A RADIO STUDY OF

METEORIC IONIZATION

by

N. Brown, B.Sc. (Hons)

A Thesis

presented for the degree of

DOCTOR OF PHILOSOPHY

at the

UNIVERSITY OF ADELAIDE

(Physics Department)

June 1972

CONTENTS

SUMMARY

This thesis presents the results of a study of radio echoes from meteor trails, with particular emphasis on low radio frequencies. Radio echoes have been observed at a frequency of 1.98 MHz using a large aerial array situated at Buckland Park near Adelaide. The results of a preliminary study of these echoes have been presented and compared with theoretical predictions. Use of meteor trails, observed at low frequencies, as atmospheric sensors has also been considered.

The distribution with height of 1.98 MHz radio meteor echoes has been measured and compared with the height distribution of radio meteor echoes observed at higher radio frequencies. It has been found that there is no significant increase in the radio echo height ceiling for radio frequencies below 17 MHz. The radio echo's polarization, electron line density, duration and decay time constant were measured, while observations of the line-of-sight velocity of the reflection point were made.

Wind profiles deduced from these observations have been compared with those measured simultaneously by a nearby radio meteor system operating at 27 MHz, and with the movement of the diffraction pattern of radio waves partially reflected from the D-region. Wind profiles obtained from the 1.98 MHz meteor observations agreed closely with the 27 MHz observations over their common height range. Using both these

systems, winds were measured from 80 to 120 km. The long echo durations found with low frequency echoes have been shown to allow the measurement of electron attachment rates.

Some work at a frequency of 27 MHz, on the measurement of possible variations in the ionization line density along the trail is also presented.

To the best of the author's knowledge this thesis contains no material previously published or written by another person, except where due reference is made in the text. It contains no material which has been submitted or accepted for the award of any other degree or diploma in any University.

(N. Brown)

ACKNOWLEDGEMENTS

The work described in this thesis was carried out in the Physics Department of the University of Adelaide under the supervision of Dr W. G. Elford. The author is grateful to Dr Elford for help and encouragement throughout the course of the work. For his interest and helpful suggestions, the author would like to thank Dr B. H. Briggs.

Many of the author's colleagues in the Radio-Physics group of the Physics Department gave valuable assistance towards this project. In particular, Dr R. A. Vincent made many helpful suggestions and, together with Mr J. W. Smith, did much of the work involved in developing the system to measure the radio echo's phase. The scanning gate was developed by Dr D. G. Felgate.

For the ionospheric drift data presented in Chapter 6 the author is indebted to Mr T. Stubbs, and to Mr E. J. Welsby who operated the 27 MHz meteor wind equipment.

The author would also like to thank Professor C. A. Hurst of the Mathematical Physics Department for some helpful discussions.

Finance for the project was provided by the Australian Research Grants Committee (Grant B65/15830), the Radio Research Board (Australia) and the University of Adelaide. The author was the holder of a University Research Grant postgraduate scholarship for the first year of

work, and then a Commonwealth Postgraduate Award for three years.

CHAPTER 1

INTRODUCTION

1.1 Review of Early Radio Meteor Observations

One of the first references to the effect of meteors on the ionosphere was made by Nagaoka (1929). He thought that they would reduce the level of ionization in their path, leaving the ionosphere in a disturbed state so that it behaved like a scratched mirror in reflecting the radio waves. Skellett (1932) was the first to suggest that the meteors contributed electrons, and together with Schafer and Goodall tried to make simultaneous visual and radio observations during the Leonid shower of 1931 (Schafer and Goodall, 1932; Skellett, 1935). During 1931 clouds prevented their visual observations, however intermittent reflections lasting for several seconds were observed at 4.79 MHz and these were observed to be more frequent during the shower period. These reflections were thought to occur directly overhead, so observations of the Leonids in 1932 were restricted to an area above the transmitter. Even so a number of simultaneous observations of radio echoes (at 2.4 MHz) and visual meteor trails were reported (Skellett, 1935).

During 1937, observations of transient radio echoes were made by Appleton, Naismith and Ingram (1937). At about the same time Eckersley (1937), using a frequency of 9.1 MHz, compared the phase of transient echoes on two spaced aerials and was thus able to measure the angle of

the echoes relative to the axis joining the two aerials. He showed that echoes occurred over a wide range of angles. Appleton and Piddington (1938), using a frequency of 8.8 MHz, measured the range spread of echoes and found it to be between 80 and 160 km. That these echoes were from meteor trails was not generally accepted, however, and it remained for Skellett (1938) to point out that meteor rates observed by Eckersley were consistent with visual meteor rates, and that the echoes occurred at the same height as the visual trails. It was also reported by Appleton and Naismith (1947) that Mohanty (1938, Ph.D. thesis) studied transient echoes using frequencies up to 16 MHz and concluded that they were caused by meteors; however this work was not published. Pierce (1938) suggested that meteor ionization might cause blanketing sporadic-E. A number of instances have since been reported where strong layers of sporadic-E have occurred at the same time as strong meteor showers (Appleton and Naismith, 1947), however it now seems that meteoric ions are the significant factor rather than the direct ionization (Wright et al., 1967).

Thus the first studies of radio meteor echoes were at low frequencies normally used to observe ionospheric reflections. The lowest frequency at which echoes have been observed appears to have been 1.6 MHz, when sudden decreases in the virtual height of night time reflections from the F-region were observed by Schafer and Goodall (Skellett, 1935). Radio reflections at higher frequencies were most likely responsible for some of the long range reception (284 miles) of

signals at 61 MHz and 44 MHz described by Jones (1933) who observed large increases in signal strength lasting several seconds.

During the second world war there was a rapid development in radar techniques. Meteor echoes were observed by some of these radars, but it was not until after the war that any serious studies of these echoes were carried out. Most of these were carried out at frequencies above 20 MHz in order to avoid scattering from the ionosphere; both continuous wave and pulse transmissions being used. It was found, however, that an upper limit appeared to exist to the frequencies that could be employed. American army radars at 100, 600, 1,200, 3,000 and 10,000 MHz were used but only the 100 MHz radar recorded meteor echoes (Stewart, Ference, Slattery and Zahl, 1947).

1.2 The Heights of Radio Echoes

The nature of the radio meteor echo is discussed in Chapter 2 where it is shown that most echoes occur under the conditions of specular reflection. A direct result of diffraction theory is that only a section of the trail, which is equal in length to $\sqrt{R\lambda}$, contributes most of the observed signal. This section of the trail can therefore be referred to as the reflecting region of the trail. The reflection coefficient of this section of the trail is determined by the electron line density of the column, and the diameter of the column compared to the radio wavelength. Appendix A of this thesis presents the theory behind some numerical calculations of the reflection coefficients for

a radio wavelength of 1.98 MHz. These are presented and discussed in Chapter 2. These calculations show that for electron line densities less than about 2×10^{13}/m the radio echo is attenuated as the diameter of the trail increases through the action of diffusion. Such echoes are referred to as underdense because the radio wave penetrates the column of electrons with little attenuation. Echoes from columns with electron line densities greater than 1.0×10^{14}/m are called overdense as the radio wave is totally reflected from the outer region of the column. However, such echoes make up only a small percentage of echoes observed by most radar systems of moderate sensitivity. Thus the amplitude of the majority of echoes observed is determined in part by the radius of the column of electrons. Any initial column radius can therefore have a significant effect on any radio echoes observed at wavelengths which are close to the size of the initial radius. The maximum amplitude of such echoes would be less than theory predicts for a zero column radius.

Two important effects determine the size of the initial radius. The first being the result of a rapid initial spread of the ions and electrons evaporated from the meteoroid, as these are travelling at the meteoroid's velocity until they collide with atmospheric molecules. The second effect which has to be considered is the finite time it takes the trail to form. During this time the trail radius increases through diffusion. This effect is less important as the wavelength is increased because the signal decay time is proportional to λ^2, while the time for the main reflecting section to form is proportional to both the meteor

velocity and to $\lambda^{\frac{1}{2}}$.

The height ceiling produced by an initial trail radius has been discussed by Greenhow and Hall (1960) and by Greenhow (1963), while the effects of diffusion and an initial trail radius were considered by McKinley (1961). McKinley used initial trail radii suggested by Manning (1958; to be referred to as 1), and this treatment has been extended in Figure 1.1 to include initial radii mid-way between the upper and lower limits suggested by Lebedinets and Portnyagin (1966; to be referred to as 2). In this figure curves are plotted which show the height at which a radio echo with a wavelength λ is attenuated by a factor of 40 db through; (a) the initial trail radius, and (b) the diffusion of the trail while it is forming, shown for three meteoroid velocities (the shaded region). The initial radii 1 and 2 are discussed in Chapter 2.2(a) where it is shown that the exact size of the initial radius has not yet been conclusively established. However, it will be shown in Chapter 5 that the actual values are closer to 1 than to 2. It can be seen from Figure 1.1 that if the initial radius follows 1 then diffusion sets the height ceiling for radio echoes with wavelengths shorter than about 30 m for low velocity meteors ($V < 15$ km/sec), and for wavelengths shorter than about 3 m for high velocity meteors ($V > 50$ km/sec). Above these wavelengths initial radius effects predominate. If the initial radius follows 2 then diffusion is important for wavelengths less than 1.5 m for low velocity meteors, and for wavelengths less than 0.2 m for high velocity meteors. Thus initial

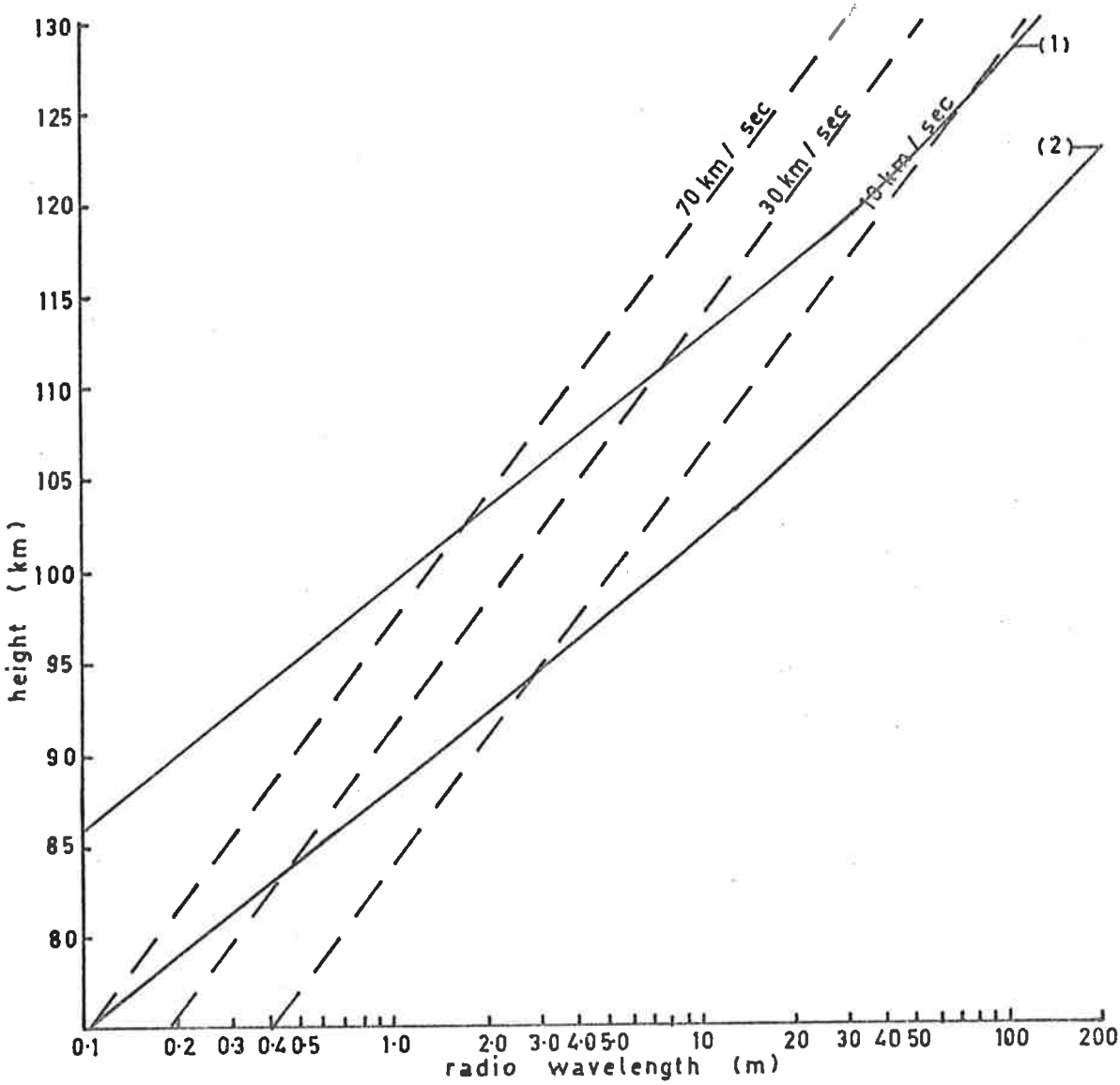

Figure 1.1 Shows the height at which a radio echo is attenuated by 40 db through initial diffusion (for 3 velocities), and through initial radii (1) and (2) (see text).

radius effects would predominate over diffusion effects for most of the wavelengths used to observe echoes if the latter initial radius were true. There is a reasonable amount of evidence to show that values proposed by Lebedinets and Portnyagin (1966) are too large and this is discussed in Chapter 8.

It can be seen from Figure 1.1 that observations at wavelengths shorter than 10 m (this includes most of present day observations; see Table 1.1) are affected by a height cut-off imposed by either diffusion or initial radius. The extent to which this affects the radio detection of the actual number distribution of meteors with height is still uncertain as the size of the initial trail radius remains in doubt. The effect of an initial radius was observed by Greenhow and Hall (1960) who found that fewer high velocity meteors were observed at wavelengths of 4.3 m, 8.3 m and 17 m than theory predicted. This effect was found to be more pronounced at shorter wavelengths. This can be explained by the fact that high velocity meteors produce their trails at the greatest heights and are thus most affected by any height ceiling. Corrections for this effect can produce significant changes to the meteor orbit distribution deduced from radio observations. (I.A.U. Symposium Number 33, 1967).

1.3 Radio Observations at Long Radio Wavelengths

Most contemporary work is being carried out at frequencies above 30 MHz. A table listing the frequency and power of a number of meteor

Station	Power	Frequency (MHz)
Adelaide, South Aust.	1.5 kW (CW)	26.8
	65 kW (pulse)	27.5
Havana, Ill., U.S.A.	3 MW (pulse)	40.9
Garchy, France	5 kW (CW)	29.8 (3 frequencies)
Durham N.H., U.S.A.	30 kW (pulse)	36.8
Stanford, Calif., U.S.A.	5 kW (pulse)	30.1
Fairbanks, Alaska, U.S.A.	1.5 kW (CW)	30.2 (2 frequencies)
White Sands, M.M., U.S.A.	30 kW (pulse)	32.8
Englin AFB, F/a, U.S.A.	5 kW (pulse)	36.8
Sheffield, England	75 kW (pulse)	25
Sheffield, England	7 kW (pulse)	17
Kharkov, U.S.S.R.	100 kW (pulse)	36.9
Kazan, U.S.S.R.	100 kW (pulse)	72
Moscow, U.S.S.R.	100 kW (pulse)	33
Hayes Isld., U.S.S.R.	75 kW (pulse)	33.5
Tomsk, U.S.S.R.	50 kW (pulse)	30.0
Obninsk, U.S.S.R.	75 kW (pulse)	24.0
Kiev, U.S.S.R.	10 kW (pulse)	34.5
Frunze, U.S.S.R.	45 kW (pulse)	38.3
Duschanbe, U.S.S.R.	80 kW (pulse)	37.4

Table 1.1: Radio-meteor systems in operation during 1970.

observing stations in operation in 1970 is given in Table 1.1. It can be seen that the lowest frequency in use is that at Sheffield which operates at 17 MHz. Thus most of the interpretations of radio meteor data could be influenced by initial radius effects discussed above. One way of overcoming this would be to observe meteor echoes at relatively long wavelengths (λ > 100 m) as such echoes are free of any initial attenuation through diffusion and probably free of any initial radius effect unless the radii 2, suggested by Lebedinets and Portnyagin (1966), are found to be correct. It has already been shown that early meteor observations were made at wavelengths of about 50 m, but subsequently very little detailed work has been carried out at λ > 17 m.

There are a number of advantages and disadvantages associated with these long wavelength observations. The principal disadvantages being the effects of ionospheric reflections. Absorption in the D and E regions and backscatter from the F region can occur to some degree at radio wavelengths longer than about 10 m. Pulse transmissions can be used to distinguish F-region reflections, but to avoid confusion the pulse repetition rate may have to be as low as 25 pulses/sec and this can prevent the observation of diffraction effects which occur during the echo's formation and are used to determine the meteoroid's velocity. Absorption in, or reflections from, the E region will hinder observations. At wavelengths longer than about 100 m this will always be the case during the day and can persist into the night with

sporadic-E ionization.

The advantages, however, go beyond the lack of an effective ceiling. The echo decay time through ambipolar diffusion is proportional to λ^2. Thus echoes at long radio wavelengths have long decay times. This makes it easier to study the effects of winds and turbulence on the amplitude of the echo, and the effect of electron attachment on the echo's duration. Wind measurements can be extended above the present ceiling of about 105 km to a height of about 115 km. Direct comparisons can be made between the movement of the diffraction pattern of radio waves reflected from the E or sporadic E regions and the neutral wind.

Resonance effects can cause the radio wave to be reflected with an increase in amplitude that may be as great as twenty. These effects are restricted to a narrow range of electron line densities around 2.0×10^{14}/m and occur when the meteor column has a diameter equal to about $\lambda/10$ (Chapter 2.3(a)). At short wavelengths this value may well be less than the initial radius of the trail so that the effect could not be observed. However, at long wavelengths this would never be the case and the transition through the resonance should be easily observed.

In this thesis results are presented of a theoretical and experimental study of radio reflections from meteor trails at a frequency of 1.98 MHz. Observations of meteor echoes have been made using the Buckland Park aerial array. This array was first phased to work as a broadside array during 1970 by the author and several of his

colleagues. Late in 1970 the first observations of meteor echoes were made, using a broadside array phased to have its maximum gain at 55° from the zenith. This work was abandoned in favour of the system described in Chapter 3, which made it possible to measure the echo's phase. Observations with this system were made between April and November, 1971. The results of these observations are presented in Chapter 4. In Chapter 5 a comparison is made between the distribution with height of meteors observed at 1.98 MHz and 17 MHz, while in Chapter 6 the wind measurements made at 1.98 MHz are compared with simultaneous measurements made using two other methods. In Chapter 7 the meteor observations at 1.98 MHz are compared with known meteor showers and with the radiant concentrations of sporadics.

1.4 Irregular Ionization along a Meteor Trail

At the present time there has not been published a completely satisfactory explanation of the large scatter present in the measured rates of decay of radio echoes from meteor trails at the same height (Weiss, 1955; Rice and Forsyth, 1963). However a number of theories have been advanced. Rice and Forsyth (1963, 1964) suggested an irregularly ionized trail and computed some decay times using a numerical model of the trail. Their work was extended by the author (Brown and Elford, 1971; see Appendix B). The possibility of deducing the variation of the electron line density along a short section of the meteor trail from the observed radio echo has also been

examined and a method of analysis developed. This analysis and some experimental results, are presented in Chapter 8.

CHAPTER 2

RADIO ECHO THEORY

2.1 Introduction

In this chapter it is intended to introduce the basic formulae used in this thesis in discussing the experimental results obtained for radio echoes from meteor trails at frequencies of 2 MHz and 27 MHz. While these formulae are widely applied in interpreting echoes from trails for the more normally used radio frequencies above 20 MHz, their use at 2 MHz has not previously been considered in detail. At a frequency of 20 MHz the length of the trail that contributes most to the observed signal is less than 2 km, while at 2 MHz this effective trail length is about 5 km. A meteor column radius of 1 m is about 1/15 of the radio wavelength at 20 MHz, however it is only 1/150 of the wavelength at 2 MHz and this has an important effect on the radio wave's reflection coefficient.

2.2 Trail Formation and the Radio Echo

2.2(a) Initial Trail Radius

A meteoroid entering the atmosphere is rapidly heated by collisions with atmospheric molecules. Atoms evaporated from the meteor's surface collide with other atmospheric molecules to produce a trail of electrons and ionized molecules. To begin with, the evaporated atoms have the same velocity as the meteor. The initial diffusion is thus very rapid and establishes a Gaussian distribution of

electron density along the radius of the column with an initial radius r_o to the point where the electron density is 1/e of its maximum value. Theoretical and experimental values of r_o are shown in Figure 2.1. Values of r_o were calculated by Manning (1958) to be equal to 3L, where L is the mean free path (shown as 1 in Figure 2.1). Kashcheyev and Lebedinets (1963) considered the effect of velocity on the evaporated particle's diffusion cross-section. Atoms evaporated from the meteor travel at meteoric velocities until they have undergone a number of collisions. The diffusion cross-section is significantly smaller at these velocities (Portnyagin, 1966) so the first mean free path L_o is greater than L. Kashcheyev and Lebedinets found $r_o = 1.5\ L_o$ (shown as 2 in Figure 2.1). Recently Lebedinets and Portnyagin (1966) found r_o satisfied the condition $0.93\ L_o < r_o < 1.5\ L_o$ (shown as 3 in Figure 2.1). Experiments to measure the initial radius have been carried out by Greenhow and Hall (1960, shown as 6 in Figure 2.1), Kashcheyev and Lebedinets (1963, shown as point 2), and by Bayrechenko (1965, shown as point 4) using a method of comparing the echo amplitude at two different wavelengths. All their height determinations were made by measuring the rate of the echo's decay. The variation of diffusion coefficient with height adopted in determining these heights, follows Greenhow and Neufeld (1955). A reason for adopting their values is discussed in Chapter 5 where it is shown to be a reasonable compromise. The theoretical variation of r_o with height was calculated using atmosphere molecular number densities from the C.I.R.A. standard

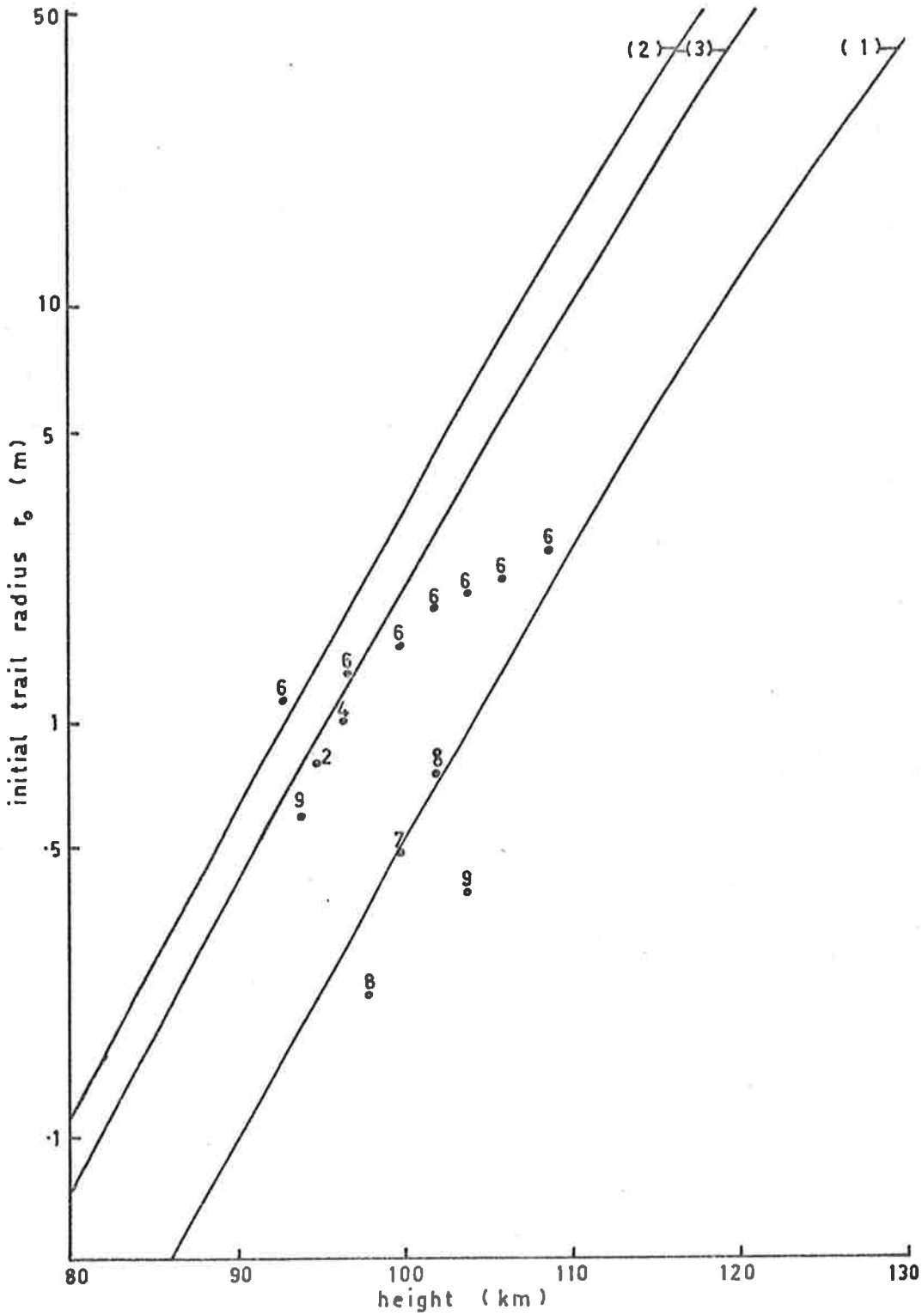

Figure 2.1 Initial trail radius - theoretical values due to (1) Manning, (2) Kashcheyev and Lebedinets and, (3) Lebedinets and Portnyagin. Point plots are experimental values discussed in text.

atmosphere (1965). It can be seen that there is a poor agreement between the experimental results and the theoretical results of Lebedinets and Portnyagin (1966). However, a line can be drawn approximately through the points 2, 4, and the centre of the height range covered by 6, this line having a slope which agrees with Manning (1), and Lebedinets and Portnyagin (3). It has been shown by Kashcheyev and Lebedinets (1963), that the method used to determine the initial radius from observations of the echo's amplitude at two different wavelengths has large errors when the amplitude ratio is either high or low. Thus there is some justification in only using those values of 6 in the centre of their height range.

Direct measurements of the radius of optical coma of meteor trails have been reported by Hawkins (1963). Observations of +6 magnitude meteors were obtained by Cook, Stienon, and Hawkins (1960) who used the 48 inch Palomar Schmidt to observe foreshortened meteor trails from the Geminid radiant. These observations showed a mean value for the radius of 0.5 m for seven trails, and this is plotted on Figure 2.1 as point 7. Two trails showed radii of 2.9 m and 2.5 m, however, these were considered to represent the peculiar case of fragmenting meteors. Mean diameters of the first and second halves of the trail were also determined and these are plotted as 8 in Figure 2.1. It can be seen that these values agree fairly well with Manning's (1958) theoretical values. Hawkins and Whipple (1958) obtained measurements of the optical comas of 51 meteors for average magnitudes of 0 and +3. These are shown as the

points 9 on Figure 2.1.

As the initial radius of the ionized column is unlikely to be larger than the optical coma (Hawkins, 1960), these optical measurements appear to contradict the results obtained by the two frequency method. Thus the actual initial radius is still doubtful.

2.2(b) Radio Echo Amplitude

The ionized column is formed along the meteor trajectory and is thus initially almost perfectly linear. The phase of radio signals reflected from a point s on the trail is given by

$$\phi(s) = \frac{4\pi R(s)}{\lambda} \qquad 2.1$$

where λ is the radio wavelength and R and s are defined in Figure 2.2(a). The echo amplitude is determined almost entirely by the trail near s = 0 so R(s) can be determined using the following approximation

$$R(s) = \left(R_o^2 + s^2\right)^{\frac{1}{2}} \sim R_o + \frac{1}{2}\frac{s^2}{R_o} \qquad 2.2$$

where R_o is defined in Figure 2.2(a). If the trail's coefficient of reflection at s is given by g(s), the signal from a short section ds will be

$$A = g(s) \exp\left(i \frac{4\pi R(s)}{\lambda}\right) ds \qquad 2.3$$

The amplitude of the signal received from the whole trail up to a point s can be found by integrating Equation 2.3 and allowing for the aerial gain. This has been carried out by Kaiser (1955) and Kashcheyev and Lebedinets (1961) and gives for the voltage, V(s), induced in the aerial,

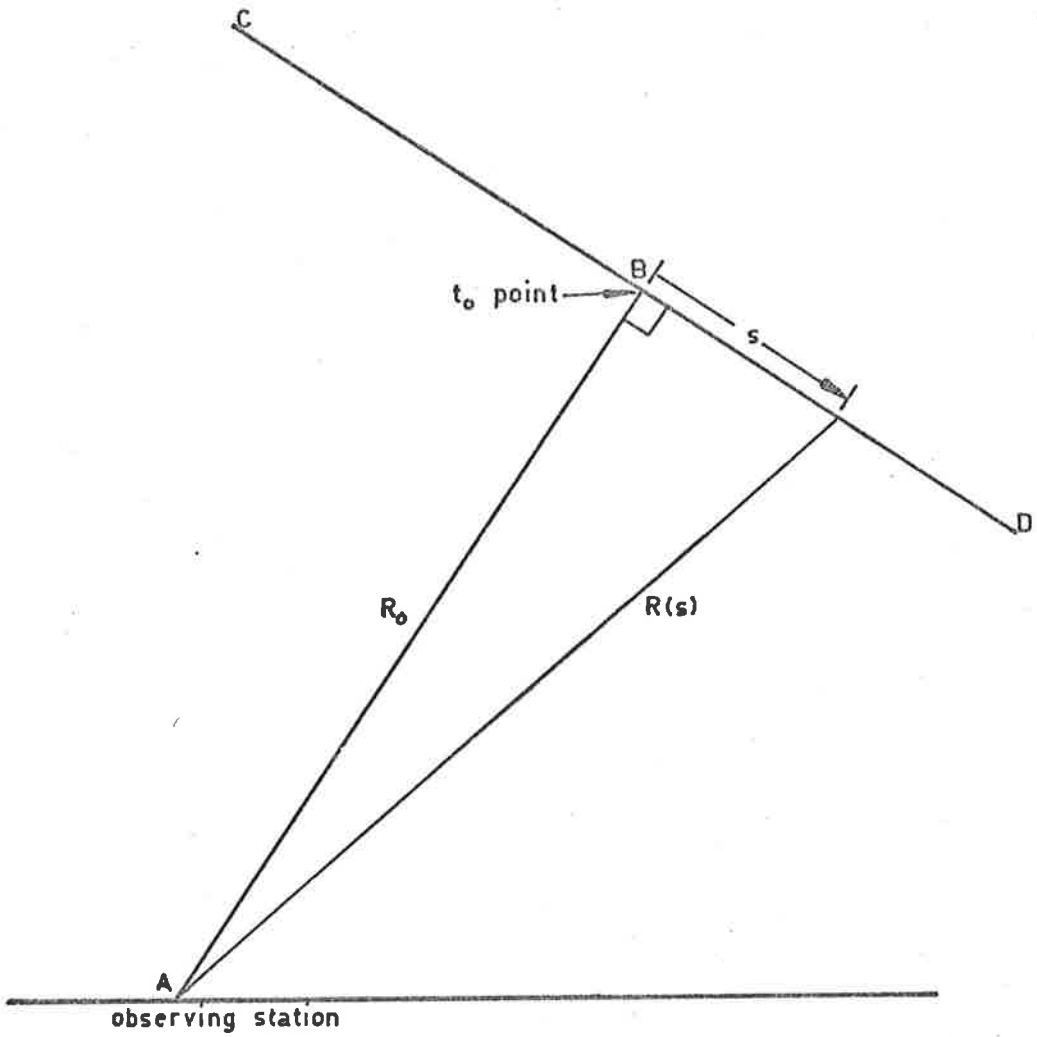

Figure 2.2(a) The t_o point of the trail where the signal is specularly reflected, is shown by the point B, where AB is perpendicular to the trail CD.

the expression

$$V(s) = \frac{G\lambda\ (2\rho)^{\frac{1}{2}}}{4\pi R_o^{\,2}} \int_{-\infty}^{S_o} g(s)\ \exp(i\ \frac{4\pi R(s)}{\lambda})\ ds, \qquad 2.4$$

where G is the aerial gain, and ρ is the input resistance of the receiver. By substituting for R(s) using Equation 2.2 this becomes

$$V(s) = \frac{G\lambda\ (2\rho)^{\frac{1}{2}}}{4\pi\ R_o^{\,2}} \exp\left(i\ \frac{4\pi R_o}{\lambda}\right) \int_{-\infty}^{S} g(s)\ \exp\left(i\ \frac{2\pi s^2}{\lambda\pi R_o}\right)\ ds. \qquad 2.5$$

This expression can be simplified by changing the variable s to a normalized variable x, often called the Fresnel length in optics. In this case

$$x = \frac{2s}{\sqrt{R_o \lambda}} \qquad 2.6$$

and Equation 2.5 becomes

$$V(x) = b \int_{-\infty}^{x_o} g(x)\ \exp(i\pi x^2/2)\ dx \qquad 2.7$$

where b is a constant defined for a particular trail by

$$b = \frac{G\lambda\ (2\rho R_o \lambda)^{\frac{1}{2}}\ .\ \exp\ (i4\pi R_o/\lambda)}{8\pi R_o^{\,2}}\ . \qquad 2.8$$

If g(x) = 1 then the integral becomes the Fresnel integral of optical diffraction theory

$$\int_{-\infty}^{x_o} \exp(i\ \frac{\pi x^2}{2}) = \int_{-\infty}^{x_o} \cos(\frac{\pi x^2}{2}) + i \int_{-\infty}^{x_o} \sin(\frac{\pi x^2}{2})$$

$$= c + is \qquad 2.9$$

this relation is plotted in Figure 2.2(b), where it can be seen to be the Cornu spiral used to solve problems of diffraction in optics. The function V(x) is plotted in Figure 2.2(c), where it can be seen that a

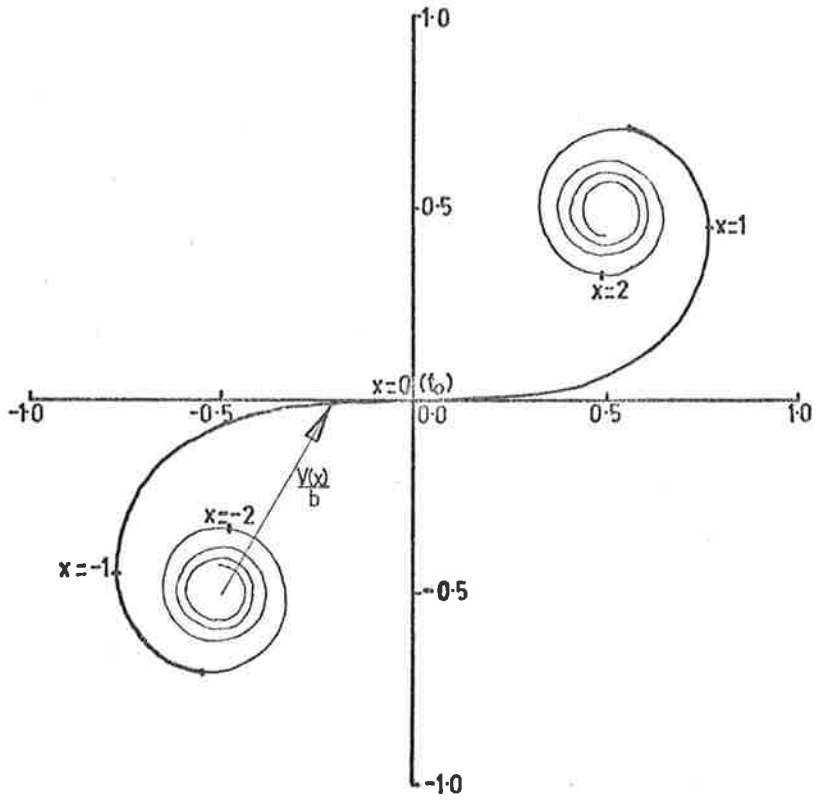

Figure 2.2(b) Cornu spiral, (Equation 2.9) showing with a heavy line the length of trail equal to $\sqrt{R_o \lambda}$.

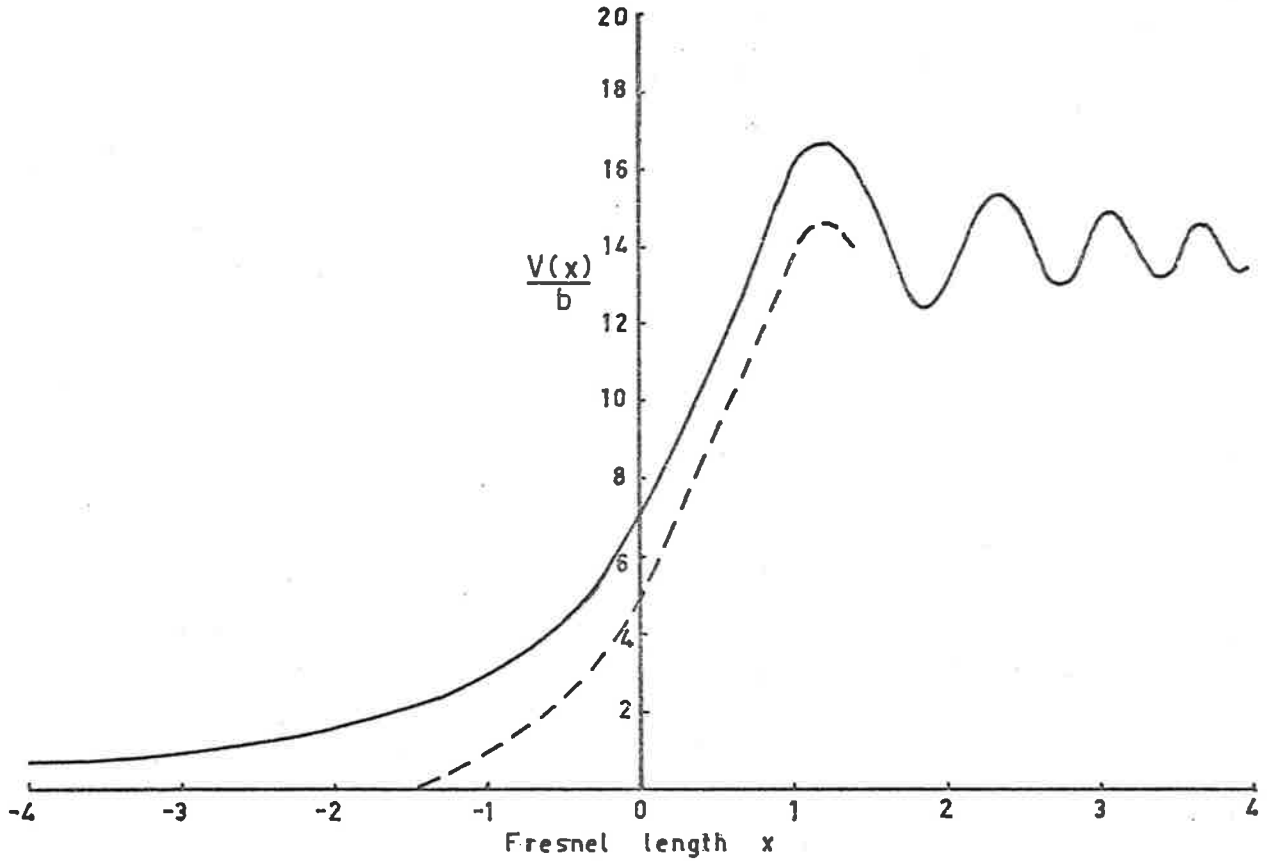

Figure 2.2(c) The echo diffraction pattern $\frac{V(x)}{b}$ plotted against x. The length of trail equal to $\sqrt{R_o \lambda}$ is shown displaced to illustrate that this length of trail contributes an amount equal to the trail's total signal.

length of trail centred about the point t_o on the trail and equal in length to $\sqrt{R\lambda}$, reflects the same signal amplitude as the whole trail. At a frequency of 1.98 MHz and range of 150 km, $\sqrt{R\lambda}$ = 4.7 km. Thus about 5 km of trail length, centred about the t_o point, is required before the maximum signal amplitude is reflected at 1.98 MHz. To a good approximation a length of trail equal to $\sqrt{\frac{R\lambda}{2}}$, reflecting the radio signal with the same phase, will return the same amplitude. Thus for large values of x, V(x) $\sim$V where

$$V = b \cdot g \cdot \sqrt{\frac{R\lambda}{2}} . \qquad 2.10$$

provided the reflection coefficient g(x) is equal to the constant value of g along the effective reflecting length $\sqrt{R\lambda}$ of the trail. In the case of an underdense trail g is proportional to the electron line densityα. Using this and the above approximation to the value of V(x), the power returned from a meteor trail P_R can be shown to be

$$P_R = 2.5 \times 10^{-32} P_T G_R G_T \left(\frac{\lambda}{R_o}\right)^3 \alpha^2 \qquad 2.11$$

where P_T is the transmitter's power, and G_R and G_T are the gains of the receiving and transmitting aerials (McKinley, 1961).

2.3 Decay of the Radio Echo

The decay of the radio echo is caused by three processes:- the radial expansion of the trail through ambipolar diffusion, the loss of electrons as they become attached to neutral atoms or molecules, and the dispersion of the trail through the action of winds. At a frequency of 1.98 MHz, most underdense echoes have durations of several seconds.

Thus Diffusion will limit echo durations above 100 km, while attachment and wind turbulence will limit durations below this height.

2.3(a) Trail Diffusion

The radius of a column with an electron density that is a Gaussian function of radius, is given by

$$r^2 = r_o^2 + 4 D t \qquad 2.12$$

where r is measured to the point at which the electron density has fallen by 1/e; r_o is the initial radius, D is the ambipolar diffusion coefficient, and t is the time after the trail's formation. The reflection coefficient of the ionized column as it expands through diffusion has been determined by many workers. Feinstein (1951) considered two relatively simple cases; where the electron density was constant throughout the column, falling abruptly to zero at the boundary, and where the electron density fell linearly to zero at the boundary of the column. The first numerical solutions for a cylinder with an electron density that was a Gaussian function of radius, were given by Kaiser and Closs (1952). These solutions were calculated by expanding the incident and reflected fields into their Fourier components. Only the first two Fourier coefficients are important for trails with low electron line densities. The trails with high electron line densities, however, require a large number of coefficients. Approximate solutions were found for these trails by considering them to behave like a metallic cylinder (Kaiser and Closs, 1952; Eshleman, 1955). These solutions were improved by Manning (1953, 1963) who

considered the effect of radio wave refraction in the outer region of the cylinder. It was shown by Herlofson (1951) that trails that were narrow compared to the radio wavelength, and with electron line densities between the above two cases, could behave as resonators and give a stronger echo for radio waves polarized perpendicularly to the trail. The approximate solutions obtained by Kaiser and Closs (1952) showed a maximum increase in amplitude of two.

Numerical solutions involving more than two Fourier coefficients became possible as the speed of electronic computers increased. The first worker to take advantage of this was Keitel (1955), who considered both a low and high electron line density with regard to both back-scatter and forward-scatter of the radio waves. Since then solutions have been obtained by Brysk et al., (1965) who considered the trail in terms of a potential well. A more systematic approach, computing reflection coefficients for electron line densities in the range of 10^{12}/m to 10^{15}/m for both transverse and longitudinal polarization, has been carried out by Lebedinets and Sosnova (1967). They showed that the resonance phenomena occurred to a much larger degree than had been predicted by the approximate solutions of Kaiser and Closs (1952).

The problem and its method of solution is given in Appendix A. There are two equations to be solved. The first of these is

$$\frac{d^2P_n(\rho)}{d\rho^2} + \frac{1}{\rho}\frac{dP_n(\rho)}{d\rho} + \left[\varepsilon(\rho)(kr_o)^2 - \frac{n^2}{\rho^2}\right] P_n(\rho) = 0 \qquad 2.13$$

where $P_n(\rho)$ are the Fourier coefficients of the electric field in the longitudinal case, so that

$$E(\rho) = \sum_o^n P_n(\rho) \cos n\theta \; ; \quad \rho = \frac{r}{r_o}$$

where r is the trail radius, and r_o is the radius to the point where the electron density has fallen to 1/e of its maximum value. The second equation, for the transverse case, is

$$\frac{d^2T_n(\rho)}{d\rho^2} + \left(\frac{1}{\rho} - \frac{d\varepsilon}{d\rho}/\varepsilon\right)\frac{dT_n(\rho)}{d\rho} + \left[\varepsilon(\rho)(kr_o)^2 - \frac{n^2}{\rho^2}\right] T_n(\rho) = 0 \qquad 2.14$$

where $T_n(\rho)$ are the Fourier coefficients of the magnetic field $H(\rho)$, given by

$$H(\rho) = \sum_o^n T_n(\rho) \cos n\theta. \qquad 2.15$$

For any practical situation the solutions to Equations 2.13 and 2.14 are almost independent of the radio frequency, and depend only on kr_o and α for values of collision frequency (ν) normally found above 80 km. The radio frequency enters Equations 2.13 and 2.14 through the terms $\varepsilon(\rho)(kr_o)^2$ and $\frac{d\varepsilon}{d\rho}/\varepsilon$, where $\varepsilon(\rho)$ is the dielectric constant and k is the wave number. The full expression for $\varepsilon(\rho)$ is given in Appendix A (Equation A.7). For the present discussion it is sufficient to define it as

$$\varepsilon(\rho) = 1 - \frac{C\,\alpha\,\exp(-\rho^2)}{(kr_o)^2}\left(1 + i\,\frac{\nu}{2\pi f}\right) \qquad 2.16$$

where C is a constant; α is the electron line density; ν the collision frequency in the column; and f the radio frequency. It can be shown

(using Equation 2.16) that

$$\frac{d\varepsilon}{d\rho}/\varepsilon = \frac{2\rho}{(kr_o)^2 \,/\, (C\ \alpha\ \exp(-\rho^2)) - 1} \qquad 2.17$$

Thus for a particular value of α and kr_o, both $\varepsilon(\rho)(kr_o)^2$ and $\frac{d\varepsilon}{d\rho}/\varepsilon$ will be independent of the wavelength (f) provided $\frac{\nu}{2\pi f} << 1$. Lebedinets and Sosnova (1967) found only a small change in the solutions to Equations 2.13 and 2.14 when $\frac{\nu}{2\pi f}$ was varied between 10^{-4} and .07. At 1.98 MHz, $\frac{\nu}{2\pi f} < .01$ above 80 km, so this case lies within the range considered.

The initial trail radius at 100 km has been shown to be of the order of 1 m. Thus at 2 MHz kr_o will initially be .042. It will be less than this below 100 km. Thus small values of kr_o are peculiar to the low frequencies. The reflection coefficients for small values of kr_o have been considered by Herlofson (1951) who showed that in the case of parallel polarization, the Born approximation for electron scatter is valid right down to vanishing values of kr_o for small electron densities. However, in the case of transverse polarization the energy scattering diameter will vanish as $(kr_o)^4$. This is brought about by the fact that the important partial wave in parallel scattering for $kr_o \to 0$ is the $J_o(k\rho)$ wave and this approaches a value of unity as $kr_o \to 0$, while in the case of transverse polarization the important partial wave is $J_1(k\rho)$ and this approaches zero as $kr_o \to 0$. If it has a value that is virtually zero throughout the ionized column, then it cannot be greatly affected by the column and will have a very small reflection coefficient.

Reflection coefficients for small values of kr_o have not been published for the transitional electron line densities between 10^{13} - 10^{15} electrons/meter. These have therefore been calculated using the method described in Appendix A and are shown in Figure 2.3 and Figure 2.4. The reflection coefficient is shown on a logarithmic scale plotted against values of $(kr_o)^2$. Thus as $(kr_o)^2$ is proportional to the time (t) it takes the trail to diffuse to a radius r_o, the horizontal axes of Figures 2.3 and 2.4 are linear with time (where t = 0 for r_o = initial radius). Time scales shown in Figures 2.3 and 2.4 were calculated assuming a zero initial radius, using Greenhow and Neufeld's (1955) values of ambipolar diffusion for the heights 80 and 95 km. It can be seen from Figure 2.4 that trails with electron line densities greater than 5×10^{13}/m have a reflection coefficient $g_\perp < g_{//}/2$ until $(kr_o)^2 = .02$. This value of kr_o can be considered to mark a transition from the trail reflecting only the component of the radio wave polarized parallel to the column (where $(kr_o)^2 < .02$ and $g_\perp << g_{//}$), to the situation where both components, parallel and perpendicular to the column are reflected ($(kr_o)^2 > .02$). In Figure 2.5 $g_\perp$ is plotted against $(kr_o)^2$ for four electron line densities between 5.0×10^{13} and 5×10^{14}/m. Over this range there is a pronounced increase in the ratio $g_\perp/g_{//}$ through the effects of resonance. For an electron line density of 5×10^{13}/m, $g_\perp$ reaches its maximum value when $(kr_o)^2 = .2$. For $(kr_o)^2 < .2$ the component of the radio wave reflected perpendicularly from the column undergoes a change in phase on reflection, which depends

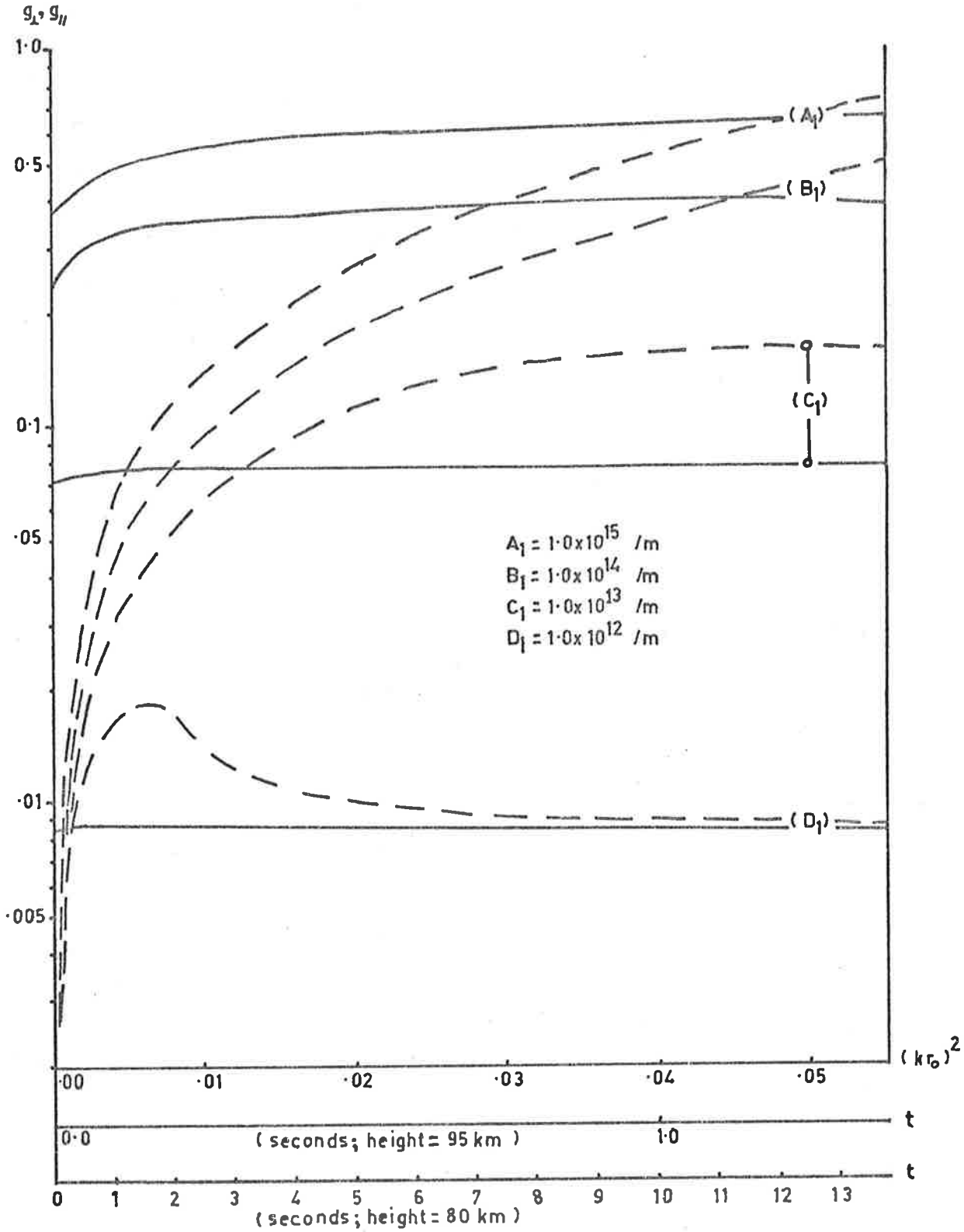

Figure 2.3 Reflection coefficient for waves polarized parallel to the column ($g_{//}$ - continuous line) and perpendicular to the column ($g_{\perp}$ - dashed line), for electron line densities shown.

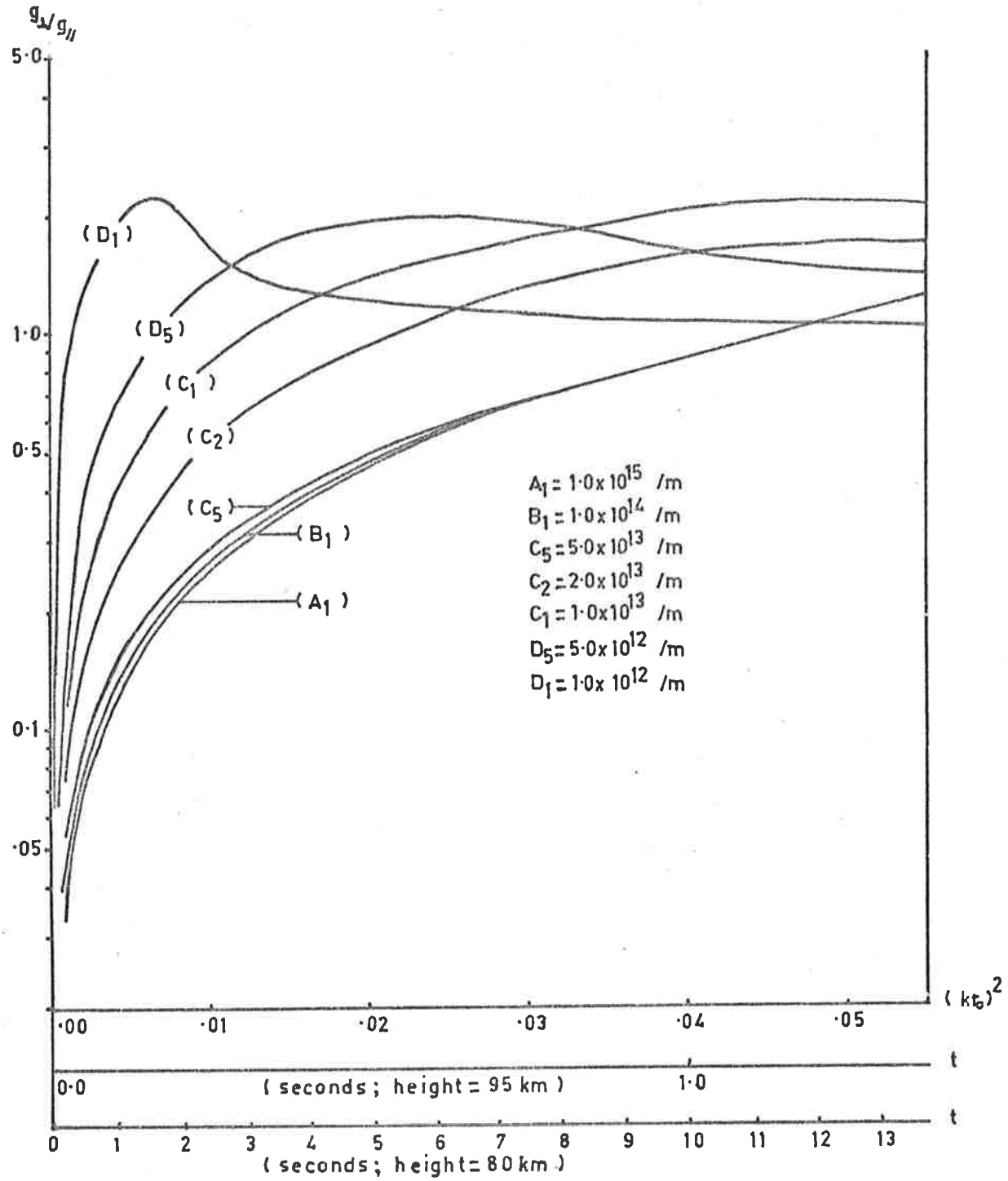

Figure 2.4 The ratio of reflection coefficients for radio waves perpendicular ($g_\perp$) and parallel ($g_{//}$) to the trail, for electron line densities indicated.

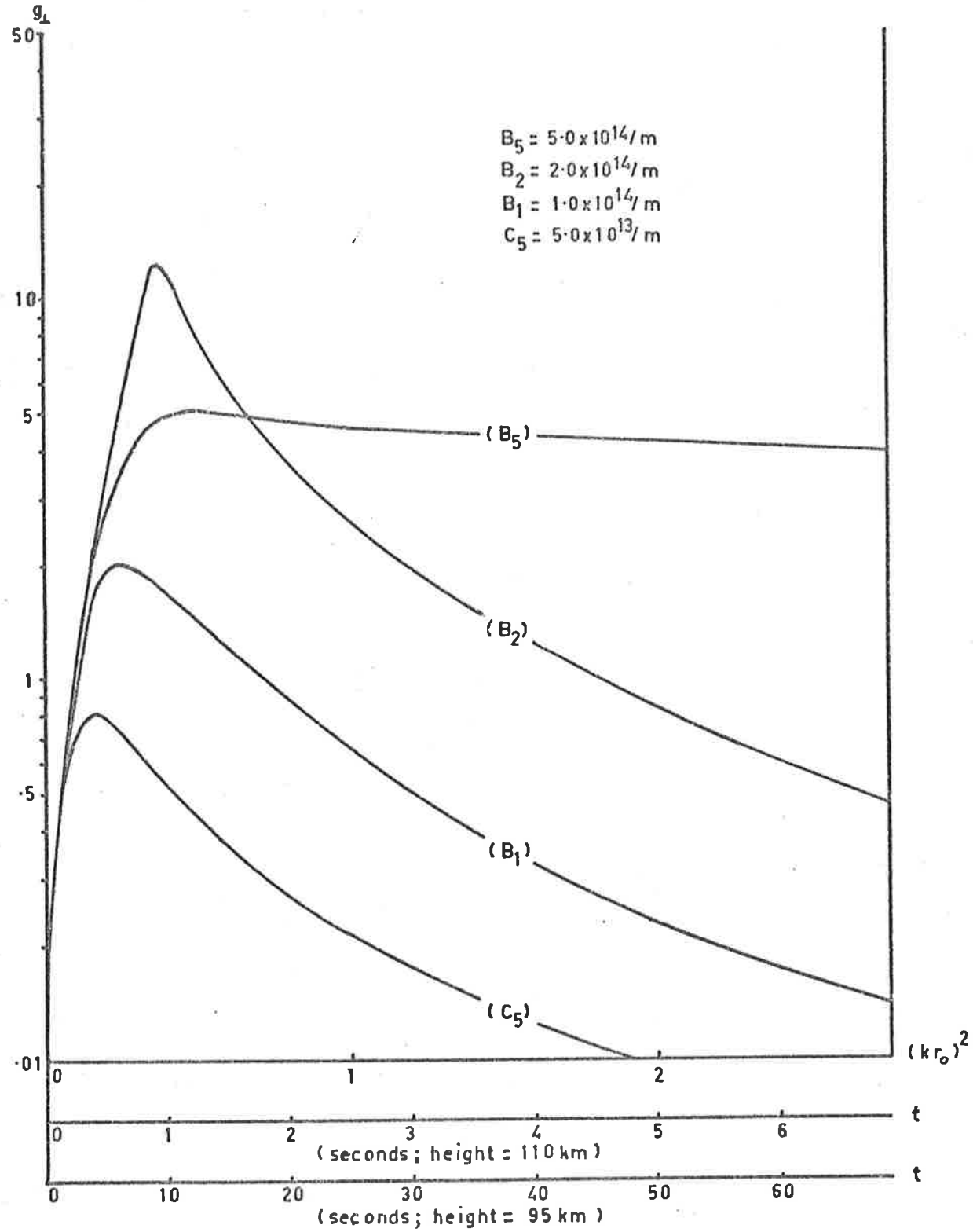

Figure 2.5 The reflection coefficient for radio waves polarized perpendicular to the trail, for electron line densities indicated.

fairly critically on the value of kr_o (see Appendix A). When $(kr_o)^2 > .2$ this phase change is constant with increasing kr_o and equal to the change which occurs to the component of the radio wave reflected parallel to the column. Thus, if a circularly polarized radio wave is transmitted, it will be reflected from the trail as a linearly polarized wave while $(kr_o)^2 < .02$. Then for $.02 < (kr_o)^2 < .2$ the reflected wave will change in both amplitude and polarization, becoming elliptically polarized for $(kr_o)^2 = .2$. For $(kr)^2 > 0.2$ $g_\perp/g_\parallel$ will approach unity and the reflected wave will become circularly polarized. The times taken for the trail to diffuse until $(kr_o)^2 = .02$ and .2 (where r = 3.3 m and 11 m at 1.98 MHz) are shown in Figure 2,6 where the region defined by $.02 < (kr_o)^2 < .2$ is shaded in.

Reflection coefficients shown in Figures 2.3 to 2.5 have been calculated assuming a plane wave incident upon an infinite column. This is a good approximation to the real case in the t_o region, where most of the observed signal amplitude is reflected. The case of a plane wave incident obliquely on a cylinder of infinite length has been considered by Wait (1955) who showed that the field gains a cross-polarized component.

It has already been shown that the effective length of trail which reflects signal at 2 MHz, is about 5 km. Over this length the coefficient of diffusion (ignoring effects due to the magnetic field) can vary by a factor of two. The more rapid decay of the reflecting

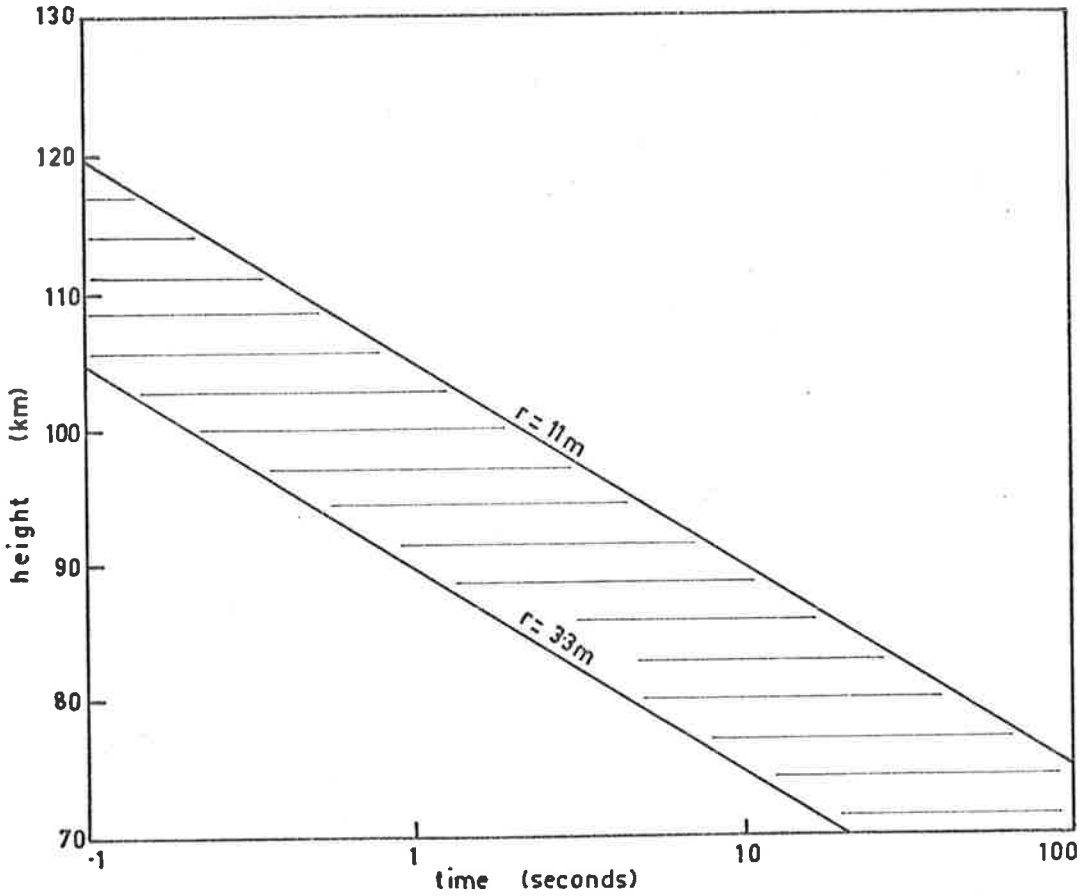

Figure 2.6 The times taken for the trail to diffuse to a radius of 3.3 m and 11 m are shown plotted against height.

region of trail above t_o will, however, be compensated for by the slower decay of the region below t_o, so that the effect is fairly small (Figure 2.7). Even if such an effect were appreciable it would be unlikely that it could be observed, except in the trails that decay rapidly. This is because winds start to distort most trails after about one second and this can produce large fluctuations in the observed signal.

The effect of very rapid diffusion on the radio diffraction pattern normally observed during trail formation, has been computed theoretically by Southworth (1962), Simek (1964, 1968), and by Lebedinets and Sosnova (1967). This effect becomes unimportant for the longer wavelengths because the decay time increases as the square of the wavelength, while the zone length is proportional to the square root of the wavelength. Thus the meteor crosses the principal zone in a time that is small compared to the signal's decay time.

2.3(b) The Effects of Winds and Wind Shears

It has been shown by Kato (1959) that ionization irregularities in the E region of the atmosphere move with the neutral wind. More recently, Kaiser et al (1969) have shown that planar irregularities move with the neutral wind unless they are field aligned. The degree of alignment required decreases with height and is about two degrees at 114 km. It can therefore be assumed that the large majority of meteor trails below about 120 km move with the neutral wind, and the reflected

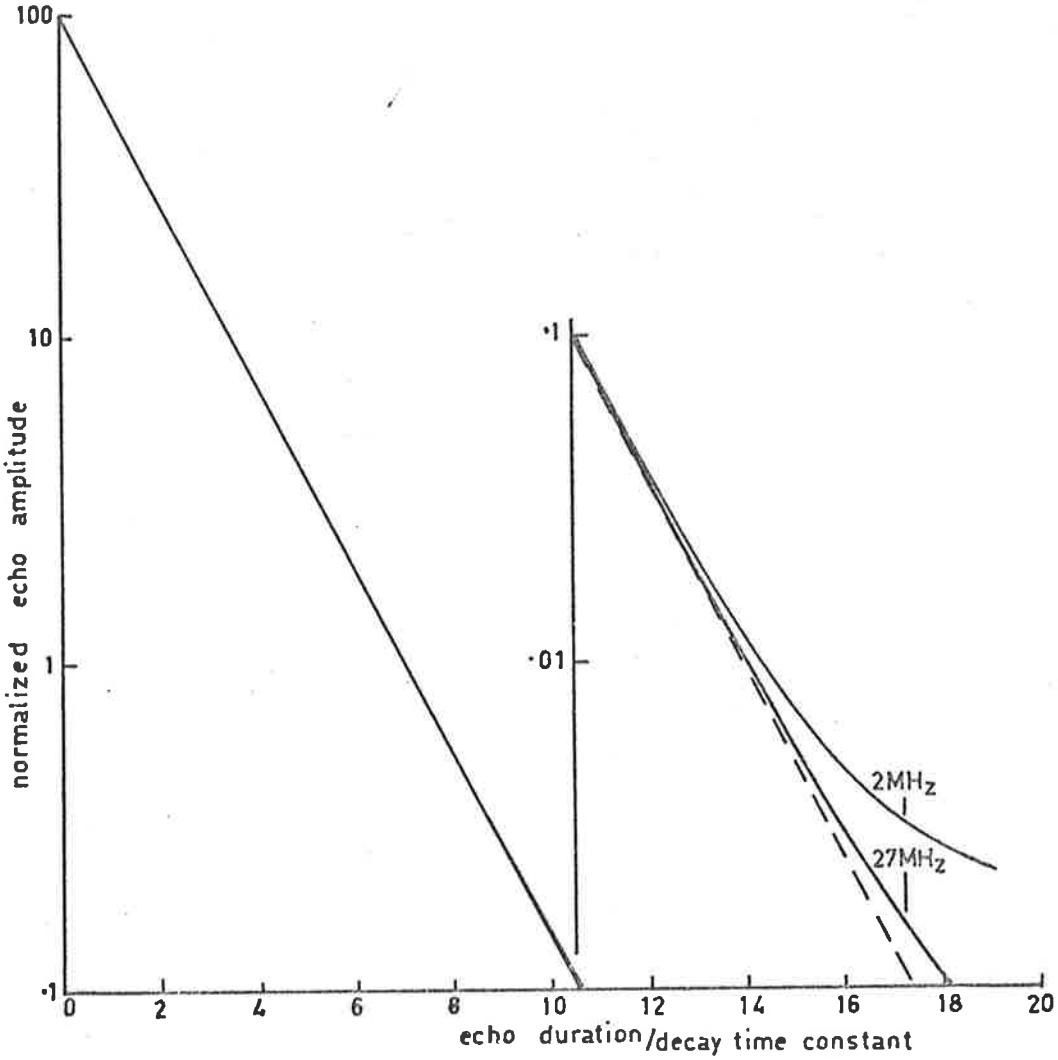

Figure 2.7 The decay of a radio echo at 2 and 27 MHz for a trail at 45° to the zenith.

radio signal will be Doppler shifted in frequency. As the frequency shift is small it is normally viewed as a continuous change in phase.

When the wind varies with height the trail inevitably becomes distorted so that the initial reflection point moves and secondary reflection points develop. When the wind varies linearly with height, the trail rotates causing the reflection point to move along the trail. This results in the reflection point's height rising or falling at a velocity V_H. In Figure 2.8 the variation of V_H with the echo's zenith angle is shown for linear wind shears of 10 and 100 m/sec/km for an echo first formed at a height of 105 km. It can be seen that for an average wind shear of 10 m/sec/km the vertical movement of the reflection point can be neglected for zenith angles less than 50°. However, the reflection point would be rapidly moved out of a region of high wind shear near 100 m/sec/km. Such a shear would seldom exist over a height range greater than 3 km and it would only take about 1 second for the reflection point of a trail with a zenith angle of 35° to be moved over this height range.

Non-linear wind variations with height cause the trail to bend and secondary reflections to develop. Signals from these reflections interfere with the original signal causing it to fade. Overdense echoes observed at radio frequencies above 20 MHz have been shown to start fading about 0.4 seconds after the trail has formed (Greenhow, 1952a). At a frequency of 1.98 MHz underdense echoes below 120 km have decay

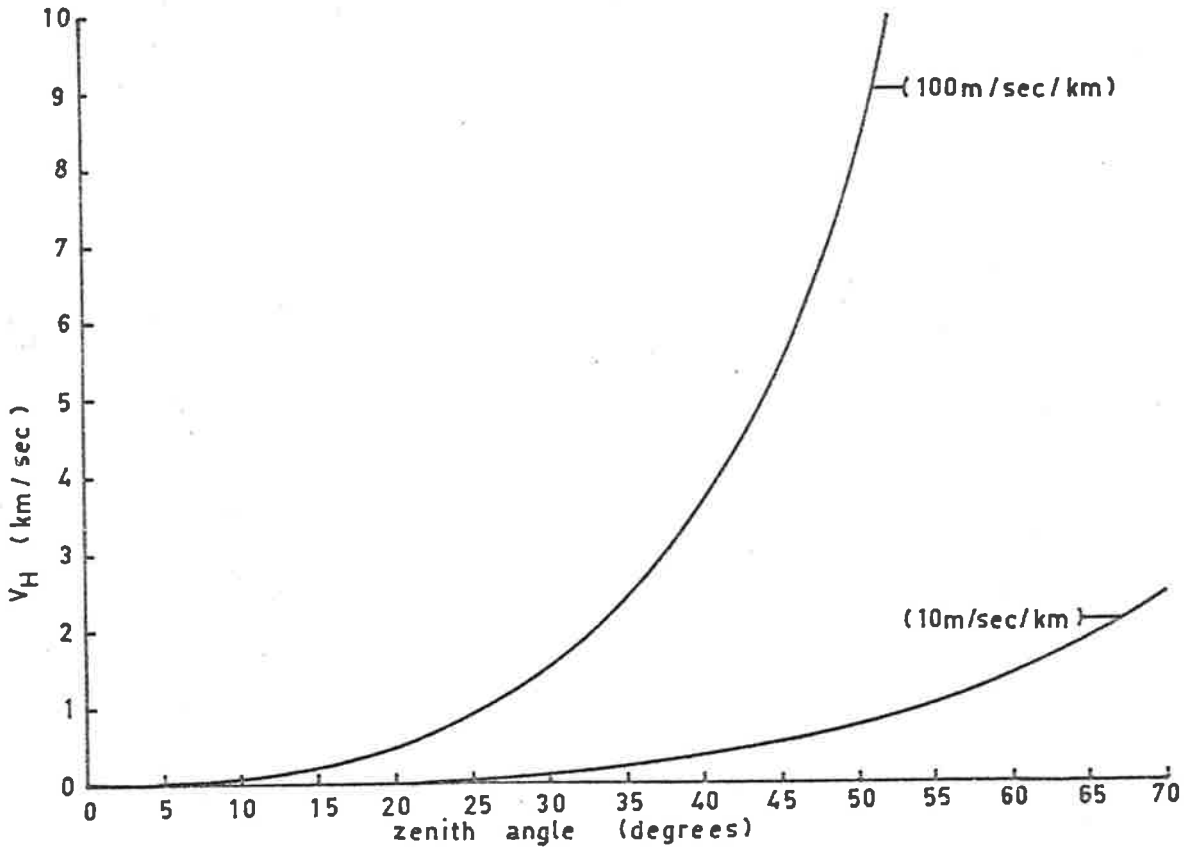

Figure 2.8 Showing how the vertical velocity of the reflection point (V_H) varies with zenith angle for two linear wind shears of 10 and 100 m/sec/km (for an echo initially at 105 km).

time constants that are > 0.4 seconds, therefore most underdense echoes at 1.98 MHz should show fading. However, because an underdense echo decays exponentially, two echoes separated by more than about 5 km will not produce a long-lasting deep fading as the relative strengths of the two echoes will change rapidly until the lower echo dominates. (In the case of an overdense echo the echo strengths remain fairly constant for most of the echo's duration until the trail becomes underdense). An additional factor which serves to reduce the effect of wind induced trail distortions at 1.98 MHz is the length of the trail contributing signal to each specular reflection. At 1.98 MHz this is about 5 km (Chapter 2.2(b)) so that wind measurements are averaged over this length of the trail.

2.3(c) Wind Turbulence

Photographic observations of meteor trails at a height of 90 km, have shown the existence of small scale turbulence with a scale of 20 m and velocity 0.7 m/sec (Greenhow, 1959). The radial expansion of a meteor trail proceeds at a rate which is proportional to $t^{\frac{1}{2}}$ (where t is the time from the formation of the trail) under the influence of diffusion, while it expands at a rate proportional to $t^{3/2}$ through turbulence. ~~Thus~~ Turbulence will eventually become the dominant factor in trail dispersal below 100 km where the normal delay, before it becomes important, is about 30 seconds (Greenhow, 1959). This is also observed with the growth rates of chemical trails which show a delay of about 30 seconds before the rapid radial growth through turbulence sets

in (McAvaney, 1970).

At a frequency of 1.98 MHz the trail diameter must be about 48 m before the reflected signal amplitude has fallen by a factor of 1/e. At 100 km the trail would take 10 seconds to diffuse to this diameter while at 90 km it would take about 50 seconds. Thus turbulence could be an important factor in the decay of radio echoes at 1.98 MHz below 100 km.

2.3(d) Electron Attachment

Long enduring echoes from overdense meteor trails are observed to be most persistent at a height of 95 km. Thus below this height the duration of the radio echo must be shortened through the action of some agent other than diffusion. Simultaneous photographic and radio echo observations of persistent meteor trails carried out by Davis et al (1959a and b) showed that the attachment of electrons to neutral oxygen molecules, could explain the shortened radio echoes. Further work on the theory of attachment has been carried out by Greenhow and Hall (1962) and by Manning (1964). Glöde (1967) has shown that attachment is significantly greater at night due to the strong detachment of electrons during the day time. By observing the change in echo durations just before and just after sunrise for the Quadrantids, Leonids and Perseids, Glöde found the attachment rate (A) to vary between .02/sec at 91 km to about 0.2/sec at 100 km.

Attachment of electrons is proportional to the number of electrons

present. It thus leaves the distribution of electrons across the trail Gaussian, although it causes an exponential decrease in the electron density. In the absence of attachment the electron density n_e is equal to the density of positive ions n_p. However with an attachment rate A, and detachment rate C, these two densities are related by

$$n_e = n_p \left[\exp - (A + C)t + \frac{C}{A + C}(1 - \exp - (A + C)t)\right], \qquad 2.18$$

where t is the time after trail formation (Glöde, 1967). During the night A >> C and this becomes

$$n_e = n_p \exp (- At)$$

If an average value for A of 0.1/second is adopted, then the electron density will fall by a factor of 1/e in 10 seconds. This would produce a similar reduction in the radio signal reflected from a trail with an underdense electron line density. However this neglects the signal decay caused by the radial diffusion of the trail electrons. At frequencies above 17 MHz the signal is reduced by a factor of 1/e through diffusion, in less than 1 second. Thus attachment has little effect on underdense echoes at these frequencies. At a frequency of 1.98 MHz this is no longer the case, as at a height of 95 km the radio echo takes about 30 seconds to decay by the above factor through diffusion alone. In Figure 2.9 the decay time constant (time for the signal to fall by a factor of 1/e) is plotted against height for diffusion and for attachment for a number of values of A. The dashed line shows the variation of A with height found by Glöde (1967). This variation with height could not be explained by Glöde who thought that

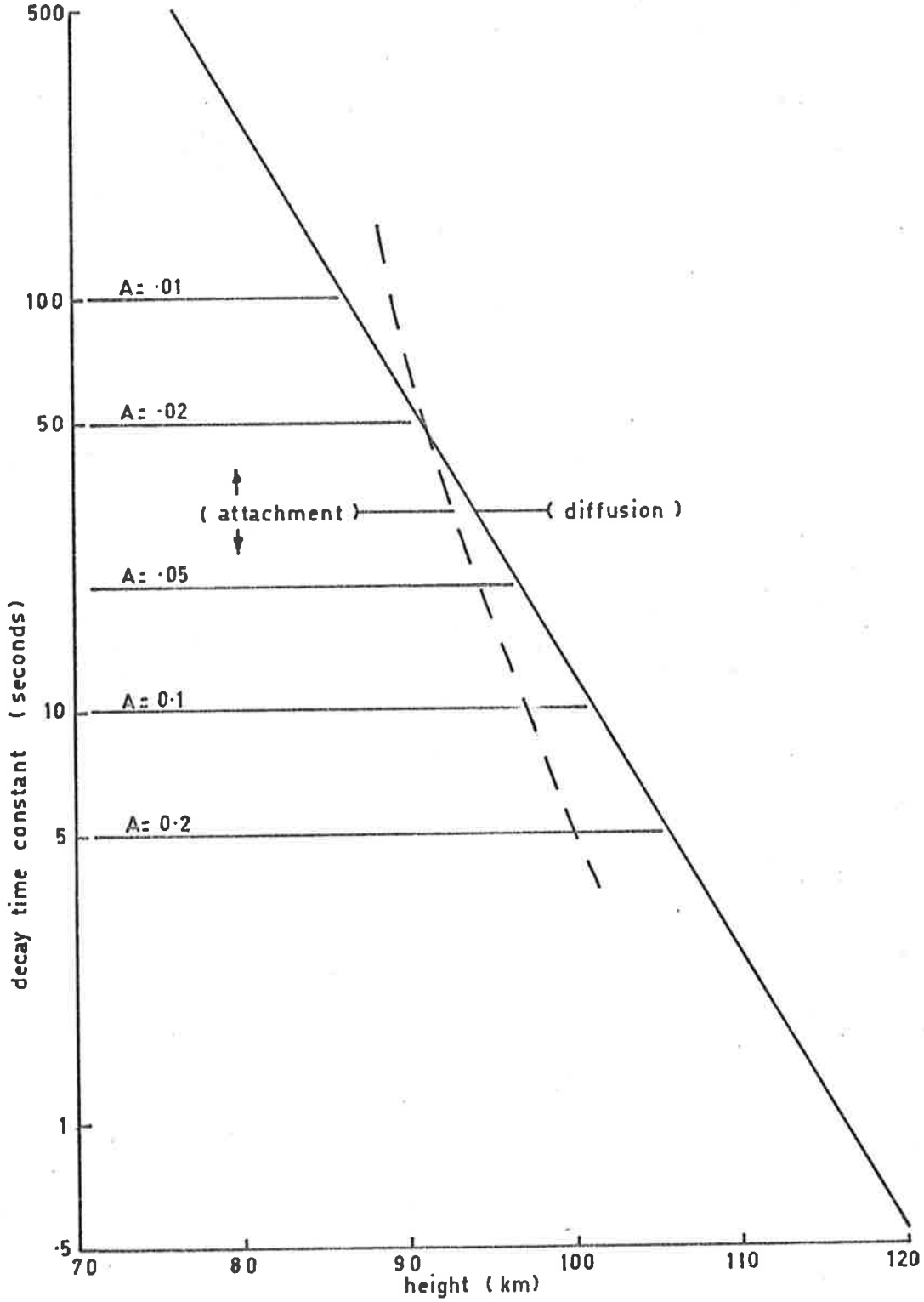

Figure 2.9 Showing the decay time constant through diffusion and attachment of underdense radio echoes at a frequency of 1.98 MHz (for five values of the rate of Attachment, A). The dashed line shows decay rates for a variation of A with height due to Glöde (1968).

it was probably not real (heights were deduced from the durations of overdense echoes).

CHAPTER 3

EQUIPMENT AND EXPERIMENTAL METHODS

3.1 The Buckland Park Research Station

The aerial array located at Buckland Park, 26 miles north of Adelaide, has been described by Briggs et al (1969). It consists of 178 dipoles arranged in the manner shown in Figure 3.1. Each dipole consists of a wire 72 m long, which is supported 11 m above the ground by timber poles. A coaxial feeder connects each dipole to the receiving hut. These coaxial cables are matched to the aerials for the frequencies 1.98 MHz and 5.96 MHz, and the length of each cable is an integral number of half wavelengths at 1.98 MHz. Each cable is connected to a socket on an aerial connection board in the central receiving hut where aerials can be combined to produce beams (Figure 3.2). The combination used is described in Chapter 3.5. A transmitter situated next to the array generates a Gaussian shaped pulse 30 msec wide at the half power points, with a maximum power of 26 kw. The transmitting aerial consists of four centre-fed half wave folded dipoles arranged in the form of a square. The polarization of the transmitted wave can be rapidly changed between left-hand, right-hand and linear by altering the phases of the currents in the four dipoles. A pulse repetition rate of 25 pulses/sec was normally used at night, although pulse repetition rates of 50 and 100 pulses/sec were available.

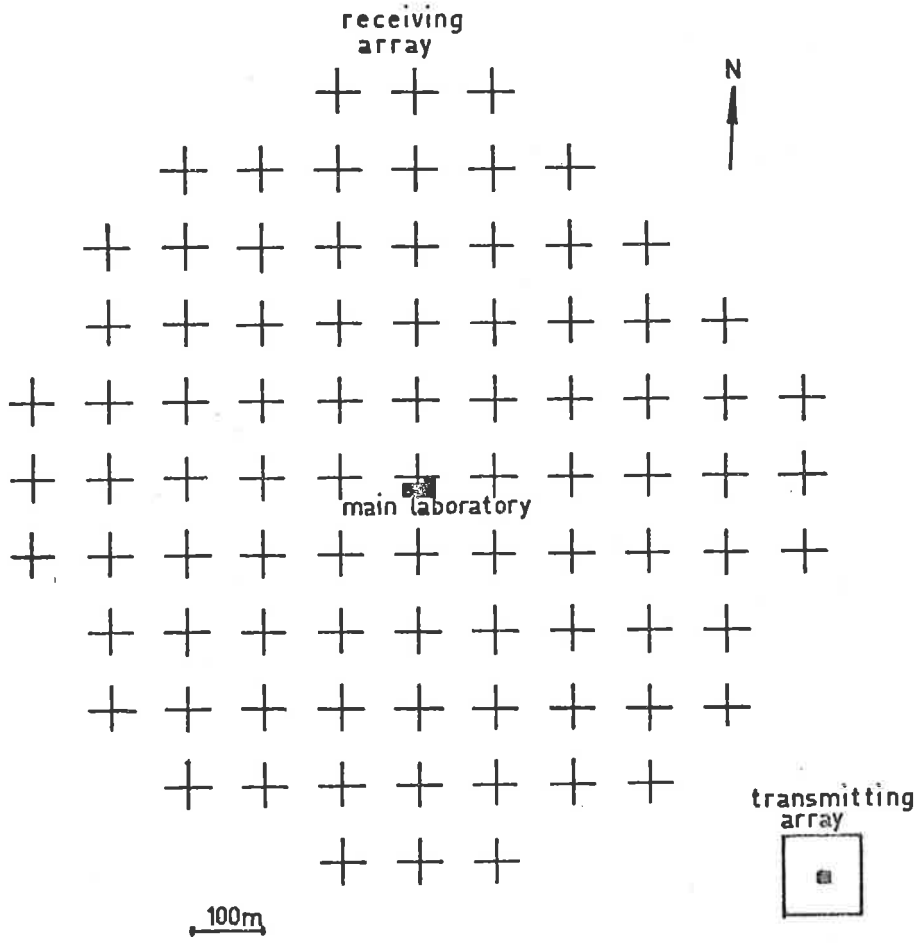

Figure 3.1 The Buckland Park aerial array.

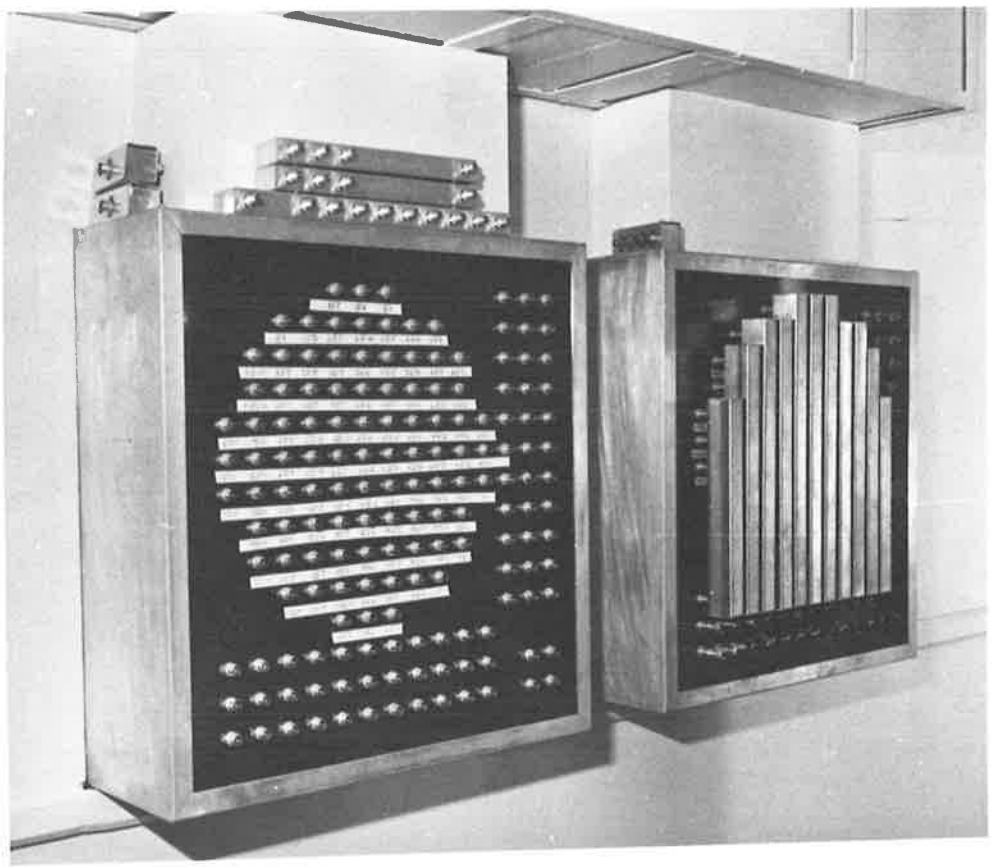

Figure 3.2 The aerial phasing boards.

Three broadband receivers with a bandwidth of 60 kHz and a gain of 120 db were used with the receiving array. Two receivers were used for measuring the radio amplitude, while the third measured radio phase. The local oscillator was suppressed except for the range of interest, and this provided a zero signal reference level.

3.2 Echo Amplitude Records

The trigger used to pulse the transmitter was also used to trigger a range gate. Signals within this gate were peak rectified so that a D.C. voltage was produced which varied with the amplitude of the gated echo. This signal was recorded on a chart recorder. The receiver's detected output was also used to modulate the brightness of an oscilloscope provided with a vertical time base. This was photographed on a film which moved horizontally, producing a time axis. An example of the record produced is shown in Figure 3.3(a).

3.3 Echo Phase

3.3(a) Theory

A method for measuring changes in the phase path of pulsed radio waves has been described by Findlay (1951) and modified by McNicol and Thomas (1960) and Vincent (1967). In principle the technique involves comparing the phase of the reflected signal with the phase of a reference oscillator which is in turn fixed in phase relative to the transmitted pulse. If the reference and received signals are added and then detected in the normal way, each echo will be modulated by the

beat frequency δf given by

$$\delta f = f_s - f_r$$

where f_s is the transmitted frequency and f_r is the frequency of the reference oscillator. The phase of the beat signal will be determined by the phase of the reflected radio pulse thus making it possible to observe directly these phase changes. This can be seen by considering the signal in a pulse of radio waves which have travelled over the phase path P to a meteor trail and back. After a time, t, the amplitude, R, of the returned signal will be (for c = velocity of light)

$$R = R_o \cos \left(2\pi f_s \left(t - \frac{P}{c}\right)\right)$$

The amplitude, L, of the reference oscillator at time, t, will be

$$L = L_o \cos (2\pi f_r t)$$

These two signals are mixed together and the high frequencies removed during the process of detection. The resultant is a signal whose amplitude is given by (for K = constant)

$$A = K R_o L_o \cos 2\pi \left(\delta f \, t - \frac{f_s . P}{c}\right)$$

If the phase path changes by δP then the signal changes in phase by $2\pi \frac{f_s \delta P}{c}$. If the beat frequency within an echo is observed to move in range a distance of one wavelength (λ), then

$$\frac{2\pi f_s}{c} \delta P = 2\pi$$

$$\delta P = \frac{c}{f_s} = \lambda$$

Thus a change in the phase path of one wavelength results in the phase

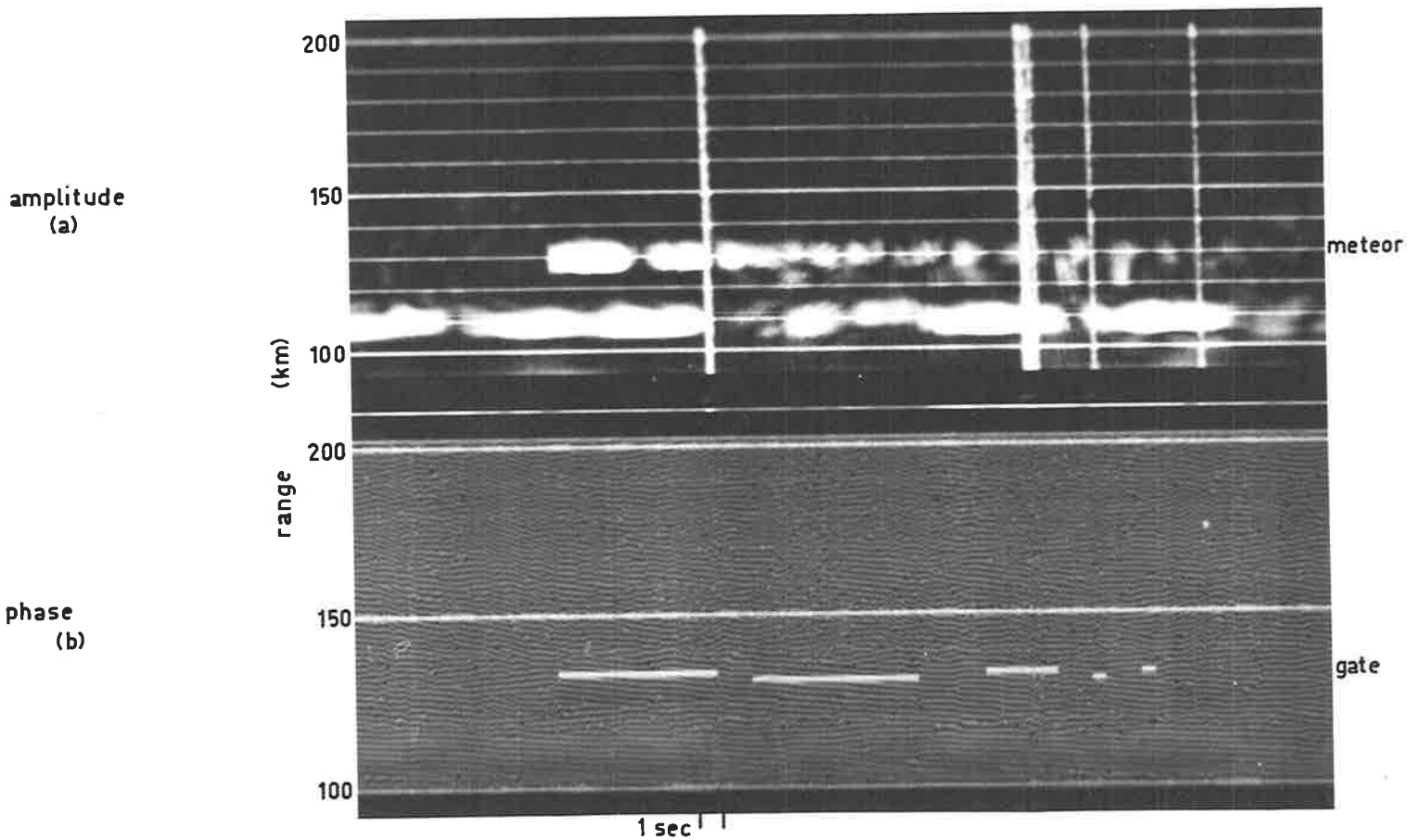

Figure 3.3 Film record. The transmitted pulse had a Gaussian shape, thus fast rising echoes started abruptly with a broad trace, and slow rising echoes showed an initial broadening.

of the beat frequency changing by 2π radians. The sense of the change in phase of the beat frequency within the pulse will be in the direction of the change in P if $f_r > f_s$.

3.3(b) Equipment

A block diagram of the system is shown in Figure 3.4. The transmitter pulse was derived from an oscillator running continuously at 1.98 MHz. The phase reference was obtained from this signal by mixing it with 85 kHz. The lower sideband (1.895 MHz) was then fed to the receiving hut where it was mixed with the receiver's local oscillator and the lower side band (1.685 MHz) used as a reference to be added to the receiver's intermediate frequency (1.600 MHz) before detection. With a transmitter pulse width of 30 msec, approximately three cycles of the beat frequency were present within an echo. The phase of the reference signal was locked to the start of the transmitted pulse by using the 85 kHz reference signal as the trigger. This was achieved by squaring the 85 kHz and then differentiating it. One of the resulting spikes was then gated out and used to trigger both the R.F. pulse and the displays and gates used to record the echoes.

Mixing the intermediate frequency with a reference signal has two advantages. Firstly the reference signal does not have to pass through the I.F. of the receiver; the beat frequency δf can therefore be greater than the receiver's bandwidth. Secondly the receiver can also be operated in the normal manner to record the echo's group path. An

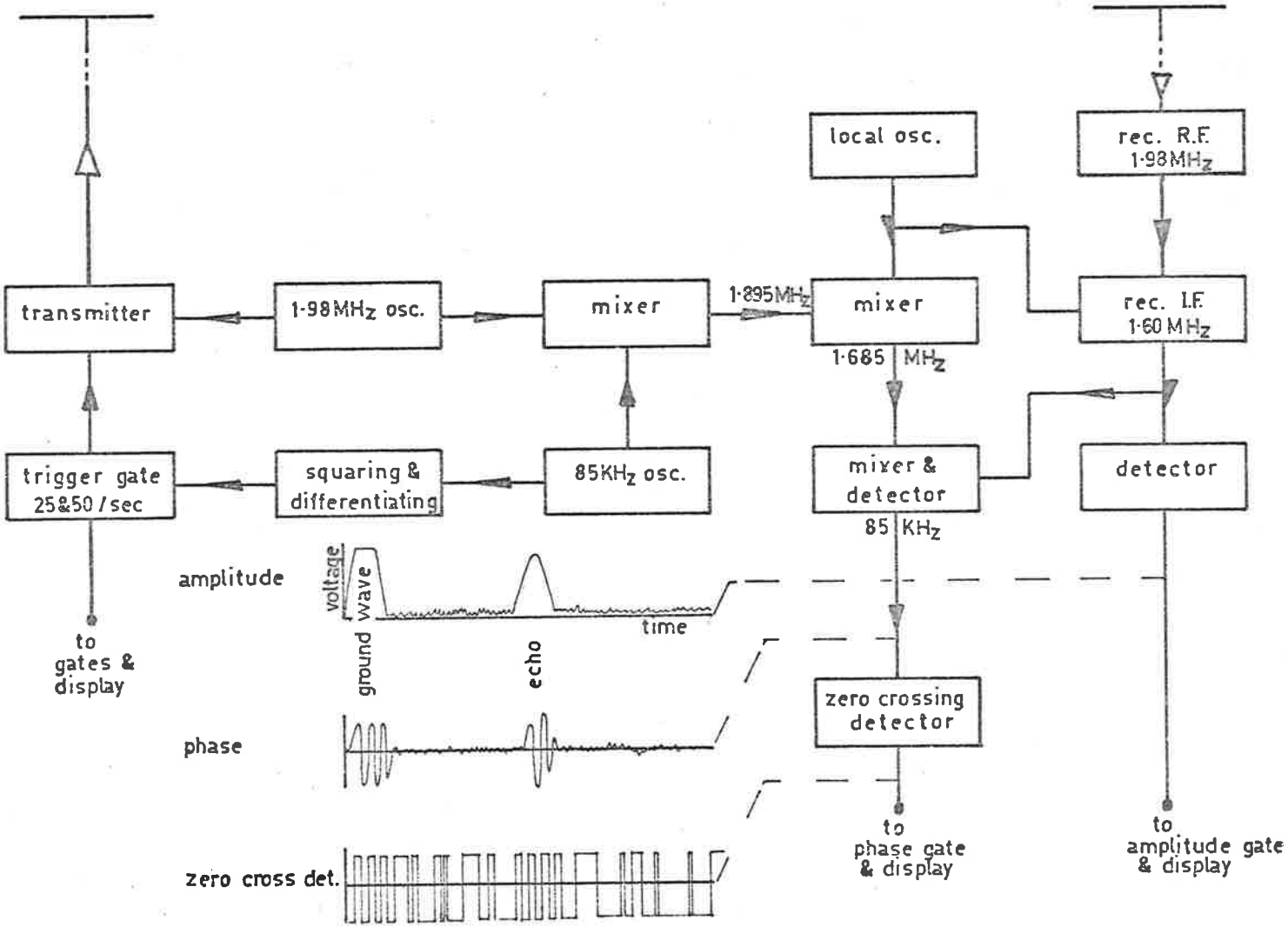

Figure 3.4 Block diagram of the transmitter and receiver showing the system used to obtain a phase-locked pulse.

isolated output of the receiver's intermediate frequency is all that is needed.

Changes in receiver gain can often result in changes in the phase shift produced by the receiver. To avoid this the receiver gain was held constant and the beat signal was amplified and clipped in a zero crossing detector. This had the result of making all echoes equal in amplitude, although it did not alter the phase of any echo. While noise will also have the same amplitude as that of the echo, it will be phase incoherent, so the beat pattern will vary randomly where only noise exists. The signal-to-noise ratio is, in fact, improved because the reference signal is phase coherent with all of the components of the frequency spectrum of the wanted echo, but not with the noise (McNicol and Thomas, 1960).

3.3(c) Records

A record of the range variation of the beat pattern with time, for a fairly wide range, was obtained by modulating the brightness of an oscilloscope with the clipped beat signal. The beam was deflected vertically by an amount proportional to the echo range and this was recorded on a film moved horizontally to provide a time axis. Thus an echo that did not change in range mapped out three horizontal lines on the film. Examples of this kind of record are given in Figure 3.3(b).

Direct records of the phase variation in a particular echo were obtained by centring a range gate within the echo, triggered by the

amplitude gate and with a duration equal to the period of one cycle of the beat frequency (δf). A pulse was generated with a width equal to the time delay between the leading edge of the gate and a negative going edge of the clipped beat signal. This pulse was integrated by using its width to determine the charging time of a capacitor that was discharged just before each pulse. A receding echo caused the phase pulse width to decrease steadily to zero and then jump back to its maximum width as each cycle of the beat signal moved through the gate. The voltage from the pulse width integrator thus appeared as a sawtooth with each ramp representing a change in the echo's phase of 2π radians. This is a change in phase path of 75 m at a frequency of 1.98 MHz. The echo phase was thus recorded together with the echo's amplitude, on a chart recorder.

3.4 Aerial Switching

Echoes returned at some angle to the vertical arrive at two spaced aerials with different phases. By measuring the phase difference between three aerials the echo's elevation and azimuth can be determined. If three receivers are used for this purpose, any difference in the phase shifts produced by the receivers in their function of amplifying the signal must be allowed for. This difficulty can be overcome by using only one receiver and chopping both the input and output in sequence between three aerials and three phase-measuring circuits. The signal from the aerial was fed through an emitter-follower. By reverse biasing the transistor's emitter the aerial signal was attenuated by up to 100 db.

The phase output, in the form of the variable width pulse generated by gating the echo, was switched in sequence between three pulse-width integrators. Each retained its voltage for three trigger pulses before being updated by the phase pulse produced by the phase signal from the corresponding aerial. The phase difference between the aerials was then formed by feeding the two phase signals into a difference amplifier. The output from this amplifier was then proportional to the phase difference. The phase comparison was made between consecutive transmitter pulses and not simultaneous pulses. Where the echo's phase is varying continuously with time the difference output has a chopped appearance (Figure 3.7) which can easily be corrected for.

3.5 Recording Sequence

3.5(a) Scanning Gate

The meteor echo's range was recorded on the film display, and the echo amplitude and phase were recorded on the chart recorder by gating out the echo. Once an echo appeared, the gate had to be set at the echo's range. As the echo typically lasted for from one to ten seconds, some automatic means of scanning the gate through the range of interest was required. This was done by moving a gate 2 km wide in 2 km steps through a predetermined range interval. The range steps were triggered by the transmitter trigger so that the scanned range was completely sampled by each scan. The range scanned was normally 80 km so 40 pulses were required to step the gate through this range. With a pulse rate of 25 pulses/sec a scan took 1.6 seconds (see Figure 3.5 for a block diagram of the complete system).

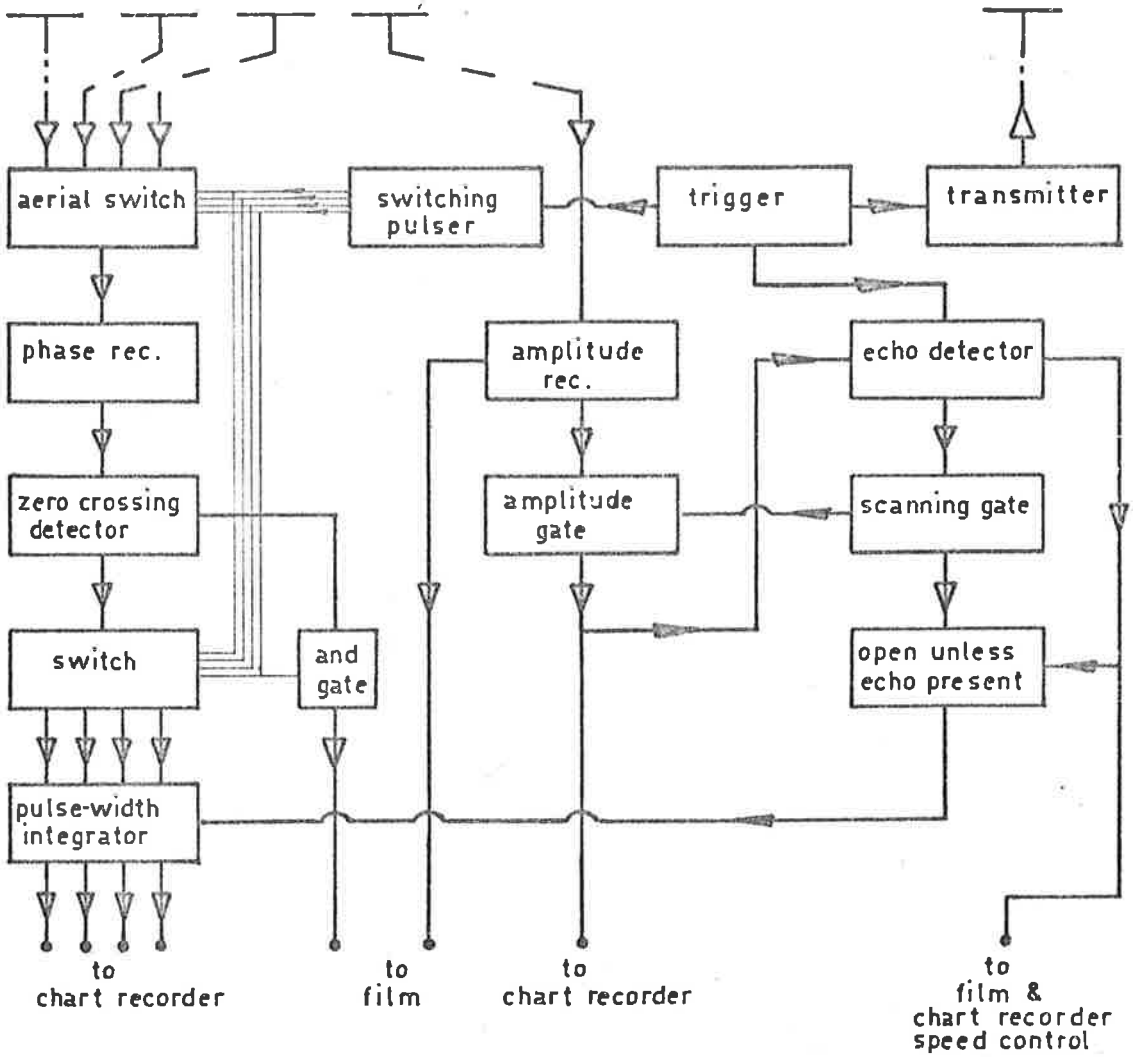

Figure 3.5 The arrangement used to detect and record the meteor echo.

3.5(b) Echo Detection

Whenever an echo appeared within the gate the signal level derived from the gate would rise. If this rise was above a predetermined level (x) it triggered a monostable which controlled the recording sequence (see Figure 3.6). When this monostable was in its triggered state no transmitter triggers were allowed to reach the scanning gate which thus stayed at the range of the echo. The monostable also increased the speed of the chart recorder from 0.1 mm/sec to 2.5 mm/sec. The duration of the monostable was set between 4 sec and 10 sec. After this time it reverted to its original state, allowing the scanning gate to continue scanning and the chart recorder to run at its reduced speed. The monostable could be triggered by noise pulses in the gate and by very short lived echoes. To prevent a needless waste of chart the monostable was reset when the signal level fell below a predetermined level (y). Thus the triggering level could be set just high enough to avoid small persistent ionospheric echoes and the resetting level set sufficiently low to prevent losing the echo when its amplitude varied through fading. While the gate was scanning, the phase signal fluctuated wildly in a manner which could eventually damage the pens. To avoid this, the gate was only fed to the phase receiver when the monostable was in a triggered state. This had the added advantage of making the phase output between records equal zero, so the chart record was continuously calibrated and records were easily separated. Identifying the echoes on the time-range film that triggered the monostable was made possible by

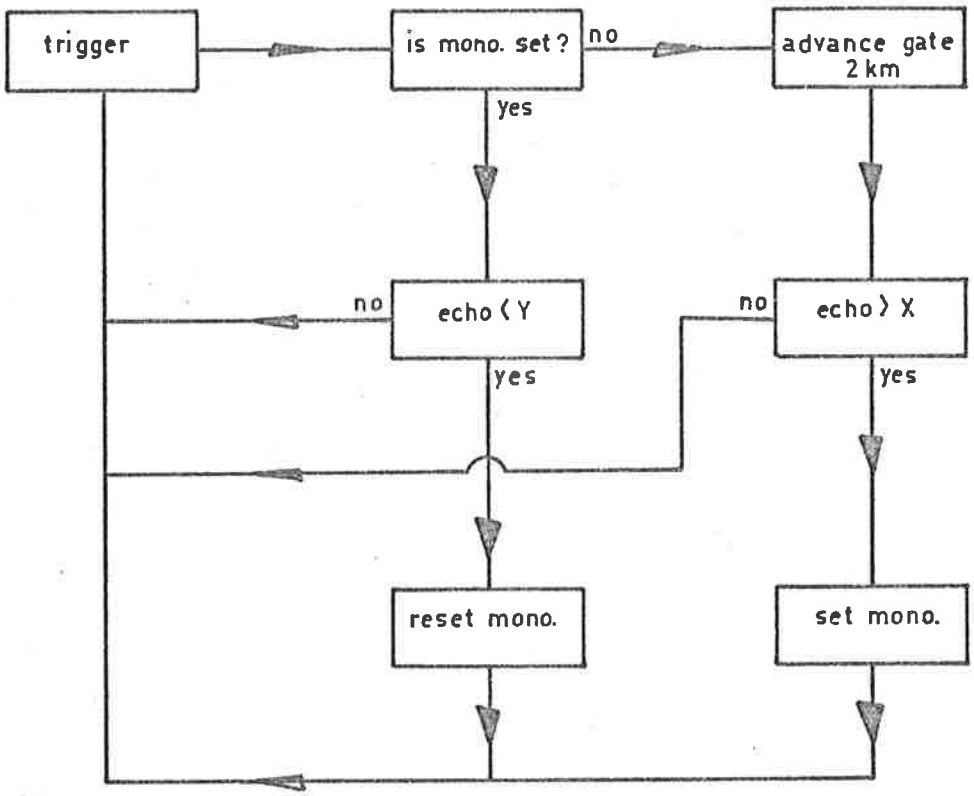

Figure 3.6 Showing how a monostable multivibrator was used to stop the scanning gate from scanning when an echo occurred within the gate at a signal level greater than x.

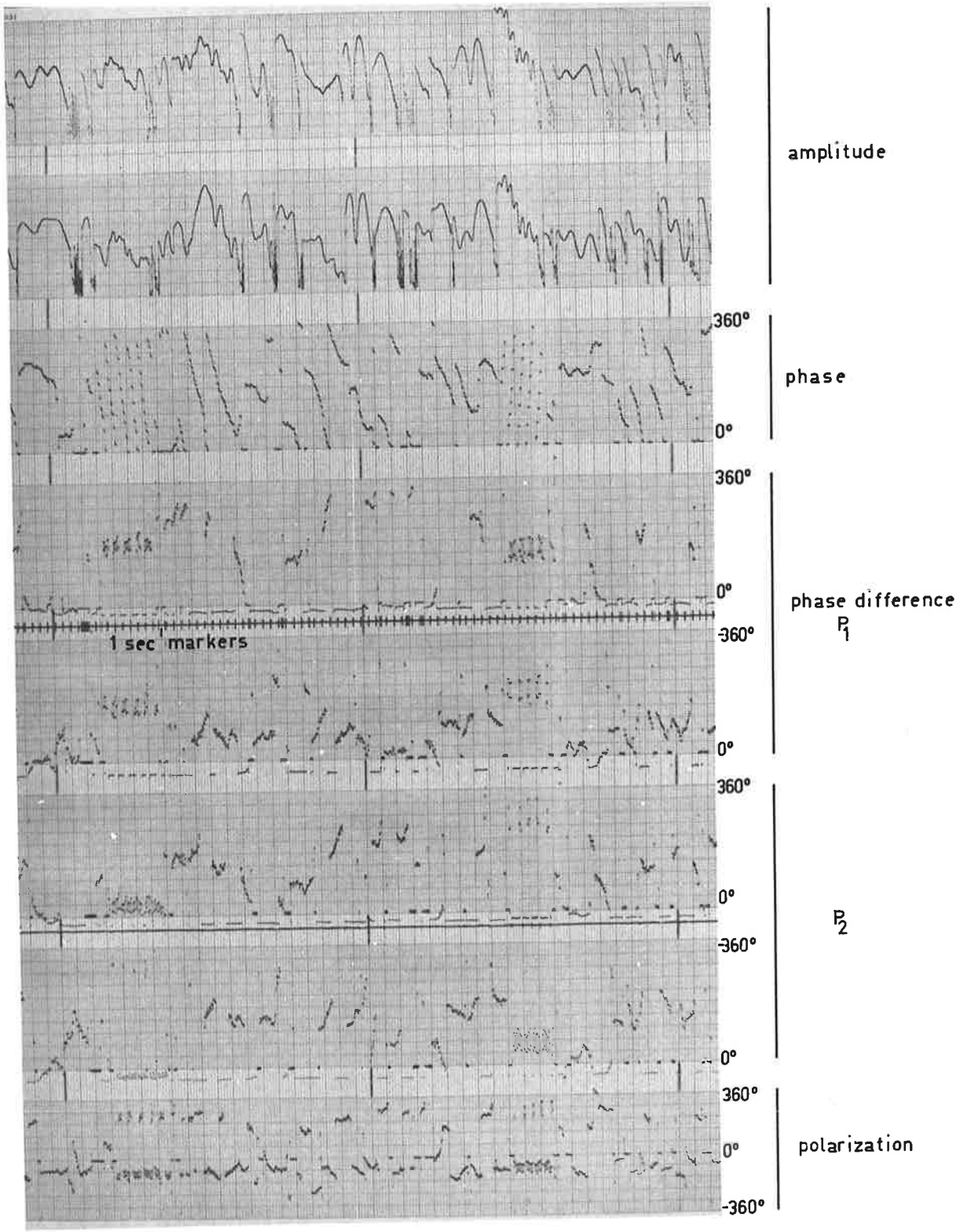

Figure 3.7 Chart record.

brightening the oscilloscope at the range of the scanning gate whenever the monostable was in a triggered state. The gate is easily seen superimposed on the phase record as shown in Figure 3.3.

3.6 Aerial Beams and Records

Determining echo directions with three aerials, as suggested, was not in fact the method employed in this experiment. The night time noise level was generally too great to obtain reasonable signal-to-noise ratios from one dipole. Instead, eleven dipoles arranged in a row were added together in phase. The directional response of this broadside arrangement perpendicular to the row, was the same as a single dipole. However, the response parallel to the row was that of a beam $\pm 4^{o}$ wide at the half power points. Thus a row of aerials lined up in a north-south direction received signals from all angles of elevation within 4^{o} of the east-west azimuth. This response can be described as a fan response and is shown in Figure 3.8. A density plot is shown in Figure 7.1. The narrow beam produced by the row of aerials defined the echo's azimuth, while the elevation of the echo was determined by measuring the difference in the echo's phase from two adjacent rows. To improve the accuracy of this measurement, the phase from three rows was in fact measured. These three rows were treated as two pairs .61 wavelengths and 1.22 wavelengths apart. For most of the echoes observed a fourth phase difference between two rows of crossed dipoles was recorded. This, together with the recorded amplitude of the signals from a second row of crossed dipoles, made it possible to deduce the echo polarization.

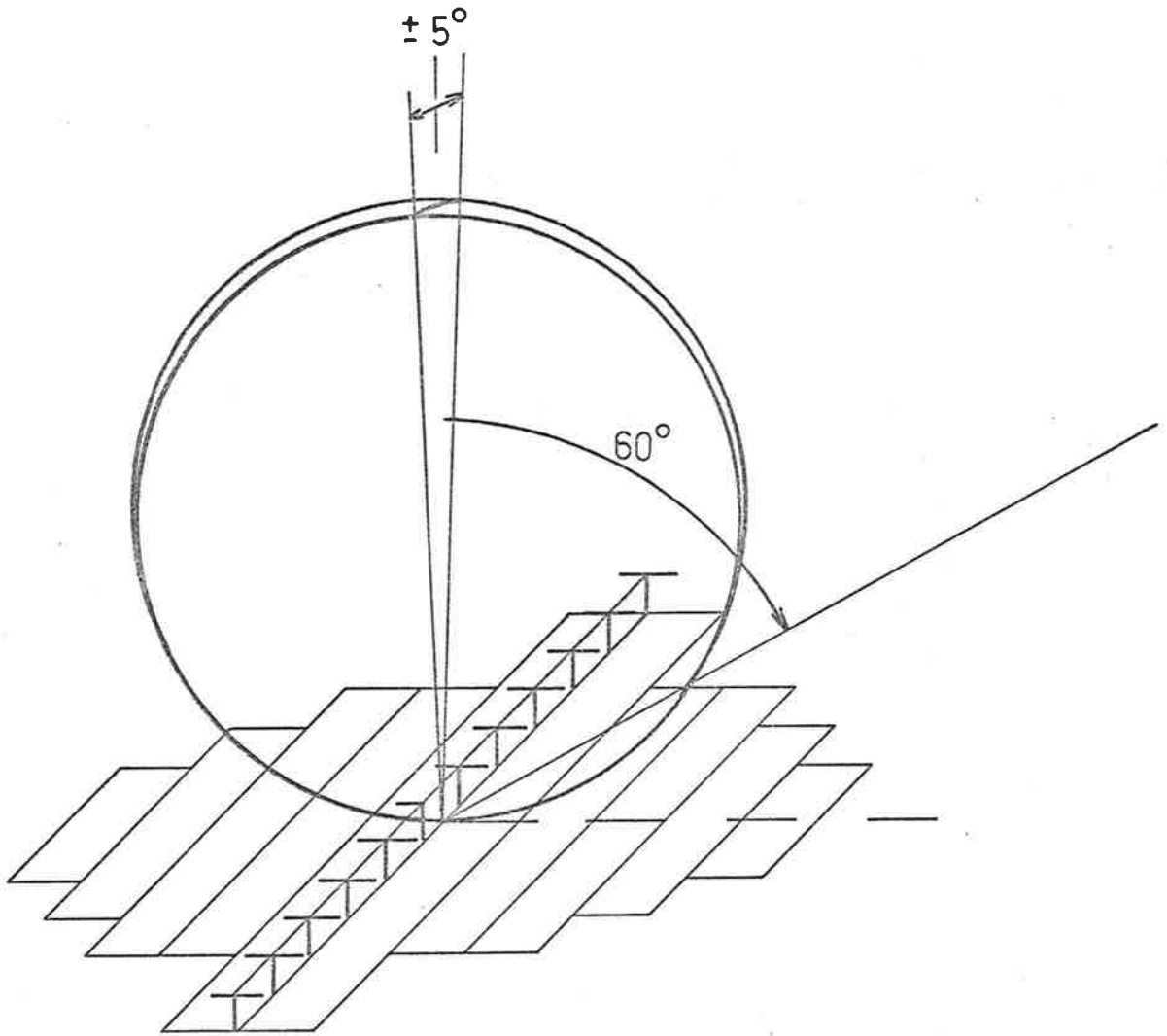

Figure 3.8 Amplitude response of one row of the Buckland Park array. Half amplitude points are given in degrees.

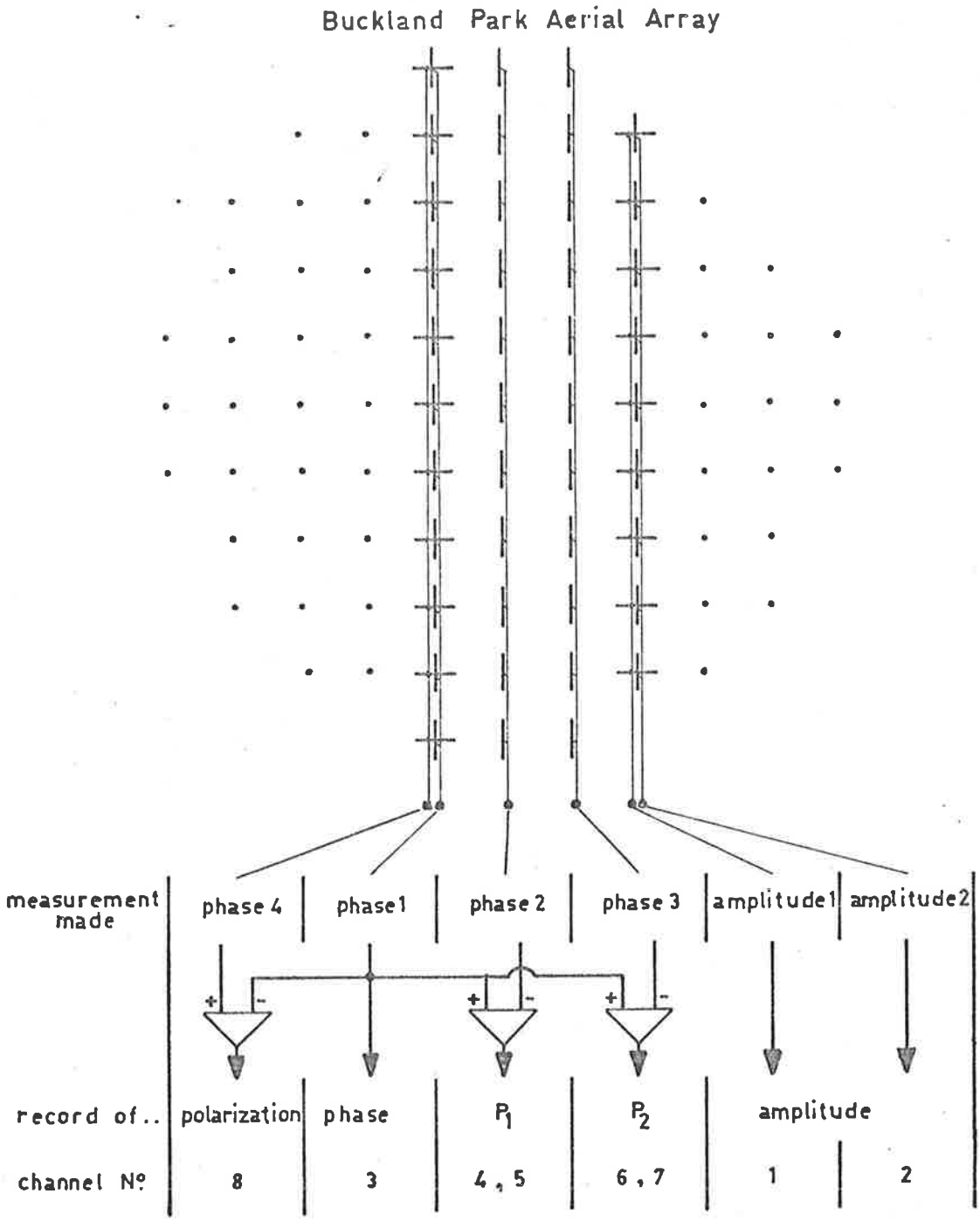

Figure 3.9 The aerials used and the records recorded on the 8-channel chart recorder.

Figure 3.9 shows the aerials used and the measurements made from them. The phase difference measurements P_1 and P_2 were each recorded separately on two channels so that a phase difference of + 360° represented full-scale on the first channel and - 360° was full-scale on the second channel. A sample of chart record is presented in Figure 3.7. Most of the records were made with a Sanborn hot wire recorder. The pen deflections were accurate to 0.5 mm and could respond to frequencies up to 150 Hz. The pen heats were automatically controlled by the chart speed, which in turn could be controlled remotely through electromagnetic clutches.

3.7 Echo Rise Time Records

Towards the end of the observational period, a second oscilloscope and camera were set up to record the rise time of the meteor echoes. The oscilloscope's beam was deflected vertically by an amount proportional to the received signal from one of the aerial beams described above. The echo range of interest was selected by only brightening the beam while a signal was being received from this range. The maximum signal strength within the selected range was thus recorded on a film which moved at a rate sufficient to separate the records obtained after each transmitted pulse. A typical record of an echo is shown in Figure 4.19.

CHAPTER 4

RADIO ECHOES AT 2 MHz

4.1 Introduction

The experimental arrangement and the records made have been discussed in Chapter 3. In this chapter it will be shown how these records were reduced and checked for inconsistencies and errors. Two fan shaped aerial beams were used, one sensitive to echoes to the north and south of the receiving array, the other sensitive to echoes east and west of the array.

The echoes observed fell into two categories; those from layers of ionization such as sporadic-E; and reflections from meteor trails and ionospheric irregularities. During the summer months the sporadic-E layers often persisted throughout the night, with a critical frequency above 2 MHz. At such times very few off-axis echoes were observed. During the winter the sporadic-E ionization was often transparent to the ordinary ray, although the extraordinary ray was nearly always partially reflected by a weak, but persistent layer of ionization at about 100 km. While these conditions lasted, the ordinary ray suffered very little absorption and multiple F-region reflections could be observed above the noise level for about 30 msec after the transmitter pulse. This limited the pulse repetition rate to 25/sec. The night-time noise level was particularly high from about 2200 - 0300 hours, local time, when the noise power received from a row of dipoles, was about 30×10^{-12} watts,

with frequent bursts or impulses considerably above this level. From 0300 hours onwards this level decreased and the impulsive noise became much less frequent. The helion and antihelion sporadic meteor radiants can be observed over this period and the rate of sporadic meteor echoes reaches its peak near 0600 hours. For these reasons most echoes were recorded between 0300 - 0700 hours, the formation of the E region with sunrise preventing observations beyond about 0700 hours.

During periods when the sporadic-E was at a low level of ionization the transmitter was phased to transmit the ordinary ray. This reduced the reflections from the sporadic layer to a low level. The two aerial elements phased to produce the ordinary ray have different off-vertical gains so that the radiation becomes increasingly elliptical as the angle from the zenith increases. The elliptically polarized radio wave can be viewed as a linear addition of two circularly polarized waves with opposite rotations. In Figure 4.1 the normalized amplitudes of ordinary and extraordinary polarization transmitted is shown for a range of zenith angles. It can be seen that the extraordinary polarization is less than 35% of the ordinary polarization, for zenith angles less than 45^{o}.

Echoes that rose suddenly to a level close to their maximum and then decayed slowly were considered to come from meteor trails which formed to give a specular reflection, the rise time of the echo being determined by the time taken for the meteor to cross the principal Fresnel zone . Many echoes did not show a rapid rise and thus were

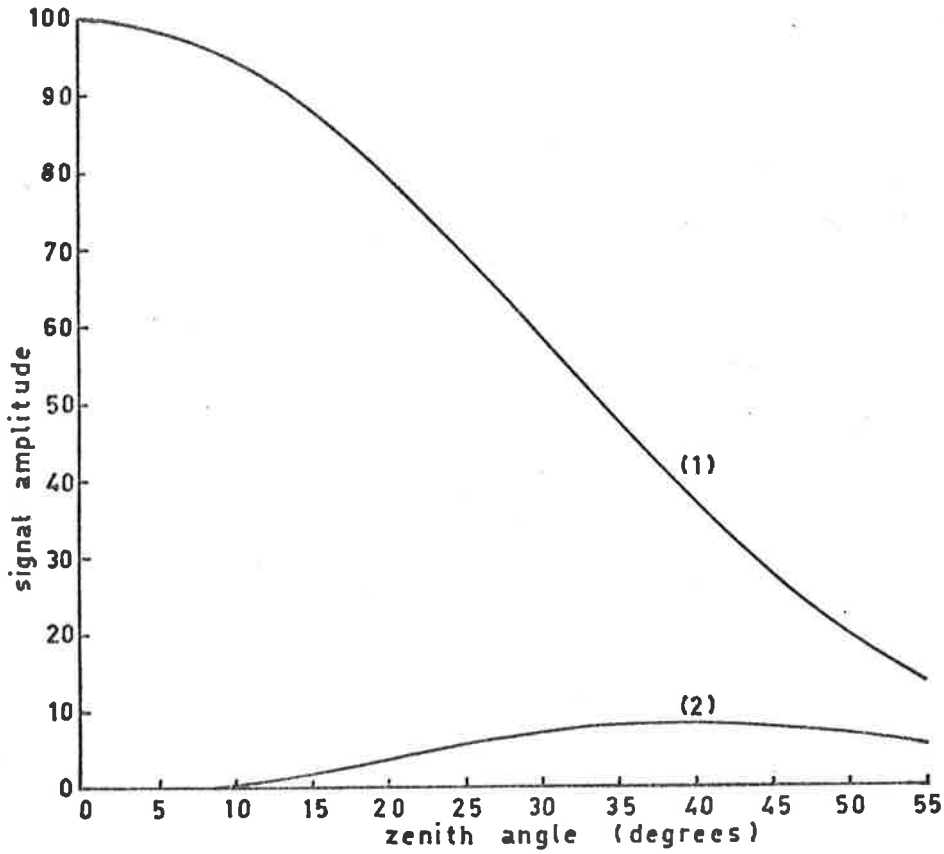

Figure 4.1 The normalized amplitudes of ordinary (1) and extraordinary (2) polarization transmitted out to a zenith angle of 55 degrees.

assumed to be either from old trails that had been sufficiently distorted by the wind to form a specular reflection some time after the trail's formation, or from ionospheric irregularities. A flare, or region of increased ionization at some point on a trail, will reflect a signal for some time after the rest of the trail has become too diffuse to produce a signal. Where the electron line density in the flare is above a critical level so that it is overdense, the signal from the flare region will increase in amplitude as the ionization diffuses into a larger echoing area. Flares can therefore produce echoes with a slow rise time.

All echoes that produced a phase record free of obvious interference effects were digitized and then analysed with the aid of a computer program. Three echo classes were recognised: rapid rising echoes, slow rising echoes, and those echoes that were not clearly in the first or the second class. The film record of the echo's range, shown in Figure 3.3, was used to determine the echo's class as this record was continuous throughout the recording period. Height and angular distributions were produced for the first two classes. However, the three classes were combined in determining the component of the neutral wind towards or away from the receiving station.

4.2 Analysis of Echoes

It has been shown in Chapter 3 how the records of range, phase difference and phase were obtained. The phase differences between two

adjacent rows .61 wavelengths apart (P_1) and between two rows 1.22 wavelengths apart (P_2) were recorded between the limits + 360° to - 360°. For a plane wave, the phase difference varies linearly over the ground such that $-220 < P_1 < 220$ and

$$P_2 = 2\,P_1.$$

However as P_2 is only recorded between the above limits this becomes

$$P_2 + n\,360^\circ = 2\,P_1 \qquad 4.1$$

where $n = -1$ for $-220 < P_1 < -180$;

$n = 0$ for $-180 < P_1 < 180$;

$n = 1$ for $180 < P_1 < 220$.

Thus a corrected value for P_2 can be formed such that

$$PC = P_2 + n\,360 \qquad 4.2$$

for n defined in Equation 4.1. The effects of noise will generally mean that PC only approximately equals $2P_1$. The height of the echo was calculated using the phase difference P which was a weighted mean of P_1 and PC defined by

$$P = \left(\frac{P_1}{X_1} + \frac{PC}{X_2}\right)\left(\frac{X_1 X_2}{2X_1 + X_2}\right) \qquad 4.3$$

where X_1 and X_2 are estimates of the error in the reading of P_1 and P_2 from the chart. These were assessed from the spread of the phase differences which were recorded for an average five second interval. P is related to the zenith angle z of the echo by the relation

$$z = \text{arc sin}\left(\frac{(P/360)}{0.61}\right) \qquad 4.4$$

for two aerials .61 wavelengths apart where the azimuth of the echo is

defined by a line connecting the two aerials. In this experiment each aerial was a row of dipoles connected in phase so that the main response was perpendicular to the row. Thus all echoes in the aerial beam fulfilled the above condition. Equation 4.4 is shown graphically in Figure 4.2, where it can be seen that z is ambiguous for all values of P between 140° and 220°. An echo with a phase difference P of 140° can have a zenith angle of 40° or -90°. In this case -90° can be discarded as a possible zenith angle. Figure 4.3(a) shows the region in the atmosphere where echoes between the heights 70 and 130 km can be interpreted unambiguously. This region transformed into range-z space is shown in Figure 4.3(b). The unambiguous region can be approximately defined for echoes with $z < 55^{\circ}$ by the condition that

$$R < (340 - 4.P) \qquad 4.5$$

where R is the echo's range. The boundary of this region is shown in Figure 4.3(b) by dashed lines. This condition was imposed on all analysed echoes included in the results presented in this and later chapters. The height of an echo satisfying Equation 4.5 could be found using the relation

$$H = R \cos z. \qquad 4.6$$

At the same time a height error EHT could be found, defined by

$$EHT = R \cos z_1 - R \cos (zc/2) \qquad 4.7$$

where z_1 and zc are the zenith angles for the aerial phase differences P_1 and PC (obtained from Equation 4.4).

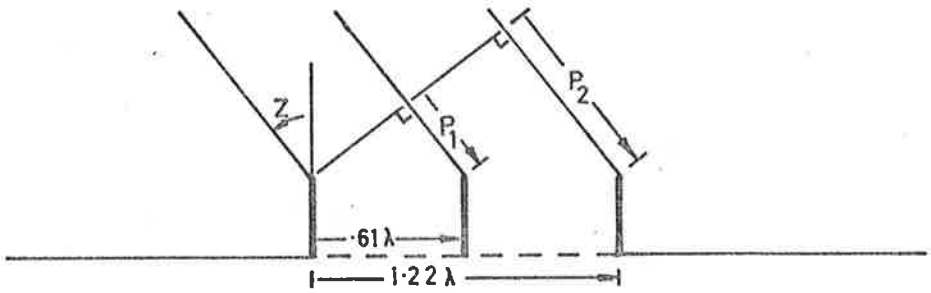

(a)

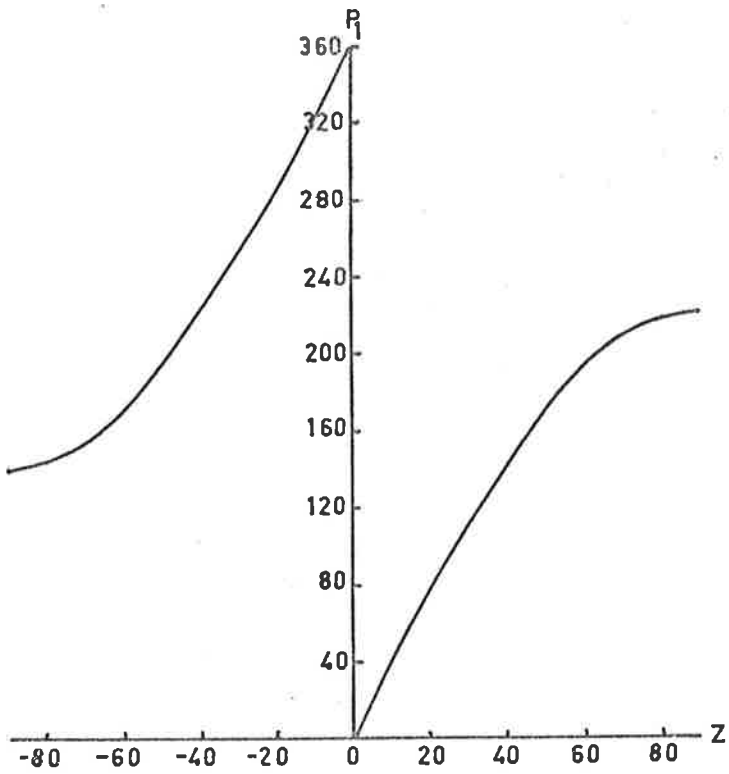

(b)

Figure 4.2 (a) The three aerials used for direction-finding. (b) The relation between zenith angle (Z) and phase difference (P_1).

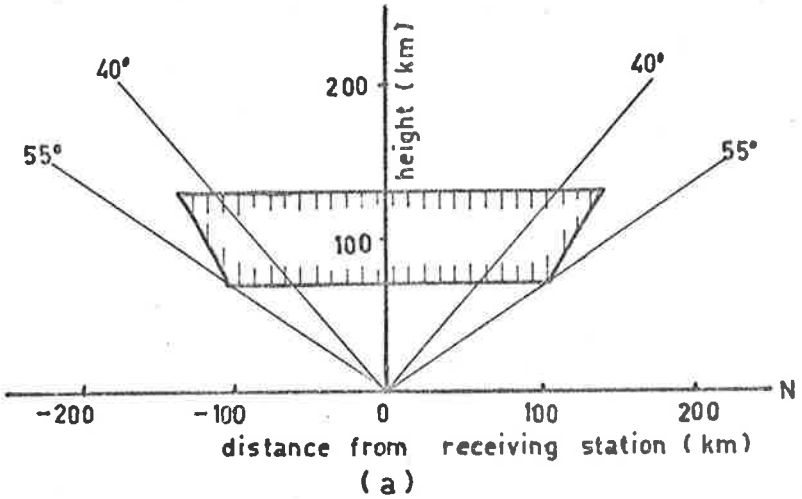

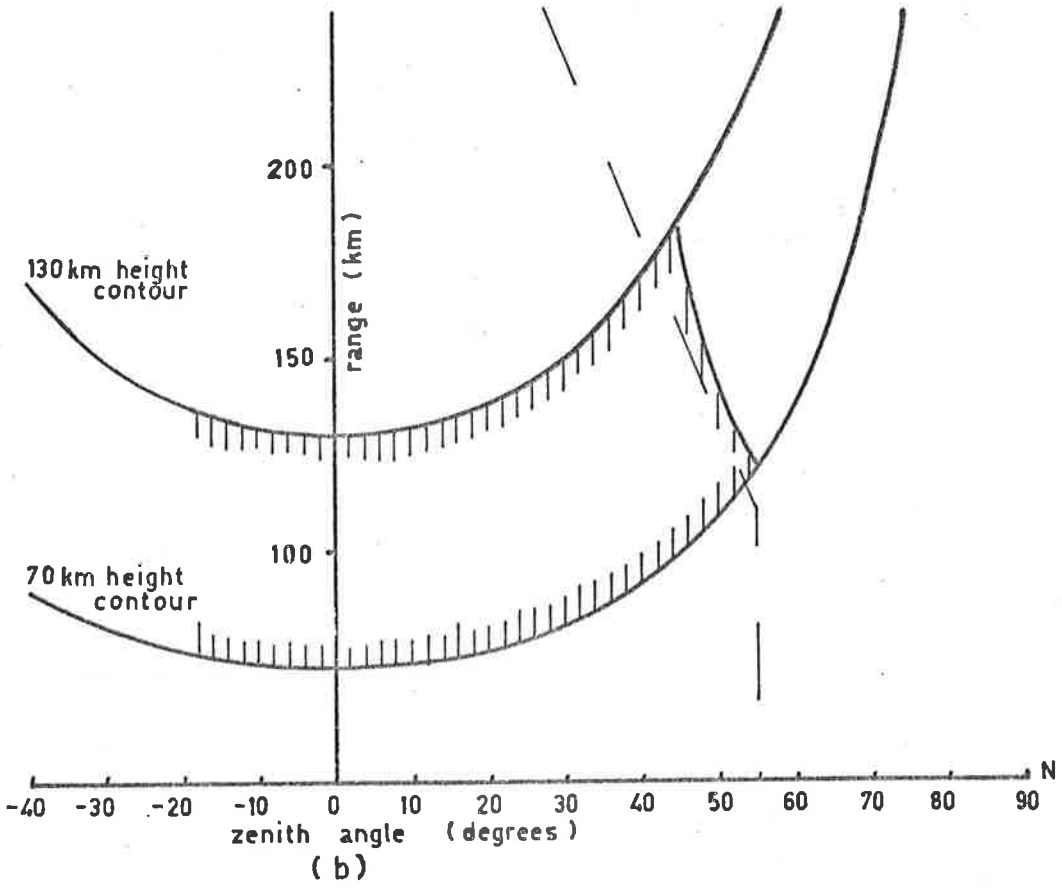

Figure 4.3 The region of the sky where echoes could be observed unambiguously in the axis of the north beam is shown in (a), and this region is transformed to ranges and zenith angles in (b).

4.3 Periods of Observation - Rates

Two factors dictated the periods when meteor echoes were observed. The major one was the level of ionization present between 80 - 160 km. During the daytime the D and E region ionizations make any observation of meteor echoes very unlikely. Sporadic E ionization can exist throughout the night, making observations equally improbable. However, during the winter and spring months the ionization in the sporadic-E layer often fell to a level sufficiently low for meteor echoes to be detected. The second restriction on observations was the level of radio noise present. This varied considerably, as it was determined to a large extent by the thunderstorm activity and by signals reflected from the F-region.

The general level of interference was worst around midnight and improved towards sunrise. The noise level from a row of nine dipoles connected in phase is shown in Figure 4.4 for a night which was free of sporadic ionization.

Most observations were made after 0300 hours as this combined the lower noise levels with the higher rate of sporadic meteors. A diagram showing the days and hours when meteor echoes were recorded is shown in Figure 4.6. Summer time sporadic-E persisted throughout the first three months of the year preventing any recording. A delay occurred during May when the transmitter had to be modified to reduce the bandwidth of the transmitted pulse. The most successful periods occurred during

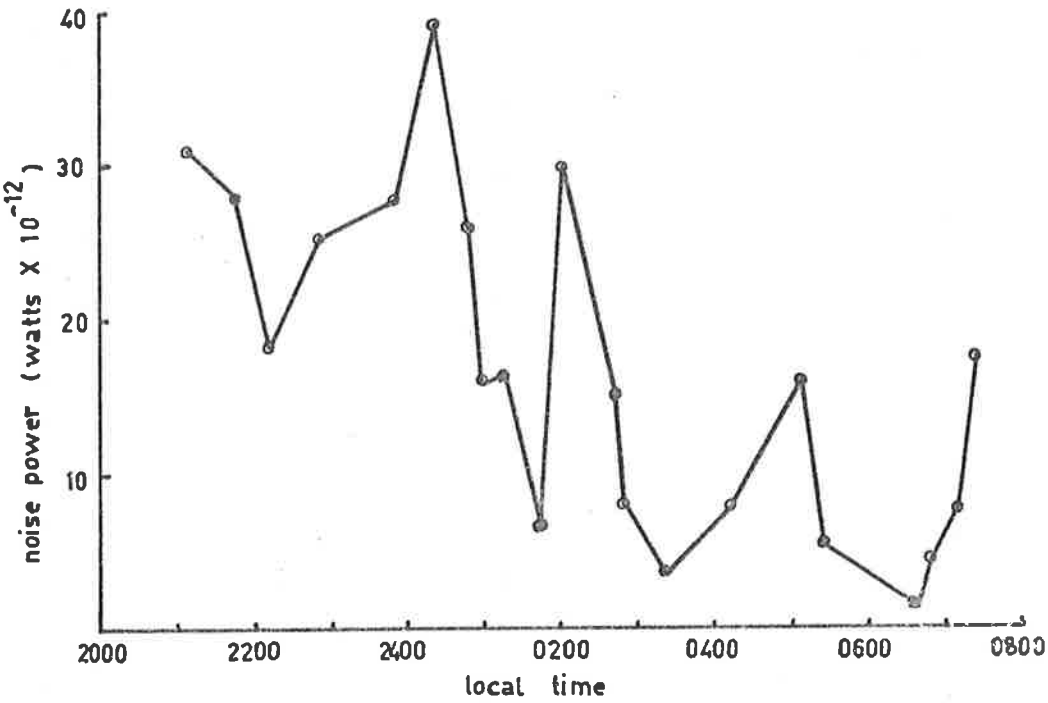

Figure 4.4 The noise power from nine dipoles added in phase from observations made on 21-22/7/71.

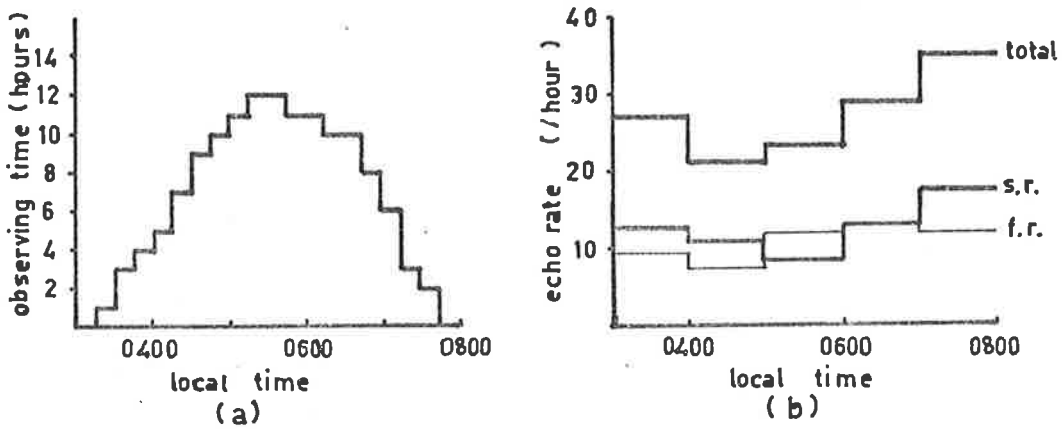

Figure 4.5 (a) Total number of echoes observed in 15 minute intervals. (b) Hourly echo rate for fast-rising (f.r.) and slow-rising (s.r.) echoes.

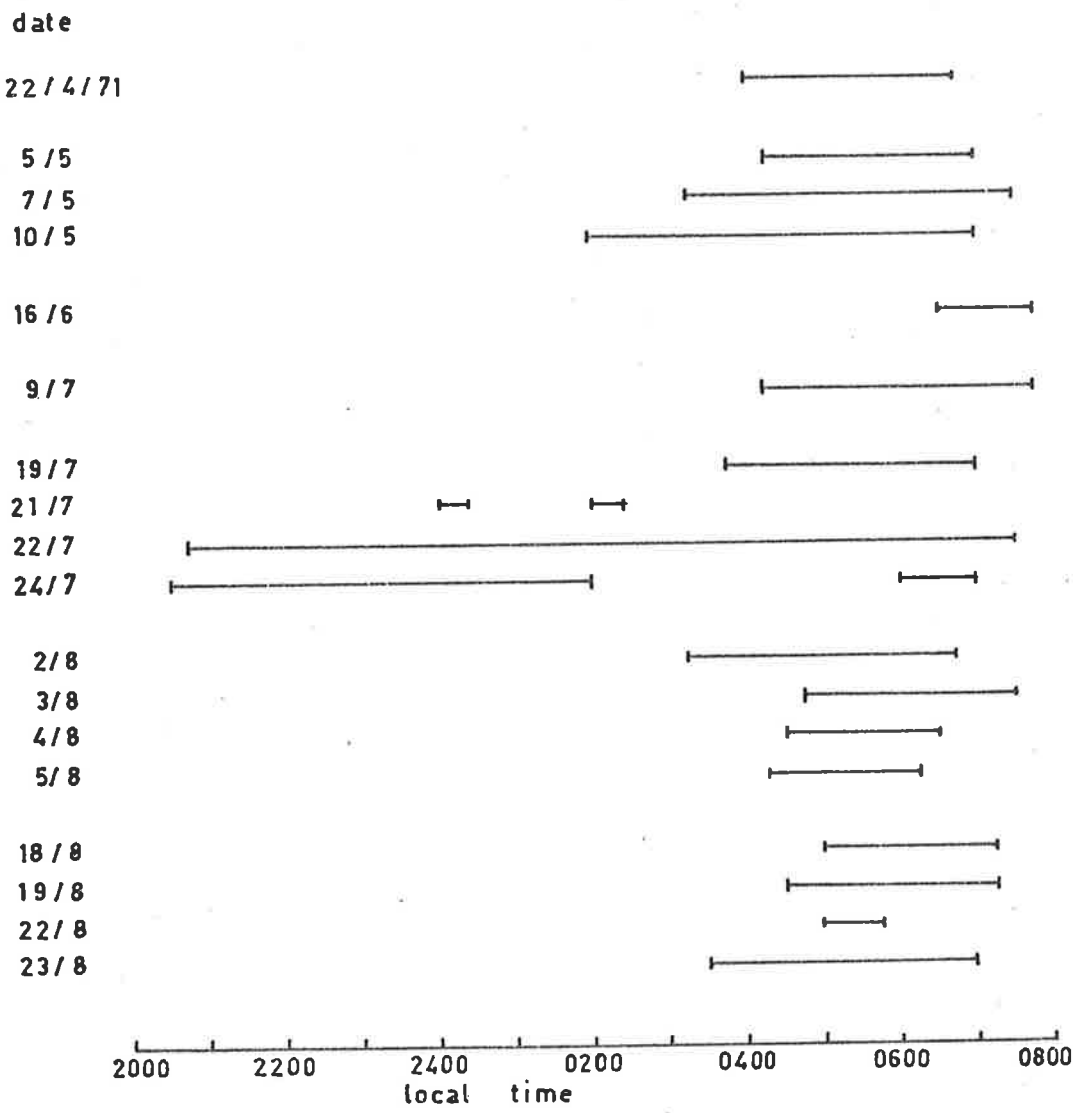

Figure 4.6 Periods when meteor echoes were observed. The date given is that of the following day in cases where observations were made before 0000 hours.

August and September when the general level of sporadic-E ionization was low. The number of hours of observations of meteor echoes is plotted against time in Figure 4.5(a). By determining the total number of echoes successfully analysed each hour between 0300 and 0700 hours, an average rate of echoes in the two categories was determined and is shown along with the rates for all echoes in Figure 4.5(b). It can be seen that, of the meteor echoes recorded, the average number to be successfully analysed was 10/hour. In fact, an average meteor rate of 40/hour was observed between the ranges 80 and 190 km on mornings when there was a relatively low amount of ionization between these ranges. On a number of occasions this rose to about 60/hour just before sunrise. The presence of a weak layer of sporadic-E could reduce this rate to about 10/hour.

All periods of recording had to be carefully supervised by the author. Although the equipment automatically detected echoes within a fixed range, it could not distinguish persistent echoes from new ones. The maximum time spent on recording an echo's phase and amplitude was normally set at seven seconds. While many echoes decayed during this time to a level below the detection level, strong persistent echoes were repeatedly detected as new echoes and this could cause a large wastage of 8-channel chart. This was overcome by changing the searched range until the echo had decayed away. The detector could also be over-ridden. Much of the recording was timed to coincide with the operation of the 27 MHz meteor wind patrol, operated for a week in each month. Recording

was also attempted during major meteor showers.

4.4 Height Distribution

The distribution of 295 meteor echoes with height is shown in Figure 4.7(a) for height intervals of 2.5 km. The peak of the distribution is close to 102 km with an r.m.s. spread of approximately 15 km, assuming the profile has a Gaussian form about the mean. In fact the distribution is asymmetric, with fewer echoes below 100 km than would be expected. This is largely due to the method used to record echoes and a possible correction is discussed in Chapter 5.2. The height distribution for 312 slow rising echoes recorded at the same time as the meteor echoes, is given in Figure 4.7(b). This distribution has a peak at about 95 km and is particularly asymmetric with a fairly sharp fall off below the peak. It is well known that persistent meteor echoes have their longest durations at a height near 95 km. Above this, height diffusion reduces the echo duration, while below it attachment and wind turbulence become increasingly important. The mean height error, calculated from the individual values of EHT defined by Equation 4.7, is shown in Figure 4.8 for the two classes of echoes. It can be seen that the mean error is approximately independent of height and less than 2 km, so that the histogram step in height of 2.5 km is justified.

4.5 Angular Distributions

Separate angular distributions for the two classes of echoes are given in Figure 4.9 for the north-south and east-west beams. The

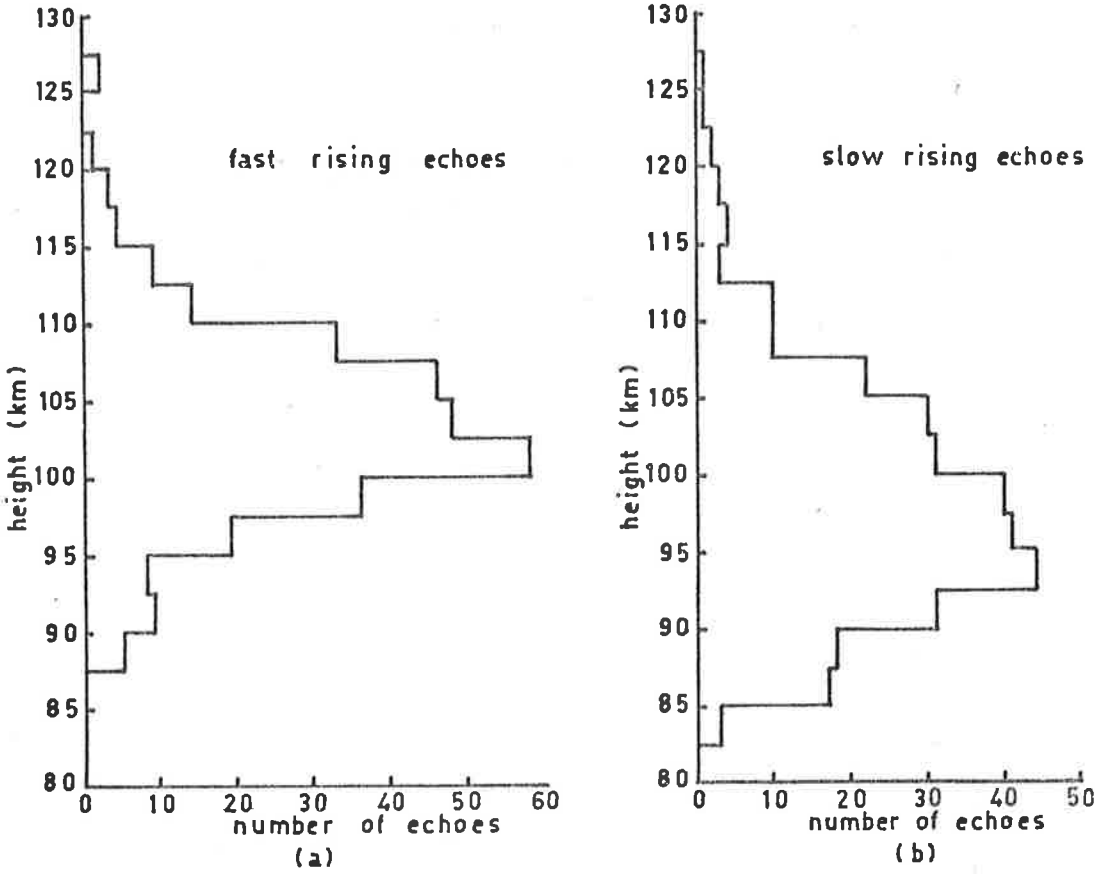

Figure 4.7 Height distribution.

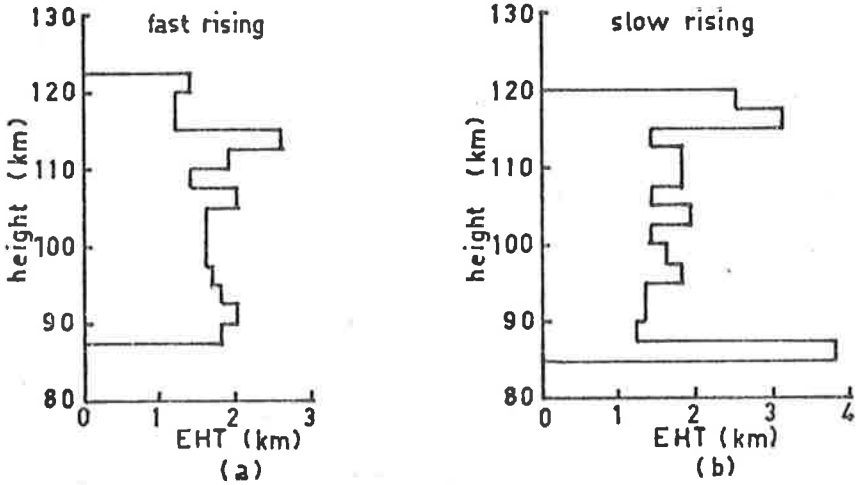

Figure 4.8 Height distributions for the average error in height (EHT).

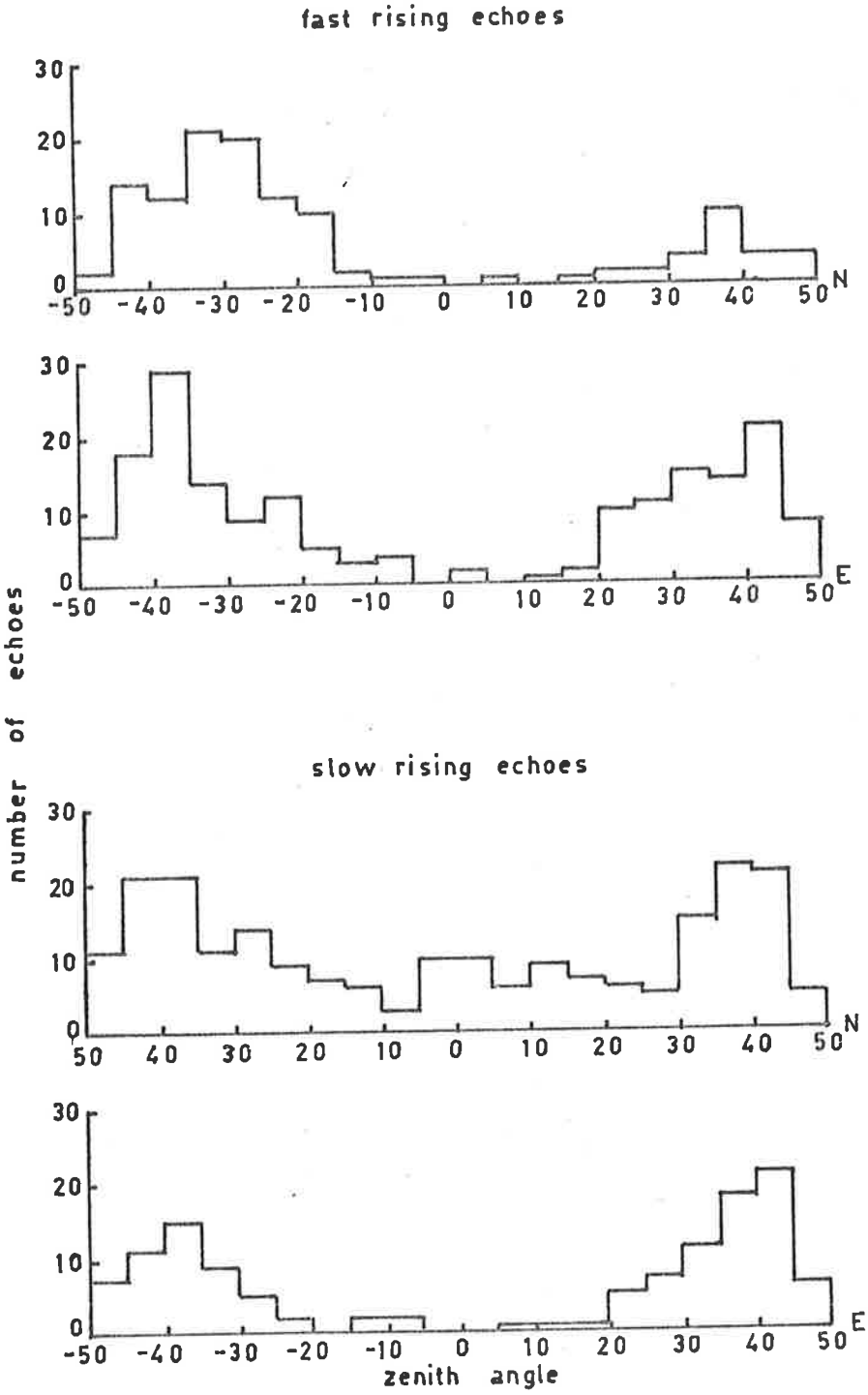

Figure 4.9 Angular distribution of echoes for the north and east beams.

north-south distribution of meteor echoes shows a definite peak at 30°S which will be shown in Chapter 7 to be due to sporadic meteors with radiants close to the apex. The north-south distribution of slow rising echoes does not show any marked trend. Most of the echoes were recorded between 0300 - 0700 hours, with the data being recorded over about four months, so this distribution is an average for this period. Most of the echoes in the east-west angular distribution were recorded over a 21 day period in August. A number of showers were present during this time. The meteor echoes, or specular meteor echoes, show an increase in occurrence as the angle increases. This is in accordance with the predicted angular distribution for echoes from underdense trails (Kaiser, 1953). The fall off in echoes after 40° is brought about by the rejection of ambiguous echoes (discussed in Chapter 4.2).

The overhead echoes present in the north-south angular distributions of slow rising echoes were mostly observed on the 9th, 21st and 22nd of July. The angular distributions of slow rising echoes on these and other days are shown in Figure 4.10. It will be shown in Chapter 6.6 that the wind varied with height in an unusually severe manner on the 9th and 22nd of July so that on these days the trails must have been rapidly bent to yield second reflection points soon after they formed. The data from three days when overhead echoes occurred is collected into one group (group A) and compared with the remaining echoes (group B) in terms of a density plot in Figure 4.11. This shows the number of echoes plotted against height and distance from the

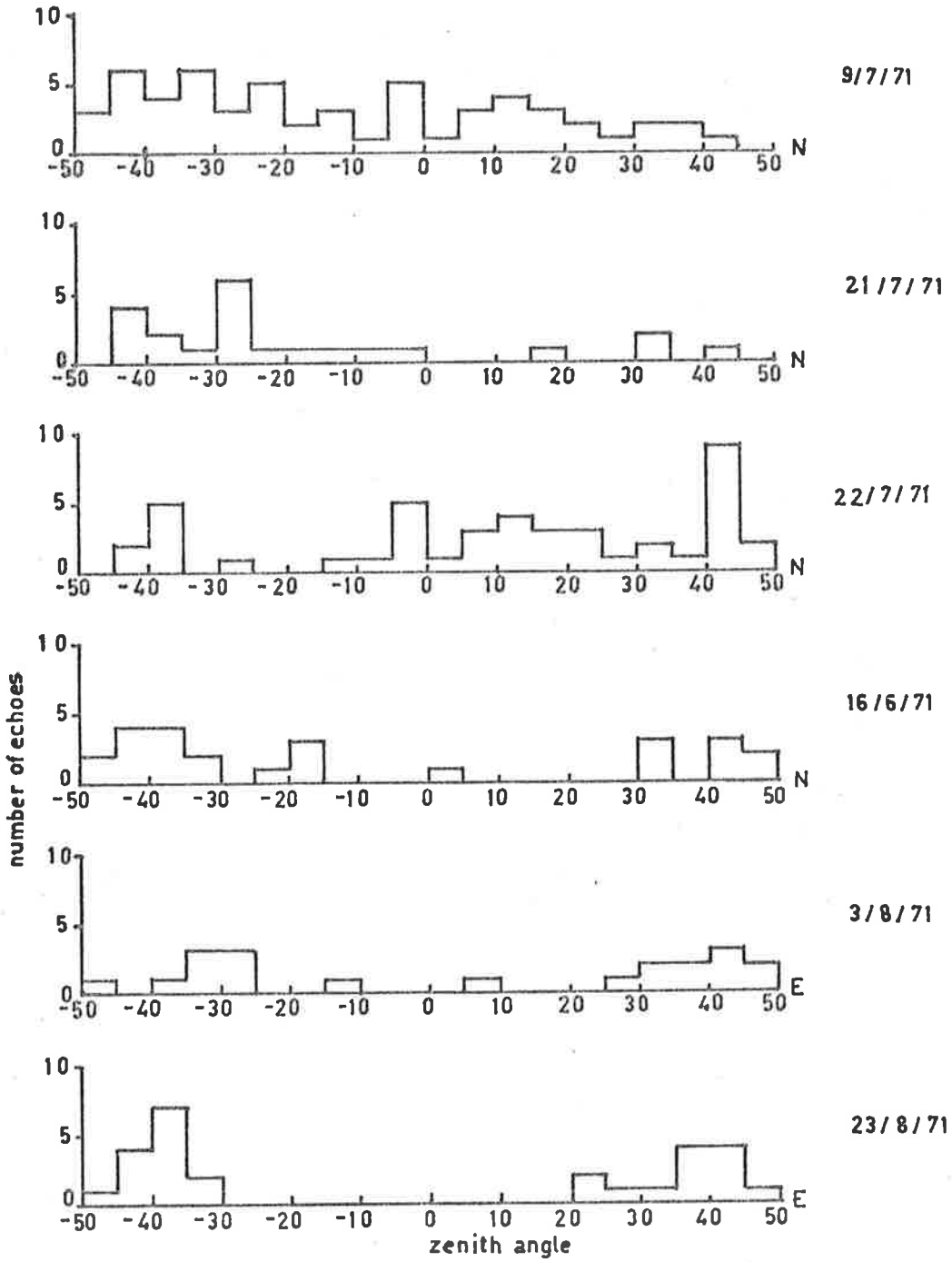

Figure 4.10 Angular distribution of slow-rising echoes for six days.

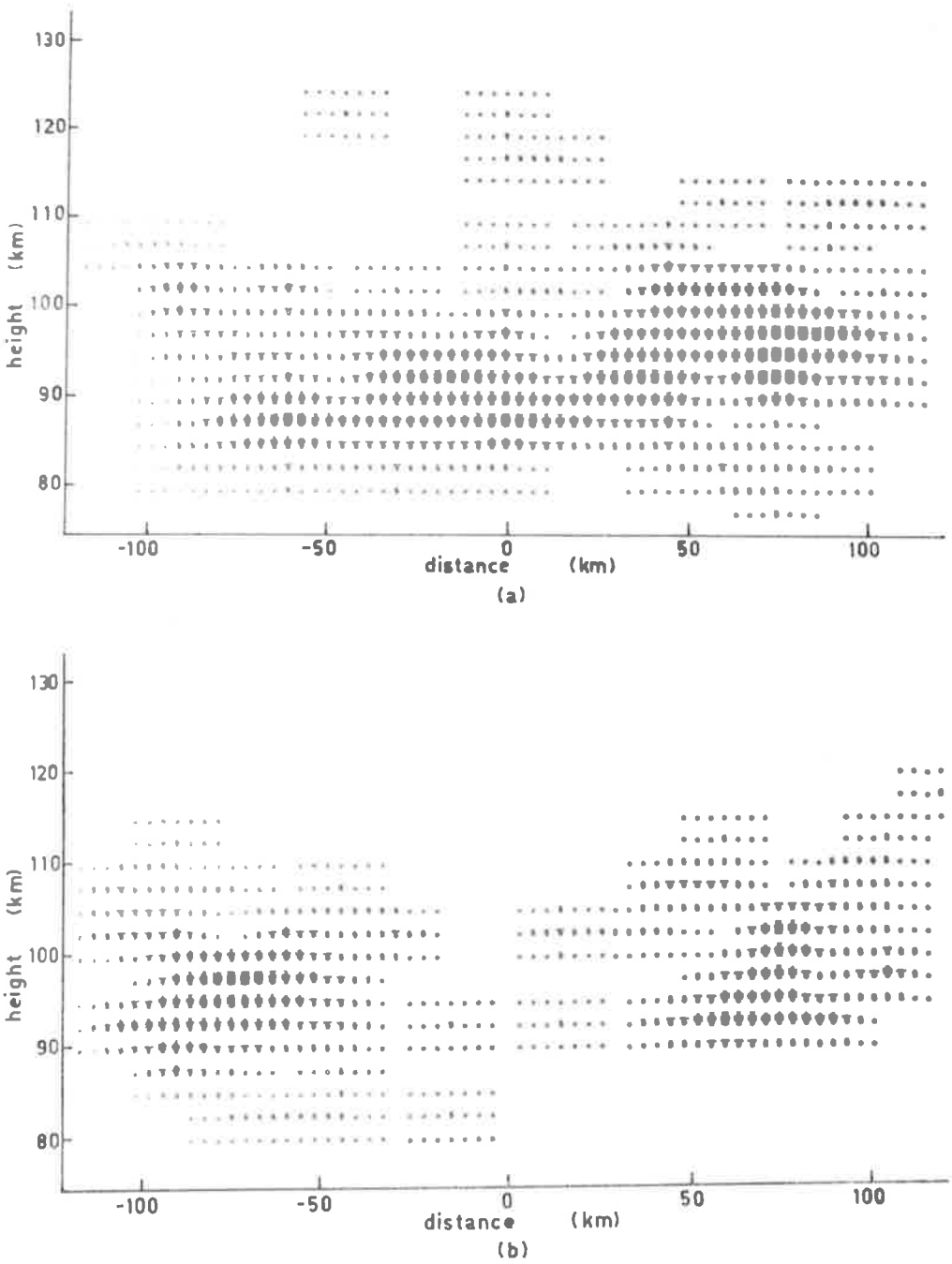

Figure 4·11(a) Group A echoes, and (b) group B.

observing station. It can be seen that the overhead echoes are generally lower than normal, which is consistent with the idea that they come from distorted trails. The large distortions required to give an overhead echo would only occur with the lower, longer lasting echoes. The slow rising echoes of group A made up 65% of the echoes observed over the three days, while slow rising echoes are only 30% of the echoes observed on the remaining days. This is to be expected, as the stronger wind shears were producing a larger number of reflections from trails which do not initially give a specular reflection. It will also be shown that the average echo duration for meteor echoes was shorter for echoes observed on the three days which form group A (Chapter 4.7).

4.6 Ionization Line Density

Two different records of the echo's amplitude are described in Chapter 3, a record of each pulse on a fast moving film and a pen recording of the echo amplitude made as soon as the echo was detected by the scanning gate. The first method gave a complete record of the echo's behaviour, but as it was very costly in film it was only used to obtain some typical echo rise times. The pen recording suffered from the fact that, in most cases, the first 1 to 2 seconds of the echo was not recorded. However, it had the advantage of being available for all echoes that were analysed. The gains of both the receiver and pen recorder were determined by feeding a radio pulse of known amplitude into the receiver's input. The scanning gate then detected this pulse as an echo and recorded its amplitude. This was done at intervals of

about 15 minutes to correct for any drifts in equipment gain.

A formula for the power returned from an underdense trail with an electron line density α, (for $\alpha < 1.0 \times 10^{14}$/m) is given in Chapter 2 (Equation 2.11), where the received power P_R from an aerial of gain G_R is given by

$$P_R = 2.5 \times 10^{-32} P_T G_R G_T \left(\frac{\lambda}{R}\right)^3 \alpha^2 \qquad 4.8$$

where P_T is the power transmitted from an aerial with a gain G_T; R is the echo's range; λ is the radio wavelength; and α is the electron line density. At a frequency of 1.98 MHz Equation 4.8 gives for the electron line density

$$\alpha = 1.1 \times 10^{17} \left[R^3/(G_R \cdot G_T \cdot P_T \cdot \rho)\right]^{\frac{1}{2}} \cdot V \qquad 4.9$$

where ρ is the input resistance of the receiver, and V is the voltage of the received signal. As Equation 4.8 was derived assuming a specular reflection from an underdense trail that has a zero initial radius, these conditions apply to Equation 4.9. Thus the voltage (V) of the received signal should be measured before the trail has time to diffuse or become distorted.

Typical records of the echo amplitude are given in Figure 4.12 where it can be seen that most echoes were affected by interference from secondary reflections. Thus in many cases, only a rough estimate could be made of the initial amplitude because of the delay of about 1 second which occurred between the echo's formation and the start of the record of the echo's amplitude (which started as soon as the echo was detected

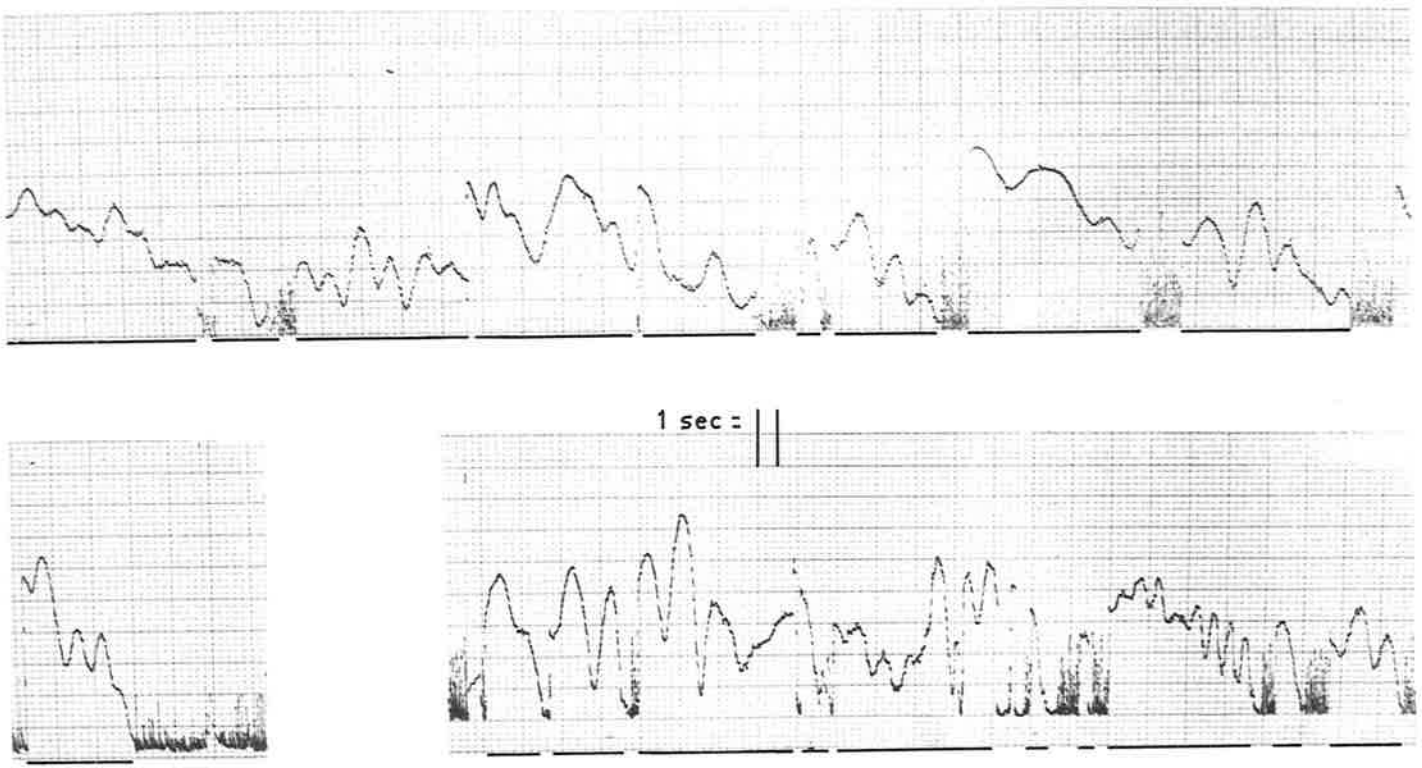

Figure 4.12 Typical records of echo amplitude.

by the scanning gate). As there is no way of knowing the echo's azimuth the echo was assumed to be in the centre of the beam. Thus values of G_R and G_T were computed for all zenith angles in the beam's centre using the method described in Chapter 7 (see Figure 4.1 for G_T and Figure 7.1(b) for G_R).

In Figure 4.13(a) the frequency of observing meteor echoes with a given electron line density is plotted. It can be seen that 75% of the echoes have electron line densities between 2.0×10^{13} and 5.0×10^{13}/m. Only 60% of the meteor echoes had suitable amplitude records to be included in this plot. The remaining echoes were either badly distorted by the effect of winds or their amplitude exceeded the maximum range of the pen recorder. Most echoes in the latter category would have been overdense (with an electron line density above 1.0×10^{14}/m) and only a few were observed. Figure 4.13(b) shows the average electron line density plotted for 2.5 km height intervals.

4.7 Echo Decay Time Constants and Durations

The amplitude records used to determine electron line densities were also used to determine the echo's decay time constant in cases where the echo was relatively free from interference effects. A number of such echoes are shown in Figure 4.14. Even with these, the rate of decay could be influenced by distortions to the trail brought about by the action of winds, as they nearly all have decay time constants greater than 1 second (discussed in Chapter 2.3(b)). Echoes which showed a reasonably exponential decay (although fading could be present) made up

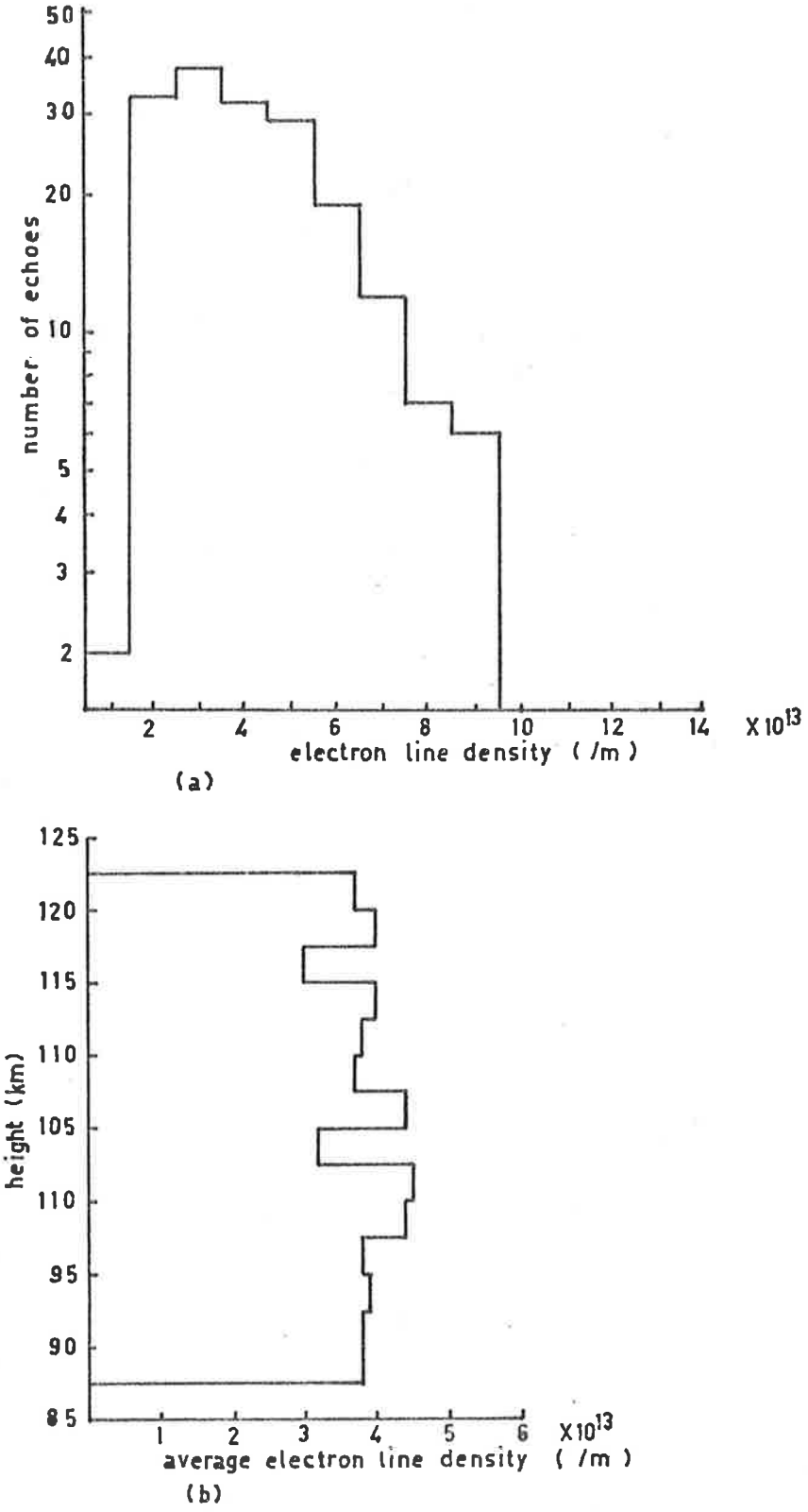

Figure 4.13 Electron line density.

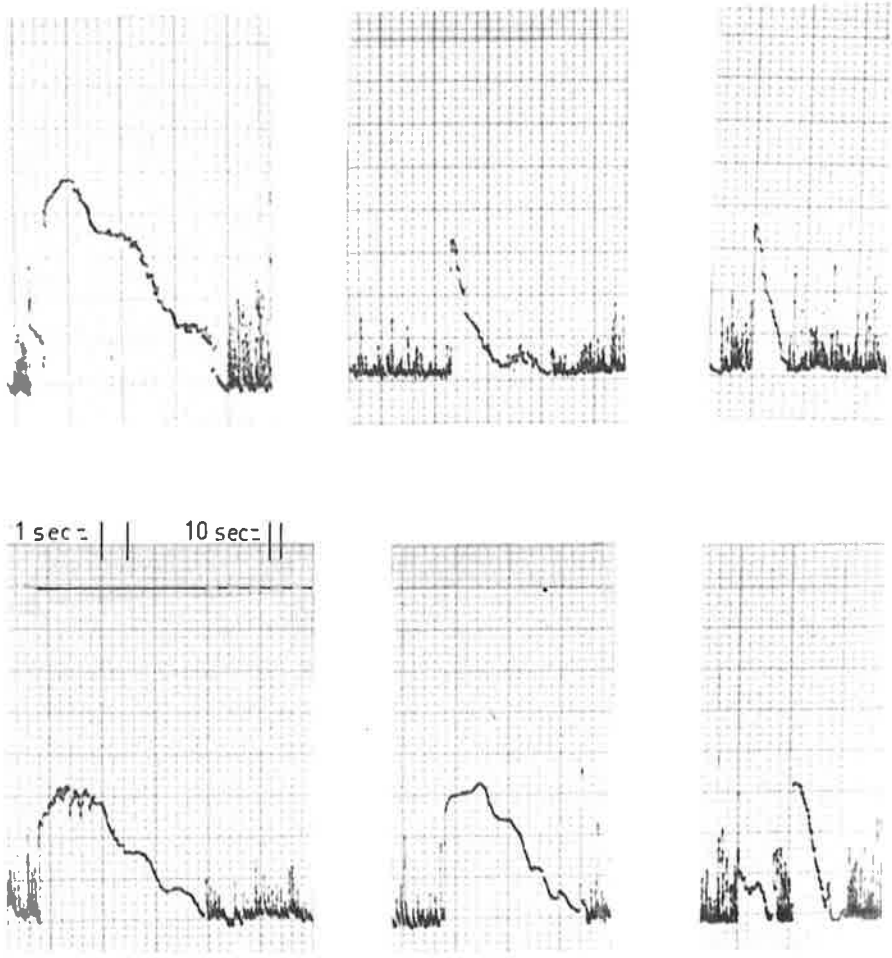

Figure 4.14 Six meteor decays.

55% of the echoes recorded, and of these 21% showed a rise in amplitude before decaying (this rise being much slower than their formation rise time). Those echoes in the latter category were probably influenced by resonance effects (discussed in Chapter 2.3(a)) or by the trail being distorted by the wind.

The time for the echo to decay to 1/e of its maximum amplitude was read for all rapid-rising (or specular meteor echoes) which showed a reasonable exponential decay. Those echoes which showed an increase in their amplitude before decaying were considered as a separate group. Decay time constants are plotted for individual echoes in Figure 4.15. Theoretical decay times are also shown for values of ambipolar diffusion found by Greenhow and Neufeld (1955).

Echo durations were determined from the film record of the echo range, an example of which is shown in Figure 3.3 (discussed in Chapter 3). The duration was obtained by measuring the time the echo's trace was visible on the film. The trace was only recorded while the signal exceeded a set level, which was close to the level of the noise signal, and was determined from the calibration pulse described in the previous section of this chapter. Durations were measured for all echoes, both fast and slow rising and are shown in Figure 4.16 averaged over 2.5 km height intervals. The duration of an echo will depend on the echo's initial amplitude and decay constant. As the initial amplitude is determined by a number of factors, including echo range and the aerial

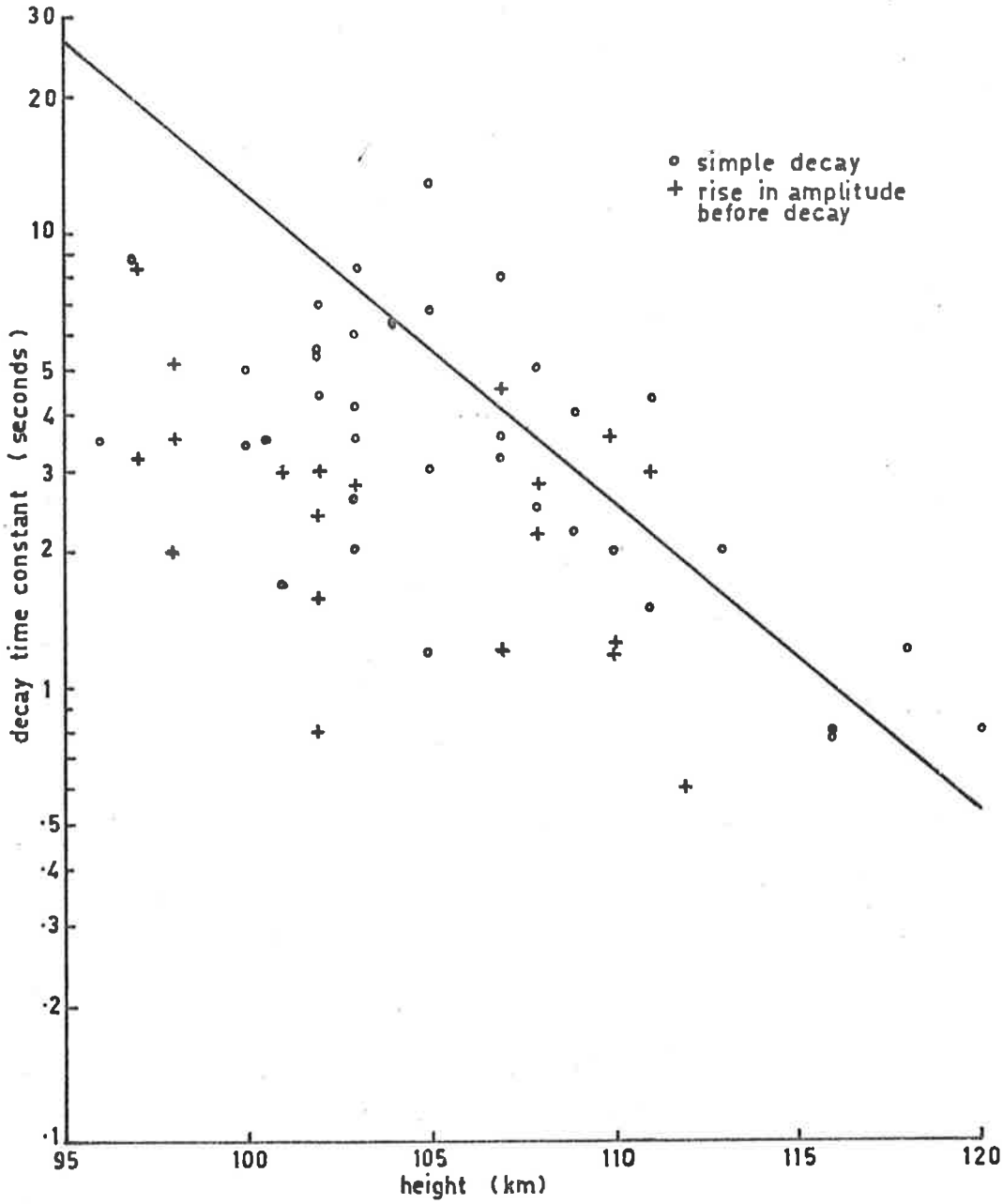

Figure 4.15 The measured decay rates of two types of echo with the theoretical decay rate shown by a continuous line.

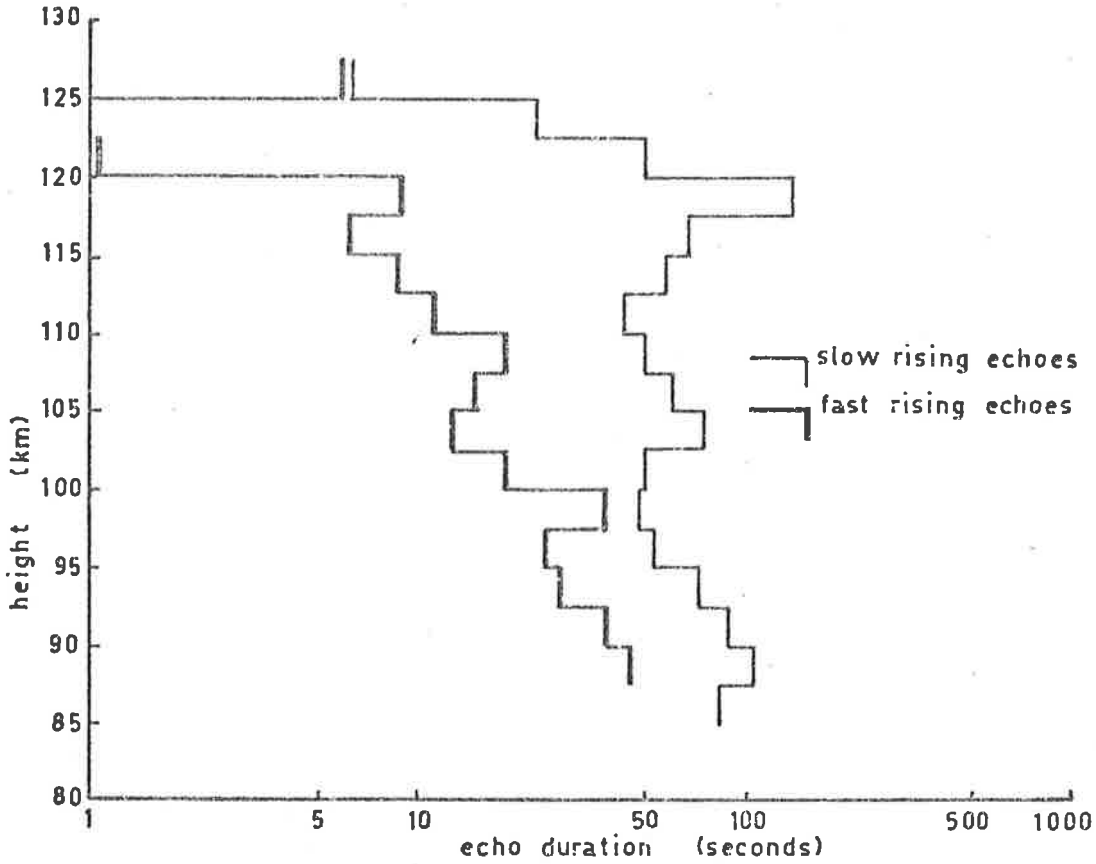

Figure 4.16 Echo durations for fast and slow-rising echoes.

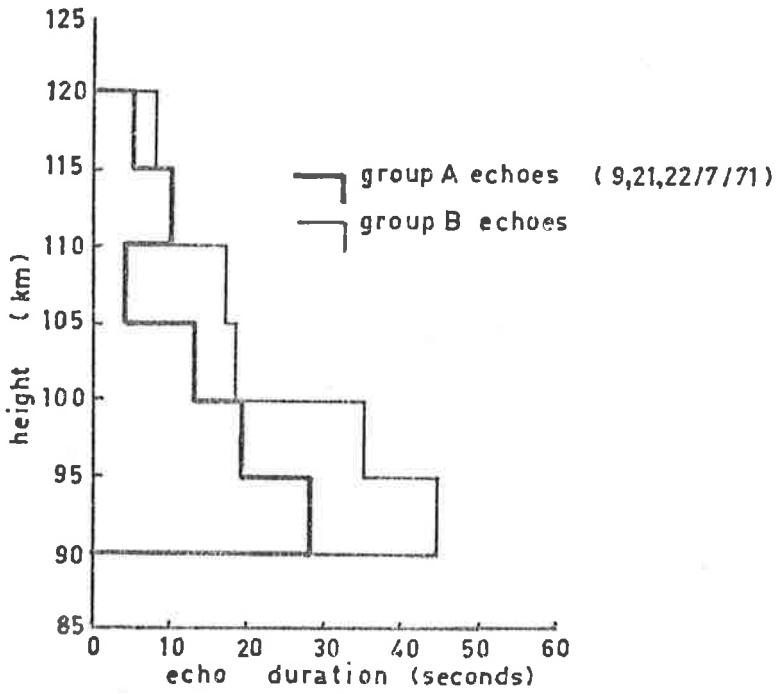

Figure 4.17 Echo durations for the two groups mentioned in the text.

gain, it is usual to correct the duration to some constant range and aerial gain (McKinley, 1953). This correction assumes an exponential decay and determines an echo duration for an echo which decays at the same rate, but has its amplitude corrected to the level it would have had if observed at the fixed range. As most echoes at 1.98 MHz do not decay exponentially, due to the action of winds, such a correction would be meaningless. Thus no attempt has been made to correct the duration distribution. **Corrections were applied to the fast rising echo durations but they did not significantly affect the shape of the distribution.**

The echo decay time constants shown in Figure 4.15 are scattered evenly about the expected decay times (computed from Greenhow and Neufeld's 1955 values of ambipolar diffusion) above 105 km. Below this height the decay times level off with the simple decays scattered about a decay time of approximately 4 seconds, while the decays which showed a rise in amplitude before decaying are scattered about 3 seconds. This variation of decay time with height is also evident in the plot of average echo duration shown in Figure 4.16. It was shown in Chapter 2.3(d) that an attachment rate of 0.2/second gave a decay time constant of 5 seconds. Values of attachment rates as high as this were measured by Glöde (1968) for overdense echoes with short durations (approximately 3 seconds). While Glöde obtained lower attachment rates for echoes with durations greater than 16 seconds, he did not take into account the effects of wind turbulence and, as these will be more pronounced with the longer enduring echoes, his values may well be lower than they should be for these echoes.

Wind turbulence was shown in Chapter 2.3(c) to become important about thirty seconds after the trail formed. However there is evidence that the wind can reduce echo durations. In Figure 4.17 echo durations are shown for days when overhead echoes were observed (group A in Chapter 4.5) and when they were not (group B). It can be seen that echoes in group A were significantly shorter than those in group B. This shows that the strong wind shears present with echoes in Group A (Chapter 6.3) were reducing the echo durations by distorting the trails. Further evidence for the effect of winds on the echo decay can be seen in Figure 4.15 where echoes that show a rise in amplitude before decaying generally have faster decay rates than those echoes which have a simple decay. Interfering signals from a secondary reflection frequently superimpose a cyclic variation of the signal amplitude on an exponential decay. Thus a rise in the signal will be followed by a fall, which will increase the signal's rate of decay. Above 105 km, resonance effects could also be responsible for an initial rise in the signal before it decays, and these will also result in increased decay times (Lebedinets and Sosnova, 1968).

The durations of slow rising echoes, shown in Figure 4.16, are fairly constant with height and about an order of magnitude greater than the meteor durations above 115 km. The peak in echo durations at about 120 km was caused by a single reflection from an overhead patch of sporadic-E ionization. It was found to be impossible to separate reflections from D and E region irregularities (which were generally

long enduring) from specular reflections from meteor trails brought about through wind-induced distortions to the trail after it had formed.

Slow rising echoes would also have come from trails which produced a flare, resulting in a densely ionized region which had diffused into a sufficiently large volume to reflect an observable signal. Such a volume would be overdense, reflecting only at its boundary. Hence electron attachment would only affect the echo by reducing the electron volume density to a level where the volume became underdense. The echo duration would therefore depend on the initial concentration of electrons.

4.8 Echo Polarizations

As stated in the introduction of this chapter, most observations were made by transmitting a circularly polarized radio wave with right hand polarization, this being the ordinary wave in the ionosphere. Thus the phase difference of the observed signal on two crossed dipoles was + 90°, provided the radio wave was reflected without unusual phase changes occurring. Where the extraordinary polarization was transmitted, the phase difference was - 90°. The observed polarization for 77 echoes is plotted against height in Figure 4.18. It can be seen that most were recorded while ordinary circular polarization was transmitted, a small number being recorded while extraordinary polarization was transmitted. These latter echoes appear to show a larger scatter about - 90° than do the echoes with ordinary polarization (about + 90°) and this is

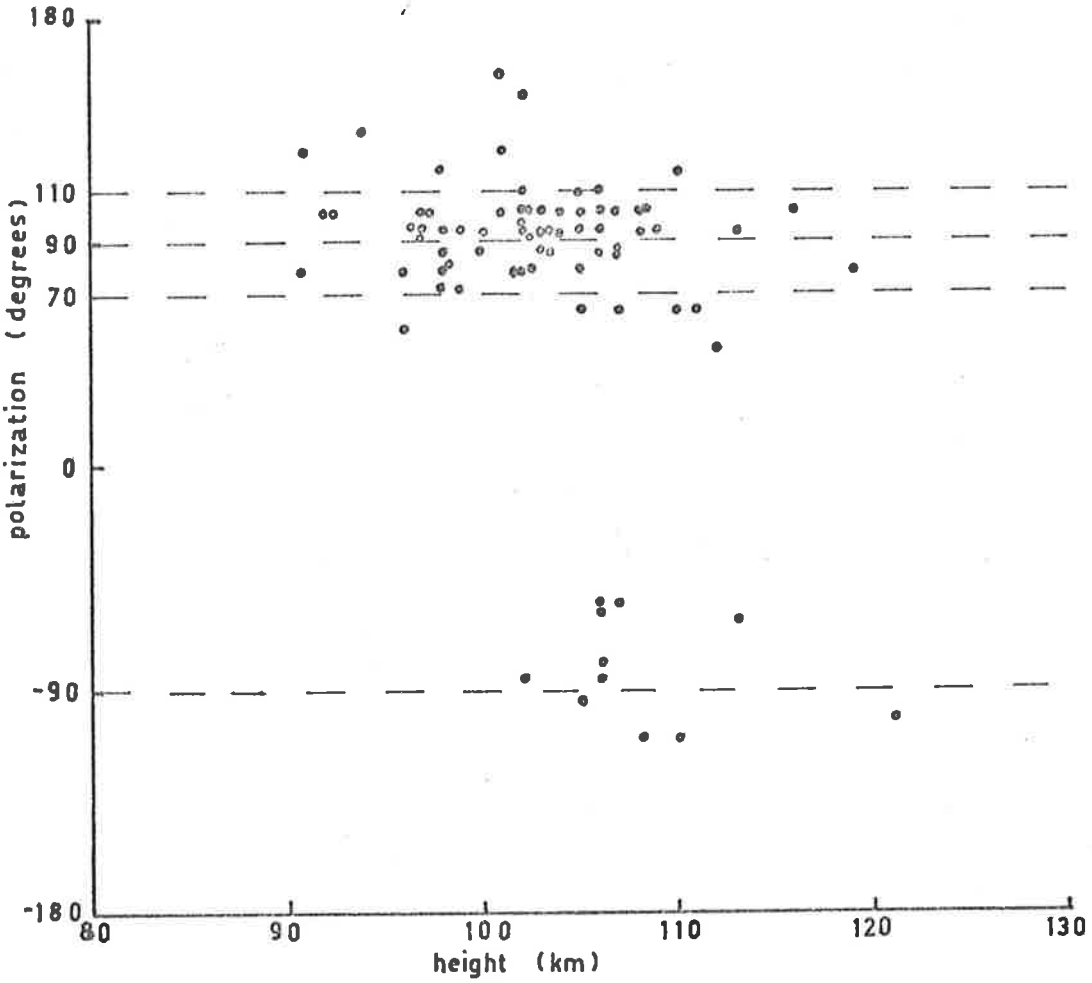

Figure 4.18 Echo polarization.

probably due to the fact that the extraordinary wave is influenced by ionospheric absorption to a much greater extent than the ordinary wave. Thus the small amount of ordinary signal transmitted in off-vertical directions while the transmitter was phased to transmit extraordinary, would influence the observed signal to a much larger degree.

The effects of resonance on the trail's reflection coefficient are discussed in Chapter 2.3(a) where it is shown that trails with an electron line density between 5.10^{13} and 5.10^{14}/m should reflect the circularly polarized wave initially as a plane wave, then as a changing ellipse, before finally returning a circular wave. Resonance effects were not considered in determining the electron line density (Chapter 4.6) as the echo amplitude could, in any case, only be approximately determined. However the range of observed electron line densities should be close to the actual range, indicating that about one quarter of the observed echoes had electron line densities greater than 5.10^{13}/m.

It was shown in Figure 2.6 that trails with the above electron line densities reflect a plane polarized wave while the trail radius was less than 3.3 m. It is unlikely that the present system of recording would be capable of observing this stage, as very few echoes were seen below 90 km. Above this height the effect lasts for less than 1 second, the average time taken by the scanning gate to detect an echo. With the trail radius between 3.3 m and 11 m, trails with electron line densities

between 5.10^{13} and 5.10^{14}/m reflect a circularly polarized wave as a relatively narrow, changing ellipse. This effect lasts for a time that is greater than 1 second below 106 km (see Figure 2.6) and should therefore be observed below this height.

In Figure 4.18 there are 13 echoes with an angle of polarization that is $> 110^{\circ}$ or $< 70^{\circ}$ (considering only those recorded while the ordinary wave was transmitted). Of these echoes 8 occur within the height range 90 to 106 km, this group containing the more extreme examples. These angles of polarization, which indicate that the reflected wave was a relatively narrow ellipse, are thus examples of resonance. However, as the orientation of the trail relative to the two crossed dipoles is not known, the degree of resonance cannot be determined.

4.9 Echo Rise Times

The rise time of an echo reflected specularly from a meteor trail is determined by the time the meteor takes to cross the principal Fresnel zone. This time will be reduced if the trail does not extend right through the zone. For a typical range of 120 km, a meteor travelling at 40 km/sec has a rise time of 0.1 seconds. Five radar pulses can be transmitted during this time, and thus the rise can be resolved. However, only in the case of very slow meteors will the diffraction pattern be resolved at this slow pulse rate. Many of the records were made at a pulse rate of 25/sec, making it even less likely that the

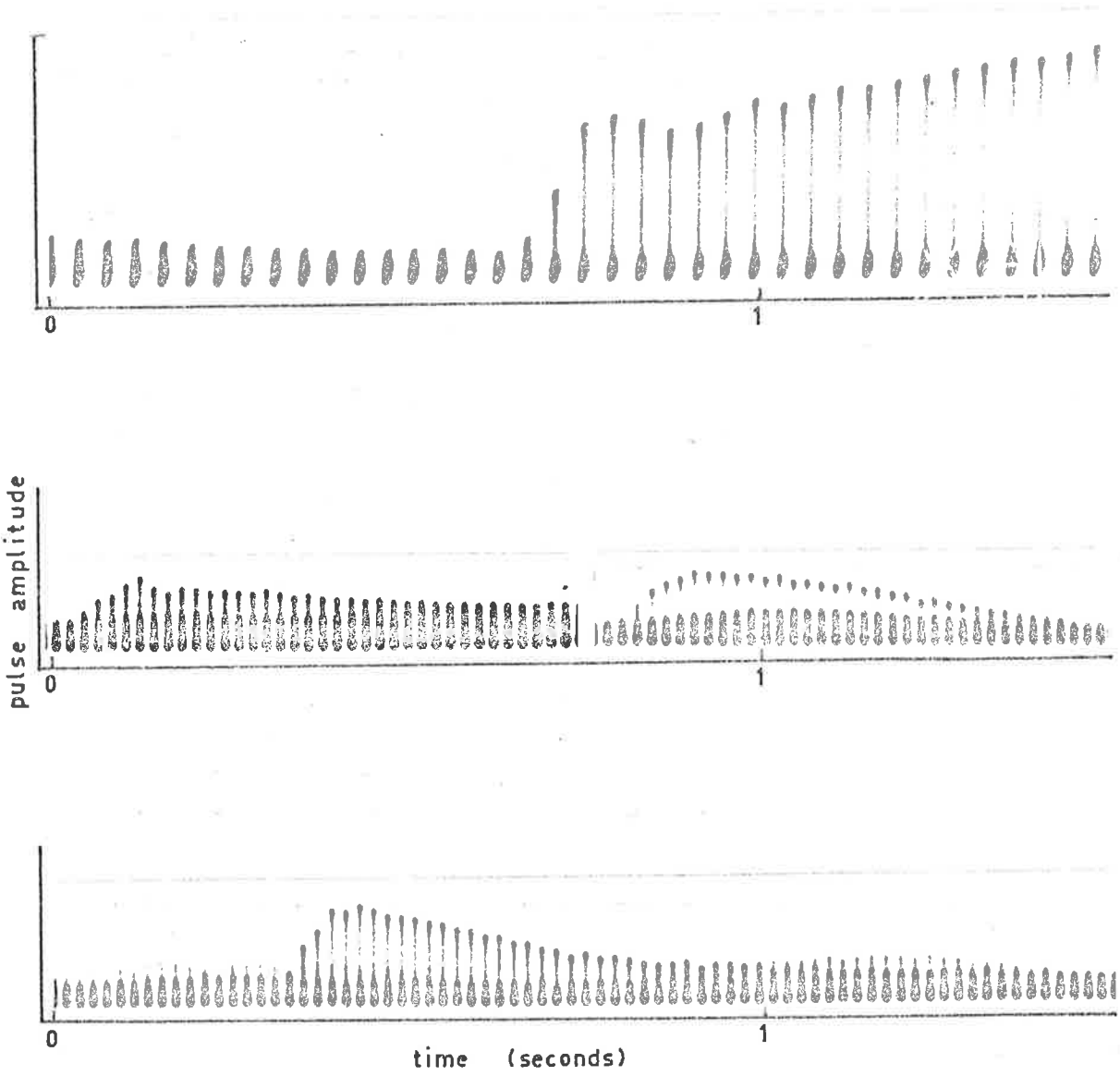

Figure 4.19 Typical echo rise times at pulse rates of 25 & 50/sec.

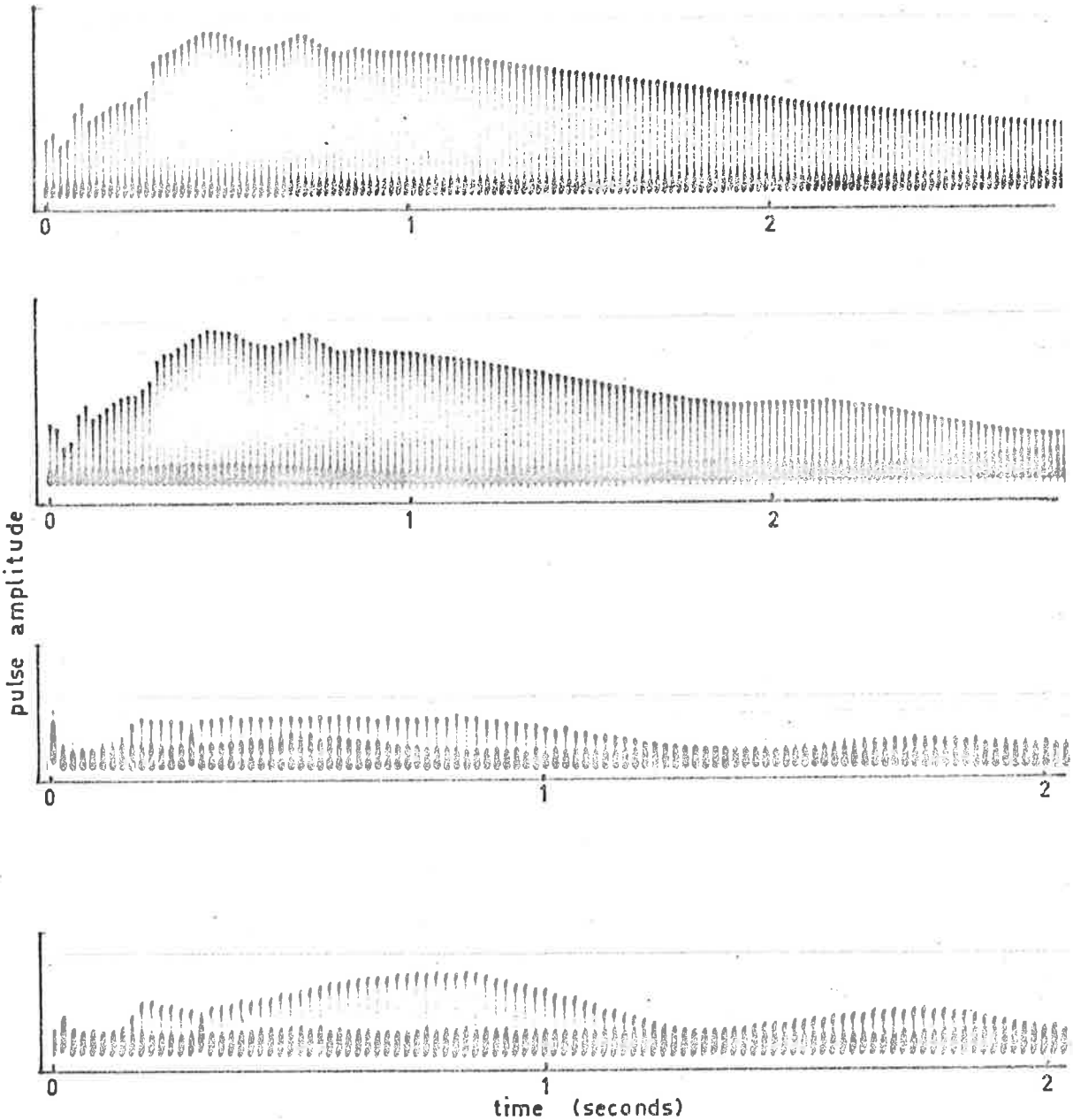

Figure 4.20 Two unusal echoes, showing both polarizations.

diffraction pattern would be resolved.

A number of echoes are shown in Figure 4.19. Some of these show very short rise times, indicating that the trail has not extended right through the principal zone. In Figure 4.20 several echoes not commonly recorded are shown. The first shows a definite diffraction pattern, while the second shows a much slower rise in echo amplitude after the echo was formed. This could be due to interference effects; however it could also be due to resonance effects discussed in Chapter 2. It was shown in that chapter, that for an electron line density of $2 \times 10^{14}/m$, as the column expanded, the transverse reflection coefficient would increase by a factor of about 20 through resonance effects.

CHAPTER 5

METEOR HEIGHT DISTRIBUTIONS

5.1 Introduction

The effects of the trail's initial radius on the observed height distribution of radio echoes from underdense meteor trails has been considered in Chapter 1. It was shown in Chapter 2 that the size of the initial radius is still uncertain, with measurements made by radio techniques giving larger values than direct measurements made of the optical coma. While this disagreement remains to be resolved, the effects of theoretical initial radii suggested by Manning (1958) and by Lebedinets and Portnyagin (1966) will be considered.

A comparison between the height distributions of echoes observed at 17 MHz and 1.98 MHz would show whether or not the initial radius effects are important at 17 MHz, as they are unlikely to be significant at 1.98 MHz (discussed in Chapter 1). The height distribution used in the following comparison was obtained from Greenhow and Hall (1960), who measured the echo decay time constant. They obtained echoes from roughly the same population of meteors since the echoes at 1.98 MHz are from meteors with electron line densities greater than 2×10^{13}/m, while the 17 MHz echoes had a mean magnitude of + 6.5, which is roughly equivalent to an electron line density of 4×10^{13}/m. The aerial used to receive echoes at 17 MHz was a single full wave dipole at a height of $3\lambda/8$ above the ground, while a row of eleven half wave dipoles, each $\lambda/15$

above the ground was used at 1.98 MHz. As it is the higher part of the echo distribution which is important and this will most likely result from trails entering the atmosphere with large zenith angles, it is the beam's response at zenith angles out to about 45 degrees which matters. Both polar diagrams will be similar over this range if only the response perpendicular to the row of dipoles at 1.98 MHz is considered. In addition it has been shown by Kaiser (1954a) that the aerial polar diagram has a relatively small effect on the observed height distribution. The two height distributions should therefore be identical if no initial radius effects are present. Calculations based on Lebedinets and Portnyagin's (1966) values of initial radius indicate that the 17 MHz height distribution should be severely attenuated above 105 km, while Manning's (1958) initial radii show that severe attentuation occurs for echoes above 115 km. Before a comparison of the height distributions can be made, the 1.98 MHz height distribution must be corrected for selection effects.

5.2 Corrections to the 1.98 MHz Height Distribution

The meteor height distribution shown in Figure 4.8(a) is for all echoes with durations greater than about one second observed within the range scanned by the gate described in Chapter 3.4(a). Thus echoes with durations greater than 1 second could be analysed. Echoes with durations less than this would have occurred above 115 km where the decay time constant becomes less than 1 second. The height distribution falls off evenly between 105 and 115 km where the echo

duration was, on average, about ten seconds. From this part of the curve it can be inferred that few echoes would be expected above 115 km. Thus it seems unlikely that many echoes were lost because the echo duration was too small. However, the range scanned by the gate will have affected the distribution, reducing the number of echoes observed below 105 km. The scanned range was normally started at 80 km. However, partial reflections from ionization between 80 km and 100 km were occasionally strong enough to be detected by the gate. Slow rising echoes in the height range 85 - 95 km had an average duration of about 90 seconds. At a zenith angle of 30° this height interval occupies the range interval 98 - 110 km. To prevent repeated detection by the gate of these echoes, the gate's scan was often started at 110 km. On a few occasions the scan was started at 130 km because of persistent echoes. Unfortunately no record was kept of the periods when the scanned range was altered, but it is roughly estimated that it was from 110 km for half the time, thus a corrected height profile can be constructed. This was done by assuming that echoes from 85 to 105 km had the same angular distribution as all the echoes observed. The percentage of echoes thus present in each 5 km height interval from 70 to 105 km is shown in Table 5.1. The correction is only approximate, but a more exact analysis is not justified as the echo count for each height range is only known approximately. The corrected height distribution is shown in Figure 5.1 superimposed on the observed height distribution.

This distribution shows a sharp cut-off below 97 km. The

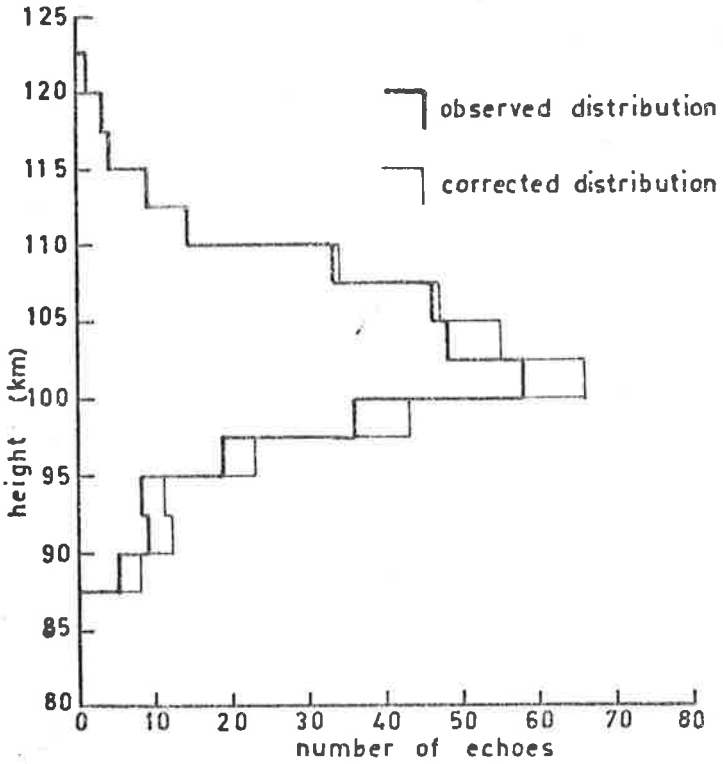

Table 5.1

% of echoes lost	height (km)
0	110
3	105
12	100
18	95
27	90
87	85
43	80

Figure 5.1 The observed and corrected height distributions at 1.98 MHz.

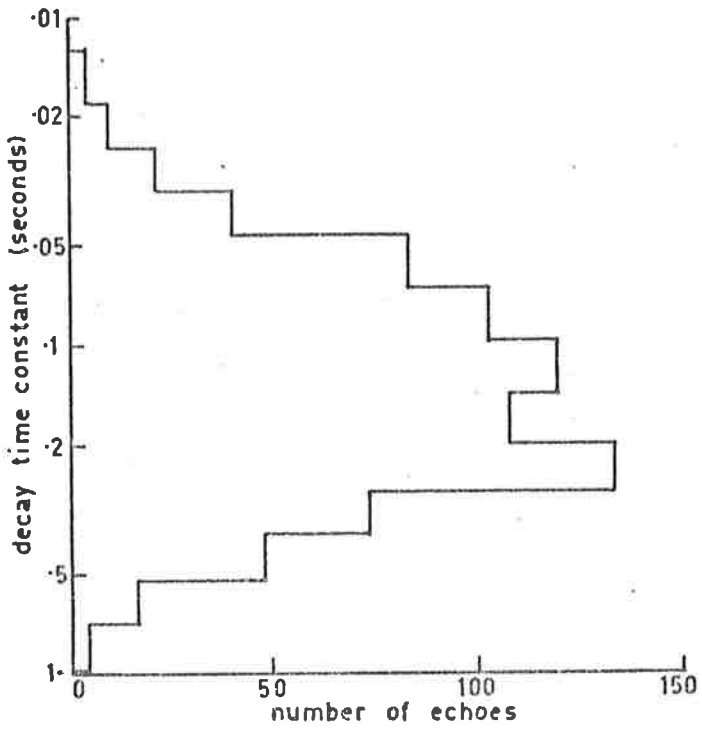

Figure 5.2 The observed distribution of decay time constants at 17 MHz by Greenhow and Hall (1960).

correction factor for these heights is large; at a height of 85 km, 37% of the echoes were most probably excluded because of the range scanned. The observations were limited to echoes with zenith angles < 50°. This would tend to reduce the number of echoes observed at low heights (below 100 km) because the point of maximum ionization of the meteor trail occurs where the atmospheric density is equal to ρ_m and

$$\rho_m \propto \cos z$$

where z is the zenith angle. An additional cause of low altitude cut-off could come from polarization effects. In Chapter 2 it was shown that at low radio frequencies trails initially reflect a plane polarized wave. This can reduce the amplitude of the observed echo by a factor of 2 or more in many cases. While this amplitude reduction only lasts for a short period until the column has expanded sufficiently through diffusion, it would cause the echoes from low heights to take several seconds to rise to their maximum amplitude. Such an echo would be classified with the slow rising echoes which were observed down to 82 km.

5.3 Comparisons of Height Distributions at 17 and 1.98 MHz

Of the echoes observed by Greenhow and Hall (1960) at a frequency of 17 MHz, 750 showed an exponential signal decay. The resulting distribution of signal decay rates (time taken for the echo amplitude to decay to 1/e of its maximum value) is given in Figure 5.2. This distribution can be interpreted as a height distribution using the expression for the decay time constant T,

$$T = \frac{\lambda^2}{16\pi^2 D} \qquad 5.1$$

where λ is the radio wavelength, and D the ambipolar diffusion coefficient (Herlofson, 1948). The variation of D with height above 95 km is affected by the earth's magnetic field. This is because the electrons will tend to diffuse at a greater rate along the field than across the field.

Herlofson (1948) proposed that the observed ambipolar diffusion (D_o) was given by

$$D_o = D_{\parallel} \sin^2 \phi + D_{\perp} \cos^2 \phi \qquad 5.2$$

where $D_{\parallel}$ and $D_{\perp}$ are the ambipolar diffusion coefficients for diffusion parallel and transverse to the field lines, and ϕ is the angle between a line normal to the magnetic field, and a line drawn from the observing station to the magnetic field line. At heights below 95 km $D_{\parallel} = D_{\perp}$ (Poole and Kaiser, 1967) however above this height it has been suggested that $D_{\perp} < D_{\parallel}/2$ (Weiss, 1955; Francey, 1964). As no obvious correlation has been found between ϕ and echo decay rates, it has been suggested that $D_{\perp}$ is close to $D_{\parallel}/2$ (Poole and Kaiser, 1967). Recent theoretical work by Kaiser, Pickering and Watkins (1969) has shown that meteor trails closely aligned with the magnetic field diffuse at a very slow rate. This has been confirmed by experimental observations made by the same authors who showed that the echo decay rate is inhibited for trails that lie within a degree or so of the direction of the magnetic field. They also found that trails not parallel to the field could have long decays, however this only occurred when the aerial beam's axis was

within a degree or so of being normal to the magnetic field. Thus the magnetic field only inhibited the decay of a small percentage of echoes, and the effect has been ignored in this treatment.

The variation of D with height for a zero magnetic field (D_z) has been calculated by Kaiser, Pickering and Watkins (1969). Assuming that $D_{//} = D_z$ then $D_\perp < D_z/2$. Values of $D_{//}$ and the upper limit of $D_\perp$ ($D/2$ - dashed line) are shown in Figure 5.3. Also shown are the experimentally determined values found by Greenhow and Neufeld (1955; to be referred to as D_G), extended to a height of 115 km. It can be seen that D_G is close to $D_z/2$ above 95 km, where the effect of the magnetic field becomes important. Thus, above 95 km D_G can be considered a reasonable compromise between $D_\perp$ and $D_{//}$. Below 95 km the magnetic field becomes unimportant and D_G can again be used as it approaches D.

Thus using D_G in Equation 5.1 the 17 MHz echo decay rate distribution of Figure 5.2 can be plotted as a height distribution, and this is shown in Figure 5.4 together with the corrected height distribution of 1.98 MHz meteor echoes and a height distribution observed by Doyle (1968).

Before these height distributions can be compared, a number of factors have to be considered. The method of selecting 17 MHz echoes will have influenced this distribution to some extent. Only those echoes with reasonably undistorted decays were analysed. As distortion to the decay is most likely to occur with the lower echoes which decay

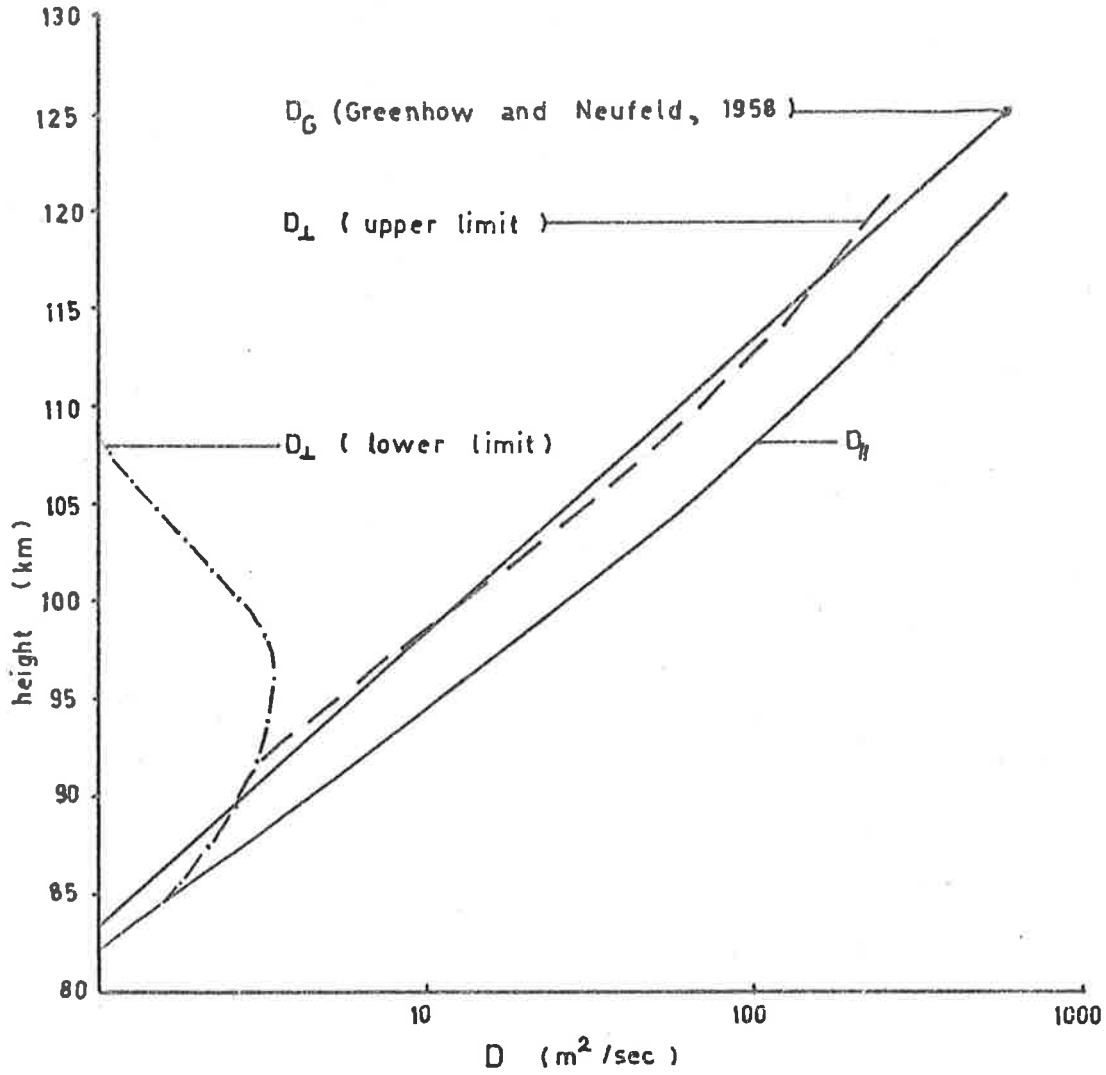

Figure 5.3 Variation of the coefficient of diffusion (D) with height.

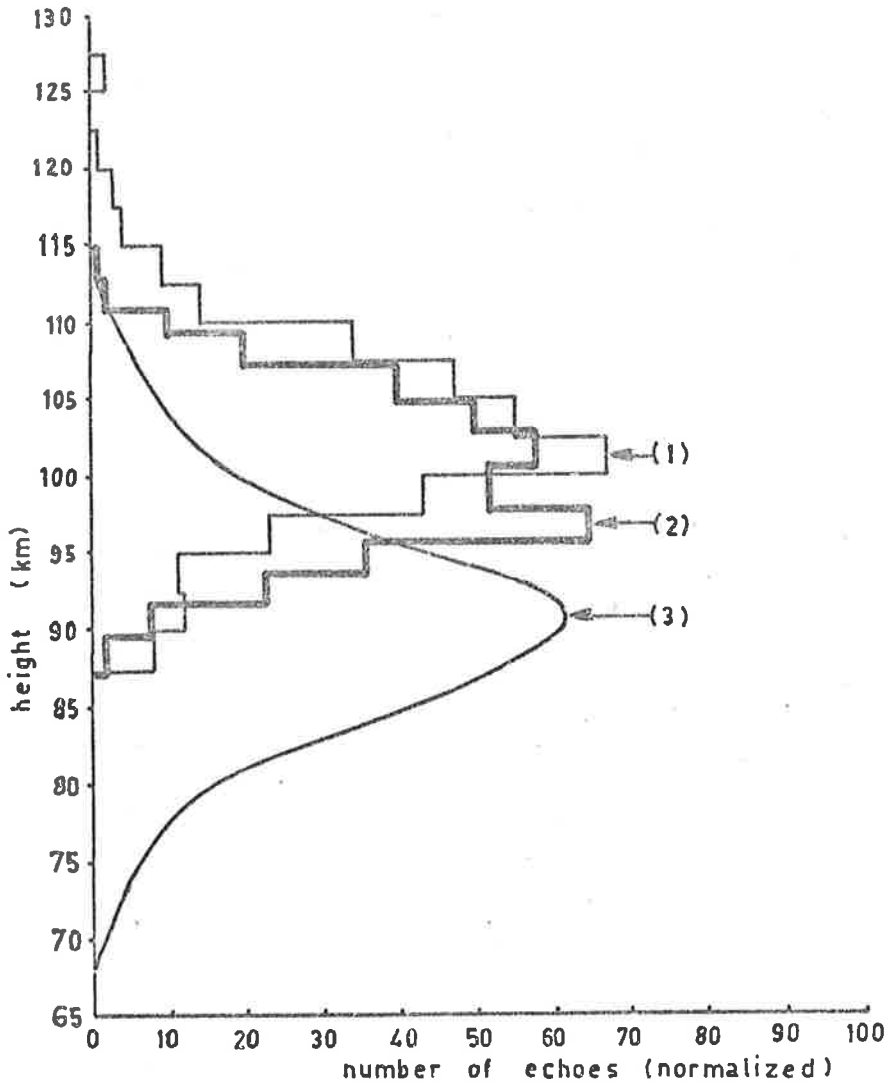

Figure 5.4 The corrected height distribution for radio echoes with a frequency of; (1) 1.98 MHz (295 echoes), (2) 17 MHz (750 echoes), and (3) 27 MHz (54,000 echoes). **Note that the 17MH$_z$ distribution does not extend above 115km because decay times greater than .01 seconds could not be analysed.**

more slowly, these are most likely to be excluded. At 90 km the decay time constant of a meteor echo at 17 MHz is about 0.6 seconds. On average it takes 0.4 seconds for interference effects to occur with overdense echoes. An underdense echo should not be affected as soon, as in many cases the interfering signal will be decaying more rapidly than the initial signal. However, the lack of echoes below 87 km could be explained by the fact that these echoes were distorted.

The heights of 27 MHz meteor echoes obtained by Doyle, are actual heights obtained by recording the echo's range and zenith angle. This system requires one and a half Doppler cycles ($\sim$ 0.1 secs) to be present in a record of the echo before the necessary phase measurements can be made. Thus it discriminates against the higher echoes which decay more rapidly.

It can be seen that the 17 MHz and 1.98 MHz height distributions have the same variation with height above 105 km. Thus initial radius effects must be of little importance to radio observations of meteor echoes at 17 MHz, and therefore the initial radius must on average be less than 3 m at 110 km. This compares well with Manning's (1958) value of 2.4 m for this height. There is not much that can be deduced from the 27 MHz height distribution as the selection effects imposed by the requirement of one and a half Doppler cycles before the echo can be analysed is very severe and has resulted in a relatively large number of analysed echoes being below 90 km.

Thus the distribution of echo heights at 1.98 MHz and 17 MHz shows that at a height of 110 km the initial radius has a value which is significantly less than the theoretical predictions of Lebedinets and Portnyagin (1966), and more likely to be close to the value predicted by Manning (1958). This is consistent with the findings of Poole and Kaiser (1967) who presented indirect evidence to support their view that at 17 MHz there was no height ceiling imposed by an initial trail radius.

CHAPTER 6

WIND COMPARISONS

6.1 Introduction

Methods employed to observe winds in the atmosphere between the heights 80 km to 120 km involve observing either artificial or natural tracers, optically or by radar.

Artificial tracers are convenient in that they allow a controlled experiment to be performed at a time chosen by the experimenter. However, they are expensive and thus not a practical way of making continuous observations over an extended period of time. The type of trace to be placed in the atmosphere is determined by the height at which the wind is to be measured as the tracer must move with the neutral wind. Below 80 km an inflated balloon or rigid sphere (Bartman et al, 1956) can be ejected from a rocket and then tracked by radar. More recently a parachute carrying an instrument package (Webb et al, 1961) has been used in a similar manner. Radar chaff and chemical trails have been ejected from probes launched from a gun (Murphy et al, 1966), while rockets have been used to lay chemical trails up to 160 km. These can be observed with several ground based cameras. Alkali vapours can be used at times when the trail is in sunlight while the sky is dark, such as at sunset and sunrise (Manning et al, 1959). Night time observations can be made with trimethyl aluminium (Rosenberg et al, 1963). Rockets have also been used to carry grenades which are fired at

intervals of a few kilometers. An array of microphones on the ground recorded the angle and time of arrival of the accoustic shock wave, thus providing information for a model atmosphere (Stroud et al, 1956; Groves, 1960).

Naturally occurring tracers that can be observed optically include noctilucent clouds and long-enduring meteor trails, but as they do not occur frequently, they are of limited use. The situation changes, however, when radio observations are made. It then becomes possible to observe the drifts of the ionized columns of meteor trails. Radio reflections from ionization in the D and E regions can also be observed, and the movement of the ionization in these regions inferred.

6.2 Winds in the Upper Atmosphere

Between 80 km and 110 km the movement of the neutral atmosphere is governed by a mean flow, planetary waves, tides, internal gravity waves, and turbulence. These wind movements are predominantly horizontal.

Measurements of the wind's variation with height over a short period of time are most easily carried out by observing chemical trails laid by rockets. However, continuous measurements over a number of days, have been carried out by meteor radar systems which combine high meteor rates with accurate height determinations (Southworth, 1968; Revah, 1969).

Small scale fluctuations in the wind can be measured if the number

of meteor radar receiving stations is increased. This makes it possible to obtain more than one reflection from a single meteor trail. The separation of these reflections is determined by the angle of the trail to the various receiving stations, and is typically 2 to 5 km. This has been carried out by Greenhow and Neufeld (1959) who used three receiving stations, by Roper (1966) using three stations and by McAvaney (1970) who used five stations. A less direct method of observing the action of the wind along a meteor trail involves observing the amplitude fluctuations present in enduring radio echoes. These are caused by the interference of waves reflected from two or more regions of a bent trail. Observed fading rates have been compared with those predicted by various models by Manning (1959) and Phillips (1960). These measurements, and the more direct ones, suggest a vertical scale of between 6 and 8 km and a horizontal scale greater than 100 km. An average wind variation with height is 10 m/sec/km although variations as high as 100 m/sec/km over small height ranges have been observed to occur with many chemical trails. Vertical shears appear to be most pronounced at a height of 105 km where they have an average value of about 30 m/sec/km (Kochanski, 1964).

6.3 Meteor Trail Drifts

The effects of neutral winds on meteor trails and thus their effects on the reflected radio signal, have been discussed in Chapter 2.3(b). It was shown that the trail moves with the wind unless the trail is closely aligned with the magnetic field. Thus the large

majority of trails observed are drifting with the neutral wind.

Manning, Villard and Peterson (1950) made the first observations of winds by observing shifts in the phase of the radio meteor echo, brought about by the trail's movement. In this way the radial velocity of the reflecting region of the trail was recorded. If the position in the atmosphere of the reflection point is known, because there is very little vertical movement, the horizontal component of the wind towards or away from the receiving station can be determined. As this single measurement only yields the component of the wind towards or away from the receiving station, a number of such measurements (at least two) must be made at each height. Then by assuming the wind to have a horizontal scale > 100 km, a wind-height profile can be determined.

Various methods have been employed to measure the wind. Greenhow (1952) used a phase-coherent pulse at a frequency of 36 MHz. A directional aerial was used to observe two components of the wind, observing one component and then the other by rotating the aerial through 90 degrees. A high peak pulse power together with high gain aerials enabled a high meteor rate to be observed. However the height was only known approximately, being deduced from the rate of decay of the echo's signal strength. A phase-coherent pulse system has been combined with aerial arrays for direction finding by Southworth (1968). This has the advantage of having both a high echo rate and accurately known echo heights.

The Adelaide system is a combined continuous-wave pulse system and is described in some detail in Chapter 8. The method employed to obtain wind measurements is described by Robertson, Liddy and Elford (1953). The Adelaide system operates at frequencies of 26.773 MHz (continuous wave) and 27.540 MHz (pulse) and will be referred to as the 27 MHz system. Over this frequency range echoes are observed between 70 km and 110 km, with most echoes between 80 km and 100 km.

6.4 Ionospheric Drifts by the Spaced Receiver Method

The measurement of the horizontal drift of irregularities in the ionosphere by comparing reflected radio signals received from three separate aerials placed in a triangle, is a well established technique first tried by Mitra (1949) and Krautkramer (1950). Radio waves with a frequency of 1.98 MHz are totally reflected during the daytime by the E-region at heights between 100 - 115 km. Occasionally a layer of sporadic-E totally reflects the signal at a height between 100 - 110 km. These layers of ionization are seldom completely flat so the reflected signal forms an irregular diffraction pattern on the ground. As the pattern moves, the signal amplitude variations can be sampled by three or more aerials, or the movement rendered visible by a large array of aerials connected via receivers to an array of lights, the intensity of each light being proportional to the signal amplitude at each aerial.

The drift velocity of the pattern has been shown to be twice the velocity of the irregularities present in the reflecting layer (Felgate,

1969). Where only three aerials sample the pattern, the time displacement of the fading recorded at each aerial can be determined by correlating the records. The time displacement required for a maximum correlation gives a measure of the velocity. However, the pattern often changes as it moves over the ground. Thus care must be taken in selecting a suitable triangle size (Golley and Rossiter, 1970). A technique known as full correlation analysis developed by Briggs, Phillips and Shinn (1950) and Phillips and Spencer (1955) can be used in determining the record's time displacements. Even with these precautions the three aerial technique can give misleading and inconsistent results (see below).

Large aerial arrays overcome many of the limitations present in the above method. An array of 89 aerials described in Chapter 3 has been in operation at Adelaide since 1969. A spatial correlation analysis developed by Briggs (1968) allows the diffraction pattern's velocity to be determined from two observations of the complete pattern separated by 1 second in time. This analysis is independent of the statistical properties of the diffraction pattern. It was found by Felgate (1969) that for about 27% of the time the pattern from both the E and sporadic E regions was unsuitable for velocity determinations either by the large array or by the three receiver method. Effects which can cause this include sudden changes in the velocity of the pattern taking place in a 20 second interval. These would confuse the results from the three receiver method, which requires about three minutes of record to

produce a velocity determination. It has been suggested by Felgate (1969) that these changes in pattern velocity could be caused by the interference of radio waves from two or more reflecting regions with height changes occurring in one or more of these regions. Thus at these times the pattern will not represent the horizontal movement of the irregularities. At other times the presence of only two reflecting regions causes the pattern to consist of a single set of fringes. At these times only the component of the wind perpendicular to the fringes can be measured, as the movement of the fringes parallel to their length cannot be observed. Thus care must be taken interpreting measurements of the radio diffraction pattern's movement as being due to the neutral wind.

Recently much work has been carried out on signals partially reflected from the D-region. This is a weakly-ionized region below 90 km, thought to be produced by the ionization of nitric oxide by Lyman-α radiation from the sun, and by the ionization of the neutral atmosphere by solar x-rays and cosmic radiation. Measurements of the drifting diffraction pattern were first carried out by Fraser (1965, 1968). These patterns have been observed at Adelaide by the large aerial array, and shown to consist mainly of a small scale random structure (about 300 metres across) with a consistent direction of motion (Felgate, 1969). Comparisons of the drift velocities of these patterns with the drift velocity of the neutral wind determined by the radio meteor technique have been made by Rossiter (1970) for a number of

height ranges at different times of the year. While the two methods gave similar results, on some occasions (mostly in winter) definite discrepancies existed which were too large to be explained by the expected errors of the two methods. It has been suggested that the disagreement could be caused by internal gravity waves forming irregularities in the D-region, which are observed as partial radio reflections.

During the night, D-region reflections can be observed above 80 km. In Section 6.6 of this chapter results are presented of a comparison between the wind's north-south component, measured by observing meteor trails at both 1.98 MHz and 27 MHz, and the north-south movement of the radio diffraction pattern from the D-region and from a weak layer of sporadic E ionization. This ionization was largely transparent to the ordinary polarized radio wave but gave observable reflections when the extraordinary polarization was transmitted. Thus the observations of radio meteor echoes at 1.98 MHz were carried out using the ordinary polarization.

6.5 Wind Measurements

Wind measurements presented in this chapter were made with the Adelaide 27 MHz radio meteor system, and with the Buckland Park aerial array, used to measure D-region drifts as well as the movement of meteor trails and ionospheric irregularities at a frequency of 1.98 MHz. Most of the meteor echoes at 27 MHz lie between 80 km and 100 km. At 1.98

MHz the majority of meteor echoes were observed between 90 km and 110 km. Echoes from partial reflections were observed between 85 km and 105 km. Thus there was a reasonable overlap in the observed height ranges, so the results of the three methods could be compared.

6.5(a) 27 MHz Radio Meteor System

The amplitude and direction of the wind can be determined for each height range only after at least two echoes have been observed in that height range. In the following results all echoes observed in 5 km height intervals were grouped and used to determine the average wind acting during a specified period (about 2 hours), within each height range.

6.5(b) 1.98 MHz Radio Meteor Echoes

The methods employed to measure the phase changes and hence drifts of 1.98 MHz radio meteor echoes were described in Chapter 3. The aerial used had a narrow fan-beam response, (shown in Figure 7.1) and was sensitive to echoes in a north-south line or to echoes in an east-west line, depending on the array aerials chosen. Thus each echo gave the north-south or east-west component of the wind. Results are presented for all echoes with zenith angles greater than 20°. As the phase of the radio echo was recorded continuously there was virtually no lower limit to the velocity that could be measured. Further, the accuracy of the wind measurement was increased by averaging the reading over the life-time of the echo. This was typically five to ten seconds

in the case of specular meteor echoes and thirty to forty seconds in the case of slow rising echoes. However, with many slow rising echoes, interference effects made any reliable wind reading difficult. Thus most readings were made in the early stage of the echo's life before the trail became badly distorted. The effects of distortion can be seen in the echo shown in Figure 6.1 where the phase record shows the disruption caused by the interfering signal. It is interesting to note that the effects of interference can be allowed for with this echo. It was only when the interfering signals had the same amplitude that the record became completely unusable.

The results in this chapter were obtained at the same time as polarization results were being taken. It was then only possible to record one of the two components of the wind. Thus the following comparisons are made for a single component.

6.5(c) D-Region Drifts

Three aerials in the form of a right-angled triangle with the shorter sides 183 m long were used to sample the diffraction pattern. Each aerial consisted of four dipoles in the form of a square added in phase. The aerials of the Buckland Park array, used to form the triangle are shown in Figure 6.2. Most of the results were obtained by recording the amplitude of the signal that was within the range interval defined by a range gate. This signal was used to determine the level of a D-C signal which was recorded on a computer tape for analysis. The

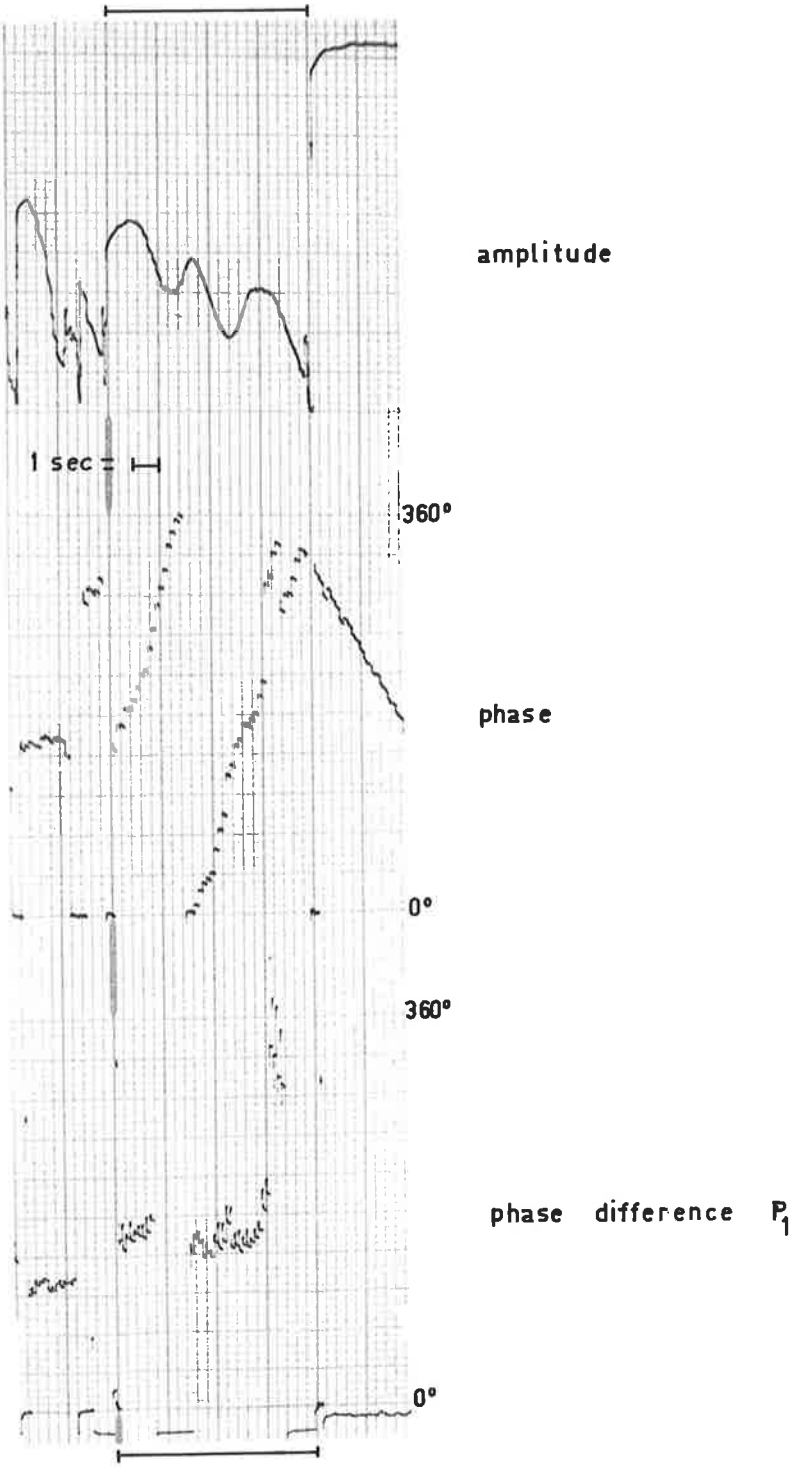

Figure 6.1 Interference effects.

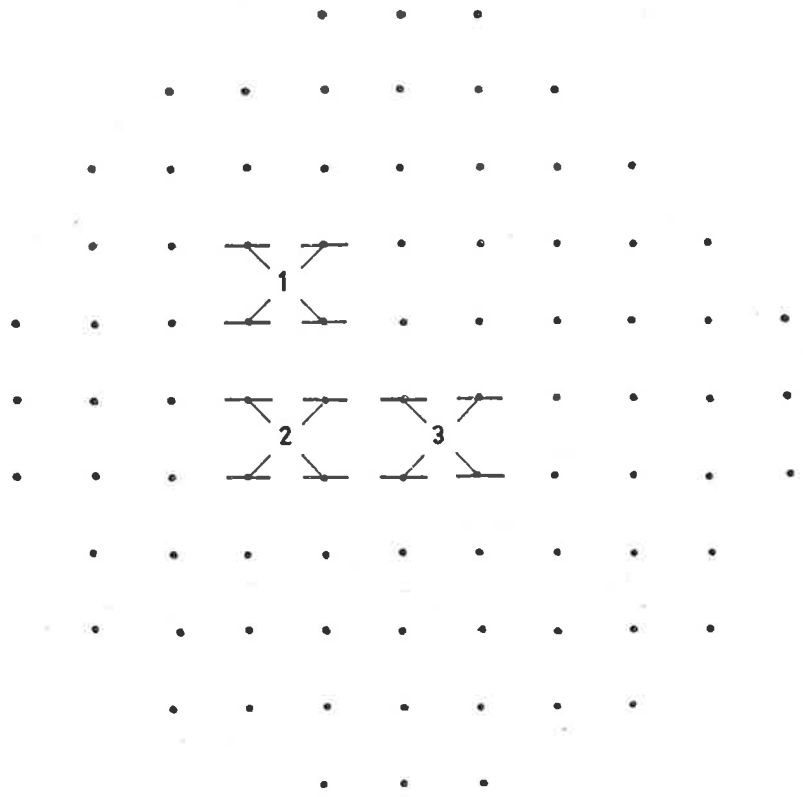

Figure 6.2 The aerial combination used to record the radio diffraction pattern from the ionosphere.

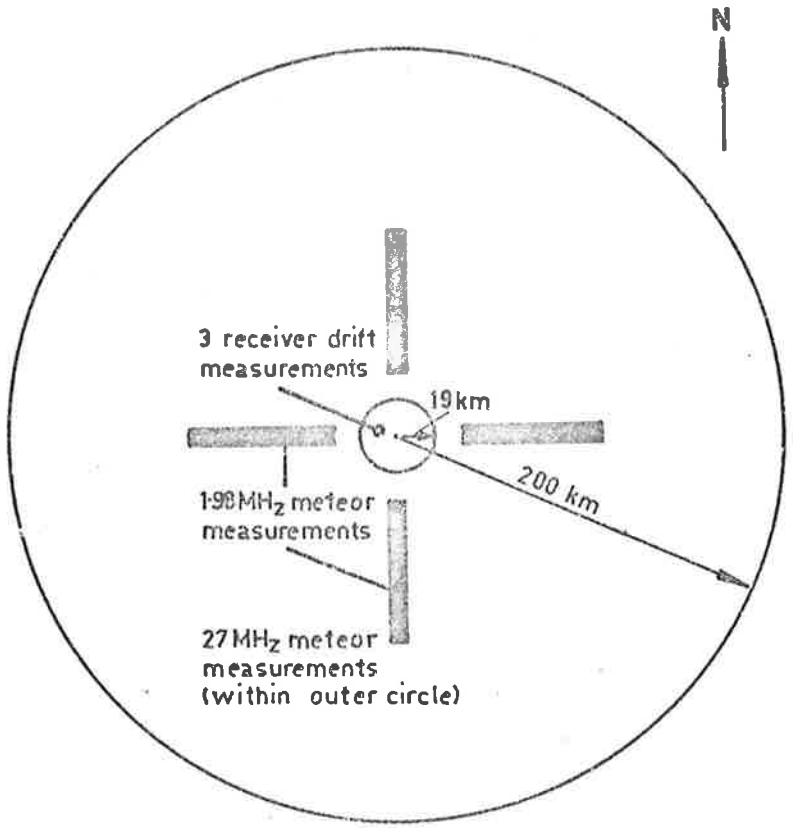

Figure 6.3 The regions in the sky where the three systems obtain wind readings, are shown projected onto the ground.

signals from the three aerials were correlated by full correlation analysis to determine the drift of the ionospheric irregularities.

6.6 Wind Height Profiles

The following results show the north or east component of the wind obtained from both slow and fast rising echoes observed at 1.98 MHz. No attempt has been made to average these results, as a plot of each value shows the scatter in the readings most clearly. Each value of the D-region drift found by the three receiver method has also been plotted. In the case of the 27 MHz meteor system, the number of meteor echoes grouped into each reading is shown by plotting this number instead of a symbol.

The projections onto the ground of the regions in the atmosphere where ionospheric and meteor echoes are observed, are shown in Figure 6.3 for the three systems.

In Figures 6.4(a) to 6.4(g) wind-height plots are shown for six days when only the 1.98 MHz system was operated. Figures 6.5(a) to 6.5(d) show plots for four days when the 27 MHz meteor system was also in operation, while Figures 6.6(a) to 6.6(e) show profiles for six days when all three systems operated. The particular days for which data was obtained are shown in Table 6.1. The wind component measured, and the time interval for which it was measured, are also shown. In the last column of this table the profile has been given a number to roughly classify it. This number system is:

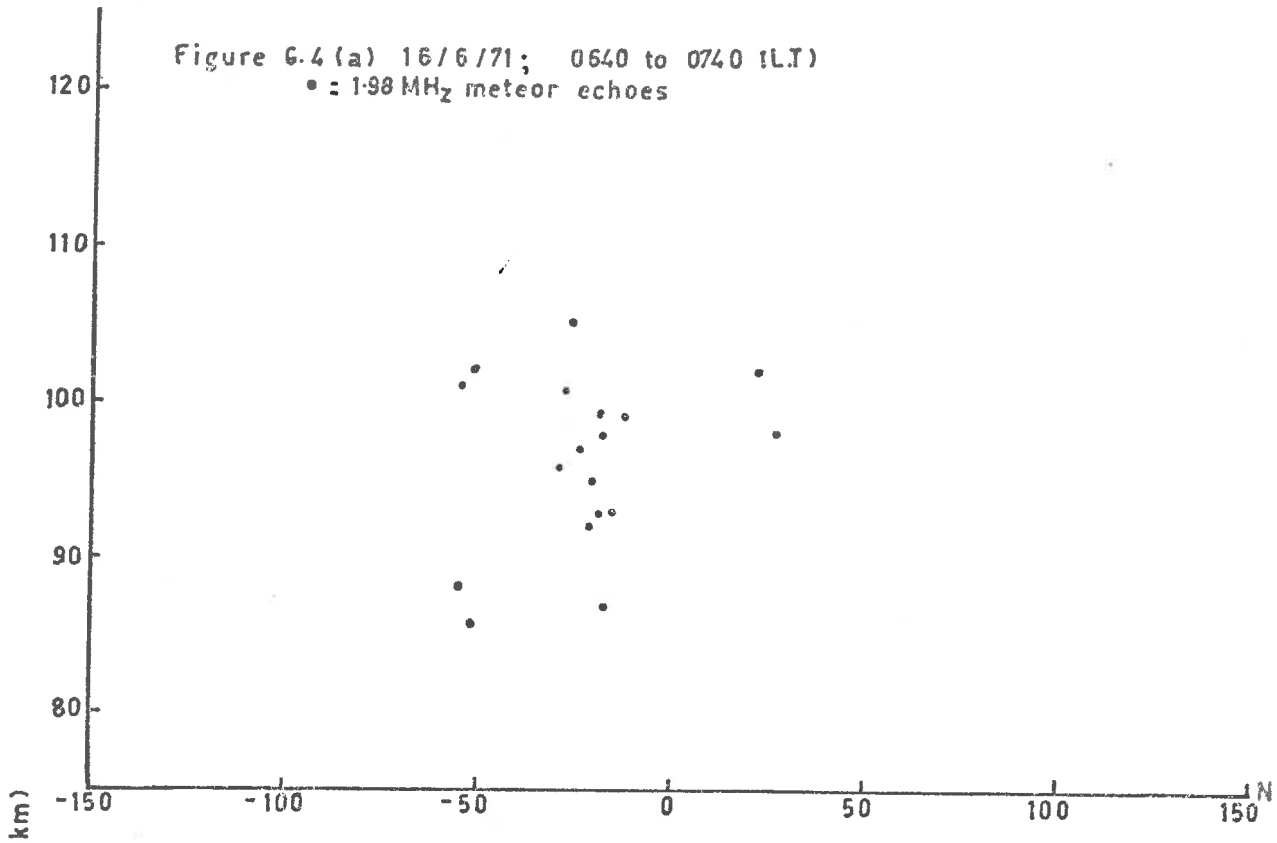

Figure 6.4 (a) 16/6/71; 0640 to 0740 (L.T)
• : 1·98 MHz meteor echoes

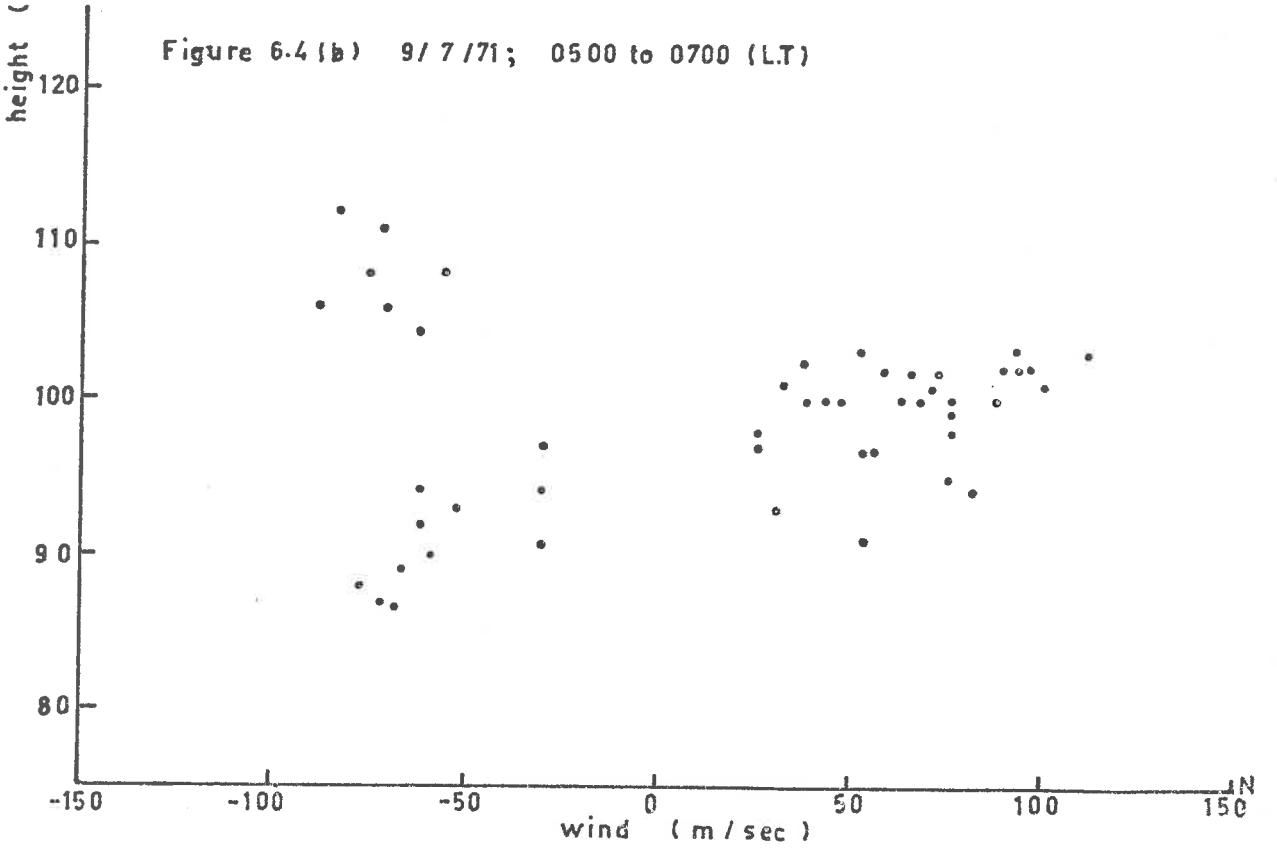

Figure 6.4 (b) 9/7/71; 0500 to 0700 (L.T)

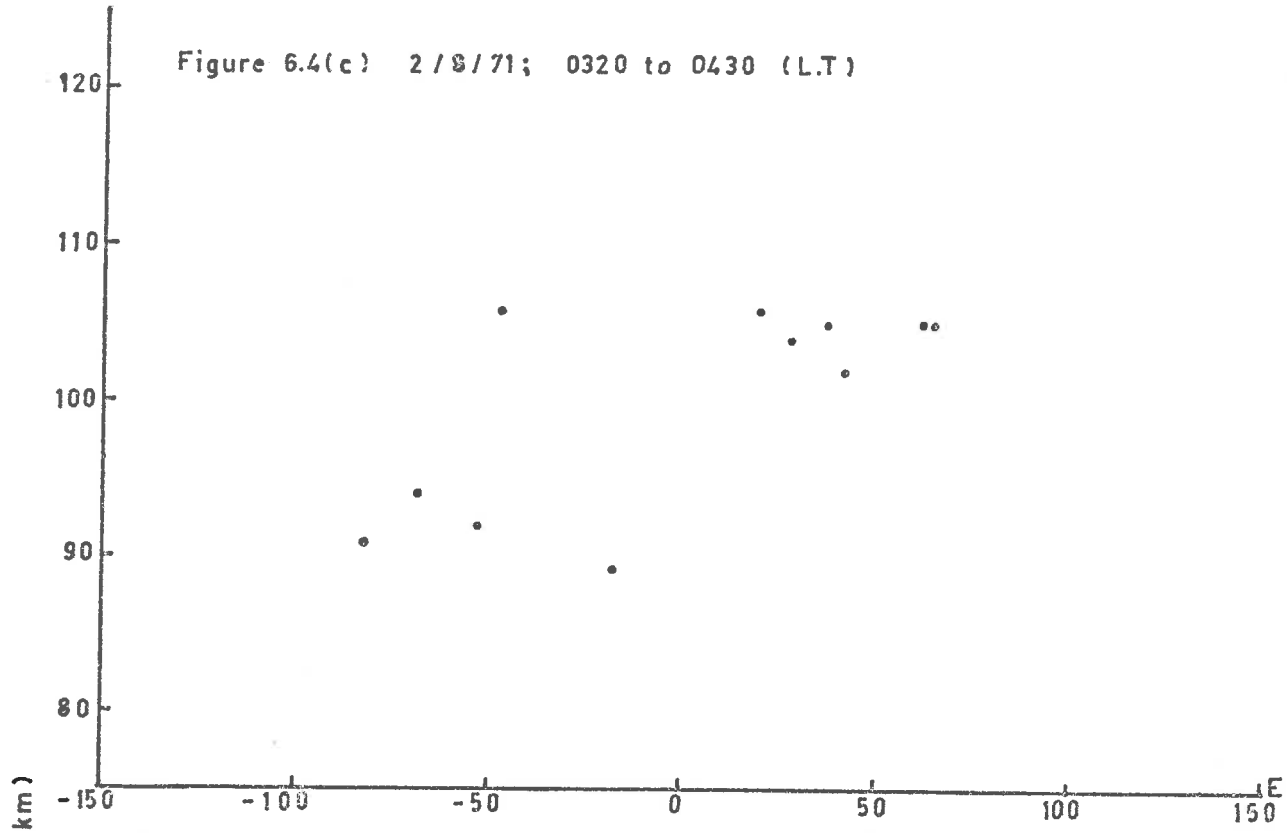

Figure 6.4(c) 2/8/71; 0320 to 0430 (L.T)

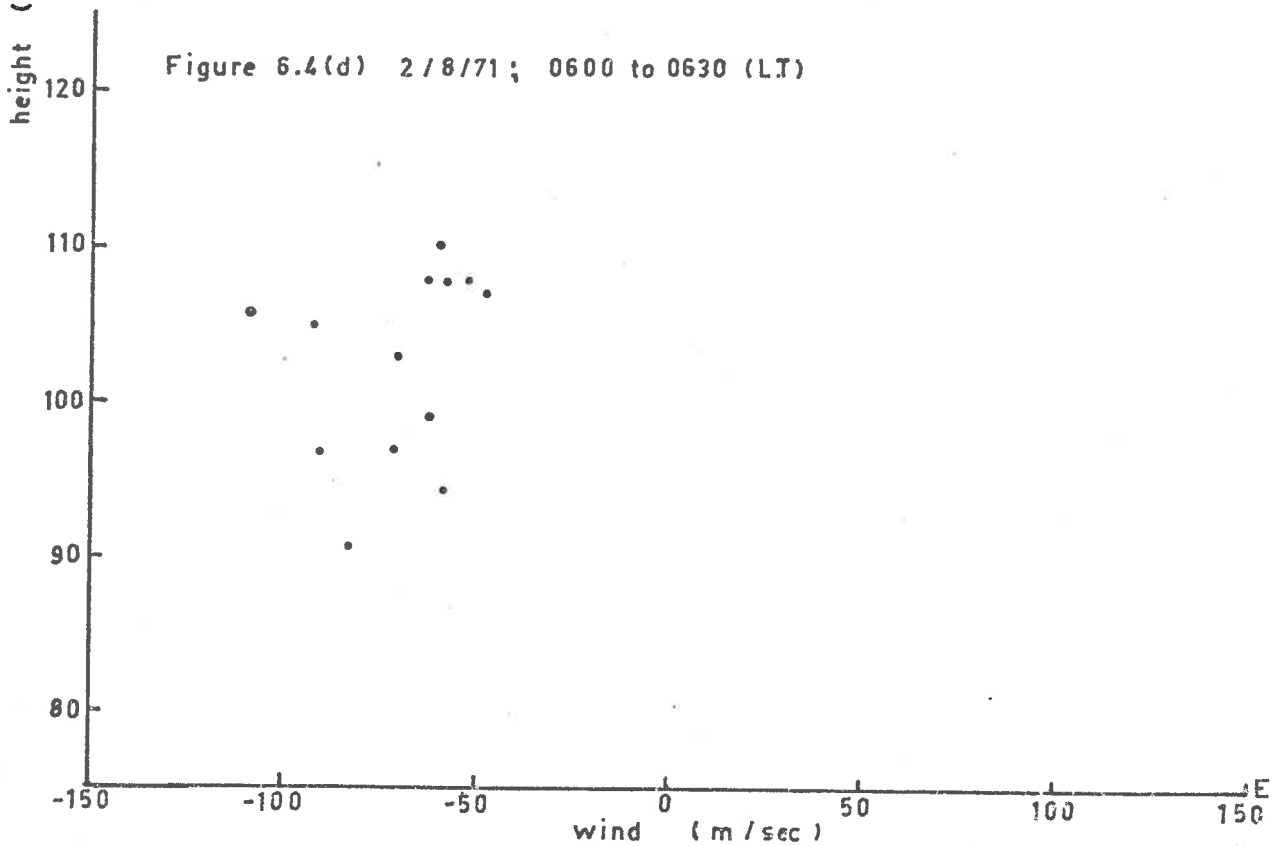

Figure 6.4(d) 2/8/71; 0600 to 0630 (LT)

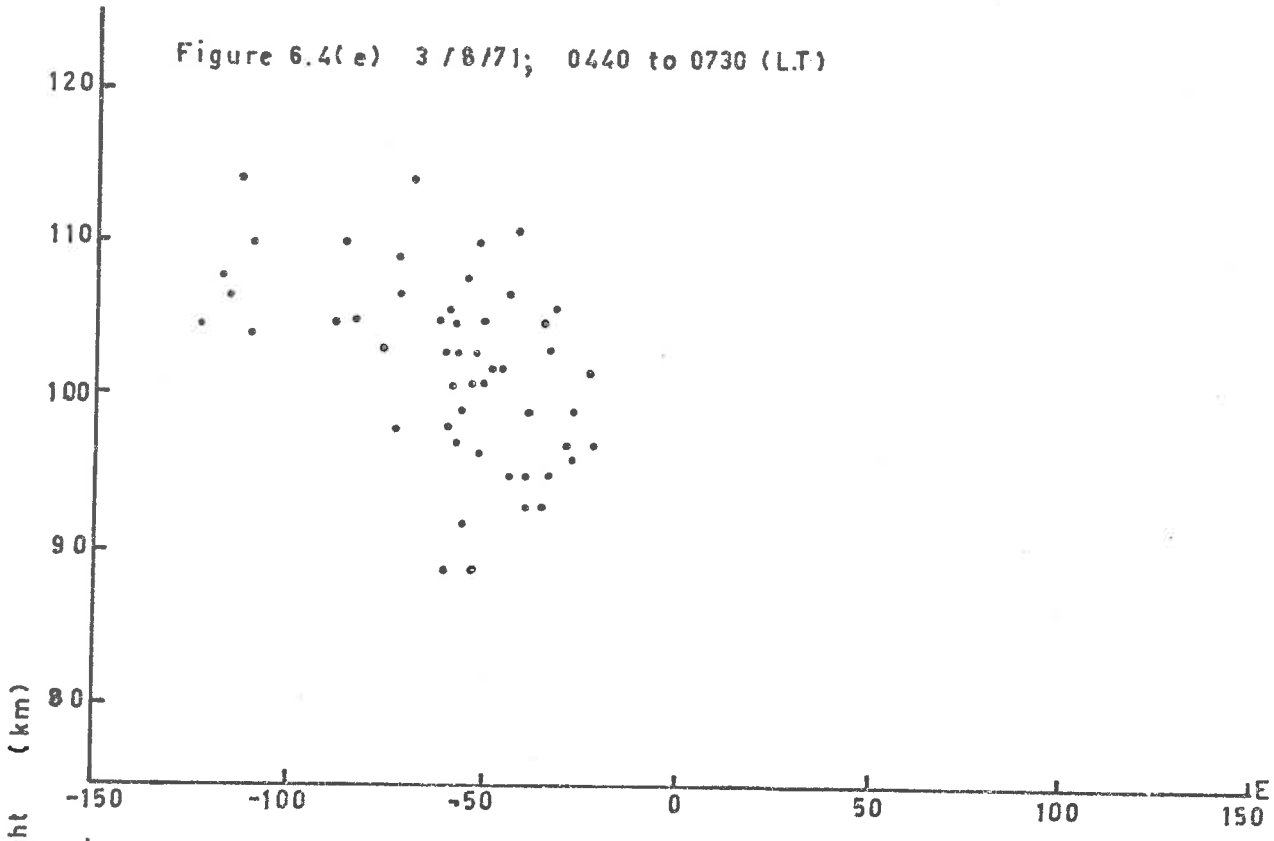

Figure 6.4(e) 3/8/71; 0440 to 0730 (L.T)

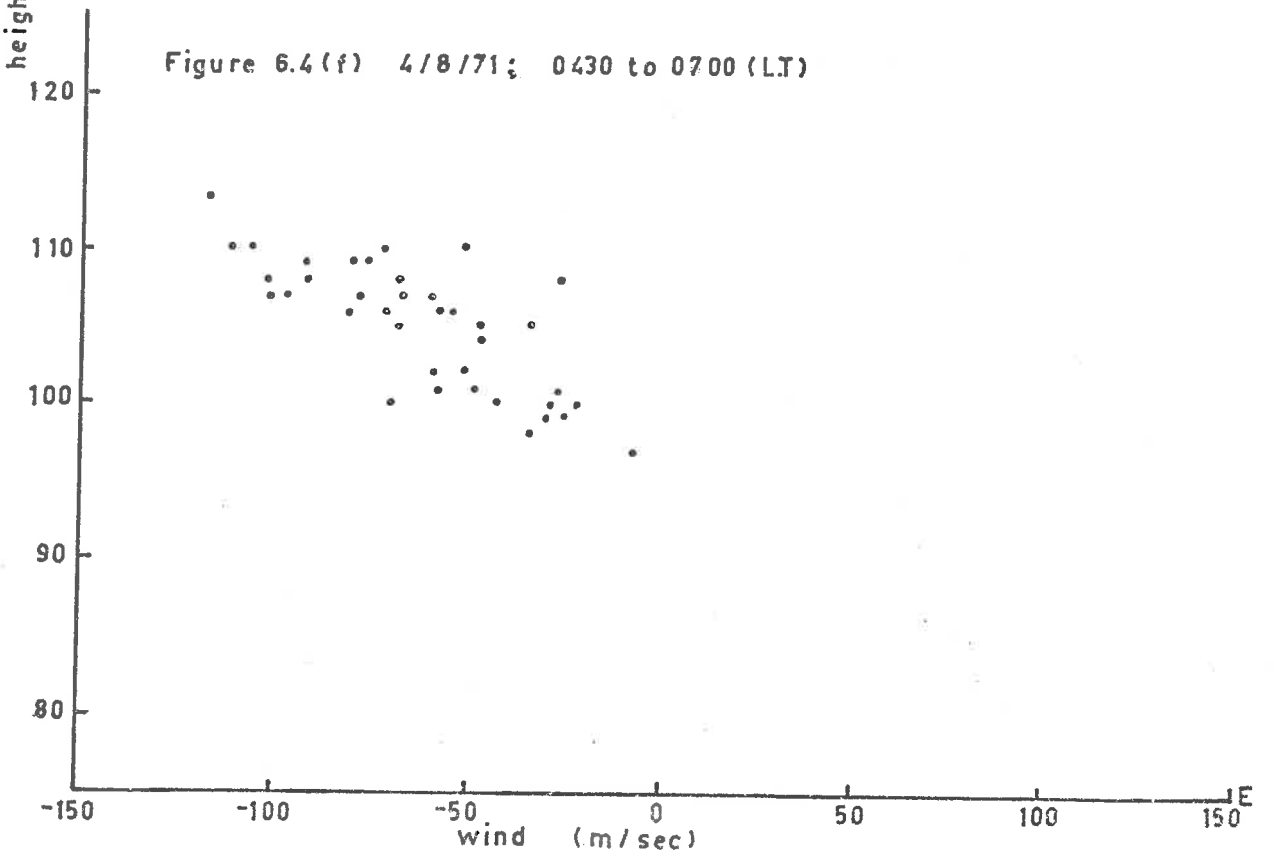

Figure 6.4(f) 4/8/71; 0430 to 0700 (L.T)

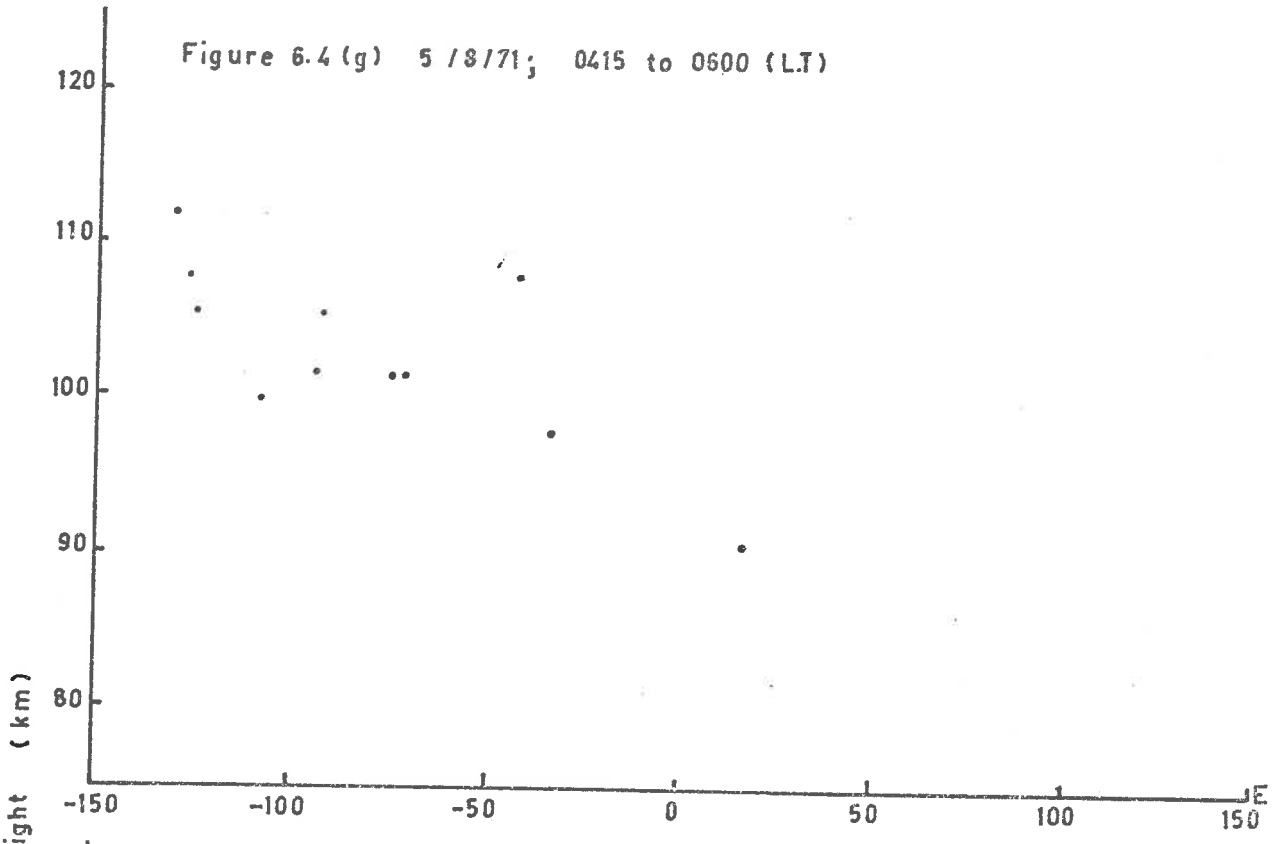

Figure 6.4 (g) 5/8/71; 0415 to 0600 (L.T)

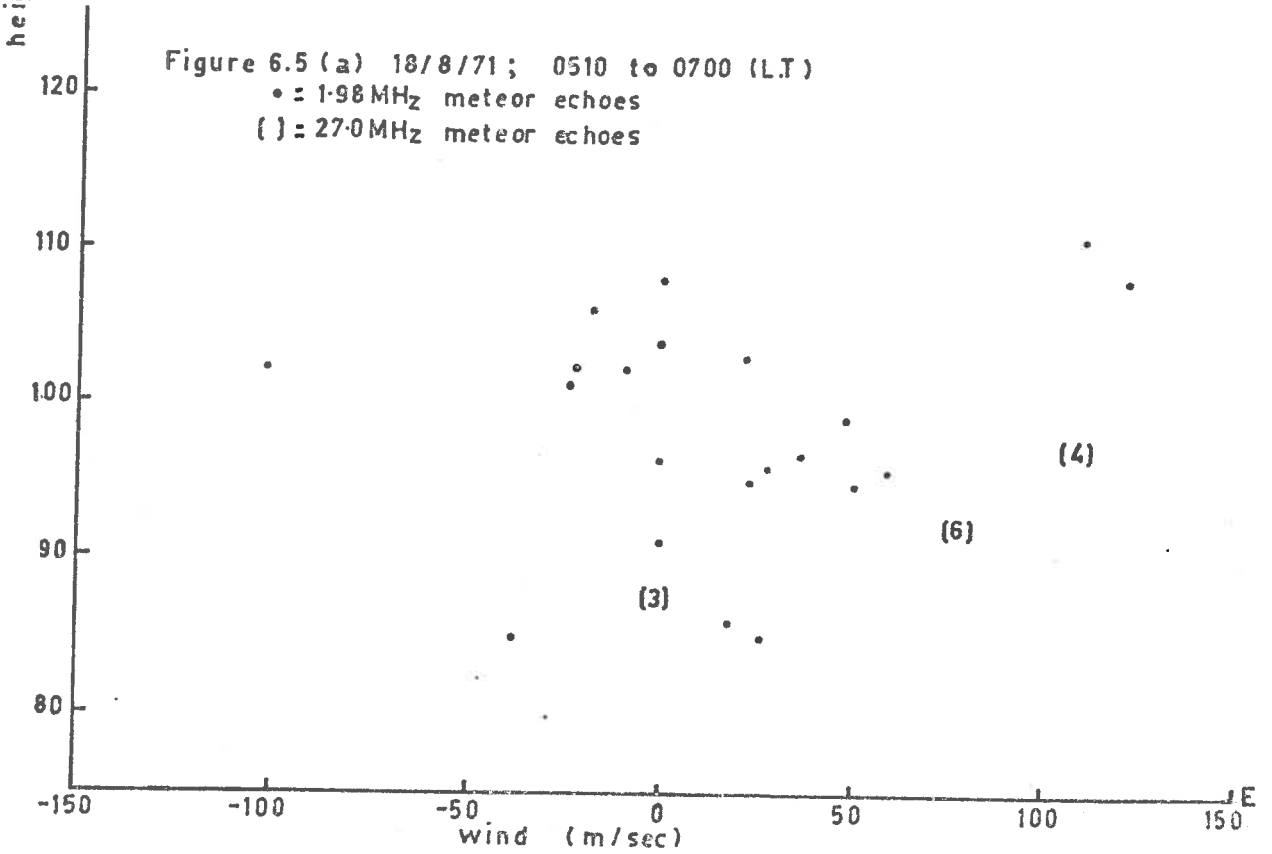

Figure 6.5 (a) 18/8/71; 0510 to 0700 (L.T)
• : 1·98 MHz meteor echoes
( ) : 27·0 MHz meteor echoes

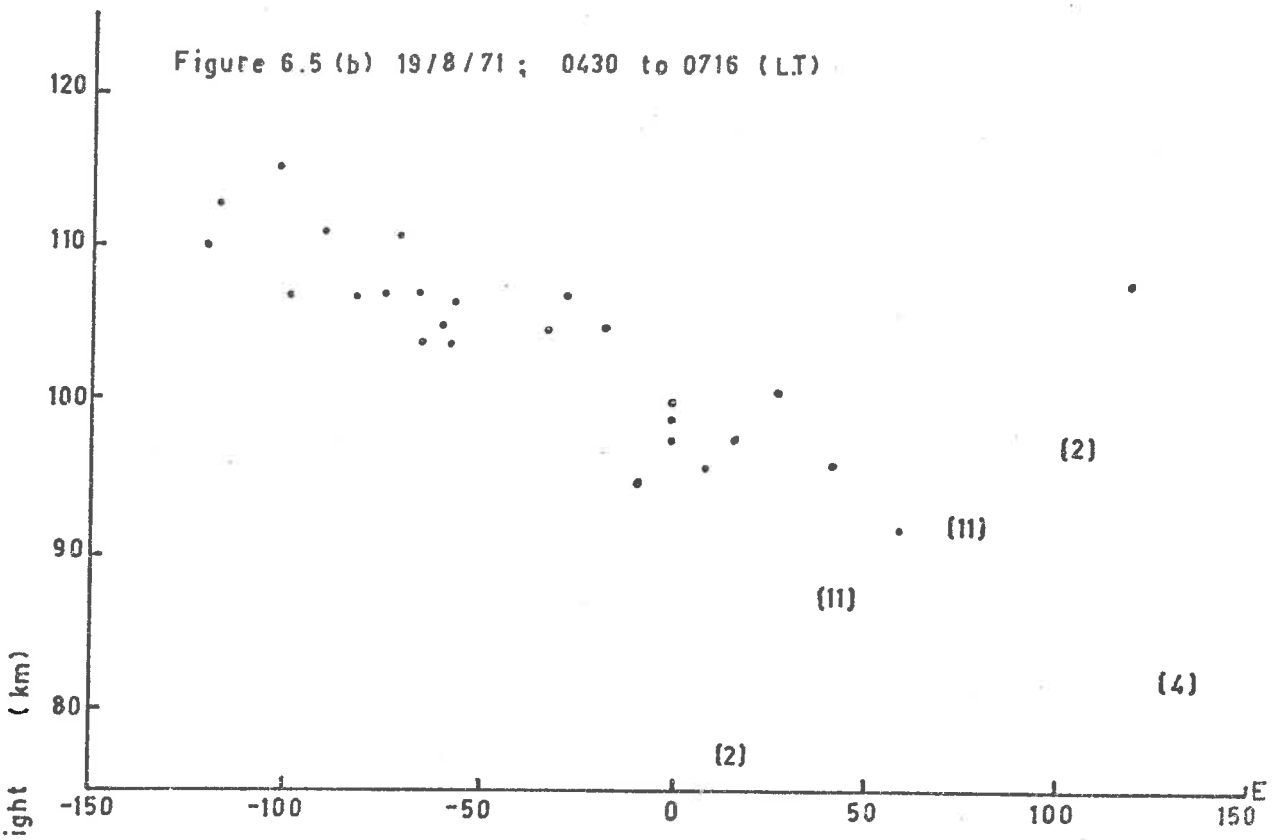

Figure 6.5 (b) 19/8/71 ; 0430 to 0716 (LT)

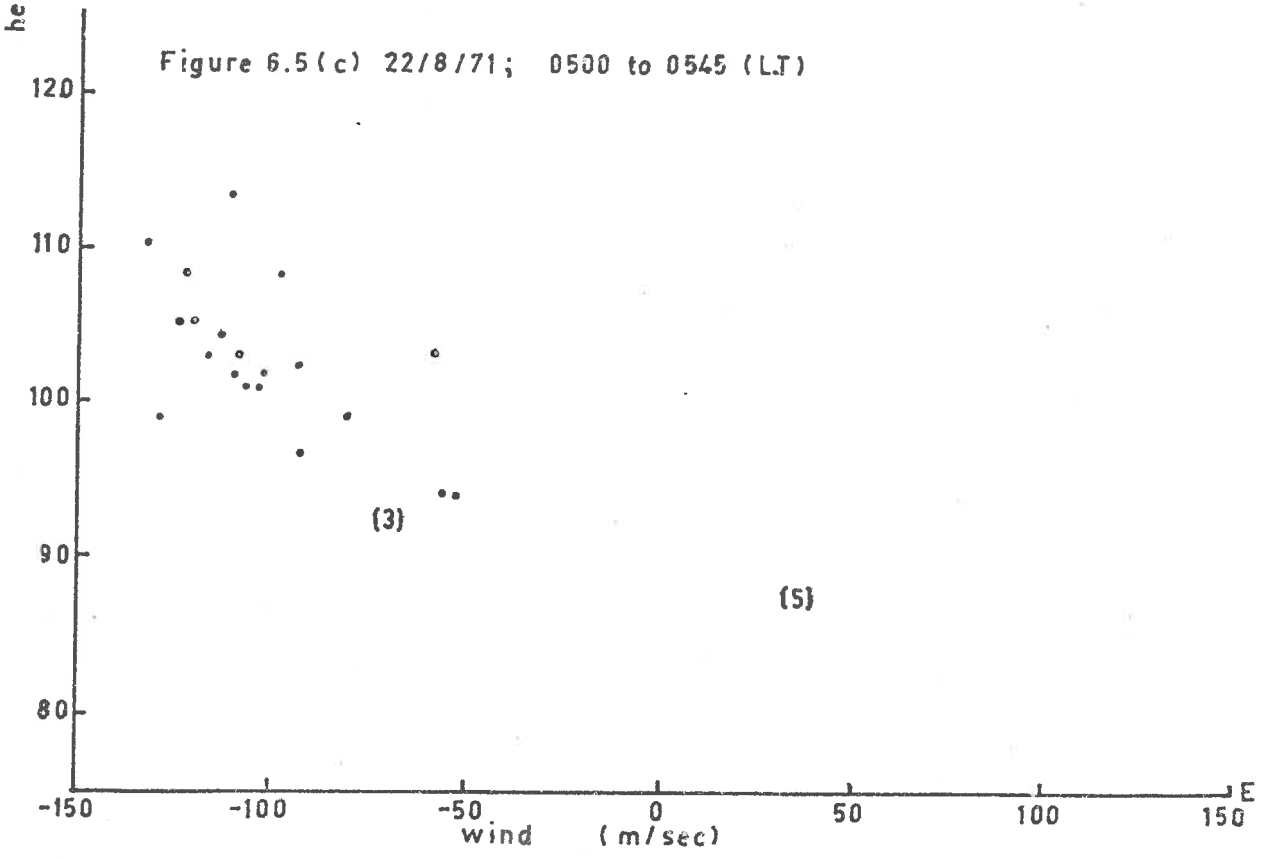

Figure 6.5 (c) 22/8/71; 0500 to 0545 (LT)

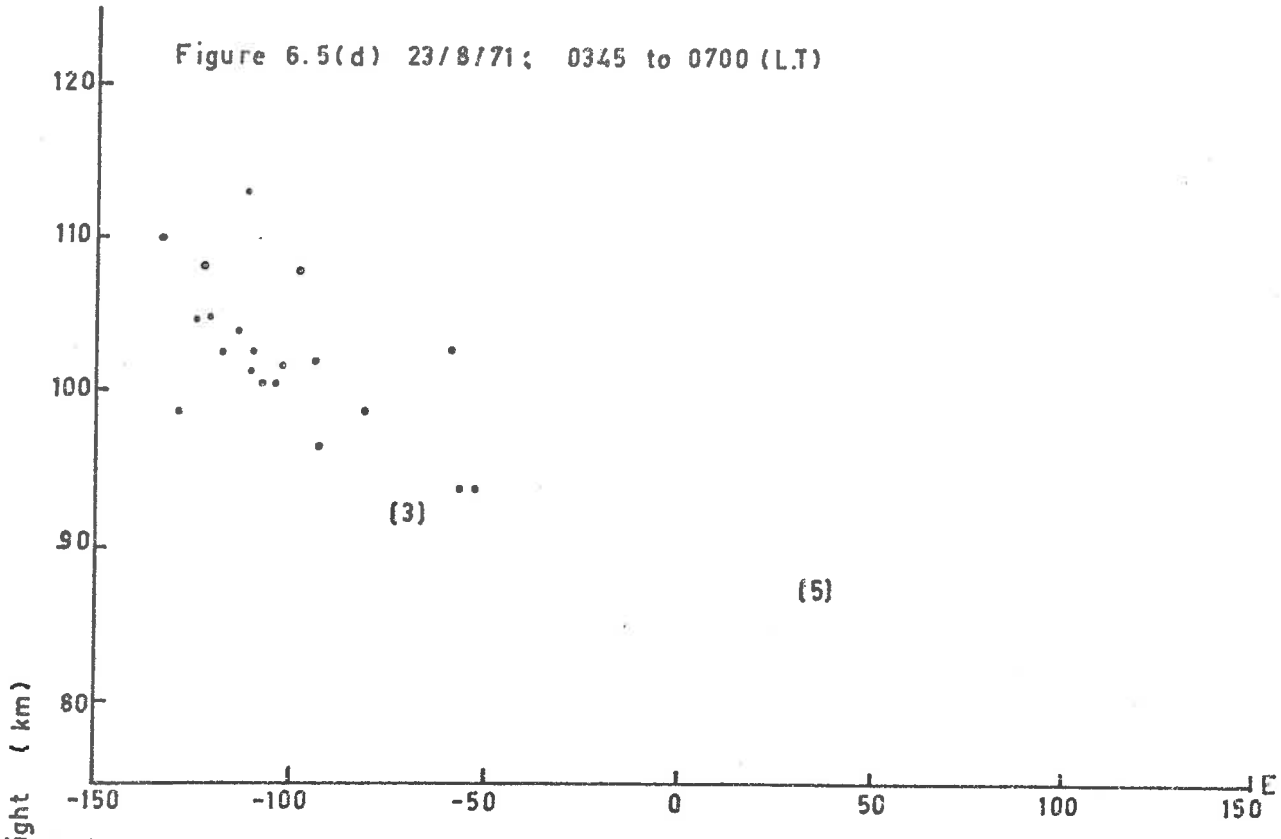

Figure 6.5(d) 23/8/71; 0345 to 0700 (L.T)

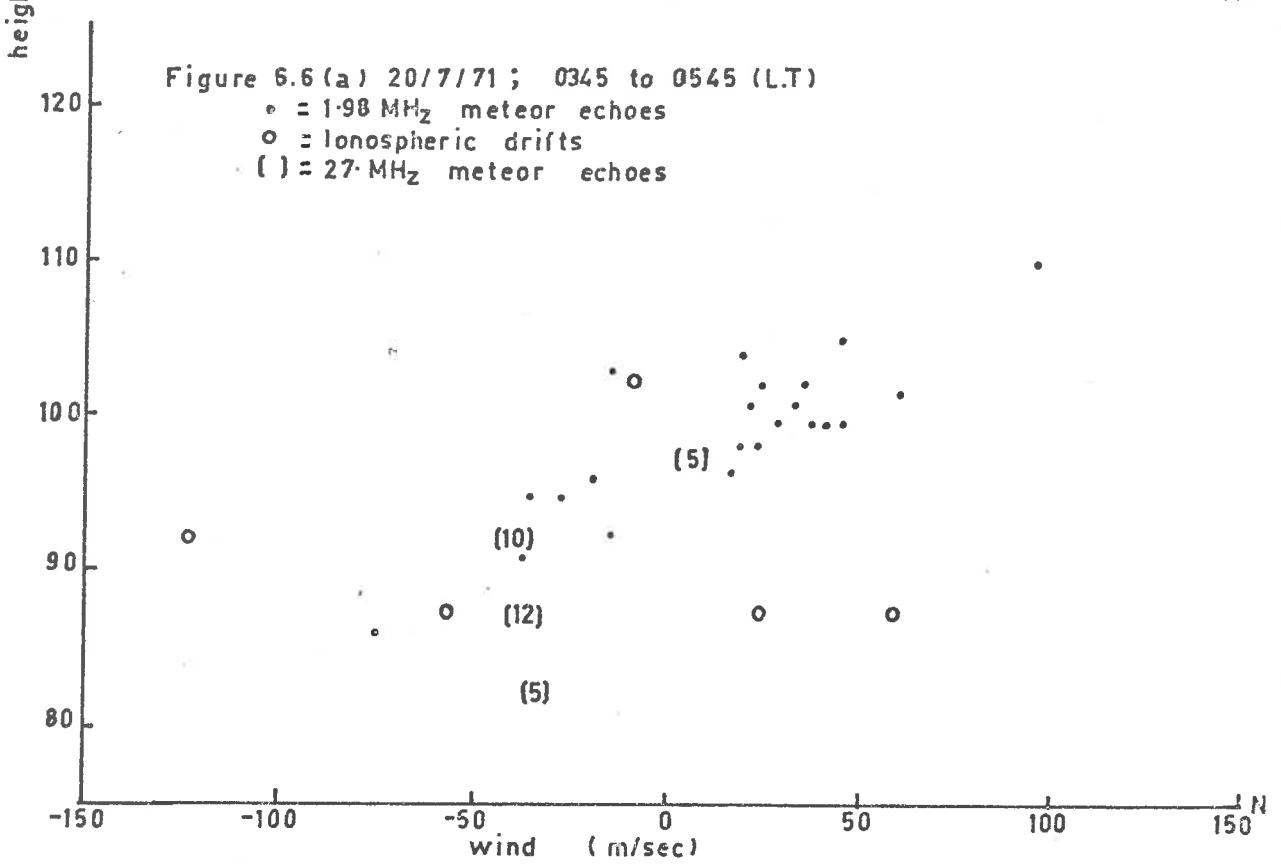

Figure 6.6(a) 20/7/71; 0345 to 0545 (L.T)
• = 1·98 MHz meteor echoes
o = Ionospheric drifts
( ) = 27·MHz meteor echoes

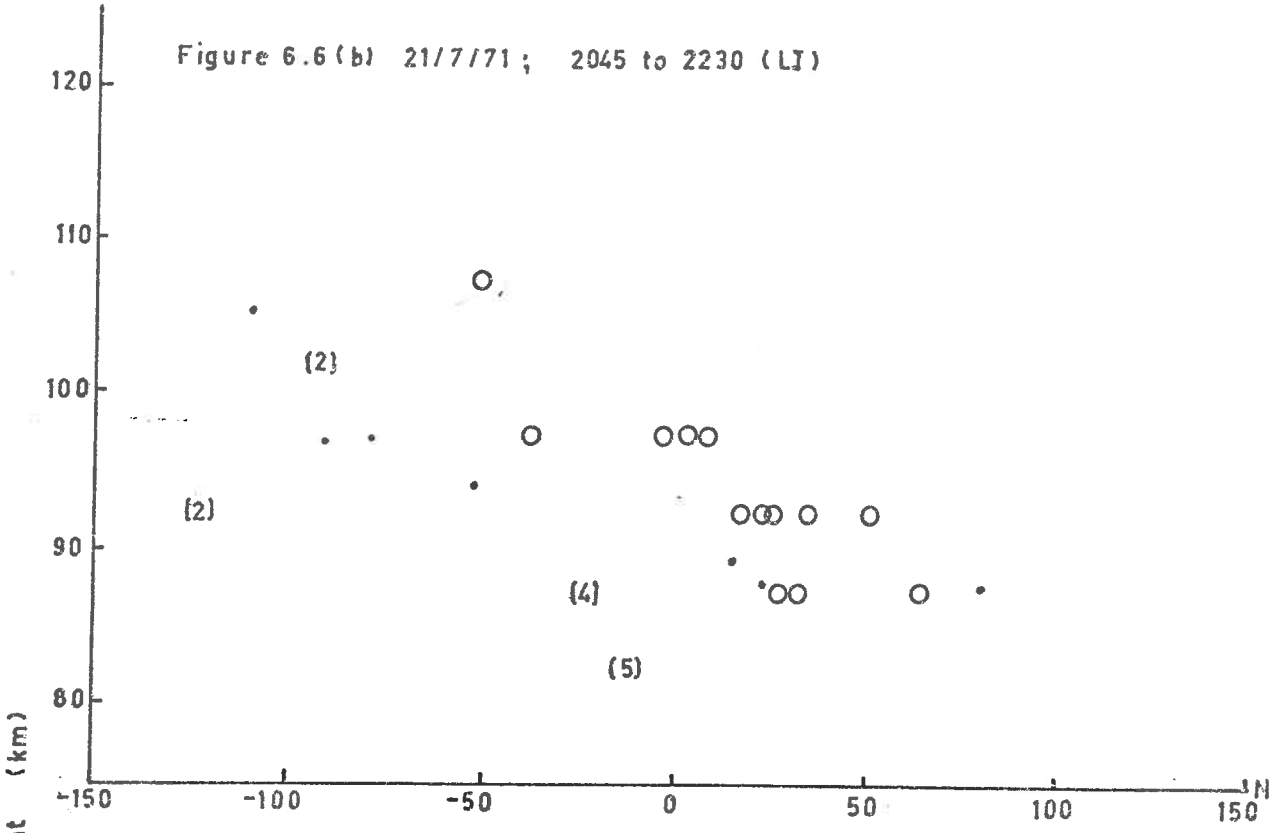

Figure 6.6 (b) 21/7/71 ; 2045 to 2230 (LT)

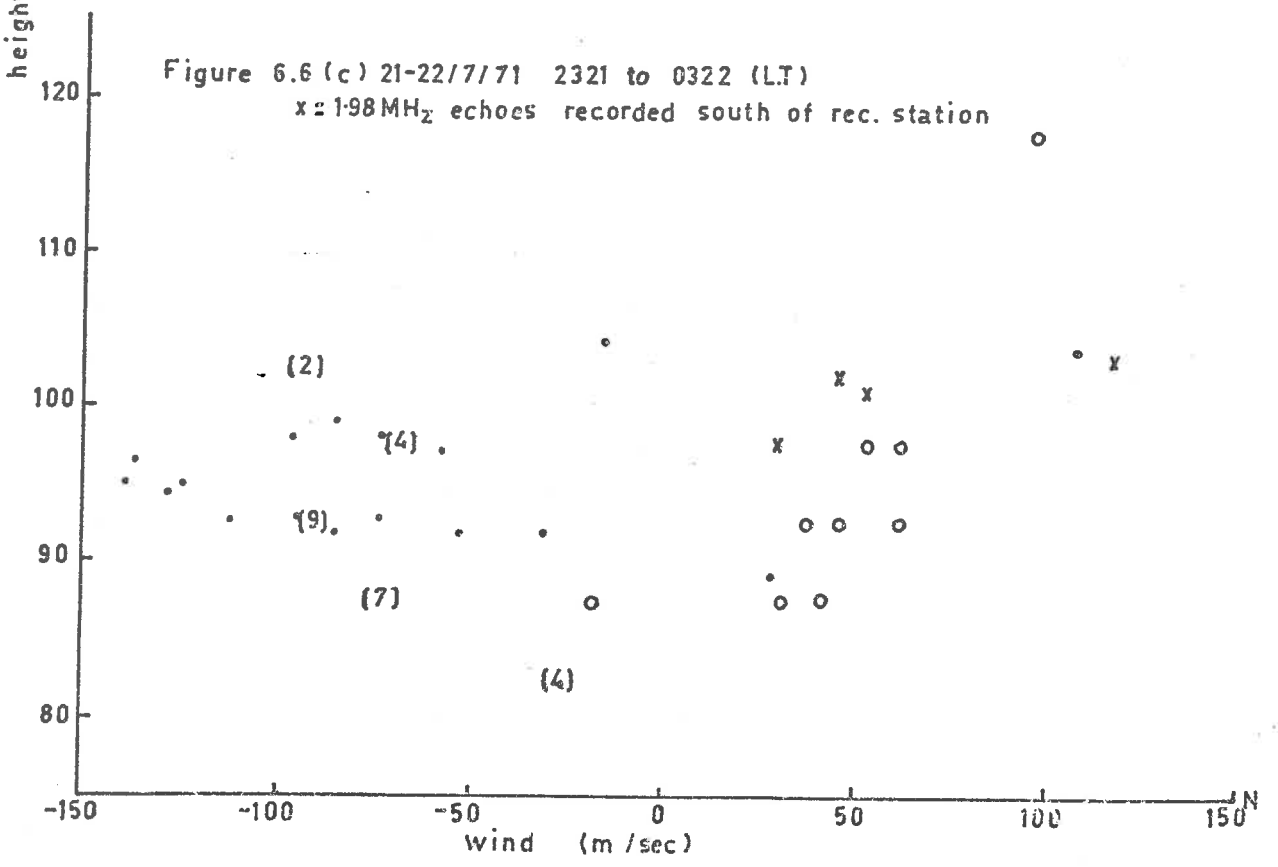

Figure 6.6 (c) 21-22/7/71 2321 to 0322 (LT)
x : 1·98 MHz echoes recorded south of rec. station

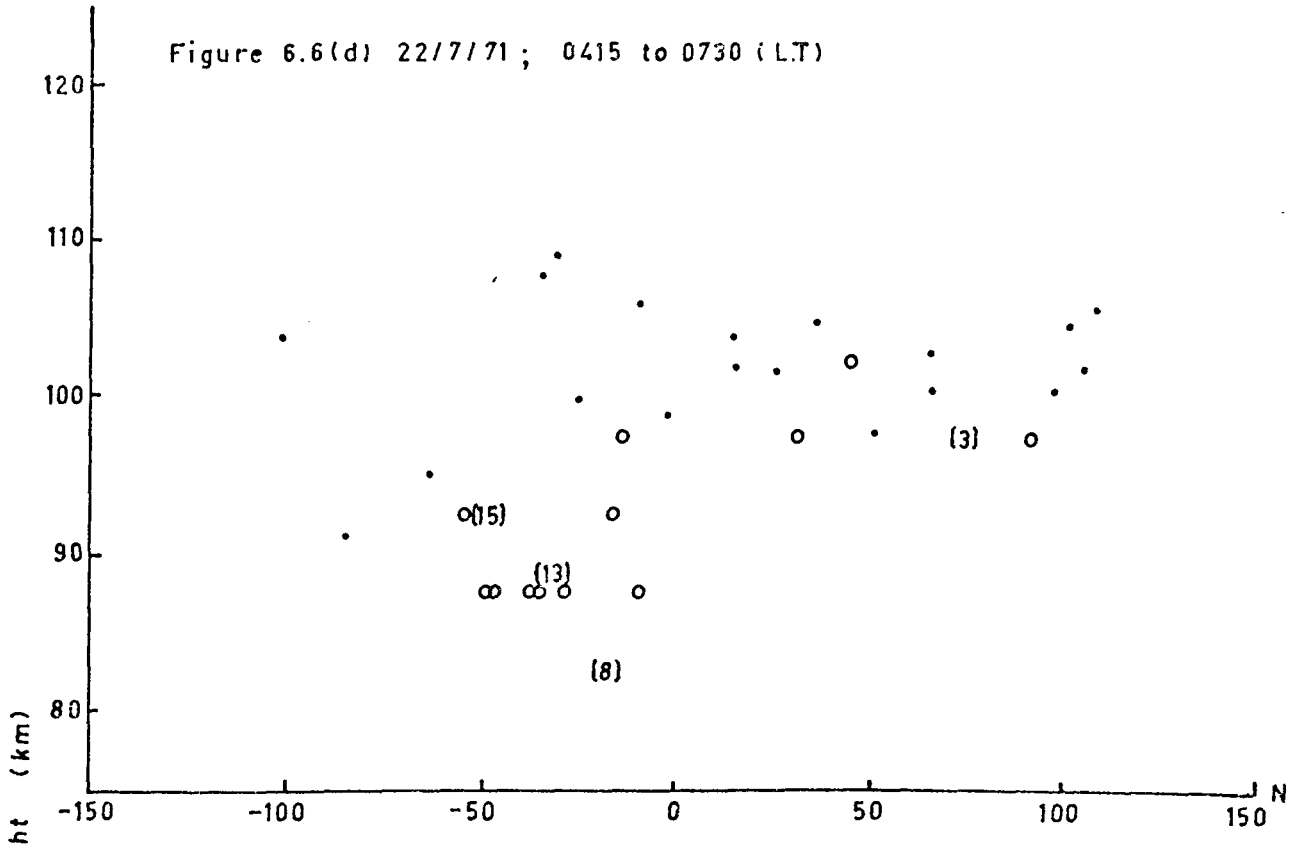
Figure 6.6(d) 22/7/71 ; 0415 to 0730 (L.T)
120
110
100
90
80
height (km)
(3)
(15)
(13)
(8)
-150
-100
-50
0
50
100
150
N

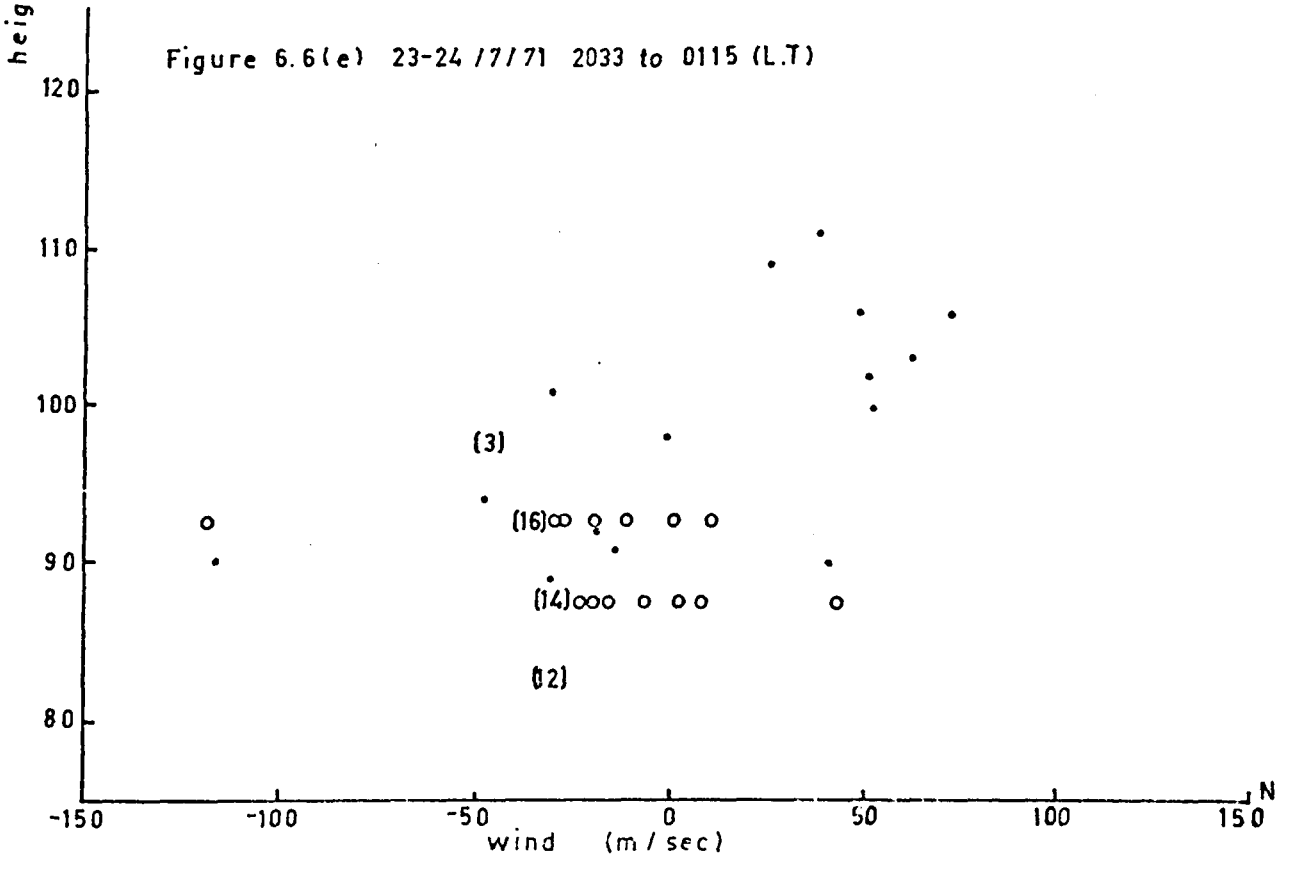
Figure 6.6(e) 23-24 /7/71 2033 to 0115 (L.T)
120
110
100
90
80
(3)
(16)
(14)
(12)
-150
-100
-50
0
50
100
150
N
wind (m / sec)

1. For little change with height.
2. For an apparent linear change with height.
3. Where the change with height is more complex than the linear model.
4. Where a scatter in the readings indicates a change in the wind during the recording period.

This classification of the profiles only describes the behaviour of the wind's component and not the wind itself. However, one component of the wind is sufficient for the purpose of a comparison. In Table 6.2 a comparison is made between the three methods of measuring the wind using the numbers:

1. To indicate a close agreement.
2. To indicate that the data points are fairly scattered, yet the agreement remains close.
3. Where the methods show the same trend without overlapping sufficiently in their height ranges to be covered by 1.
4. Where 3 would apply if the points were not as scattered.
5. For a disagreement.

6.7 Discussion

In most cases the wind component measured by the 27 MHz meteor system agrees well with that measured by the 1.98 MHz system. Only on one occasion was there a marked disagreement, (Figure 6.4(a)) and this occurred on a morning when little trend in the wind was evident. This indicates that there were one or more changes in the wind pattern

Table 6.1

FIGURE	DATE	TIME Start	TIME Finish	INTERVAL	WIND COMPONENT	PROFILE TYPE
6.4 (a)	16/6/71	0640	0740	0100	north	1
(b)	9/7/71	0500	0700	0200	north	3
(c)	2/8/71	0320	0430	0110	east	2
(d)	2/8/71	0600	0630	0030	east	1
(e)	3/8/71	0440	0730	0250	east	1
(f)	4/8/71	0430	0700	0230	east	2
(g)	5/8/71	0415	0600	0145	east	2
6.5 (a)	18/8/71	0510	0700	0150	east	4
(b)	19/8/71	0430	0716	0246	east	2
(c)	22/8/71	0500	0545	0045	east	2
(d)	23/8/71	0340	0700	0320	east	2
6.6 (a)	20.7.71	0345	0545	0200	north	2
(b)	21/7/71	2045	2230	0145	north	2
(c)	21/7/71	2321	0322	0401	north	4
(d)	22/7/71	0415	0730	0315	north	4
(e)	23/7/71	2033	0115	0442	north	4

Table 6.2

FIGURE	DATE	COMPARISON WITH 27 MHz METEORS	3 RECEIVER DRIFTS
6.5 (a)	18/8/71	5	
(b)	19/8/71	3	
(c)	22/8/71	3	
(d)	23/8/71	1	
6.6 (a)	20/7/71	1	5
(b)	21/7/71	2	2
(c)	21/7/71	2	5
(d)	22/7/71	4	1
(e)	23/7/71	4	2

during the two hour period. In contrast to this, the following morning (Figure 6.4(b)) showed a consistent wind shear of about 8 m/sec/km throughout the recording period of almost three hours.

The agreement between the 3 receiver D-region drifts and the meteor wind profile was poor on two occasions. On the first of these (20.7.71; Figure 6.6(a)) three of five readings made within the period disagree with the profile shown by both the 27 MHz and 1.98 MHz meteor systems. On the second occasion (21.7.71; Figure 6.6(c)), readings were made over a four hour period. There is evidence that the wind was changing during this period in a manner which cannot be determined because of an insufficient echo rate. Most of the 1.98 MHz meteor echoes observed north of the receiving station show the northern component of the wind to be near - 100 m/sec. This is supported by the 27 MHz meteor system. However, 1.98 MHz meteor echoes observed south of the receiving station show that at a height of 100 km the wind component is 50 m/sec and this is supported by the 3 receiver drift measurements. It is therefore possible that during the four hour period the wind had a small horizontal scale. As the three systems obtain wind readings from different volumes of the sky (Figure 6.3), a disagreement is liable to occur on these occasions. A close inspection of the 1.98 MHz wind readings did not show any trend with time; the four southerly readings occurred over the four hour period, while the 3 receiver readings were obtained on the hour and half hour, so they were evenly spaced in time.

It was shown in Chapter 4 that an unusual number of overhead echoes occurred on 9.7.71; 21.7.71; and 22.7.71. The presence of overhead echoes indicates turbulent wind conditions as the meteor trails have to be distorted at a rapid rate by the wind for overhead echoes to occur before the ionized column becomes too diffuse. On the 9.7.71 the wind's northern component changed direction twice in a 20 km height range. The two hour period was split into short time intervals and replotted to show a possible change in the wind during the period of observation. However, none could be detected. The wind on 21.7.71 and 22.7.71 showed a smaller wind shear than that which existed on the 9.7.71, however there is evidence of a small horizontal wind structure on 21.7.71.

CHAPTER 7

METEOR RADIANT COMPARISONS

7.1 Introduction

The system used to observe meteor echoes at 1.98 MHz was a single station system with a fan aerial beam. Although it is not possible to determine the radiants of individual meteors, it is possible in principle to determine the radiants of shower meteors. This was attempted with the meteors observed at 1.98 MHz, although with little success, one of the major difficulties being the fact that the periods of observation were restricted to times when there was little or no sporadic-E ionization. During August (1971), when a number of showers were active, the average meteor rate was only 10 echoes/hour because of persistent D-region echoes between 85 and 100 km, while blanketing sporadic-E prevented any observation of the Geminids during December (1970).

The method used to group meteors from a particular radiant is discussed, and the results presented for a number of showers normally observed during August. The main concentrations of sporadic meteors were also considered, and their activity compared.

7.2(a) Aerial Polar Diagram

The polar diagram of the fan beam employed in this experiment cannot be easily determined experimentally because the far field, in

the case of the large aerial array at 1.98 MHz, is tens of miles from the aerial. A theoretical polar diagram was, however, calculated by assuming the ground to be a perfect reflector and by ignoring the effects of mutual reactance. The first assumption is based on the fact that the water table at Buckland Park is close to the surface during the winter, while the mutual reactance between adjacent aerials has been measured and found to be small. The results of these calculations are given in Figure 7.1(a) where a density plot shows the response in three dimensions of an eleven element row of dipoles added in phase. In Figure 7.1(b) two cross-sections are plotted to show more clearly the shape of the beam and the strength of the side lobes. These are all plots of the amplitude response, as it was the signal's amplitude which was observed. The dipoles could be added so that their polarization was parallel or perpendicular to the fan beam. This altered the polar diagram as well as the polarization, and the effect is shown in Figure 7.1(b) where the polar diagram for the case of the polarization perpendicular to the fan beam is shown as a dashed line. The side lobes are 17 db down on the main beam and have been neglected in the analysis.

The polar diagram of the transmitter is shown in Figure 4.1 for ordinary (right hand circular) polarization. The percentage of extra-ordinary polarization (left hand polarization) transmitted when the aerial elements are phased to transmit the ordinary polarization is also shown. It can be seen that the extraordinary polarization is only

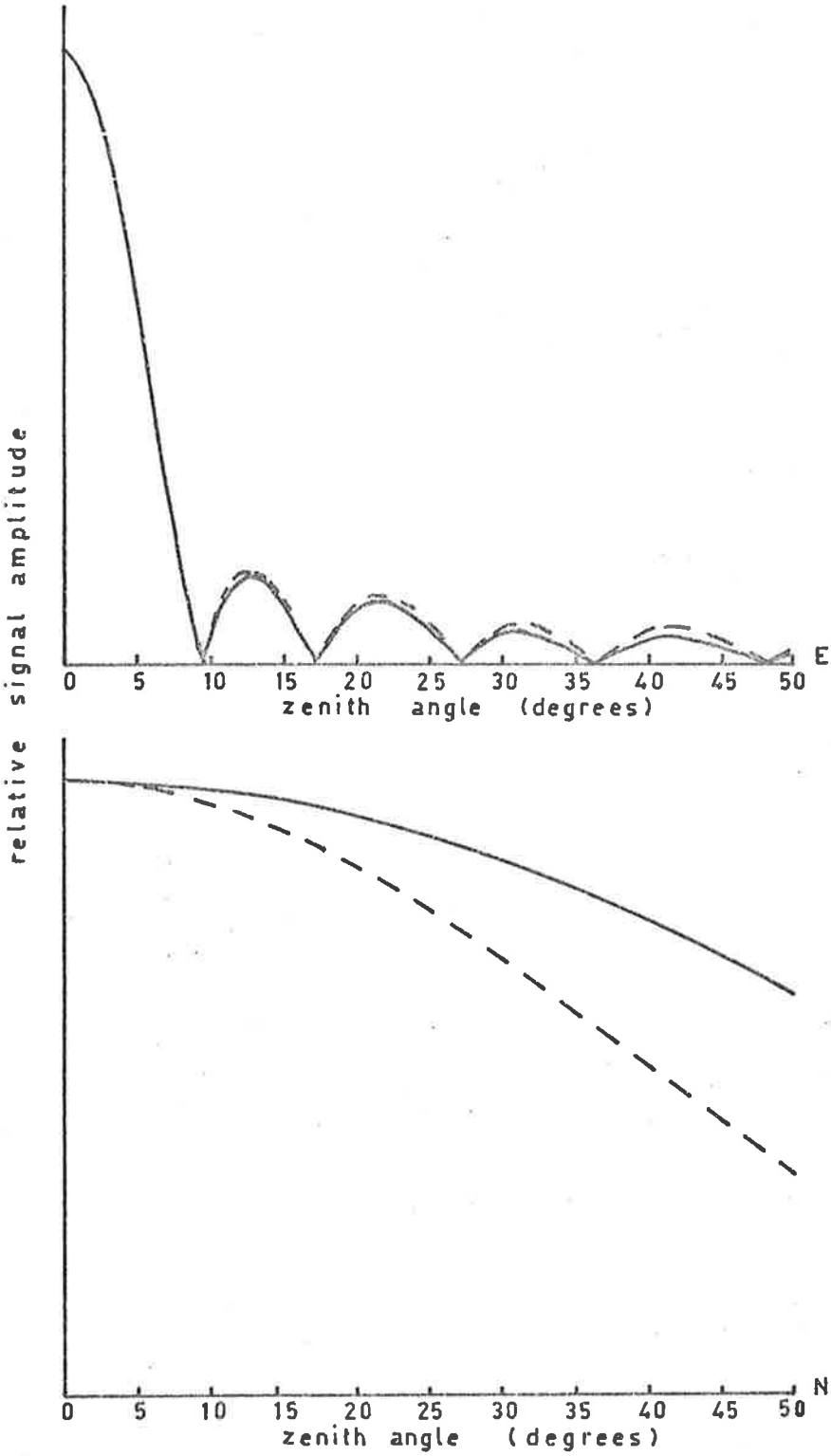

Figure 7.1(b) The amplitude response of the north aerial beam, the row of dipoles being aligned along an east-west line. Both polarizations are shown (dipoles aligned with the row shown as a continuous line).

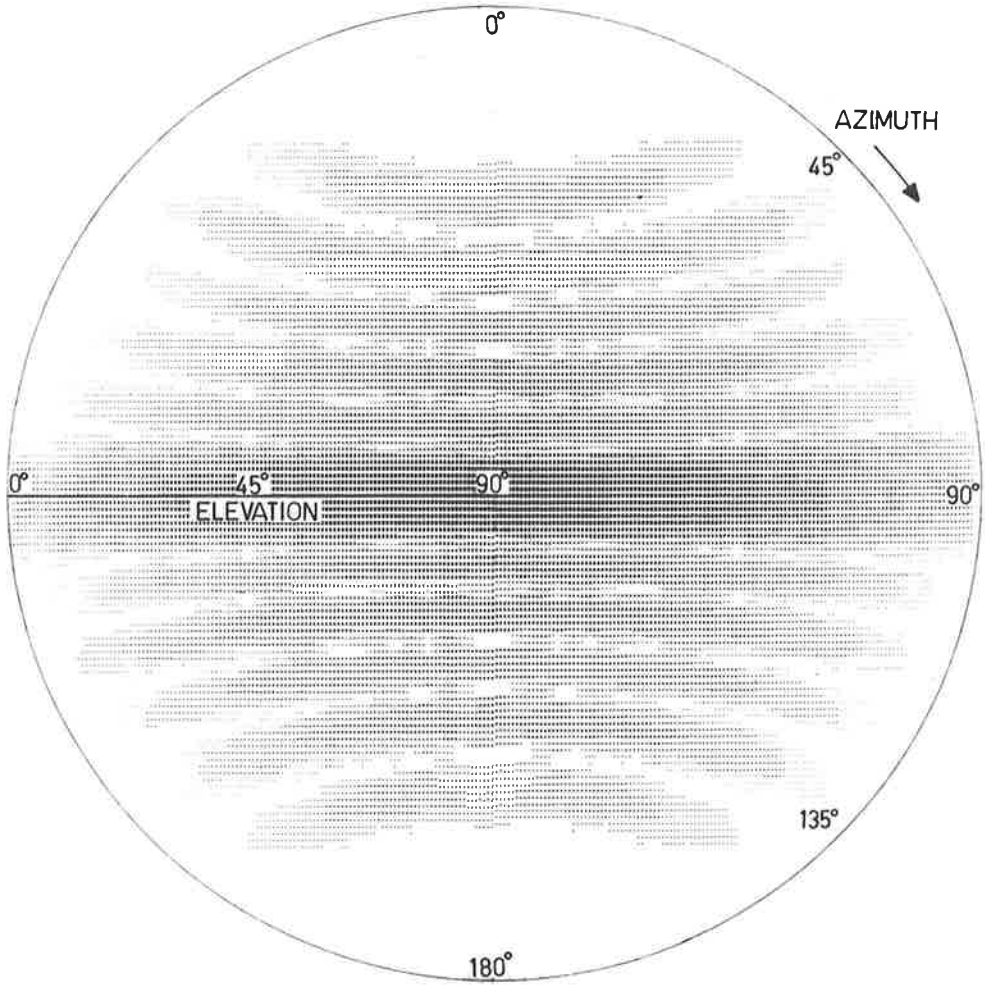

Figure 7.1(a) Aerial polar diagram.

important at large zenith angles. The polar diagram has approximately the same variation with zenith angle for all azimuth angles so only a section of the three dimensional polar diagram is shown.

7.2(b) Response Function of the System

The number of echoes to be detected from a radiant with a known elevation and azimuth is determined by several factors: the number distribution of meteors as a function of the maximum electron line density, the distribution of ionization along the trail, the nature of the reflection process, and the parameters of the radar system (such as the transmitted power, aerial polar diagrams and the limiting sensitivity of the receivers). Once these are specified, the relative response of the system can be determined for meteors from an element of the celestial sphere of unit radiant density. The response function of the system is the system's relative response to a unit radiant density placed at all possible elevations and azimuths. This problem was first considered by Kaiser (1954a, 1954b), while a computer method was developed by Elford (1964) for a system with a separated transmitter and receiver.

A meteor trail formed within the fan beam of the receiving aerial array will be detected if the orientation of the trail satisfies the geometrical conditions of specular reflection and the echo exceeds the threshold level of the system (set by the scanning gate described in Chapter 3). The condition of specular reflection for echoes from a

specified radiant is satisfied by all those meteors which form trails through the region defined by the intersection of the echo plane for the radiant and the aerial beam, the echo plane being a plane which passes through the observing station and has a line drawn from the observing station towards the radiant as a normal. This is illustrated in Figure 7.2 for the fan beam used in the observations to be described in this chapter (Section 7.4, 7.5).

The incident flux of meteors from radiants within an element of the celestial sphere of solid angle $d\Omega$, which produce zenithal line densities greater than q_z is written as $N(q_z)\, d\Omega$ where $N(q_z)$ is assumed to be represented by a simple power law of the form

$$N(q_z) = K\, q_z^c$$

where c varies slowly with magnitude and lies between - 0.4 and - 1.7 (Elford, 1965). It was found by Elford (1965) that the form of the response function is relatively insensitive to the value of c in the case of narrow aerial beams.

In Figure 7.3 the response function of the 1.98 MHz system (described in Chapter 3), is shown. It was calculated for c = - 1.0, while K was chosen to normalize the response function its actual value being unimportant. Meteor echoes with zenith angles greater than 50^o were ambiguous, so only echo ranges less than 150 km were used, as this excluded most of the ambiguous echoes.

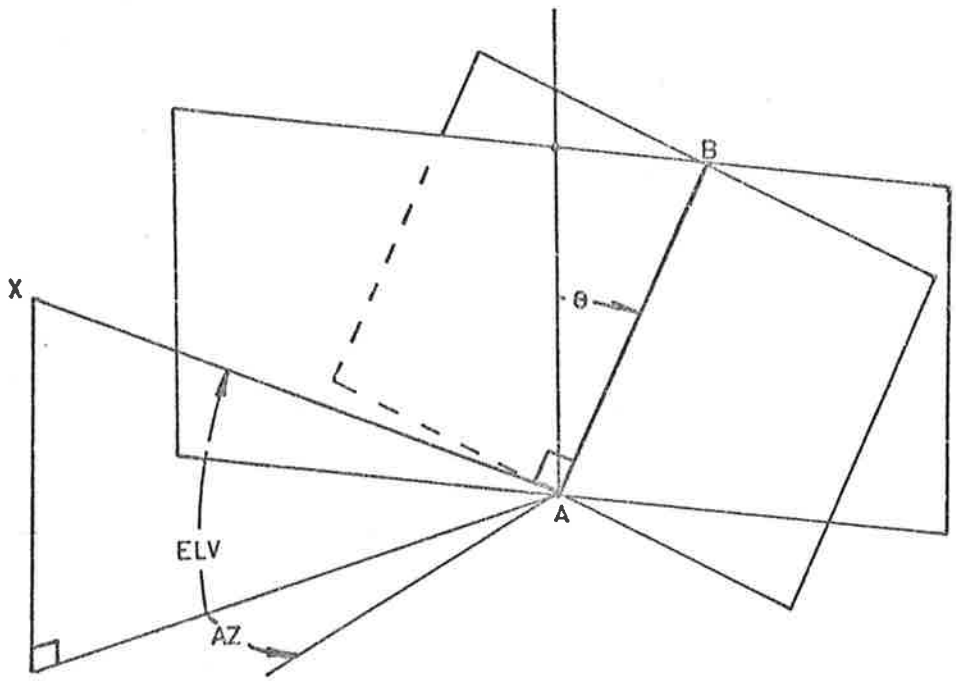

Figure 7.2 The aerial beam has been approximated by a vertical plane which intersects the echo plane (of the radiant AX) in the line AB. Thus echoes from the radiant with elevation ELV, and azimuth AZ, are observed to have a zenith angle θ.

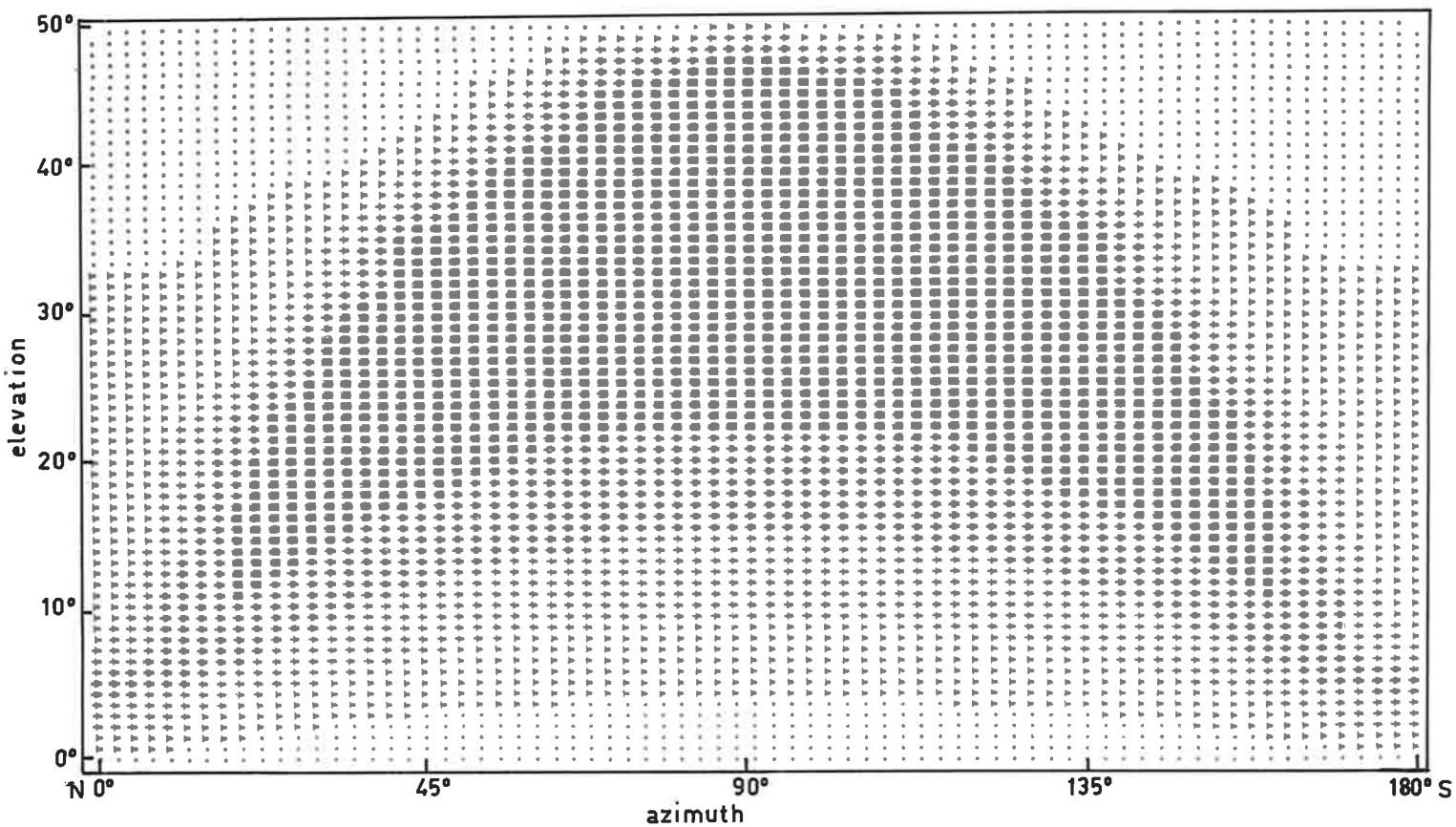

Figure 7.3 Response function of the system for the east beam.

7.3 Meteor Radiant Observations

With a narrow aerial beam meteors from a particular radiant are usually only observed for a short period of time. If the radiant is that of an active shower, the echo rate will rise and then fall as the radiant's echo plane moves through the beam. The way in which the echo rate of meteors from a known radiant changes with time can be calculated once the system's response function is known. This technique is not easily used with the fan beam because of the effect of sporadic meteors.

An alternative method is to observe meteor rates for various range intervals over a period of time. An aerial which responds to radiants over most of the sky and can observe the passage of the radiant over a period of time, will observe a steady increase in the range of echoes from the active radiant as the radiant's elevation rises. A plot of echo-rate against echo range should show a peak which increases in range until the radiant is at transit. After this time the peak will decrease in range as the radiant moves down towards the horizon. This is illustrated in Figure 7.4 where it can be seen that at any particular time the echoes from a given radiant have a spread in range determined by the spread in the height over which the trails ionize. This method could be applied to the data obtained with the fan beam employed in the present experiment. However, as the observed echo rate was low a more selective method described below was used.

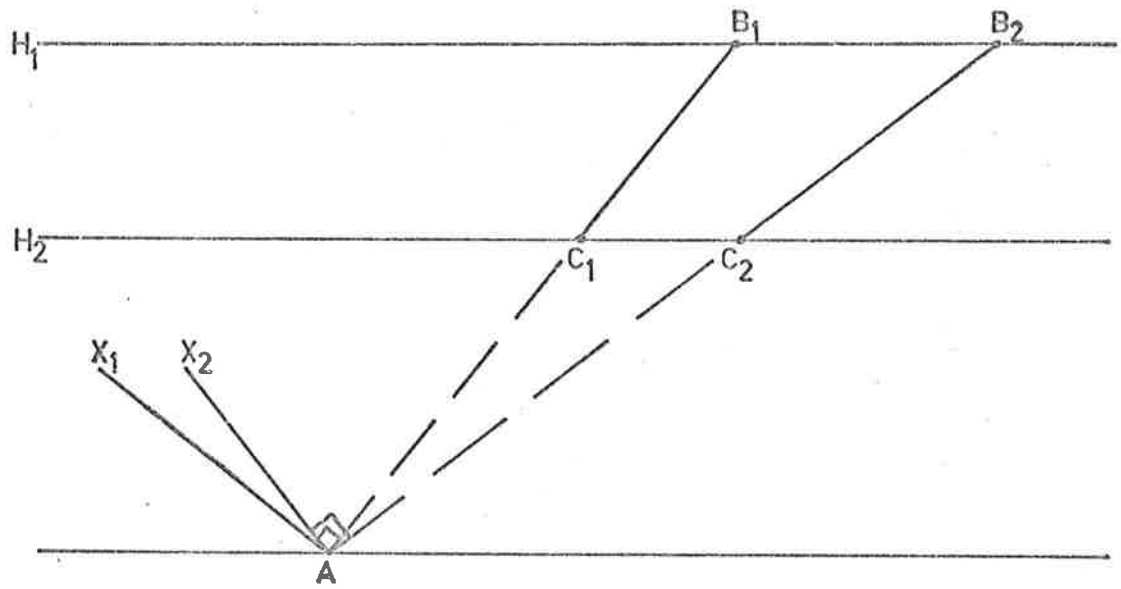

Figure 7.4 As the radiant Ax_1 rises to Ax_2 the range spread of observed echoes changes from C_1B_1 to C_2B_2 (where H_2 and H_1 define the upper and lower limits for trail formation).

The right ascension (RA) and declination (Dec) of a meteor shower can be transformed to an elevation (EL) and azimuth (AZ) at any particular local time of the observing station. It is then possible to calculate the zenith angle of reflection points of meteors in the shower by determining the angle of intersection of the echo plane with the aerial beam. In Figure 7.2 the aerial beam is approximated by a vertical plane. The intersection of this plane with an echo plane is the line AB. It can be shown that the zenith angle θ (OAB) is given by

$$\theta = \arctan (\tan EL / \cos (AZ - \psi)) \qquad 7.1$$

where ψ is the azimuth of the aerial beam. If the angle θ is determined for each echo, and a value ϕ calculated, such that

$$\phi = \theta - Z;$$

where Z is the echo's zenith, then a plot of ϕ values for a large number of echoes should show a peak at $\phi = 0^{\circ}$ if the meteor shower was an active one. The actual spread in ϕ will be determined by the spread of the radiant, which is generally small, and by the fact that the aerial beam has a finite width. The beam is ± 4 degrees to the half power points and this is an important factor for radiants with azimuths that are perpendicular to the beam, although it has very little effect on radiants with azimuths close to the beam's main response. This point is illustrated in Figure 7.5 where it can be seen that the angles θ_A, θ_B, and θ_C are almost equal in Figure 7.5(a) and could be quite different in Figure 7.5(b) where the azimuth of the radiant is close to being perpendicular to the beam. The shower radiants discussed in the

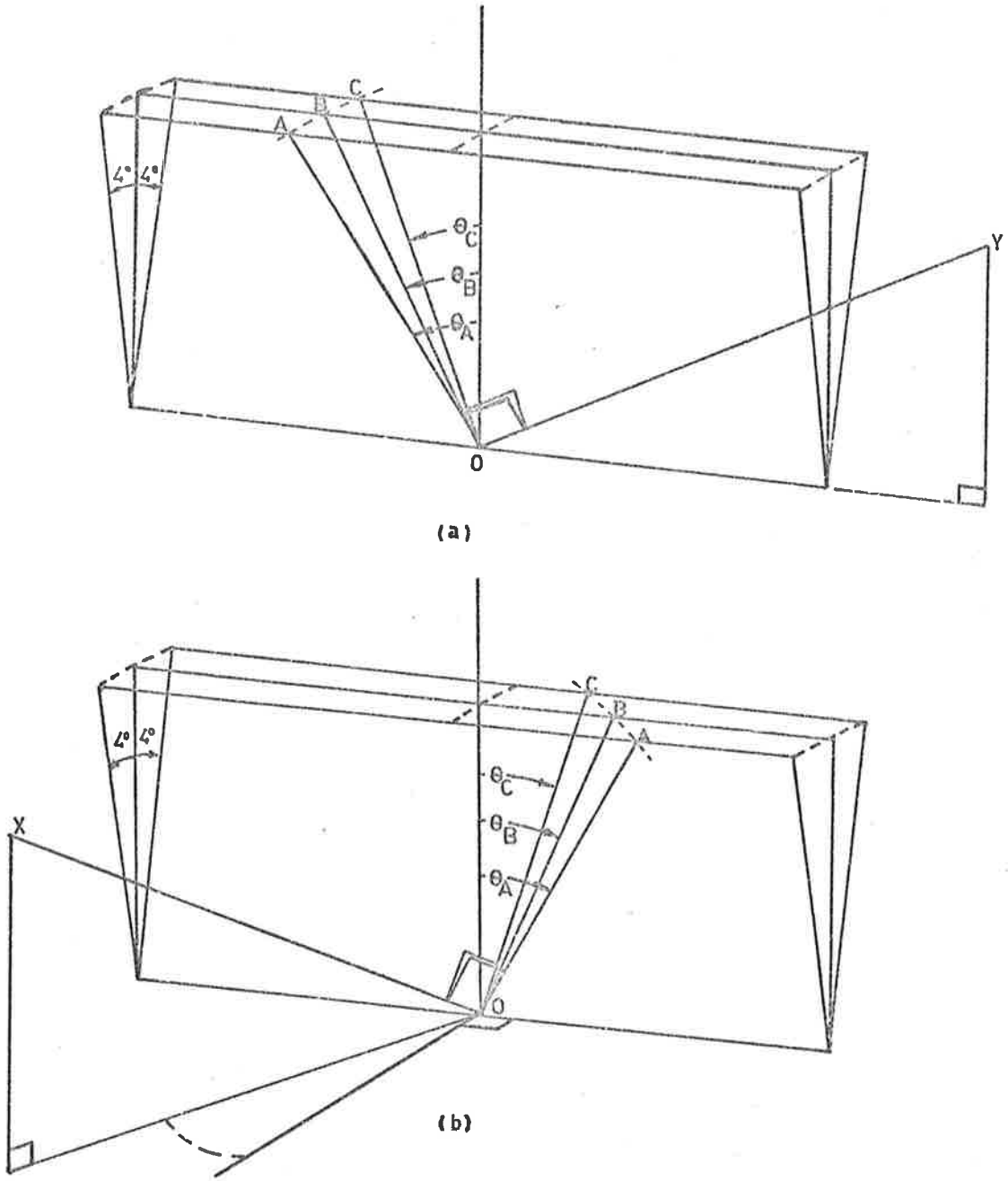

Figure 7.5 Illustrates how the angle θ varies across the beam for echoes from meteors from the radiants OY (a), and OX (b).

following section all had azimuths close to the main response of the beam during the period of observation. Thus a reasonably narrow peak at $\phi = 0$ would be expected.

The maximum electron line density of a meteor trail is on average proportional to sinELV, where EL is the elevation of the meteor radiant. Thus few echoes are observed with small angles of θ. The largest value of θ measured in the results presented is 55° (see Section 4). Thus the direction of the beam was chosen to satisfy the condition that $10^{\circ} < \theta < 55^{\circ}$, where θ was the azimuth of echoes from shower meteors in the beam, during the periods of observation. As stated in Chapter 7.2, the response of the beam could be made north-south or east-west by adding dipoles appropriately. If θ is taken to be positive to the north and negative to the south, then this beam can be called the north beam. Similarly the east-west beam shall be termed the east beam.

7.4 Meteor Showers

7.4(a) Observations

In Figure 7.6 the dates when meteor echoes were observed at 1.98 MHz are shown, together with the active periods of major meteor showers listed by McKinley (1961), which could be observed at Adelaide. Computed values of θ for the dates shown, are given in Figure 7.7 for some of these showers. The Arietids, Ophiuchids, and Eta Aquarids, are not shown because the periods when observations were made were too short

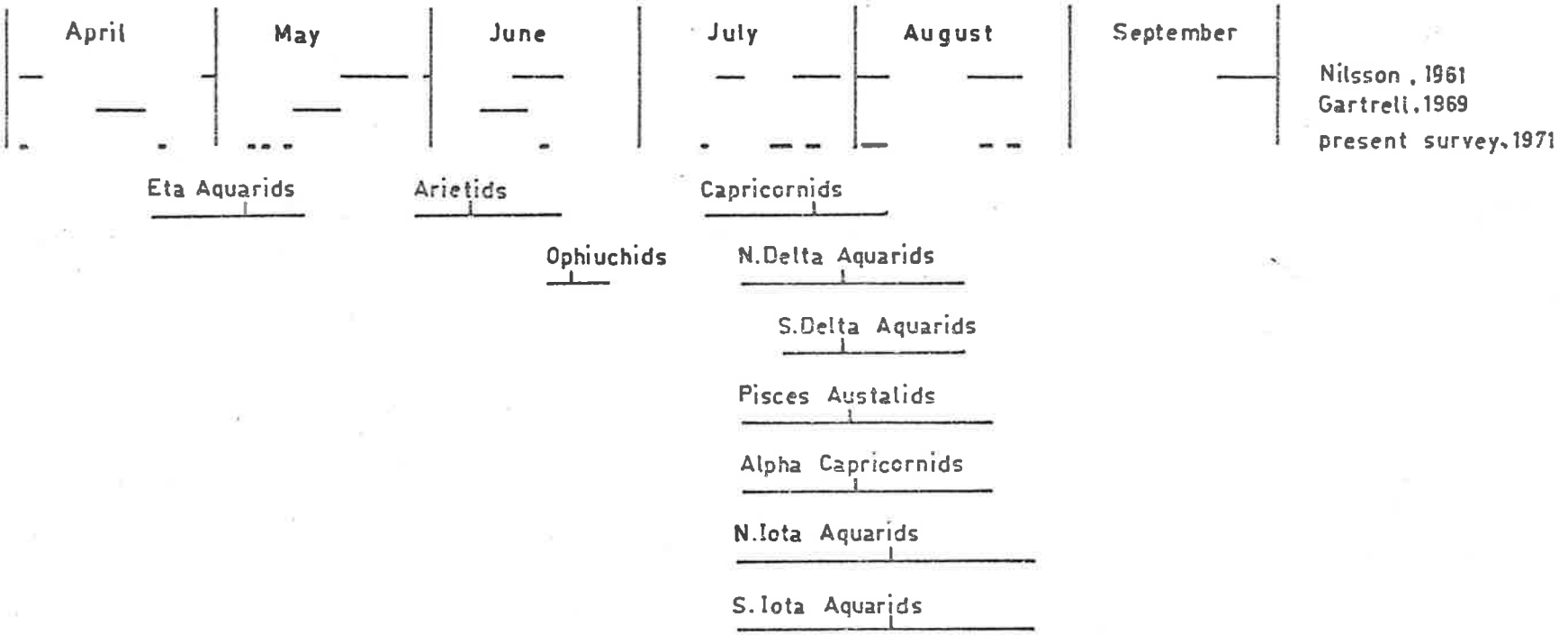

Figure 7.6 The dates of observations made by Nilsson and Gartrell are shown along with those of the present survey. The periods when particular shower meteors could be observed are shown, the peak in activity being indicates by a vertical line.

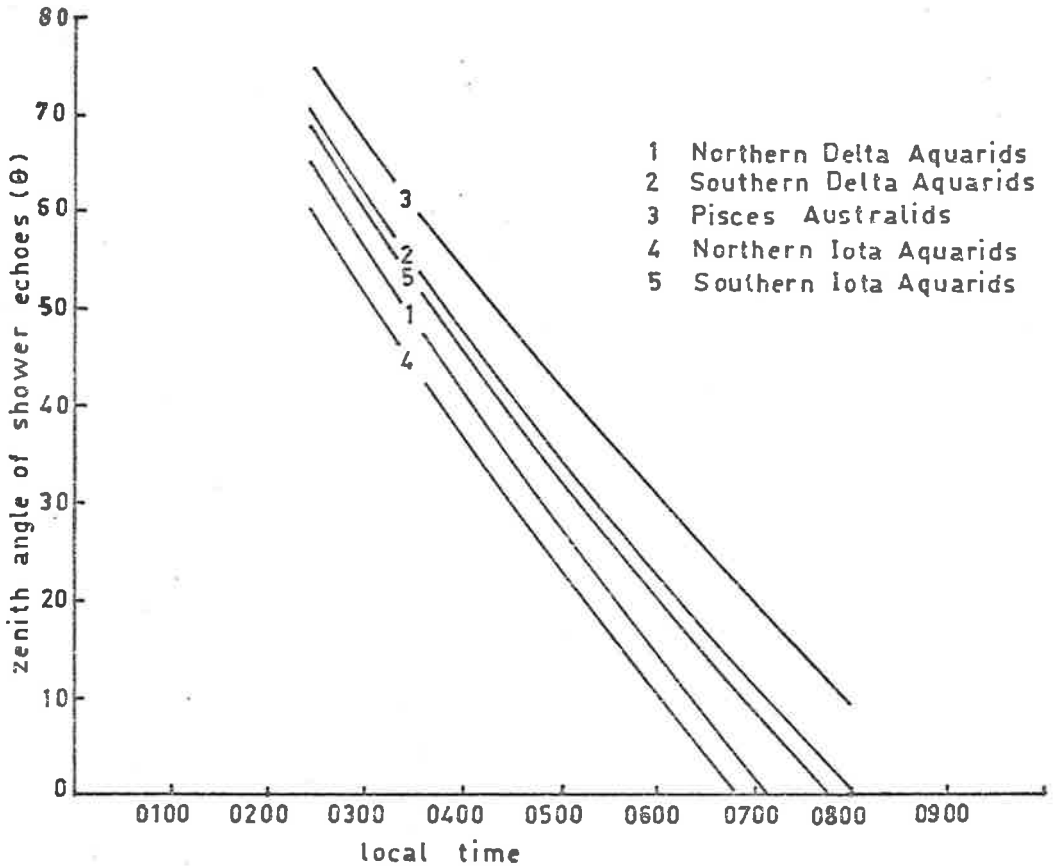

Figure 7.7 The zenith angles plotted against time for showers that could be observed during August for 4/7/71.

to obtain a useful number of echoes. All values of θ are for the east beam as there were no periods when the north beam could be used. It can be seen that values of θ for two of the showers, the Northern Delta Aquarids and the Southern Iota Aquarids are very similar, so that it is not possible to separate the effects of these showers by this method.

The relative contribution of each shower to the observed echoes, assuming that they have equal rates, can be obtained by using the system response function shown in Figure 7.3. An observation index (OI) was calculated where

$$OI = \sum_{T=1}^{11} RESPON\ (EL_T,\ AZ_T) \times H(T);$$

where RESPON (EL_T, AZ_T) is the system response to the shower at an elevation EL_T, and azimuth AZ_T; EL_T and AZ_T are the elevation and azimuth of the shower at the time T; and H(T) is the number of days that the shower was observed at the time T. The sum was formed for half hour intervals so that T = 1 at 0300 hours (local time) and T = 11 at 0800 hours, thus covering the period of observation. Values of OI are shown in Table 7.1 for 4.8.71 and 20.8.71.

The eight mornings in August when an east beam was used, were formed into two groups. The first group containing data from 2nd, 3rd, 4th and 5th of August, was close in time to the peak of the shower activity. The second group contained data from the 18th, 19th, 22nd and 23rd of August and was thus outside the active period.

Table 7.1

SHOWER	OBSERVATION INDEX 4/8/71	(OI, NORMALIZED) 19/8/71
Capricornids	3	1
N. Delta Aquarids	9	5
S. Delta Aquarids	6	3
Pisces Australids	10	8
Alpha Capricornids	1	0
N. Iota Aquarids	5	2
S. Iota Aquarids	8	4

Table 7.2

SPORADIC RADIANTS		OBSERVATION INDEX June & July (N. Beam)	(OI, NORMALIZED) August (E. Beam)
340	0	1	10
200	0	2	4
270	16	5	0
270	54	4	3
270	-16	0	0
270	-54	1	0

7.4(b) Results

Values of ϕ are presented in Figure 7.8 for five shower radiants with OI values greater than 3. The first group of data from days close to the 4th August shows possible signs of activity from the Southern Delta Aquarids, Pisces Australids and Southern Iota Aquarids. These peaks in ϕ near $\phi = 0$ are not present in the data recorded close to 19th August. However, as the showers were at different elevations and azimuths during this recording period and were in a less sensitive region of the aerial beam (note the smaller OI values), this result may be misleading. As a test, data from the period around 19th August was re-analysed as though it had been recorded on 4th August. The result of this is shown in Figure 7.9. It can be seen that a peak is again observed near $\phi = 0$ for the Pisces Australids indicating that this is due entirely to the fact that the radiant of this shower passed through a sensitive region of the beam, where most echoes were observed on 4th August. Thus nothing of significance can be deduced from these particular observations.

Nilsson (1964) observed both the Capricornids and Southern Delta Aquarids during August, 1961, with the latter shower showing a high level of activity. Thus the Southern Delta Aquarids should have been detected in the above observations at 1.98 MHz. However the observing period was between three and six days after the peak and a significant drop in the level of activity may have occurred during this time. The average elevation of this shower during the observing period was 40°.

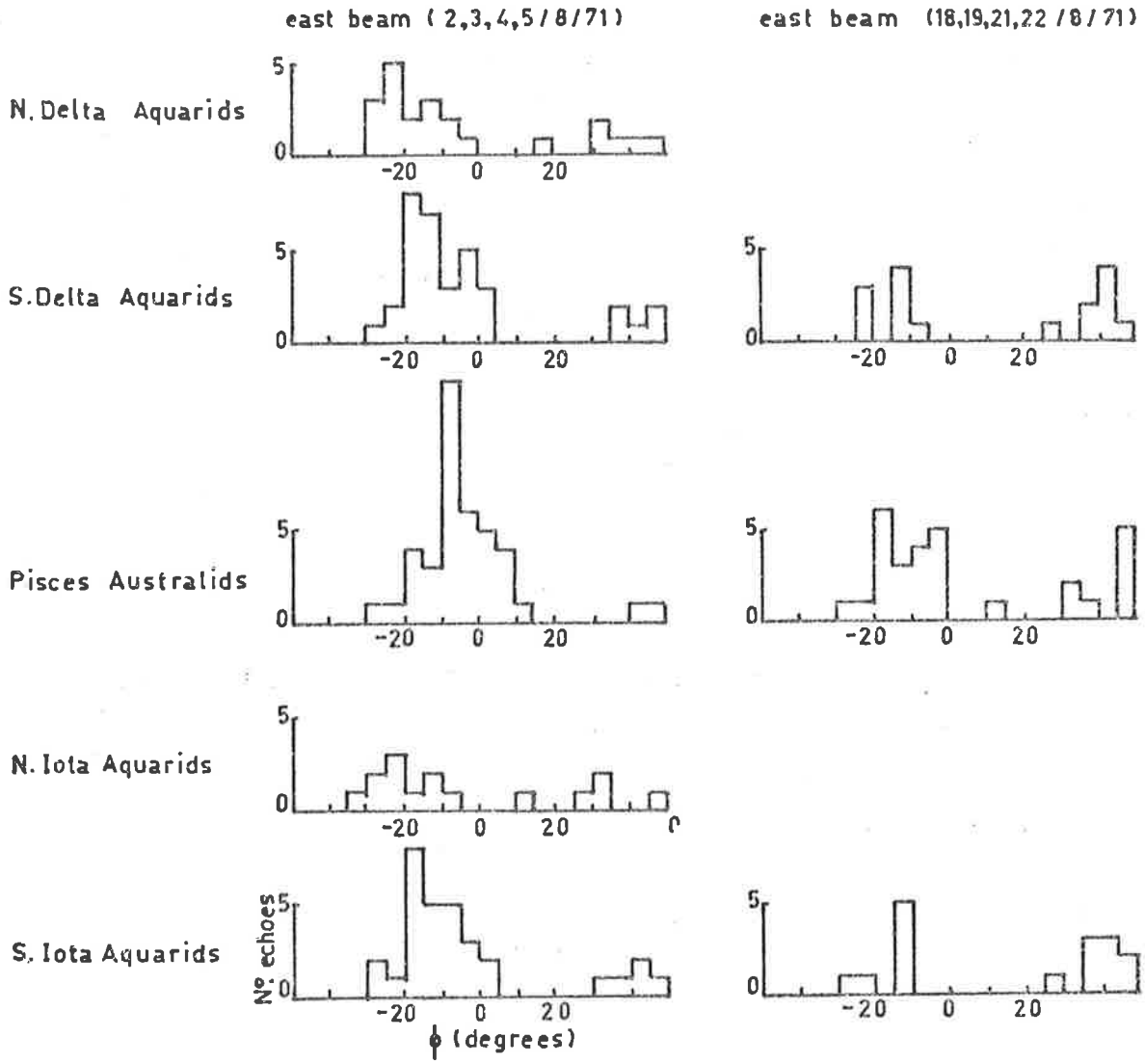

Figure 7.8 The number distribution of echoes for values of ϕ derived from five shower radiants.

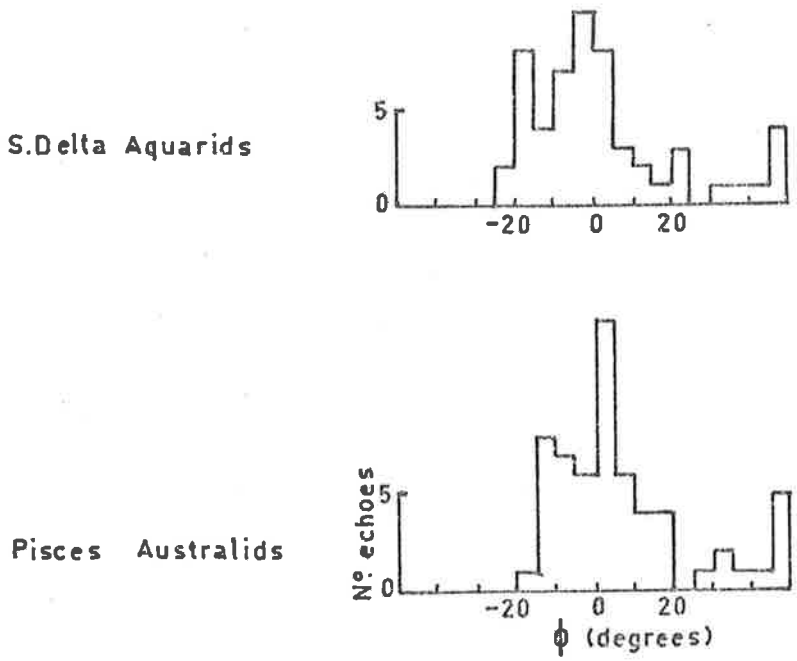

Figure 7.9 Data from 18/8/71 analysed as though recorded on 4/8/71.

Thus the echo rate would have been well below the maximum rate which would occur at transit with an elevation of 80 degrees. These two factors combined with the persistent D-region ionization (which may have been caused by the shower) probably explain the poor results.

7.5 Sporadic Meteors

7.5(a) Observations

The distribution of sporadic meteor radiants has been investigated at Adelaide by Nilsson (1964) and Gartrell (1971) and in the northern hemisphere by, Elford et al, (1964a), Stohl (1967) and Triskova (1967). Observations made by these workers show a radiant distribution which follows that used by Elford et al, (1964b) and this is shown in Figure 7.10. It can be seen that there are two concentrations on the plane of the ecliptic near the helion (340°, 0°) and antihelion (200°, 0°) positions. In addition there are four concentrations, caused by the earth's motion, with the longitude of the apex (270°, 16°; 270°, 54°; 270°, -16°; 270°, $+54^{\circ}$). Each concentration spreads over twenty to forty degrees of latitude and longitude. So that using the above radiant positions to calculate ϕ should produce a broad peak around $\phi = 0^{\circ}$ for sporadic meteors from that concentration.

Values of the observation index OI are presented in Table 7.2 for the six sporadic concentrations, for the east beam's observations during August, 1971, and for the north beam's observations during June and July, 1971. A short period of observing in May, 1971 with the east

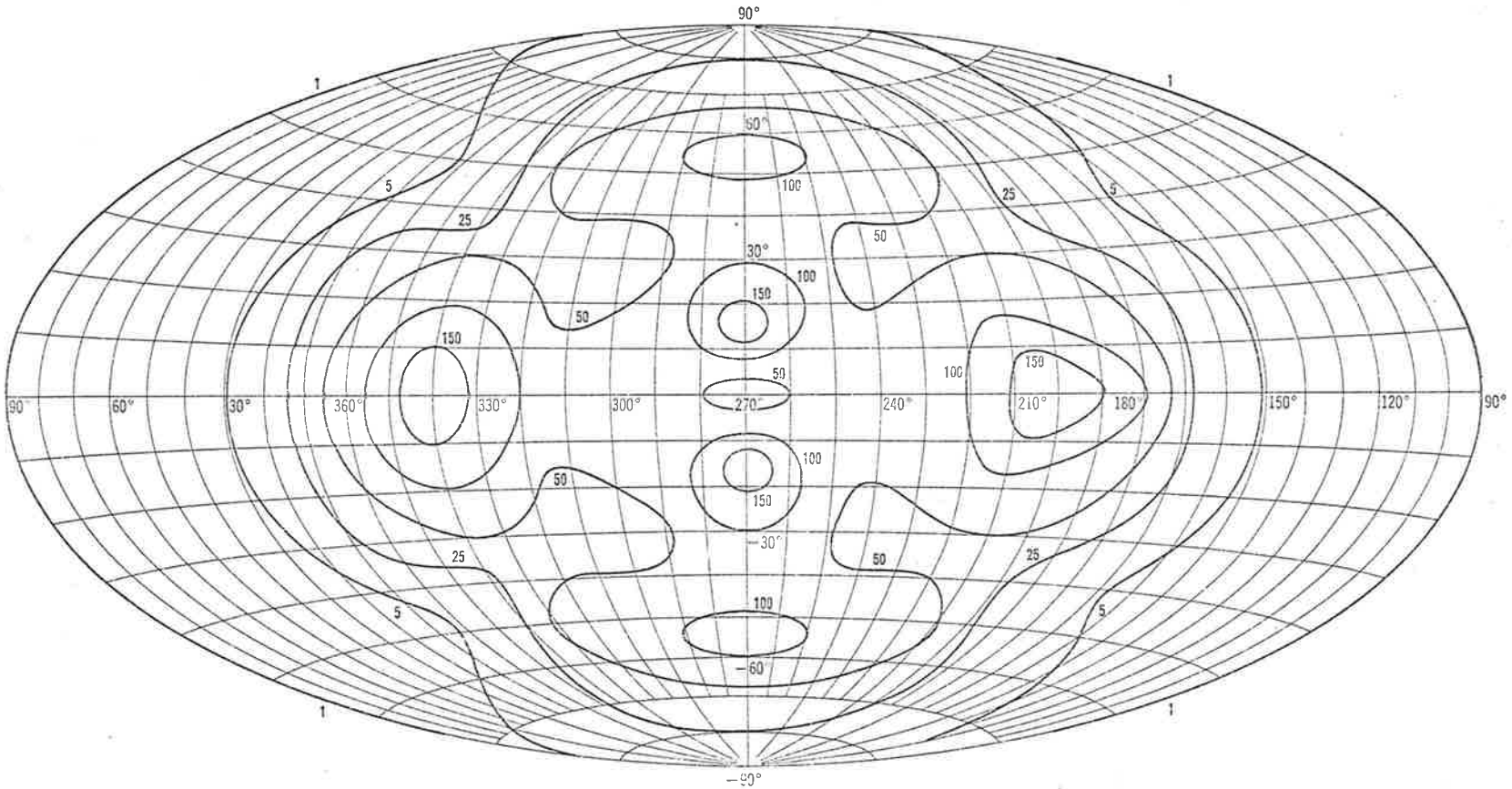

Figure 7.10 The average density distribution of sporadic radiants for the period January - August 1962.

beam has also been included.

7.5(b) Results

Values of ϕ calculated for four sporadic radiant concentrations where the normalized observation index was greater than one, are shown in Figure 7.11. It can be seen that during the period June to August, 1971, the helion and apex concentration at 270°, 16° were active, while the antihelion concentration and the apex concentration at 270°, 54° were not. During May, 1971 the antihelion concentration was, however, observed to be active, although the statistics are very poor as the observing period was short.

The observed strengths of the helion and antihelion radiants appear to contradict those found by Nilsson (1964) and Triskova (1967), who reported observing a larger number of meteors with the antihelion longitude during August. Nilsson and Triskova grouped all their echoes according to their ecliptic longitude. Thus showers such as the Southern Delta Aquarids and Pisces Australids were included in the antihelion longitude, while the present method separates these radiants as they have different zenith angles. Stohl (1967) observed only those echoes from the helion (330°, 0°), antihelion (210°, 0°) and the apex at (270°, $\pm 60^{\circ}$). He found the antihelion radiant to have a dip in activity during the period August-September, when the rate was about one-third of its maximum. Stohl also found that the apex concentrations at (270°, $\pm 60^{\circ}$) were inactive during the August period.

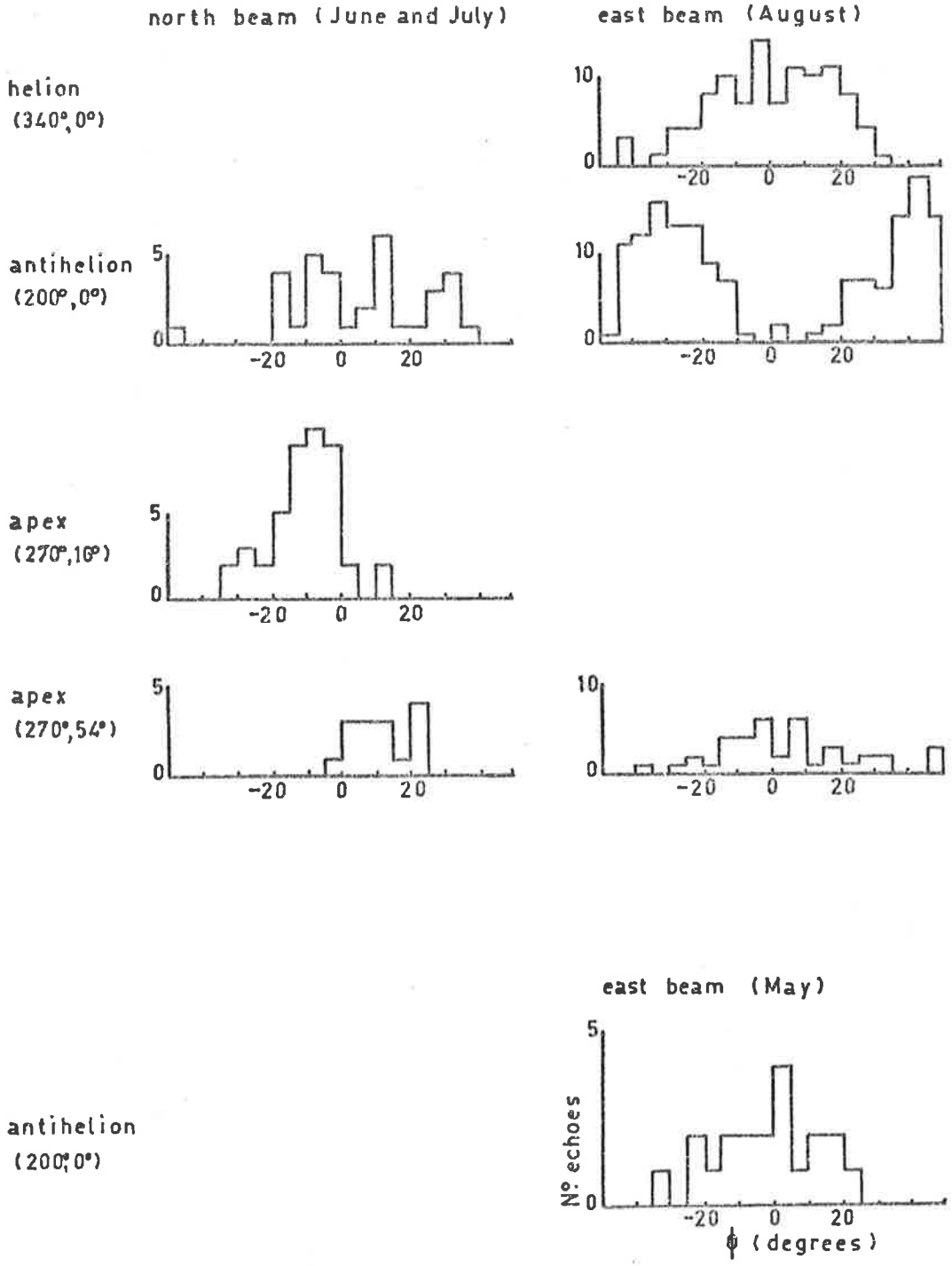

Figure 7.11 The number distribution of echoes for values of ϕ derived from four sporadic radiant concentrations.

Thus there is a reasonable agreement between the 1.98 MHz results and Stohl's results.

CHAPTER 8

RADIO METEOR REFLECTION COEFFICIENT PROFILES

8.1 Introduction

An irregular electron line density affects both the amplitude and phase of a reflected radio signal. Thus it is possible to study the irregularities in the ionization line density by observing the behaviour of the radio signal reflected from the trail. Rice and Forsyth (1963) first predicted that the dispersion in measured decay rates of radio echoes from trails at similar heights could be caused by an irregularly ionized trail. More recently Jones (1969a) has proposed a theory of the reflection process of radio waves from irregularly ionized trails. This theory makes possible the prediction of the standard deviation of the ionization from its mean level. Applied to data obtained by Greenhow and Hall (1961) this theory predicts that ionization irregularities with scales between 300 and 500 m are less than 20% of the mean electron density while those with scales between 500 m and 6 km are less than 43% of the mean. However the theory predicts a wavelength dependence in the dispersion of the normalized radio echo decay rates and this does not occur in the decay rates measured by Rice and Forsyth (1963) at wavelengths of 6, 8, and 9 m. This means that ionization irregularities are not the major cause of the dispersion in radio echo decay times. The results obtained using Greenhow and Hall's data can only be regarded as possible upper limits

to the ionization irregularities present in trails which exhibit an exponential decay.

A second method for observing trail ionization irregularities was proposed by Rice and Forsyth (1964). This involved observing both the amplitude and phase of the echo as the trail is formed. Their principal assumption is that the changes in amplitude and phase are entirely caused by new ionization produced by the meteoroid as it ablates. In most cases the echo's decay time is considerably longer than the time it takes to form, and this assumption holds. The first ionization profiles to be experimentally determined by this method were published by Rice and Forsyth (1964). A recent paper by Jones (1969) describes a method for automatically obtaining the ionization profile by differentiating the echo electronically. In this paper Jones shows that the effects of galactic noise are much greater than had been supposed. Ionization profiles obtained using this automatic processing show that small scale irregularities about 1 km in length have a root mean square deviation that is less than 30% of the mean electron line density. Used with backscatter reflections this technique is seriously affected by upper atmospheric winds so that only relatively short sections of profile can be obtained. Thus no information is yet available about ionization irregularities that are about 5 km in length. Used in conjunction with a forward-scatter meteor system, where the Doppler shifts produced in the echo by the trail's movement are nearly an order of magnitude smaller, this limitation is removed.

In the following sections of this chapter a method is developed which enables pre-t_o diffraction patterns obtained by the Adelaide meteor system to be used to determine ionization profiles. These diffraction patterns effectively contain only half of the phase and amplitude information needed to carry out the analysis described by Rice and Forsyth (1963), and Jones (1969). An approximate method of analysing these records is developed below, and some experimental results discussed.

8.2 The Adelaide Meteor System

A complete description of the system has been made by McAvaney (1970). Thus only those aspects which are important to this experiment will be discussed.

Two transmitters are located at Adelaide University, a radar used to determine the range of the echo (27.540 MHz) and a continuous transmitter which is used to determine the zenith angle and phase changes of the echo (26.773 MHz). The receiving site is 23 km north of the transmitter. The radio wave received directly across the ground from the transmitter is received at this site at a level that is greater than most of the signal levels from meteor trail echoes. The ground wave and meteor echo are mixed at the input to the receiver, so that phase changes in the reflected signal are converted into amplitude variations in the detected signal. These phase changes are principally caused by diffraction effects during the trail's formation and by movements of the

the trail with the neutral wind during and after the trail has formed. The early part of the diffraction pattern, the so-called pre-t_o diffraction pattern (where t_o is the time at which the meteor intersects a line that is perpendicular to the meteor's path and passes through the receiving station, AB in Figure 8.1) can be used to determine the meteor's velocity and is recorded for this purpose at the Adelaide receiving station at St Kilda. The determination of a meteor's orbital elements can be carried out if radio echoes are received from several different points on the meteor trail. For this purpose four out-stations were built and equipped to receive the continuous wave transmitter. Signals received at these stations are transferred to the main receiving station at St Kilda by radio links operating at a frequency near 60 MHz. The diffraction patterns received at these out-stations can therefore be displayed and recorded at St Kilda.

8.3 Calculation of the Reflection Coefficient

Each out-station's diffraction pattern will carry information about different sections of the meteor trail's ionized column (Figure 8.2). If these diffraction patterns are analysed to yield the ionization profiles of these sections, then the ionization line density will be known for a relatively long section of the trail. This was the original idea behind the project. However, it was found that the signals from the four out-stations were badly affected by noise contributed by the radio links. The experiment was then conducted using five separate aerials and receivers located at the main receiving

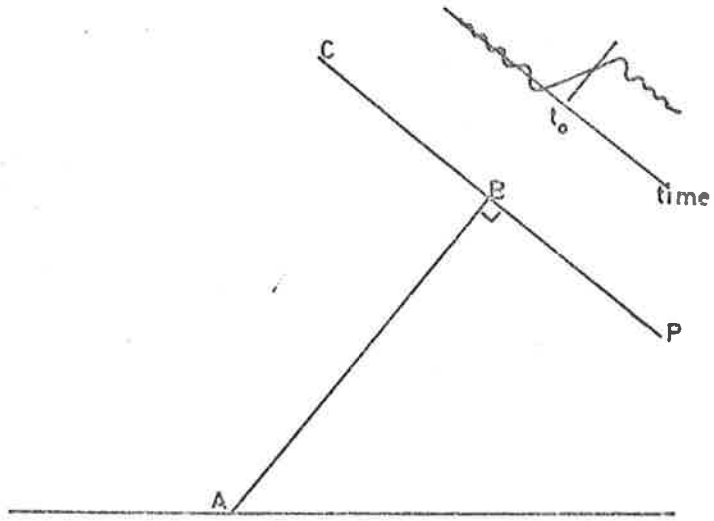

Figure 8.1 The geometry of a specular echo from a meteor trail CD showing a typical diffraction pattern obtained when a ground wave is present at the receiving aerial.

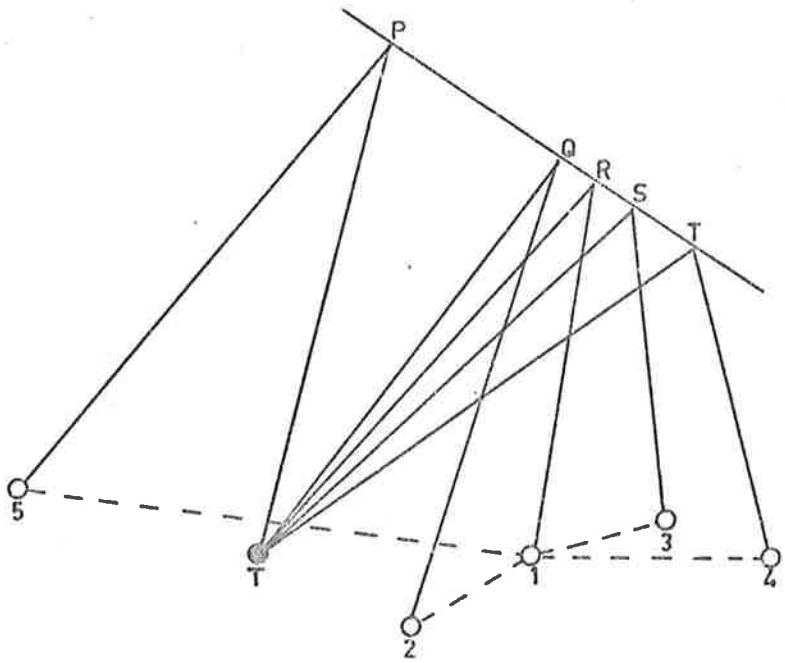

Figure 8.2 The transmitter T and five receiving stations which are linked to the main receiving station at 1 by radio links. The five diffraction patterns observed come from different sections of the trail at p, q, r, s and t.

station. The five diffraction patterns could thus be used as checks on each other, and could be combined to improve the signal-to-noise ratio.

8.3(a) Theory of Method

The radio signal reflected from the column of electrons produced by the meteoroid can be represented as the sum of signals reflected from all parts of the column. The resulting signal strength can be written as

$$\underline{E}(x)\exp(i\omega t) = b\int_{-\infty}^{x} g(x)\exp\left[i\left(\omega t - \frac{\pi x^2}{2}\right)\right]dx \qquad 8.1$$

Where $\underline{E}(x)$ is the complex echo amplitude for a trail extending from minus infinity to a point x; b is a constant defined in Chapter 2 (Equation 2.8); and g(x) is the reflection coefficient. The distance x along the trail has been defined in Chapter 2 (Equation 2.6) as

$$x = \frac{2s}{\sqrt{R_o\lambda}} \qquad 8.2$$

where s is the distance along the trail from the t_o point; R_o is the distance of the t_o point from the receiving site; and λ is the radio wavelength. Thus x is a dimensionless quantity called the Fresnel length in optics. In the experiment being considered, a ground wave is mixed with this signal so the resulting signal strength becomes

$$\underline{F}(x)\exp(i\omega t) = \underline{W}\exp(i\omega t) + \underline{E}(x)\exp(i\omega t),$$

$$\underline{F}(x) = f(x)\exp(i\alpha(x)), \qquad 8.3$$

$$\underline{W} = \omega\exp(i\phi).$$

The functions f(x) and $\alpha(x)$ are the amplitude and phase of the detected signal, where $\alpha(x)$ is determined by the range of the trail and its

length; and w and ϕ are the amplitude and phase of the ground wave, where ϕ is determined by the separation of the receiver from the transmitter. The time dependence can be dropped from this equation. It can also be simplified by rotating through ϕ and setting $\psi(x) = \alpha(x) - \phi$ and $\theta(x) = -\frac{\pi x^2}{2} - \phi$ so $\underline{F}(x)$ becomes

$$\underline{F}(x) = f(x) \exp(i\psi(x)) = w + b \int_{-\infty}^{x} g(x) \exp(i\theta(x))\, dx \qquad 8.4$$

and this rotation is shown in Figure 8.3.

The first step towards obtaining an expression for g(x) is to differentiate Equation 8.4 with respect to x. Thus

$$\frac{d}{dx} \underline{F}(x) = \frac{d}{dx} \underline{E}(x)$$

$$\frac{d}{dx} \left(f(x) \exp(i\psi(x)) \right) = \frac{d}{dx} \left(b \int_{-\infty}^{x} g(x) \exp(i\theta(x))\, dx \right)$$

$$\frac{d f(x)}{dx} \exp(i\psi(x)) + i f(x) \exp(i\psi(x)) \frac{d \psi(x)}{dx} = b\, g(x) \exp(i\theta(x)) \qquad 8.5$$

If the angle between $\frac{d \underline{E}(x)}{dx}$ and $\underline{F}(x)$ is Z(x), then it can be seen from Figure 8.4(a) that

$$f(x)\, \delta\, \psi(x) \sim b\, g(x)\, \delta x \sin Z(x)$$

or

$$\frac{d \psi(x)}{dx} = \frac{b\, g(x) \sin Z(x)}{f} \qquad 8.6$$

substituting this in Equation 8.5 yields

$$\frac{d f(x)}{dx} \exp(i\psi(x)) + i\, b\, g(x) \sin Z(x) \exp(i\psi(x)) = b\, g(x) \exp(i\theta(x))$$

which simplifies to the expression

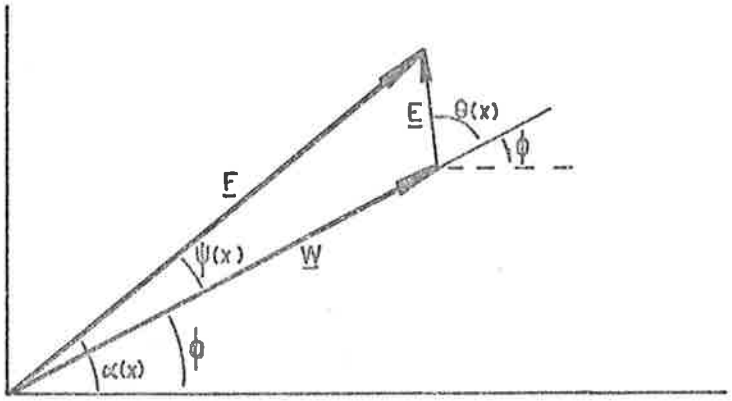

Figure 8.3 The ground wave W and the sky wave E add together in the receiver to yield the observed signal F.

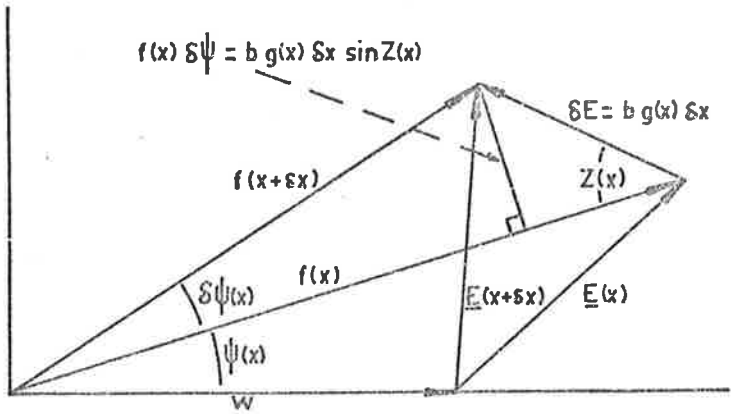

(a)

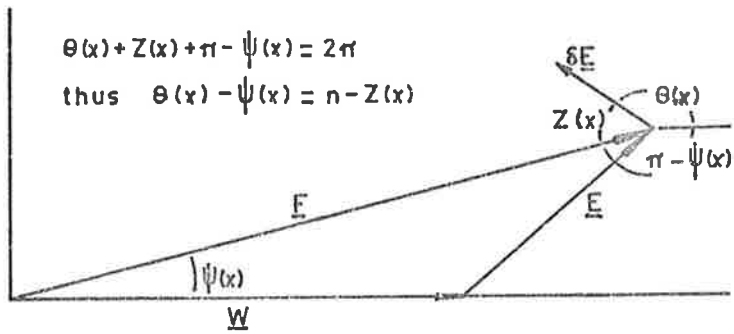

(b)

Figure 8.4 (a) shows with an exaggerated $\delta\psi(x)$ the relation used to derive Equation 8.6, while (b) demonstrates Equation 8.3.

$$g(x) = \frac{d\ f(x)}{dx} \frac{1}{b\ (\exp(i(\theta(x) - \psi(x))) - i \sin Z(x))} \qquad 8.7$$

Figure 8.4(b) shows that by definition

$$\theta(x) - \psi(x) = \pi - Z(x) \qquad 8.8$$

and using this in Equation 8.7 the expression for g(x) becomes

$$g(x) = -\frac{d\ f(x)}{dx} \frac{1}{b \cos Z(x)} \qquad 8.9$$

8.3(b) Application of Method

The pre-t_o diffraction pattern recorded by the Adelaide meteor system is a complete record of the function f(x) up to, and just beyond the t_o point. Thus $\frac{d\ f(x)}{dx}$ can be calculated, as x is defined by the pattern itself. All that remains to be determined is the function

$$\begin{aligned} Z(x) &= \pi - \theta(x) + \psi(x) \\ &= \pi + \frac{\pi x^2}{2} + \phi + \psi(x) \\ &= \pi(1 + \frac{x^2}{2}) + \phi + \psi(x). \end{aligned} \qquad 8.10$$

For a uniformly ionized trail where g(x) is constant over the region of interest, maxima and minima occur in the pre-t_o diffraction pattern wherever

$$Z(x) = \pi/2 + n\pi \qquad \text{for } n = 0, 1, 2, 3, \ldots.$$

as shown in Figure 8.5. Where g(x) is not constant the spiral becomes distorted and the maxima and minima will move randomly about the points where $Z = \pi/2 + n\pi$. However, as Figure 8.5 demonstrates, this movement is not very large even for a fairly irregular trail. Therefore it should be possible to determine Z(x) by fitting a function, by the method of least squares, to the turning points in the diffraction pattern. By

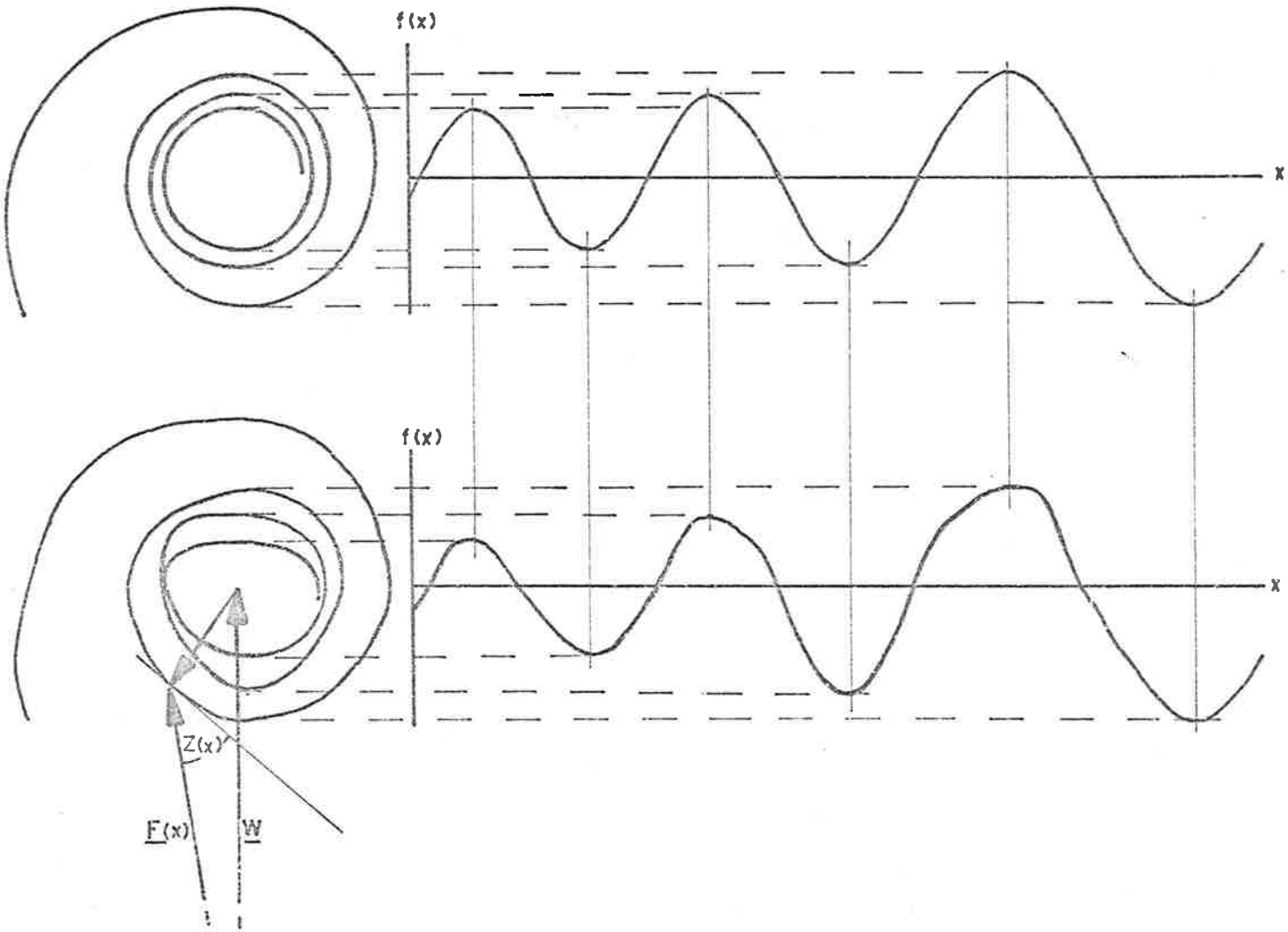

Figure 8.5 The effects of a varying function g(x), on the turning points of the diffraction pattern.

limiting the order of the function to a power of two, any badly displaced turning points in the diffraction pattern will be prevented from seriously affecting the result. Such an approach, however, ignores the function $\psi(x)$ which is not a simple quadratic function. The only way to determine $\psi(x)$ accurately depends on a knowledge of the field $\underline{E}(x)$ returned from the meteor trail. This cannot be found from the pre-t_o diffraction patterns recorded at Adelaide. However, under certain conditions $\psi(x)$ can be ignored as it is a function which oscillates about zero and has a maximum amplitude given by

$$\psi(x)_{max} = \arctan\ (|\underline{E}(x)|/w).$$

Thus when w is large compared to $|\underline{E}(x)|$, $\psi(x)$ can be set equal to zero. The effect this has on the calculated values of $g(x)$ is, in fact, made even smaller because $\psi(x)$ reaches its maximum values when $Z(x) \sim 0 + n\pi$. Since $Z(x)$ enters Equation 8.9 as cos $Z(x)$, these errors in $Z(x)$ have less effect on $g(x)$. The condition that w be large compared to $|\underline{E}|$ is met by most echoes. This is because w is set to be equal to the total signal reflected by the larger trails. The signal amplitude in the pre-t_o diffraction is on average only 10% of this.

8.4 Errors and Corrections

8.4(a) Galactic Noise

Galactic noise is the limiting factor at a frequency of 27 MHz. The effect this noise has on the differentiated signal returned from a meteor trail has been considered by Jones (1969), who derived the relation

$$S_o = S_1 \frac{V}{2\pi f_1} \sqrt{\frac{3}{R_o \lambda}} \qquad 8.11$$

where S_o is the signal-to-noise ratio of this differentiated signal and S_1 is the ratio before differentiation; V is the velocity of the meteor; R the range of the echo; λ the radio wavelength; and f_1 is the bandwidth of the system. For present purposes this can be expressed as

$$S_o = S_1 \frac{\frac{dx}{dt}}{(2\pi f_1)} \frac{\sqrt{3}}{2} \qquad 8.12$$

where $\frac{dx}{dt}$ is the velocity of the meteoroid through the Fresnel zones. Where this velocity is high, the diffraction pattern varies rapidly so that $\frac{d\underline{E}(x)}{dt}$ has large values. However, this ignores the bandwidth of the system which places an upper limit on the rate at which $\underline{E}(x)$ can change. Phase variations in $\underline{E}'x)$ have been shown to be equal to

$$\Theta(x) = \frac{-\pi x^2}{2}$$

This represents a frequency f_x given by

$$f_x = \frac{1}{2\pi} \frac{d\Theta(x)}{dt} = \frac{-x}{2} \frac{dx}{dt}$$

The maximum length of trail x_m that can be analysed is found by setting f_x equal to the bandwidth f_1 and this results in

$$x_m = -2\, f_1 / \frac{dx}{dt} \,. \qquad 8.13$$

Substituting this in Equation 8.12 gives

$$S_o = \frac{S_1}{x_m} \cdot \frac{\sqrt{3}}{2\pi}$$

thus the ratio of the signal-to-noise after differentiation (S_o),

compared to the signal-to-noise of the received signal (S_1) is given by

$$\frac{S_o}{S_1} = \frac{\sqrt{3}}{2\pi x_m}. \qquad 8.14$$

Equations 8.13 and 8.14 make it possible to determine the optimum bandwidth f_1 if a reflection coefficient profile of a given length x_m is to be obtained. To begin with, S_1 should be maximized by selecting echoes with a minimum range. The system bandwidth and the velocity of the meteor will then determine the ratio $\frac{S_o}{S_1}$ and hence the length of trail that can be analysed (x_m). This is illustrated in Figure 8.6 where $f_1(x)$ is shown for two different meteor velocities for a meteor with a range of 150 km. A more flexible approach to this problem would be to record signals with a fairly large bandwidth f_1, and then pass the resulting reflection coefficient profile through a low pass filter. In the present case this is done by using a numerical filter in the last stage of the computer analysis. The degree of smoothing imposed on the profile determines the minimum length of irregularities that can be resolved, however the available trail length that can be analysed is not affected.

In the present case the differentiated signal is divided by cos Z(x) to obtain the reflection coefficients g(x). Thus the signal-to-noise, where g(x) is the signal, will also be divided by cos Z(x). This is the major disadvantage of this method of obtaining g(x), as it means that g(x) cannot be determined near the turning points in the diffraction pattern. This can be overcome to some extent by recording

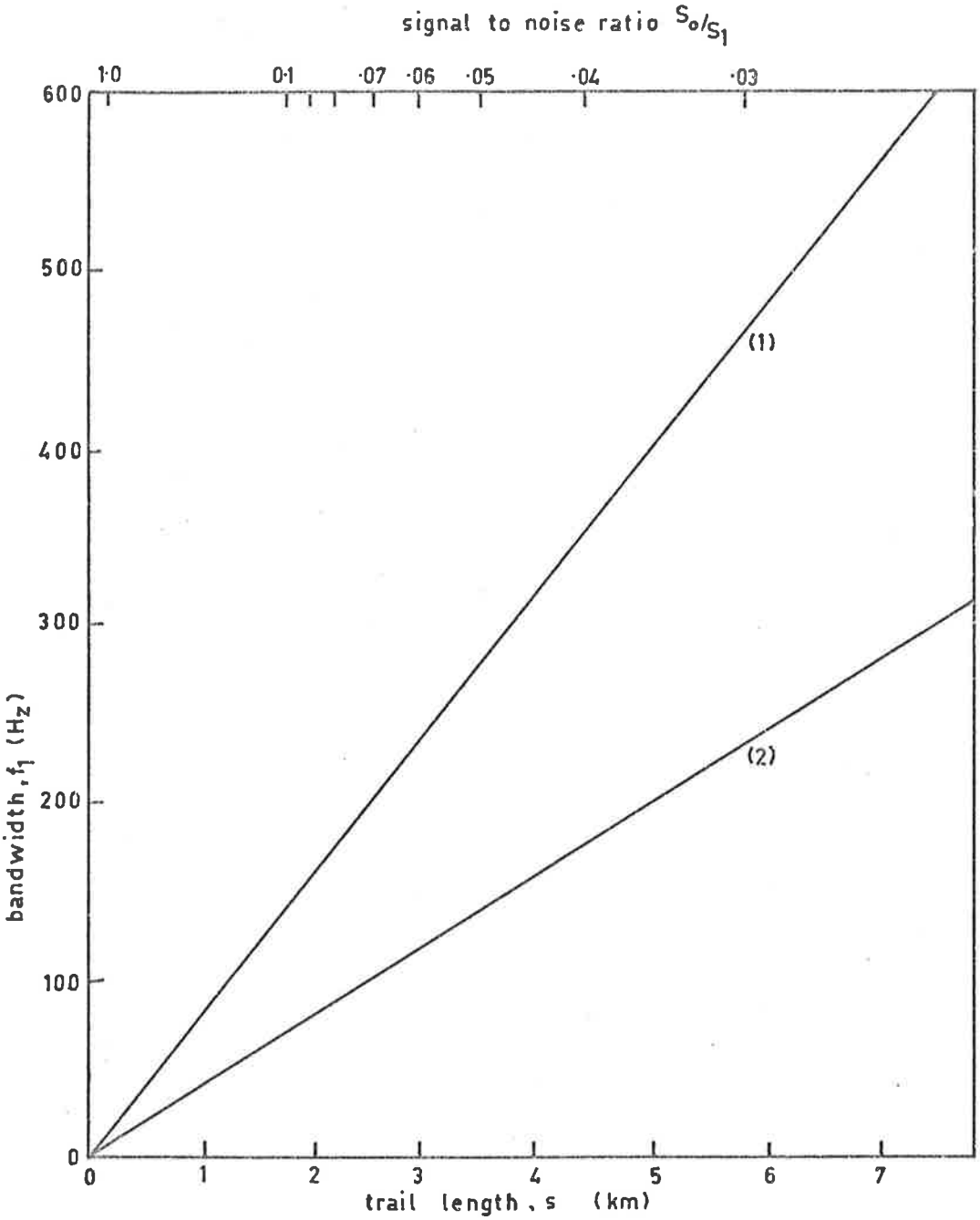

Figure 8.6 The bandwidth (f_1) required to pass the signal reflected from the trail a distance, s, from the t_o point is shown for a meteoroid velocity of 60 km/sec (1), and 30 km/sec (2).

the diffraction pattern from a number of aerials and combining the resulting g(x) profiles. Each profile can be weighted by the function cos Z(x) so that the weighting factor approaches zero as the profile becomes unreliable. Thus the resultant mean profile G(x) is given by

$$G(x) = \frac{\frac{df1(x)}{dx}\frac{1}{b\cos Z1(x)} \cdot \cos Z1(x) + \frac{df2(x)}{dx}\frac{1}{b\cos Z2(x)} \cdot \cos Z2(x) + ..}{\cos Z1(x) + \cos Z2(x) + ..}$$

$$\text{so } G(x) = \frac{1}{b}\left(\frac{df1(x)}{dx} + \frac{df2(x)}{dx} + \frac{df3(x)}{dx} + ..\right)\frac{1}{\cos Z1(x) + \cos Z2(x) + ..} \quad 8.15$$

In this case the signal-to-noise ratio for the mean profile is not constant, but proportional to a function N(x) defined by

$$N(x) = \cos Z1(x) + \cos Z2(x) + \cos Z3(x) + ...$$

If this function is fairly constant the profile G(x) will be reliable; however, marked variations in N(x) could produce a profile G(x) with noisy bursts corresponding to the low values in N(x). Thus only those records which combined to yield a reasonably constant N(x) were chosen.

8.4(b) Wind and Wind Shear

Winds are nearly always present at the height at which meteor trails are formed. The trail is carried along by them and often distorted by changes in the wind structure with height. Such distortions occur slowly compared to the duration of the Fresnel diffraction and can, in most cases, be ignored. However, a steady wind causes a continuous change in phase which must be allowed for when converting the Fresnel trail length x into true distance s. This is normally done by considering the angular function Z(x) described in

Chapter 8.3(a) and defined for $\psi(x) = 0$ in Equation 8.10 as

$$Z(x) = \pi(1 + \frac{x^2}{2}) + \phi.$$

With a wind present this becomes

$$Z_U(x) = \pi(1 + \frac{x^2}{2}) + \phi + U \frac{\pi}{V} \sqrt{\frac{R_o}{\lambda}} \cdot x \qquad 8.16$$

Where U is the component of the wind towards or away from the receiving station; V is the meteor's velocity; R_o the trail's range; and λ the wavelength. The function $Z_U(x)$ is determined experimentally by using consecutive maxima and minima of the diffraction pattern as points where

$$Z_U(x) = \pi/2 + n\pi, \qquad n = 0, 1, 2, ...$$

and then using these points in a least square fit procedure. When the trail has formed, the only phase changes present in the signal will be due to the wind. Thus U can be measured and $Z_U(x)$ corrected to give $Z(x)$. In carrying out this correction ϕ must be altered until $Z(x)$ has the correct form. However, in practice ϕ can often be determined by the shape of the echo as it passes through the t_o point. This procedure has been successfully carried out on a very large number of echoes, analysed by McAvaney (1970) and Gartrell (1971) in determining the meteor's velocity and t_o point. In the present investigation x was only approximately converted to s as range information was lacking.

Wind shear cannot be corrected for, although its effects can be gauged; when a linear wind shear exists the end of the trail is bent toward or away from the receiving station. Trail elements thus reflect radio waves with different phases so that the vector spiral changes its

shape after it has been formed. In the case of a wind that is the same at all heights the vector spiral of reflected signal amplitudes rotates as a whole retaining its shape. However, a wind shear imposes different rates of rotation on the various sections of the spiral, thus changing its shape. Only fairly severe cases of wind shear can significantly alter the spiral in the time it takes to form, so this effect has been ignored.

8.4(c) Diffusion

Diffusion has very little effect on the pre-t_o diffraction pattern except in cases where the diffusion is very rapid. This is because signals add together in the form of a spiral which largely cancels out the effect of earlier signals, so their decay becomes unimportant. This is not the case for the post-t_o diffraction, which is considerably affected by the decay of the principal zone's signal (Lebedinets and Sosnova, 1967).

8.5 Recording Equipment

Four of the receivers used in this experiment were low noise valve receivers with an overall bandwidth of ± 4.0 KHz at the 3 db points. The fifth receiver was a Racal communication receiver and this was used with a bandwidth of 1.2 KHz. These receivers were connected to half wave dipole aerials, mounted one quarter of a wavelength above the ground. The detected outputs from these receivers were passed through low pass filters (600 Hz at the 3 db point) and applied to the vertical

deflection plates of three double-beam oscilloscopes by D.C. amplifiers. A 35 mm camera with a film speed of 1.9"/sec, then recorded this vertical deflection across the film. The horizontal movement of the film thus mapped the deflection along the film. As echoes are only present for a small part of the total time, the camera was not operated continuously. Instead the signals were recorded on a six channel tape recorder, the tape of which was made up as a loop so that the signals were effectively delayed for two seconds before being read and displayed. The fully developed echo from the meteor could thus be used as a trigger, turning the camera on and allowing it to record the delayed signal and therefore the build up of the echo. The sequence of operations after receiving the trigger was as follows:-

(a) The camera was turned on and the oscilloscope tubes brightened.
(b) The recording continued for a pre-determined period and then the camera turned off and the oscilloscope tubes darkened.
(c) A clock face and counter were illuminated by an electronic flash and the counter incremented.

A block diagram of the receivers, tape delay and recording system is shown in Figure 8.7 . A more detailed account of the tape delay is given by McAvaney (1970).

8.6 Results

8.6(a) Film Reading

Samples of records obtained are shown in Figure 8.8. These were

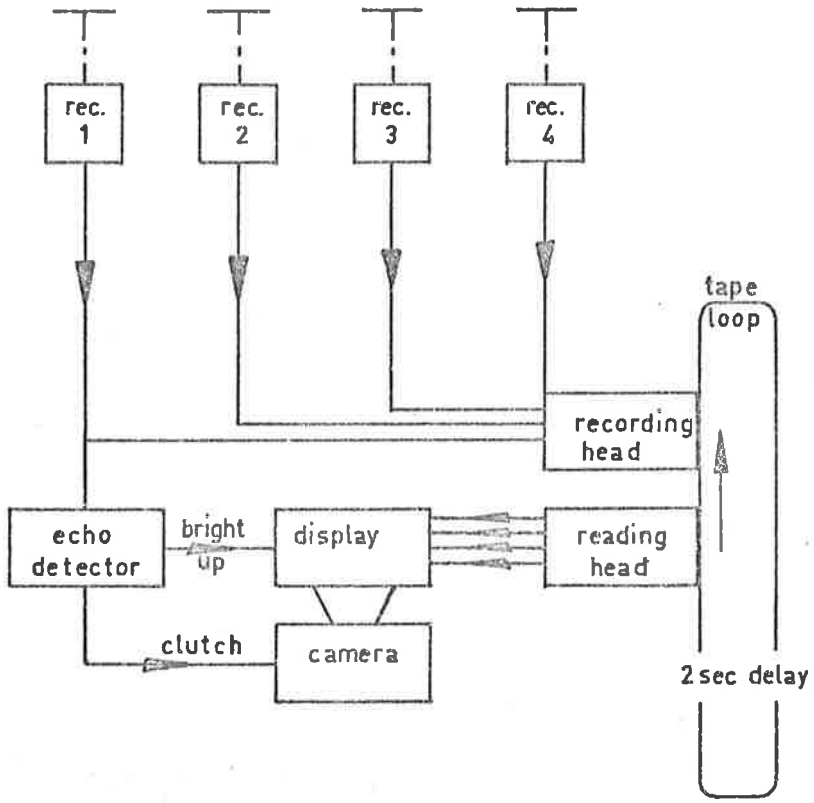

Figure 8.7 The system used to record the pre-t_o diffraction patterns.

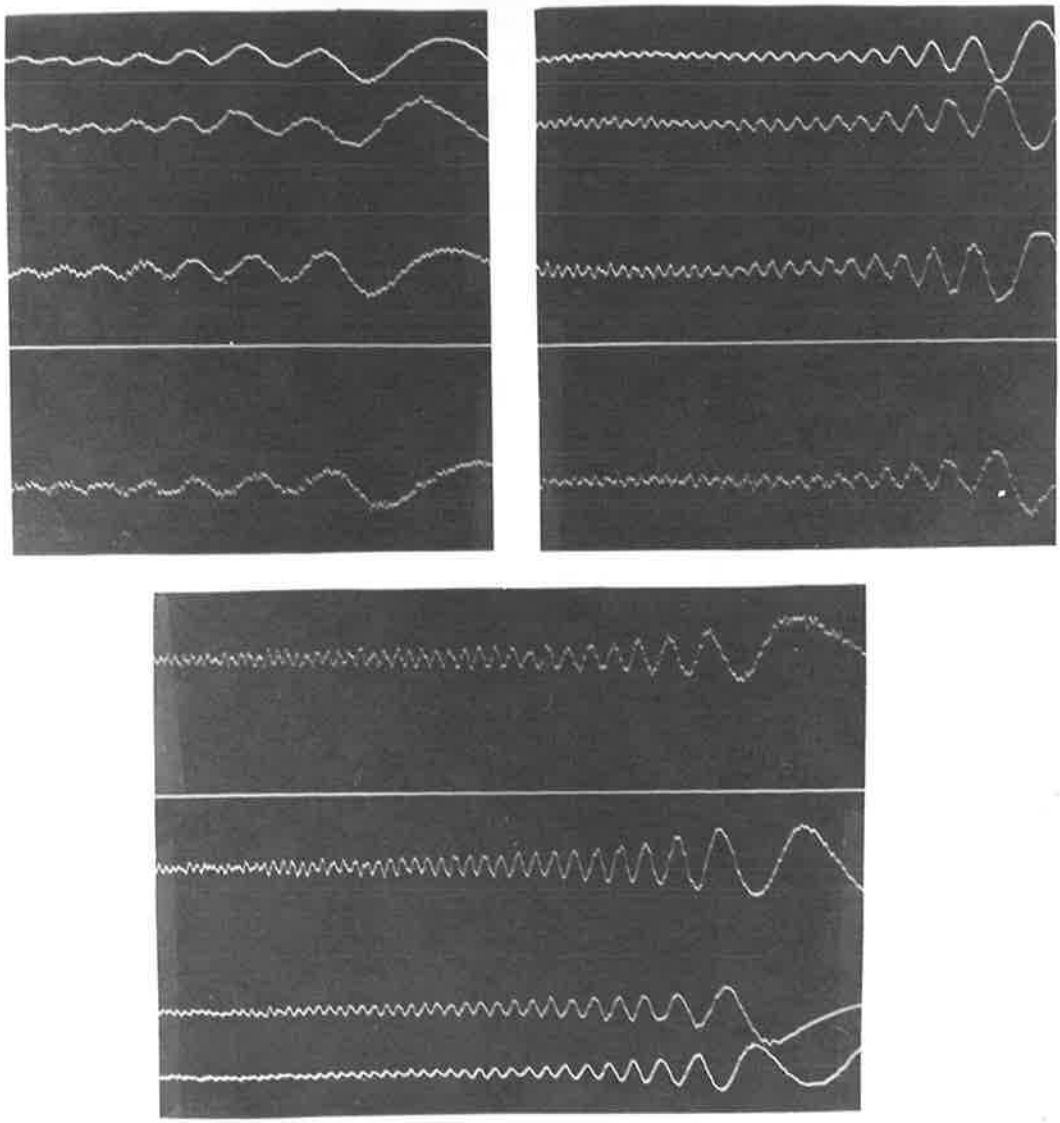

Figure 8.8 Three records of pre-t_o diffraction patterns.

digitized using a film reader (Stone, 1966) which punched onto computer cards the positions of two perpendicular wires on the display screen. The cards were then read by a computer program and analysed in the manner already described. The time interval used in digitizing was chosen to suit the diffraction pattern so that a minimum of about ten points described the smallest Fresnel cycle of the record length considered. The positions of maxima and minima of the Fresnel oscillations were recorded separately.

8.6(b) Reflection Coefficients

A reflection coefficient was calculated for each of the points of the digitized pattern. The resulting reflection coefficient profiles, and their error, were smoothed with a weighted running mean. The weights used were the function cos Z(x) which becomes equal to zero at the turning points of the diffraction pattern. The number of points in the running mean was chosen to smooth out scales less than 240 m as this removed most of the obvious noise present. These profiles are shown in Figure 8.9. The trail length indicated for these profiles assumes an echo range of 150 km. As the trail length is proportional to $\frac{x}{\sqrt{R}}$, this should represent a reasonable value for most echoes.

In all five cases the smoothed profiles show that for scale lengths between 240 m and 1 km, fluctuations are less than 10% of the mean value. The profile for echo 1 has a change in reflection coefficient of about 30% over a 2 km length, and this is clearly present in all the

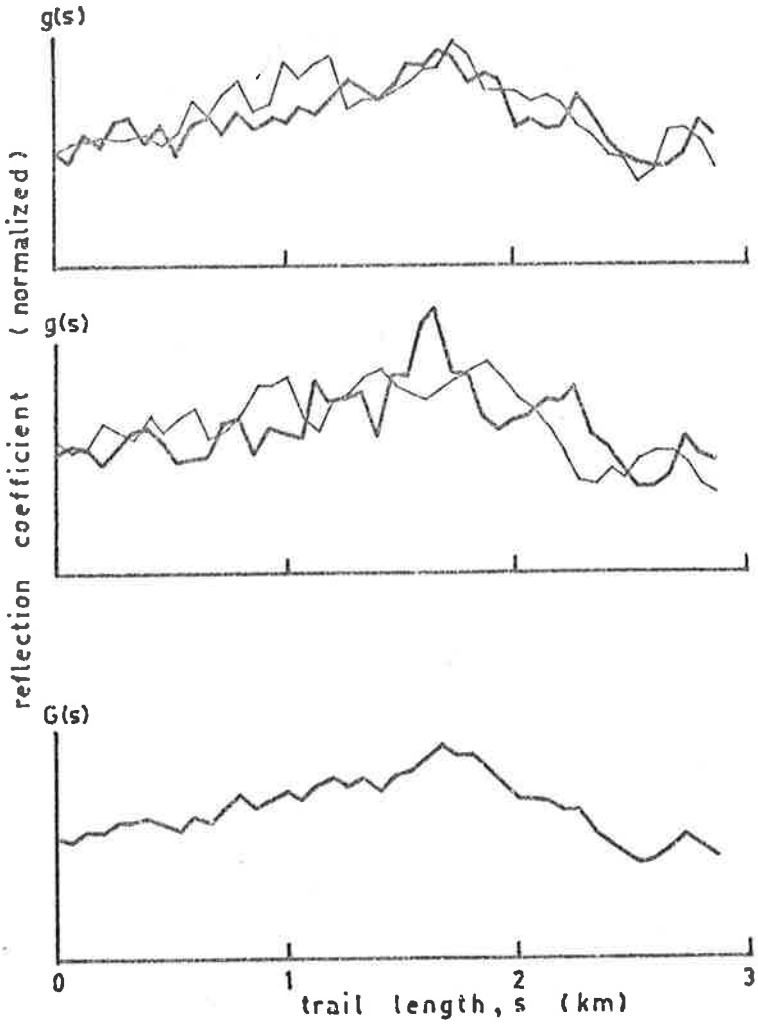

Figure 8.9(a) Echo number 1 showing four profiles g(s), which were obtained from four pre-t_o diffraction patterns, and a mean profile G(s), derived from these.

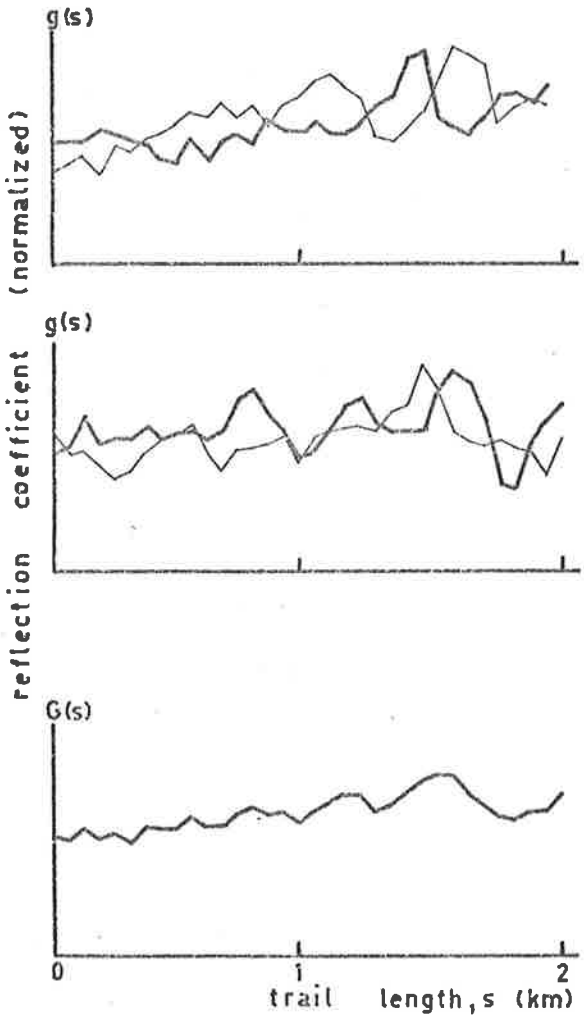

Figure 8.9(b) Echo number 2.

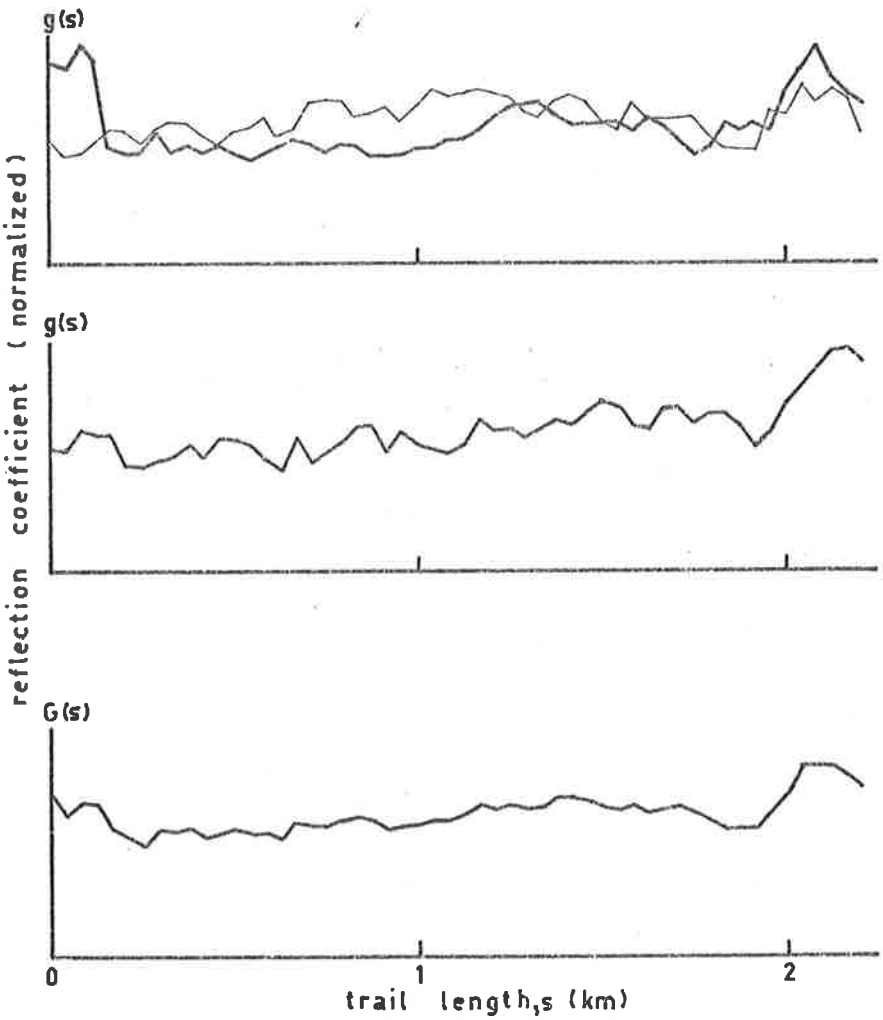

Figure 8.9(c) Echo number 3.

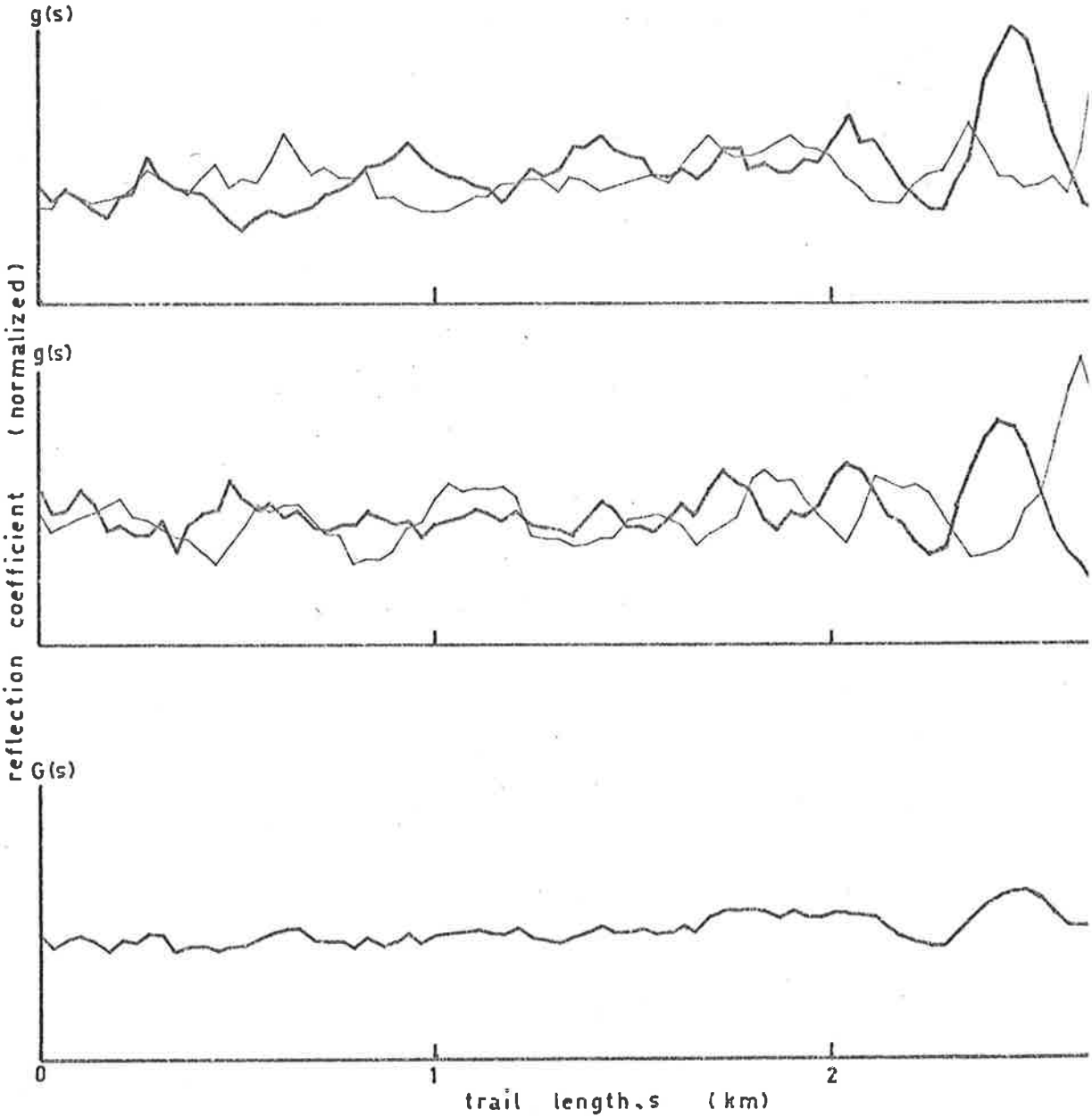

Figure 8.9(d) Echo number 4.

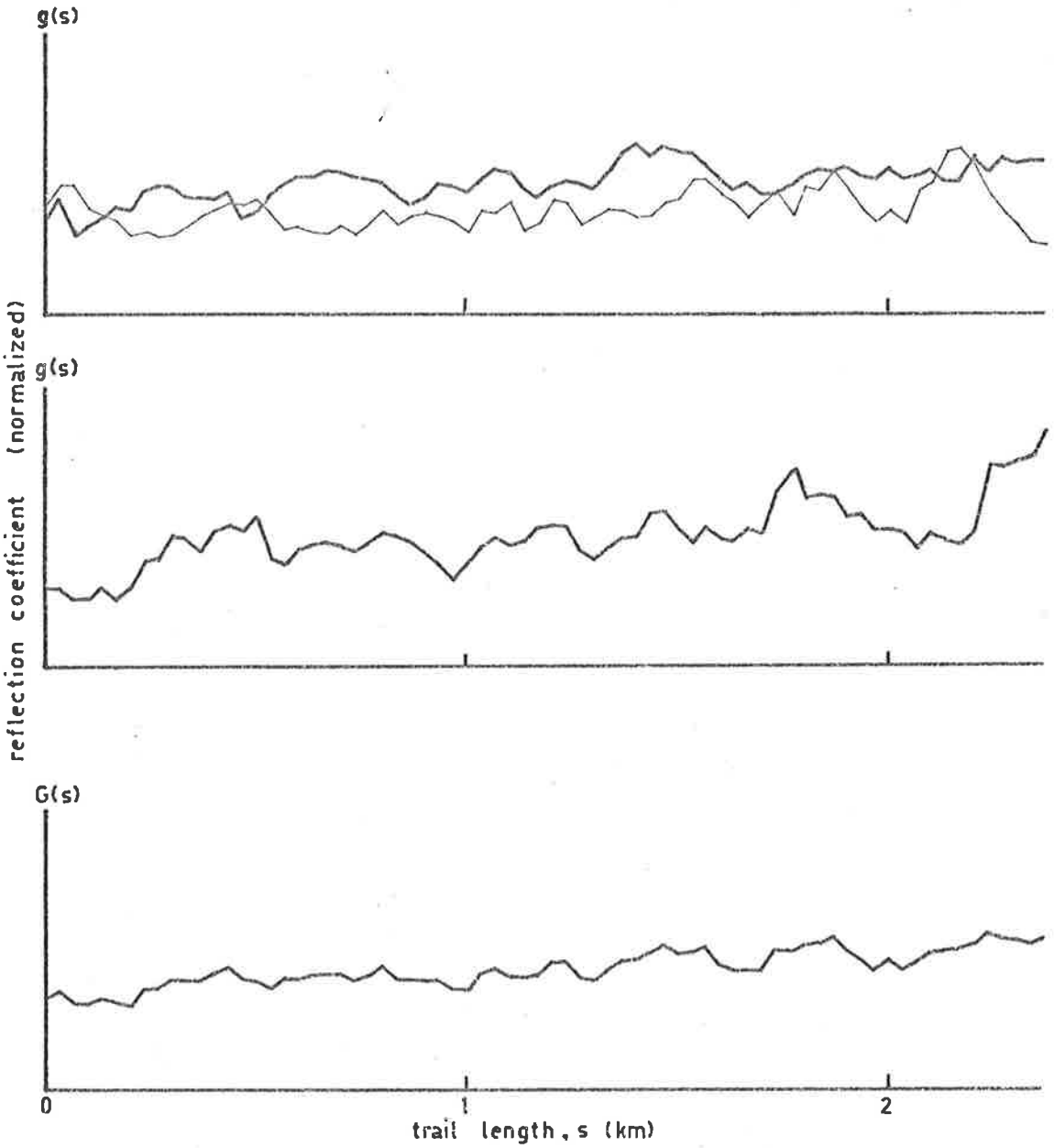

Figure 8.9(e) Echo number 5.

independent profiles for this echo. Echo 2 has a gradually increasing reflection coefficient, while the remaining three are largely constant for the 2 - 3 km for which they are determined.

8.6(c) Electron Line Density

The relationship between electron line density and reflection coefficient has been discussed in Chapter 2.3 for a column of electrons with a Gaussian electron density cross-section. If a trail element is defined as being about 100 m long with a radius of about 1 m, it should be reasonably safe to assume that these results can be applied to it. For electron line densities less than about 5.0×10^{13} electrons/m the reflection coefficient should be proportional to the electron line density. The reflection coefficients for waves polarized transversely to the column should, however, be greater than those for waves polarized longitudinally for line densities greater than about 5.0×10^{13} electrons/m. Electron line densities greater than 5.0×10^{14}/m reflect signals strongly and should, therefore, not be dismissed entirely. For longitudinal polarization the reflection coefficients will be closely proportional to the electron line density, provided the trail shows a near-exponential decay. Otherwise the echo is in the overdense category and the reflection coefficient is fairly constant and independent of the electron line density. Radio waves polarized transversely to the column resonate with it and for electron line densities greater than 5.0×10^{13}/m this resonance makes the reflection coefficient depend on line density and trail radius in a complicated manner. At the same time the

reflected wave undergoes a phase change of up to 180° and so any interpretation of the reflection coefficient in terms of a line density will be almost impossible.

8.7 Conclusions

It could be inferred from these profiles that most ionization irregularities have a scale length that is greater than 1 km. However, the echoes analysed were chosen for a reasonably good signal-to-noise ratio and therefore would be echoes that are approaching an overdense form. Echoes that were easily seen to be underdense by the exponential form of their decay were, in general, too weak to be digitized until the last few Fresnel cycles. However, all five examples show the same lack of small scale irregularities and it is unlikely that they all are borderline underdense-overdense echoes. Preliminary results given by Jones (1969) indicate that small scale irregularities about 1 km in length have a root-mean-square deviation of less than 30% of the mean electron line density. The five examples shown here indicate that this value may be an upper limit rather than a typical value.

CHAPTER 9

CONCLUSIONS AND FUTURE WORK

9.1 Introduction

It has been shown that radio echoes can be observed from meteor trails at a frequency of 1.98 MHz. The results of a preliminary study of these echoes have been presented and compared with theoretical predictions based on observations at higher frequencies. As this study is the first to be made of radio echoes at such a low frequency, it has been broadly based. It therefore remains to outline the merits of low frequency observations and to thereby indicate the direction of future work.

It was shown in Chapter 5 that the radio echo height ceiling does not increase significantly for radio frequencies below 17 MHz. The main advantages of low frequency observations thus lie in the greatly increased echo durations. The disadvantages, however, come from radio reflections from the E-region which are constantly present during the day and often extend into the night when sporadic-E ionization exists. These reflections overpower the reflections from meteor trails, severely restricting the periods when meteor echoes can be observed. Thus observations of meteor showers (Chapter 7) are difficult. The possibility of working at an intermediate frequency, such as 6 MHz, thus combining long echo durations with extended periods of observing, will be discussed in this chapter.

9.2 Winds

The 1.98 MHz wind observations shown in Chapter 6 were obtained from records that were also intended for observations of the echo height distribution, and the echo polarization. Only one component of the wind could be measured because of equipment limitations. This was, however, sufficient to show that the wind observations agreed well with the 27 MHz observations where they overlapped. It was also shown that the height range over which the wind could be measured was substantially increased, enabling direct comparisons to be made between the movement of the neutral wind and the movement of the diffraction pattern of radio waves reflected from the D region and weak layers of sporadic-E. (Strong reflections from sporadic-E layers prevented any observations of meteor echoes at 1.98 MHz). Future wind comparisons of this type can be arranged so that both the north and east components of the wind are measured simultaneously. This would halve the time required to observe a wind height profile, thereby improving the system's ability to detect changes in the wind profile.

It was shown in Chapter 4 that above 105 km the decay time constants of echoes at 1.98 MHz are close to their theoretically predicted values, which are proportional to λ^2 (where λ is the radio wavelength). Thus for a given wind, the phase change which has occurred before the echo has decayed to 1/e of its maximum amplitude (P_t), is proportional to λ. This effect is illustrated in Figure 9.1 where P_t is plotted against height for 2, 6, 20 and 60 MHz for an echo with a zenith angle of 45° and

a wind of 50 m/sec away from the station. It can be seen that there will be a maximum difference of 15 km between the height ceilings of echoes observed at 2 and 20 MHz if the minimum phase shift required by both systems to record the wind is the same. This is a maximum difference, under these conditions, because the height ceiling may be set by the actual height distribution of trails, as at 1.98 MHz only a few echoes were observed above 115 km. The above effect can be seen in the wind results shown in Chapter 6 where the wind readings at 27 MHz are mostly near 90 km, while those at 1.98 MHz are centred around 103 km (see the height distributions in Figure 5.4). Increasing the radio frequency to 6 MHz would lower the height ceiling of wind measurements because the echo duration (compared to echoes at 1.98 MHz) is reduced by a factor of 9, while for a given wind the rate at which the phase changes is only increased by a factor of 3. This can be seen in Figure 9.1 where the height ceiling for wind measurements at 6 MHz is about 7 km below the 2 MHz ceiling.

9.3 Electron Attachment

The echo decay rates (at 1.98 MHz) below 105 km are shorter than diffusion theory predicts. They were shown in Chapter 4 to be scattered around an average value of about 4 seconds. It was shown in Chapter 2 that the radial spread of the trail is governed by diffusion for the first 30 seconds. After this time wind turbulence becomes more important. Thus some process other than wind turbulence must cause the rapid decay actually observed. In fact electron attachment rates observed by Glöde

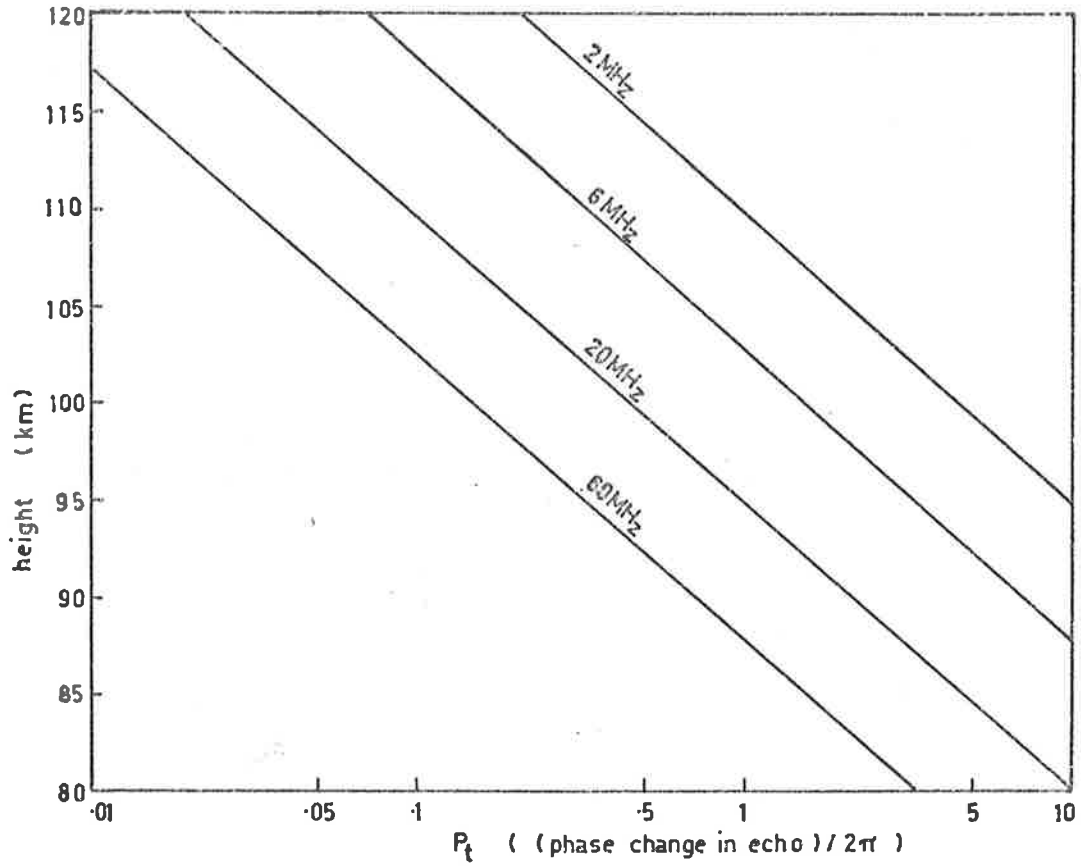

Figure 9.1 The phase change (P_t) an echo undergoes if under the influence of a wind of 50 m/sec away from the receiving station, during the time the echo takes to decay by a factor of 1/e.

(1968) for short duration overdense echoes (at 30 MHz), can be used to explain the observations.

It can thus be seen that observations of the decay rates of underdense radio echoes at frequencies near 2 MHz provide a powerful measure of electron attachment rates. At higher frequencies attachment can only be observed to affect the durations of overdense echoes which do not occur very frequently compared to the occurrence of underdense echoes. Low frequency observations are, however, limited to those times when ionization in the D and E regions is small. Measurement of the decay rate is also hampered by the almost inevitable fading of the returned signal (through secondary reflections) which occurs with most radio meteor echoes with durations greater than one second. This fading will adversely affect any study of rate of attachment using radio meteor echoes, as the effects of attachment are slow compared to the rate at which trail distortions occur. If the radio frequency is raised to 6 MHz, the trouble with ionospheric reflections in the E region can be overcome and echo decay rates can be measured during both the night and day. However, because the decay rates of underdense echoes through diffusion will be nine times faster than they are at 2 MHz, the rate of decay through attachment will only compare with the rate of decay through diffusion for heights below 90 km.

9.4 Echo Polarization

Attempts to observe resonance effects present in the echo's

polarization were reported in Chapter 4. These were found to be less pronounced than the effects predicted by theoretical calculations described in Chapter 2. A possible reason for this could be that the electrons do not have a Gaussian distribution across the trail, their diffusion being influenced by the magnetic field or by small scale turbulence. However, any conclusions drawn from the small amount of data obtained (concerning echoes with an electron line density intermediate between underdense and overdense) must be treated with a great deal of caution. There would be considerable value in observing meteors at 6 MHz, as the resonance effects would still be easily observed and the extended periods of observation would enable a much larger number of echoes to be observed.

A reduction in the average detection time of the scanning gate described in Chapter 3 would make it possible to observe the plane polarized wave reflected from the trail while the trail's radius was very small compared to the radio wavelength. Such observations would make it possible to determine the orientation of the trail from single station observations (and hence allow the determination of the meteor's radiant) and may lead to a method of observing the trail's initial radius.

9.5 Recommendations for Future Work

The comparison made in Chapter 6 between D and E region movements and the neutral wind should be extended to include both north and east

wind components. This work would be more easily carried out at 6 MHz, provided the wind can be determined from echo phase shifts of about $\pi/5$ radians.

Measurement of attachment rates between 90 and 100 km should also be extended. It was shown in Chapter 5.2 that the present system discriminates against echoes below 105 km. This could be overcome by adopting a different system of detecting echoes where persistent echoes exist. Work at 6 MHz would be valuable in measuring attachment rates below 90 km.

Further work on the echo's polarization should be directed towards observing the plane polarized wave initially reflected from the trail at 1.98 MHz, while resonance effects would be most profitably observed at 6 MHz.

APPENDIX A

REFLECTION COEFFICIENTS OF RADIO WAVES FROM METEOR TRAILS

A.1 Introduction

The method outlined in this appendix follows that described by Keitel (1955) and Lebedinets and Sosnova (1967).

A.2 Equations to be Integrated

The electric field E and magnetic field H within the meteor's ionized column satisfy Maxwells equations where

$$\text{curl } H = -i \varepsilon k E; \qquad \text{div } B = 0 \qquad \text{A.1}$$

$$\text{curl } E = i k H; \qquad \text{div } D = 0$$

These equations can be reduced to the form

$$\text{Grad } \frac{1}{\varepsilon} \times \text{Curl } H + \frac{1}{\varepsilon} \text{Curl} \cdot \text{Curl } H = k^2 H \qquad \text{A.2}$$

$$\text{Curl} \cdot \text{Curl } E = \varepsilon k^2 E$$

Where the electric field is either parallel or perpendicular to the column, the equations can be simplified. If cylindrical co-ordinates r, θ, Z are used then in the case of parallel polarization $E = E_{\parallel} = E_z$, and $E_x = E_y = 0$. Expressing the fields E and H as a Fourier series such that

$$E = E_z = \sum_o^n P_n \cos.n\,\theta; \quad H = H_\theta = \frac{-1}{ik} \sum_o^n P_n^{\,1} \cos n\,\theta \qquad \text{A.3}$$

then the Fourier coefficients satisfy the equation

$$\frac{d^2 P_n}{dr^2} + \frac{1}{r} \frac{dP_n}{dr} + \left(\varepsilon k^2 - \frac{n^2}{r^2}\right) P_n = 0 \qquad \text{A.4}$$

In the transverse case $H = H_{\parallel} = H_z$, $H_x = H_y = 0$ and Equations A.2 become

$$\frac{d^2T_n}{dr^2} + \left(\frac{1}{r} - \frac{\frac{d\epsilon}{dr}}{\epsilon} \right) \frac{dT_n}{dr} + \left(\epsilon k^2 - \frac{n^2}{r} \right) T_n = 0 \qquad \text{A.5}$$

and

$$H = H_z = \sum_o^n T_n \cos.n\theta; \quad E = E_\theta = \frac{1}{i\epsilon k} \sum_o^n T_n{}^1 \cos.n\theta \qquad \text{A.6}$$

The dielectric constant ϵ is defined by

$$\epsilon(r) = 1 - \frac{4\pi e^2 N(r)}{k^2 mc^2 \left(1 - i\frac{\nu}{\omega}\right)}, \qquad \text{A.7}$$

where e and m are the electronic charge and mass; k is the radio wave number; c is the velocity of light; ν is the electron collision frequency; and $\omega = 2\pi f$ where f is the radio frequency. For a Gaussian electron density distribution across the column

$$N(r) = \frac{\alpha}{\pi r_o^2} \exp\left[- \left(\frac{r}{r_o} \right)^2 \right] \qquad \text{A.8}$$

where α is the electron line density, and r_o is the radius of the column to the point where the electron density has fallen to 1/e of its maximum value.

A normalized column radius can be used such that

$$\rho = \frac{r}{r_o} \qquad \text{A.9}$$

In this case Equation A.8 becomes

$$N(\rho) = \frac{\alpha}{\pi r_o^2} \exp(-\rho^2), \qquad \text{A.10}$$

and Equations A.4 and A.5 become

$$\frac{d^2P_n}{d\rho^2} + \frac{1}{\rho} \frac{dP_n}{d\rho} + \left[\epsilon (kr_o)^2 - \frac{n^2}{\rho^2} \right] P_n = 0 \qquad \text{A.11}$$

and

$$\frac{d^2T_n}{d\rho^2} + \left(\frac{1}{\rho} - \frac{\frac{d\varepsilon}{d\rho}}{\varepsilon}\right)\frac{dT_n}{d\rho} + \left(\varepsilon(kr_o)^2 - \frac{n^2}{\rho^2}\right) T_n = 0 \qquad \text{A.12}$$

Because $\varepsilon(r)$ is a complex quantity, both functions P_n and T_n will also be complex. If they are written as

$$\begin{aligned} P_n &= A_n + i\, b_n \\ T_n &= C_n + i\, d_n \end{aligned} \qquad \text{A.13}$$

then in operator form the Equations A.4 and A.5 become

$$F_n(A_n) = M(b_n); \quad F_n(b_n) = -M(A_n) \qquad \text{A.14}$$

and

$$G_n(C_n) = N(d_n); \quad G_n(d_n) = -N(C_n) \qquad \text{A.15}$$

Let $\varepsilon(r) = \varepsilon_R + i\varepsilon_I$. Then for the longitudinal case these operators are

$$\begin{aligned} F_n &= \frac{d^2}{dr^2} + \frac{1}{r}\frac{d}{dr} + k^2\,\varepsilon_R - \frac{n^2}{r} \\ M &= \varepsilon_I\, k^2, \end{aligned} \qquad \text{A.16}$$

and for the transverse case

$$\begin{aligned} G_n &= F_n - \frac{1}{\varepsilon_R}\frac{d\varepsilon_R}{dr}\cdot\frac{d}{dr} \\ N &= M + \frac{1}{\varepsilon_I}\frac{d\varepsilon_I}{dr}\cdot\frac{d}{dr}. \end{aligned} \qquad \text{A.17}$$

Equations A.14 and A.15 can be numerically integrated out through the ionized column to a point $r = x$ where $\varepsilon(x) = 1$ (to the accuracy of the solution). This is effectively free space. The fields can then be matched to the external fields which are made up of an incident plane wave

and a reflected cylindrical wave. The incident wave can be expanded as a series of Bessel functions of the first kind

$$E_{INC} = \exp(ikx) = \sum_{n=0}^{\infty} \tau_n i^n J_n(kr) \cos n\theta \qquad A.18$$

where τ_n is Neumann's constant and $\tau_n = 1$ for $n = 0$, $\tau_n = 2$ for $n = 0$. The reflected wave can be expressed in terms of Hankel functions which have amplitudes $q_n + i\, s_n$. Thus the external wave is

$$E_x(r) = \sum_{n=0}^{\infty} \tau_n J_n(kr) \cos n\theta + \sum_{n=0}^{\infty} (q_n + i\, s_n) H_n(kr) \cos n\theta \qquad A.19$$

where the Hankel function

$$H_n(kr) = J_n(kr) + i\, N_n(kr) \qquad A.20$$

and $N_n(kr)$ is a Bessel function of the second kind. At the boundary this field will be both equal to, and continuous with, the internal field. This condition yields two complex equations which can be solved to yield two complex constants which determine the amplitude of the reflected wave, and the amplitude of the wave inside the column. The plane wave scattering coefficient defined by Eshleman (1952) can then be calculated. This is defined as

$$A = \sqrt{\frac{\pi k R_o}{2}} \left| \frac{F(R_o)}{F_o} \right| \qquad A.21$$

where $F(R_o)$ is the scattered field strength at a distance R_o from the column; and F_o is the incident field strength at the column. The reflection coefficients are thus

$$A_{||} = \sum_{n=0}^{n} \tau_n \frac{P_n^1 J_n - k J_n^1 P_n}{-H_n^{(1)} P_n^1 + k H_n^1 P_n} \cos n\theta$$

$$A_{\perp} = \sum_{n=0}^{n} \tau_{w} \frac{T_n^{1} J_n - k J_n^{1} T_n}{-H_n^{(1)} T_n^{1} + k H_n^{1} T_n} \cos n\theta \qquad A.22$$

A.3 Numerical Solution

As r approaches zero, Equations A.4 and A.5 become Bessel's equation for the Bessel function of the first kind $J_n (k\sqrt{\epsilon} \cdot r)$. Thus the functions $P_n (r)$ and $T_n (r)$ can be set equal to $J_n (k\sqrt{\epsilon}r)$ at the start of the numerical integration. When $\epsilon(r)$ is negative the argument of the Bessel function is complex. The expressions valid for small arguments can in fact be used so that

$$P_o (r) = T_o (r) = 1 - (k \sqrt{\epsilon} \cdot r)^2/4$$

$$P_n (r) = T_n (r) = (k \sqrt{\epsilon} \cdot r/2)^n/n! \quad \text{for } n = 0 \qquad A.23$$

are satisfactory initial conditions where $r = 1.0 \times 10^{-6}$.

Integration was performed by the Runge-Kutta method with the step size automatically adjusted to give the accuracy required. The number of Fourier coefficients required depends on both the accuracy needed in the answer as well as the value of kr_o (where r_o is the radius of the Gaussian to the 1/e point) being computed. The reason for this is that the Bessel function does not achieve a significant value until a point is reached close to where the argument becomes equal to the order. Beyond this point the function rises rapidly and then undergoes oscillations of decreasing amplitude. If the Bessel function is virtually zero throughout the column it will not be significantly affected by the column and will have a reflection coefficient that is virtually zero.

A.4 Results

Reflection coefficients have been computed for a number of electron line densities for waves polarized parallel and perpendicular to the column. In the case of parallel polarization, the amplitude and phase of the reflection coefficients follow those deduced by Lebedinets and Sosnova (1967). However, in the case of perpendicular polarization the amplitudes of the reflection coefficients appear to be consistent with their calculated values, while the phase angles do not. Figures A.1 and A.2 show the two sets of values. There are two aspects to the disagreement over phase angles, first in the limiting value of phase for $kr_o \to 0$. Values obtained in the present investigation converge to a common point in the same manner as the phase angles calculated for parallel polarization. The second region of disagreement lies in the sign of the complex part of the reflection coefficient. In the present case this sign is negative, so that the phase angle for low electron line densities approaches 90° instead of 270°.

The first point of disagreement is not particularly important from an observational point of view, because the amplitude of the reflection coefficient as $kr_o \to 0$ is very close to zero, so the phase could not be observed. In fact, the very small values of reflection coefficient may be responsible for the behaviour of the phase in Figure A.2 as errors in their calculated values of amplitude could be large. The second point of disagreement is, however, significant. As stated in Chapter 2, the problem can be solved in the case of a small electron line density by

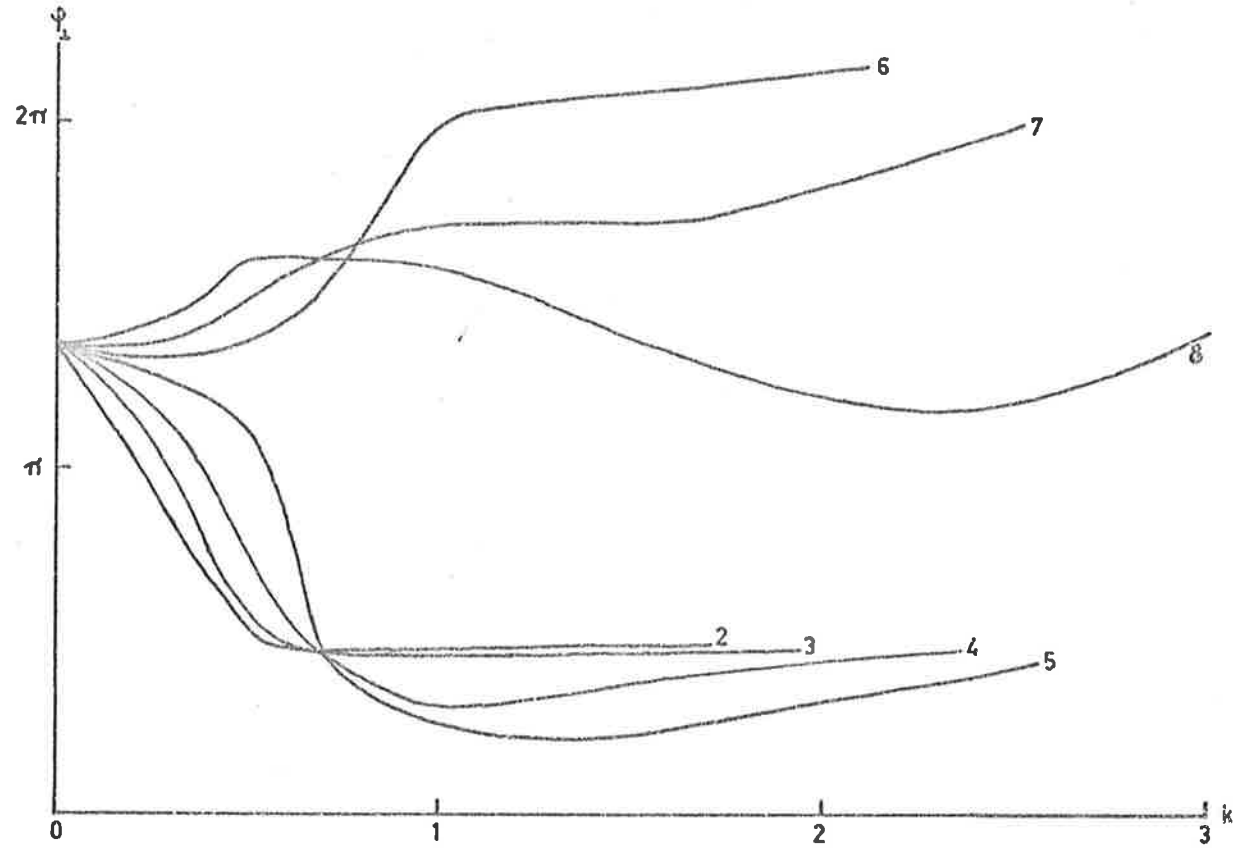

Figure A.1 Values of $\varphi_\perp$ ($\varphi_\perp$ = arctan (A_{im}/A_{re}), where $A = A_{re} + iA_{im}$) found in the present calculations.

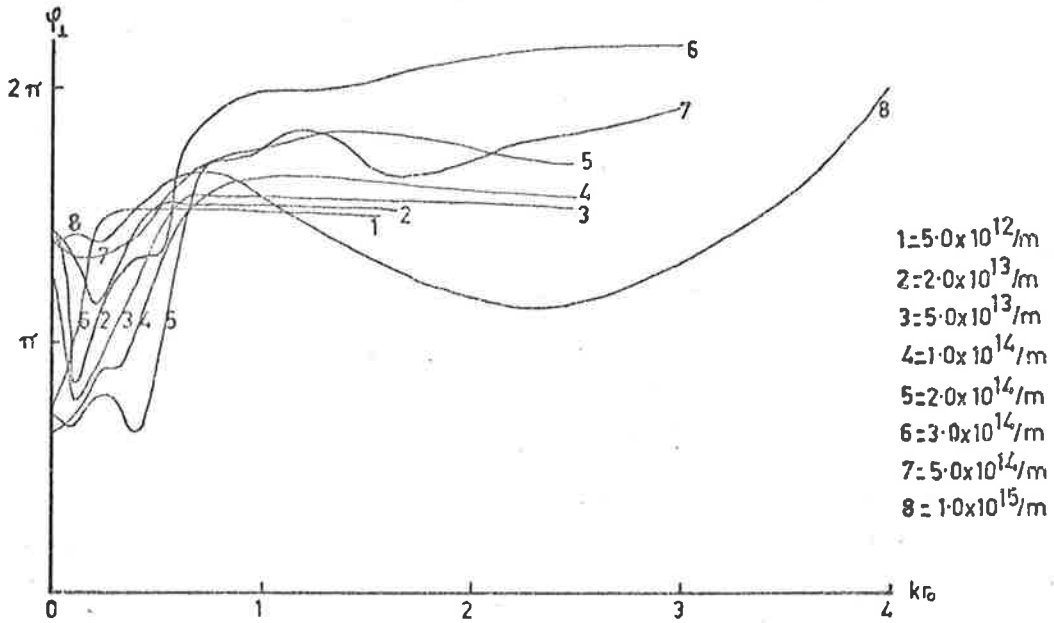

Figure A.2 Values of $\varphi_\perp$ found by Lebedinets and Sosnova (1967) for electron line densities indicated.

only considering the first three Fourier coefficients. The results of these calculations agree with Lebedinets and Sosnova (1967), so the error appears to be in the present calculations. As only the amplitudes of the reflection coefficient are used by the author, and these agree with those published by the above workers, the difficulty with the phase angles has been ignored.

BIBLIOGRAPHY

Appleton, E. V. and Naismith, R. (1947), Proc. Phys. Soc., A 109, 621.

Appleton, E. V., Naismith, R. and Ingram, L. J. (1937) Phil. Trans. Roy. Soc., 236, 191.

Appleton, E. V. and Piddington, J. H. (1938), Proc. Roy. Soc., A 164, 467.

Bartman, G. K., Chaney, L. W., Jones, L. M., and Liu, V. C. (1956) J. Applied Phys., 27, 706.

Bayrechenko, I. V. (1965), Geomagnetizm i Aeonomiya, 5, 460.

Briggs, B. H. (1968), J. Atmos. Terr. Phys., 30, 1777.

Briggs, B. H., Elford, W. G., Felgate, D. G., Golley, M. G., Rossiter, D. E. and Smith, J. W. (1969), Nature, 223, 1321.

Briggs, B. H., Phillips, G. H., and Shinn, D. H. (1950), Proc. Phys., Soc., B 63, 106.

Brown, N. and Elford, W. G. (1971), J. Atmos. Terr. Phys., 33, 1659.

Brysk, H. and Buchanan, M. L. (1965), Can. J. Phys., 43, 28.

Cook, A. G., Stienon, F. M. and Hawkins, G. S. (1960), Harvard Radio Meteor Proj. Interim Rept. No. 47.

Davis, J., Greenhow, J. S. and Hall, J. E. (1959a), Proc. Roy. Soc., A 253, 121.

Davis, J., Greenhow, J. S. and Hall, J. E. (1959b), Proc. Roy. Soc., A 253, 130.

Doyle, E. M. (1968), Ph.D. Thesis, University of Adelaide.

Eckersley, T. L. (1937), Nature, 140, 846.

Elford, W. G. (1964), Harvard Radio Meteor Proj., Res. Rep. No. 8.

Elford, W. G. (1965), Smithson. Contribs. Astrophys., 11, 121.

Elford, W. G., Hawkins, G. S. and Southworth, R. B. (1964a), Harvard Radio Meteor Proj., Res. Rep. No. 11.

Elford, W. G. and Hawkins, G. S. (1964b), Harvard Radio Meteor Proj., Res. Rep. No. 9.

Eshleman, V. R. (1955), Inst. Radio Engrs. Trans., AP-3, 32.

Feinstein, J. (1951), J. Geophys. Res., 56, 37.

Felgate, D. G. (1969), J. Atmos. Terr. Phys., 32, 241.

Felgate, D. G. (1969), Ph.D. Thesis, University of Adelaide.

Finlay, J. W. (1951), J. Atmos. Terr. Phys., 1, 353.

Francey, J. L. A. (1964), Aust. J. Phys., 17, 315.

Fraser, G. J. (1965), J. Atmos. Sci., 22, 217.

Fraser, G. J. (1968), J. Atmos. Terr. Phys., 30, 707.

Gartrell, G. (1971), Ph.D. Thesis, University of Adelaide.

Glöde, P. (1967), I.A.U. Symposium No. 33 "Physics and Dynamics of Meteors", Kresák and Millman (eds), D. Riedel Co., Dordrecht, Holland, 175.

Golley, M. G. and Rossiter, D. E. (1970), J. Atmos. Terr. Phys., 32, 1215.

Greenhow, J. S. (1952), J. Atmos. Terr. Phys., 2, 282.

Greenhow, J. S. (1952a), Proc. Phys. Soc., B65, 169.

Greenhow, J. S. (1959), J. Geophys. Res., 64, 2209.

Greenhow, J. S. (1963), Smithson. Contrib. Astrophys., 7, 5.

Greenhow, J. S. and Hall, J. E. (1960), Mon. Not. Royal Ast. Soc., 121, 183.

Greenhow, J. S. and Hall, J. E. (1961), Planet. Space Sci., 5, 109.

Greenhow, J. S. and Hall, J. E. (1962), J. Atmos. Terr. Phys., 21, 261.

Greenhow, J. S. and Neufeld, E. L. (1959), Proc. Phys. Soc., 74, 1.

Groves, G. V. (1960), Space Res., I, 144.

Hawkins, G. S. (1963), Smithson. Contrib. Astrophys., 7, 23.

Hawkins, G. S. and Whipple, F. L. (1958), Astron. J., 63, 283.

Herlofson, N. (1948), Phys. Soc. Rep. Prog. Phys., 11, 444.

Herlofson, N. (1951), Arkiv For Fysik, 3, 247.

I.A.U. Symposium No. 33 "Physics and Dynamics of Meteors" D. Reidel Publishing Co. Dordrecht, Holland, 264.

Jones, J. (1969), Can. J. Phys., 47, 1969.

Jones, J. (1969a), Can. J. Phys., 17, 1519.

Jones, L. F. (1933), Proc. Inst. Radio Engrs., 21, 349.

Kaiser, T. R. (1953), Phil. Mag. Supp., 2, 495.

Kaiser, T. R. (1954), Mon. Not. Roy. Astron. Soc., 114, 39.

Kaiser, T. R. (1954b), Mon. Not. Astron. Soc., 114, 52.

Kaiser, T. R. (1955), Spec. Supp. J. Atmos. Terr. Phys., 2, 55.

Kaiser, T. R. and Closs, R. L. (1952), Phil. Mag., 43, 1.

Kaiser, T. R., Pickering, W. M. and Watkins, C. D. (1969), Planet. Space Sci., 17, 519.

Kashcheyev, B. L. and Lebedinets, V. N. (1961), Results of the Researches of the I. G. Y., No. 7.

Kashcheyev, B. L. and Lebedinets, V. N. (1963), Smithson. Contribs. Astrophys., 7, 19.

Kato, S. (1959), Rep. Ionos. Space Res. Japan, 13, 62.

Keitel, G. H. (1955), Proc. Inst. Radio Engrs., 43, 1487.

Kochanski, A. (1964), J. Geophys. Res., 69, 3651.

Krautkramer, J. (1950), Archiv. Elekt. Ubertragung, 4, 133.

Lebedinets, V. N. and Portnyagin, Yu. I. (1966), Geomag. Aeron., 6, 544.

Lebedinets, V. N. and Sosnova, A. K. (1967), I.A.U. Symposium No. 33 "Physics and Dynamics of Meteors" D. Reidel Publishing Co. Dordrecht, Holland, 27.

Manning, L. A. (1953), J. Atmos. Terr. Phys., 4, 219.

Manning, L. A. (1958), J. Geophys. Res., 63, 181.

Manning, L. A. (1959), J. Geophys. Res., 64, 1415.

Manning, L. A. (1963), J. Atmos. Terr. Phys., 25, 182.

Manning, L. A. (1964), Radio Sci. J. Res., NBS/USNC-URSI, 68D, 1067.

Manning, L. A., Villard, O. G. and Peterson, A. M. (1950), Proc. Inst. Radio Engrs., 38, 877.

Manring, E. R., Bedinger, J. F. and Knaflitch, H. (1961), Space Res., II, 1107.

McAvaney, B. J. (1970), Ph.D. Thesis, University of Adelaide.

McKinley, D. W. R. (1953), Can. J. Phys., 31, 758.

McKinley, D. W. R. (1961), "Meteor Science and Engineering", McGraw-Hill, N.Y.

McNicol, R. E. and Thomas, J. A. (1960), Aust. J. Phys., 13, 120.

Mitra, S. N. (1949), Proc. Inst. Elect. Engr. Part III, 96, 441.

Murphy, C. H., Bull, C. V. and Edwards, H. D. (1966), J. Geophys. Res., 71, 4535.

Nagaoka, H. (1929), Proc. Imp. Acad. Tokyo, 6, 233.

Nilsson, C. S. (1964), Aust. J. Phys., 17, 1964.

Phillips, E. (1960), Planet. Space Sci., 17, 553.

Phillips, G. J. and Spencer, M. (1955), Proc. Phys. Soc., B68, 481.

Pierce, J. A. (1938), Proc. Inst. Radio Engrs., 26, 892.

Poole, L. M. G. and Kaiser, T. R. (1967), Planet. Space Sci., 15, 1131.

Portnyagin, Yu. I. (1966), Geomagnetism and Aeronomy, 6, No. 4, 707.

Revah, I. (1969), Ann. de Geophys., 25, 1.

Rice, D. W. and Forsyth, P. A. (1963), Can. J. Phys., 41, 679.

Rice, D. W. and Forsyth, P. A. (1964), Can. J. Phys., 43, 2035.

Robertson, D. S., Liddy, D. T. and Elford, W. G. (1953), J. Atmos. Terr. Phys., 4, 255.

Roper, R. G. (1966), J. Geophys. Res., 71, 5785.

Rosenberg, N. W., Golomb, D. and Allen, E. F. (1963), J. Geophys. Res., 68, 5895.

Rossiter, D. E. (1970), Aust. J. Phys., 23, 103.

Schafer, J. P. and Goodall, W. M. (1932), Proc. Inst. Radio Engrs., 20, 1941.

Simek, M. (1964), Astr. Inst. Csl. Acad. Sci., Ondrejov.

Simek, M. (1968), Can. J. Phys., 46, 1563.

Skellett, A. M. (1932), Proc. Inst. Radio Engrs., 20, 1933.

Skellett, A. M. (1935), Proc. Inst. Radio Engrs., 23, 132.

Skellett, A. M. (1938), Nature, 141, 472.

Southworth, R. B. (1962), Harvard Radio Meteor Proj. Res. Rep. No. 14.

Southworth, R. B. (1968), ARCRL Special Reports, No. 75, p. 161.

Stewart, J. Q., Ference, M., Slattery, J. J. and Zahl, H. A. (1947), Sky and Telescope, 6, No. 5, 3.

Stohl, J. (1967), I.A.U. Symposium No. 33 "Physics and Dynamics of Meteors" D. Reidel Publishing Co. Dordrecht, Holland, 298.

Stroud, W. G., Nordberg, W. and Walsh, J. R. (1956), J. Geophys. Res., 61, 45.

Trisková, L. (1967), I.A.U. Symposium No. 33 "Physics and Dynamics of Meteors" D. Reidel Publishing Co. Dordrecht, Holland, 304.

Vincent, R. A. (1967), Ph.D. Thesis, University of Canterbury, Christchurch, New Zealand.

Wait, R. W. (1955), Can. J. Phys., 33, 189.

Webb. W. L., Hubert, W. E., Miller, R. L. and Spurling, J. F. (1961), Bull. Am. Met. Soc., 42, 482.

Weiss, A. A. (1955), Aust. J. Phys., 8, 279.

Wright, J. W., Murphy, C. H. and Bull, G. V. (1967), J. Geophys. Res., 72, 1443.

APPENDIX B

Reprint of paper -

"Radio Echoes from Randomly Ionized Meteor Trails"

by N. Brown and W. G. Elford.

Journal of Atmospheric and Terrestrial Physics, 1971, Vol. 33, pp. 1659–1666. Pergamon Press. Printed in Northern Ireland

Radio echoes from randomly ionized meteor trails

N. Brown and W. G. Elford
Department of Physics, University of Adelaide, Adelaide, S. Australia 5001

(*Received* 4 *May* 1971)

Abstract—The average rate of decay of radio signals reflected from under-dense meteor trails has been shown to follow a simple dependence on trail height. However the decay of a radio echo from a single trail can vary widely from the average for its height. The possibility that this could be caused by an irregular ionization line density along the trail is examined, and decays are calculated for a trail which has a random variation in ionization along its length. The results show only small variations in the signal decay for a stationary trail. However large variations can occur if the trail is in a wind-field subject to shear.

1. Introduction

The rate of decay of radio echoes from meteor trails has been investigated experimentally and theoretically by a number of workers (Kaiser, 1953; Greenhow and Neufeld, 1955; Murray, 1959; Greenhow and Hall, 1961; Rice and Forsyth, 1963; Jones, 1969). One surprising fact is the observation that variable decay rates are observed for under-dense trails occurring at the same height, and the cause of this variation is still unresolved. A suggestion of Rice and Forsyth (1963) that has received considerable attention is that the variation is due to the presence of irregularities in the ionization density along the meteor trail. They considered the special case of a sinusoidal modulation of the ionization density. It will be shown that this does not give a good guide to the behaviour of a randomly ionized trail. The need therefore exists for similar computations with a trail which has random variations of ionization density along it. This paper gives the results of a numerical analysis of the decay of the radio echo from a trail of this type. The effects of a linear shear in the wind acting on the trail are also investigated and shown to be significant. The distribution of ionization along the meteor trail will henceforth be referred to as the 'ionization profile'.

2. Scattering of Radio Waves from Under-Dense Trails

The radio echo from a meteor trail is the sum of radiation scattered from each element of the trail. For under-dense trails the contribution from any element is defined by two parameters; the amplitude, which is initially proportional to the line density of ionization (number of electrons/unit length) and the phase which is determined by the range of that part of the trail. The decay of the amplitude of the signal from any element (for an underdense trail with a Gaussian radial distribution of ionization) is exponential. The rate of this decay, defined as the time for the signal to decay to $1/e$ of its initial amplitude, is directly proportional to the ambipolar diffusion coefficient (neglecting effects of the Earth's magnetic field) and thus inversely proportional to atmospheric pressure.

(a) *Uniform ionization*

In the case of uniform ionization, the vector diagram representing the sum of signals returned from the whole trail is the Cornu spiral. In diffraction problems this

spiral is commonly discussed in terms of half-period zones (or Fresnel zones) and it is convenient to adopt the same approach here. The foot of a normal from the observer to the trail defines the point of specular reflection; and the half period zones are centred on this point. In what follows, the first zone will be called the principal zone; successive increases in range of half a wavelength then mark off the second and succeeding zones along the trail. For a smooth trail the principal zone can be considered to contribute almost all the signal, as contributions from the higher order zones alternately cancel each other to a first approximation. Thus radio frequencies near 30 MHz can be considered to be reflected from about 1 km of the trail centred on the specular point. The rate of decay of the signal is therefore determined by the value of the diffusion coefficient at the height of the specular reflection point. However this assumption breaks down when the degree of ionization is irregular, or when the trail is distorted by turbulence or wind shears, because contributions from higher order zones then become important.

(b) *Non-uniform ionization*

To simplify the discussion the following terms will be used. The term 'trail element' will refer to the smallest section of trail considered in this numerical treatment. While the vector sum of signals for a uniformly ionized trail takes the form of the Cornu spiral, the vector sum for an irregularly ionized trail can be described as a distorted Cornu spiral. The contribution to the echo from the principal zone will be called the 'principal signal', and the contribution from the higher order zones the 'distortion signal'.

Changes in the ionization density of any trail element cause proportional changes in the amplitude of the signal scattered from that element, while leaving the positions of the half-period zones along the trail unaffected. The degree of distortion of the spiral depends on the linear scale of the ionization fluctuations. If this exceeds the length of the first Fresnel zone the distortion will be negligible. However, significant distortion to the spiral can occur where the scale coincides locally with the length of the higher-order zones. This has already been shown by Rice and Forsyth (1963) who discussed a trail in which the line density had been modulated sinusoidally. Such an ionization profile represents a special case where successive higher order zones reinforce rather than cancel each other. This causes a large distortion to the spiral in the region where the wavelength of the modulation is double the zone length (see Section 5(a)).

3. Numerical Analysis

The method used to compute the variation of reflected signal with time follows that already described by Rice and Forsyth (1963). The signal strength was computed for a wavelength of 11·2 m backscattered from a trail 10 km long at an angle of 45° to the horizontal and at a height of 100 km. The trail was divided into sections 10 m in length and the phase and amplitude of the signal from each section initially determined by the distance from the point of observation and the ionization line density of the section. By adding these signals vectorially, the total signal is determined. At any given time after the formation of the trail, the total signal was determined in the following manner. The amplitude of each element was reduced by

an amount determined by the expected exponential decay for the particular height of the element and the vector sum was again computed. The calculation was repeated until the total signal had fallen to 5 per cent of its initial value.

A wind shear (i.e. a linear variation of the horizontal wind speed with height) has the effect of rotating the trail. This was included in the calculation by an appropriate alteration of the phase of the signal from each element.

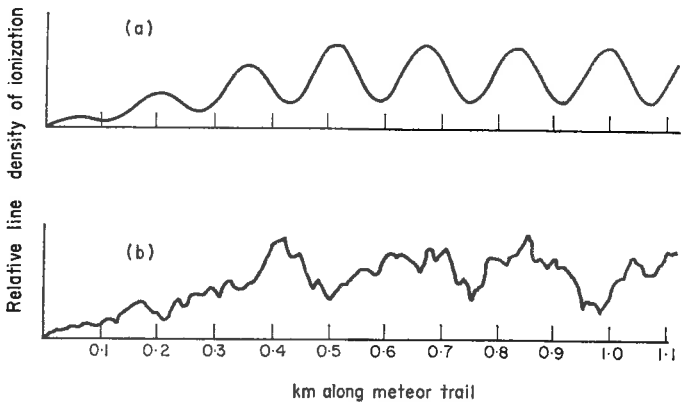

Fig. 1. Ionization profiles for (a) sinusoidal and (b) random ionization along the meteor trail. Only the first kilometer of the trail is shown.

4. Ionization Profiles

The two ionization profiles considered are shown in Fig. 1. They were constructed by taking a column of constant line density with the ends tapered to zero to avoid discontinuity. The whole profile was then modulated. One particular advantage of these profiles was that for specular reflection near the centre of the trail, small movements of the specular point do not significantly alter the average signal from the principal zone.

The sinusoidal profile was modulated to a depth of 50 per cent. The modulating function for the random profile was a sequence of random numbers smoothed by a rectangular running mean. The power spectrum of the random profile is shown in Fig. 2 with the frequency of the sinusoid indicated by an arrow.

5. Results

(a) *No wind*

Distortions to the Cornu spiral can result in significant contributions to the echo from the higher order zones. The effect that this ultimately has on the decay of the signal reflected from the trail, will depend on the phase of the distortion signal relative to that of the principal signal.

In the case of the sinusoidal profile, most distortion occurs where the sinusoidal wavelength is twice the zone wavelength. An example of a distorted spiral for this situation is shown in Fig. 3(a) and its resolution into a principal and distortion signal is illustrated in Fig. 3(b). The associated diffraction pattern is shown in Fig. 3(c). In this example the phase difference between the principal and distortion signals is

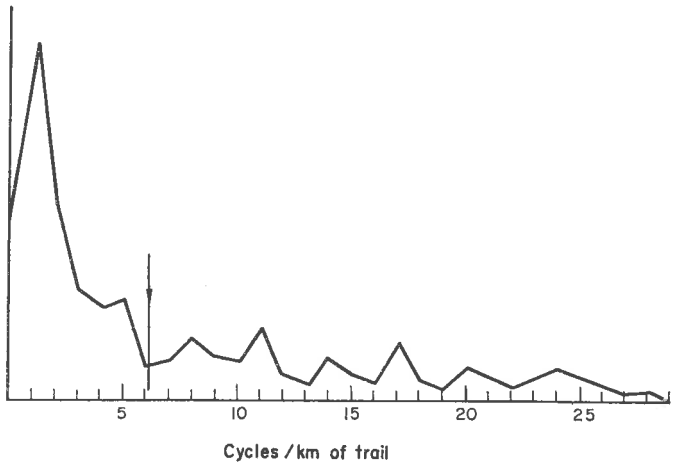

Fig. 2. Power spectrum of the random ionization profile shown in Fig. 1(b). The arrow indicates the frequency of the sinusoid of Fig. 1(a).

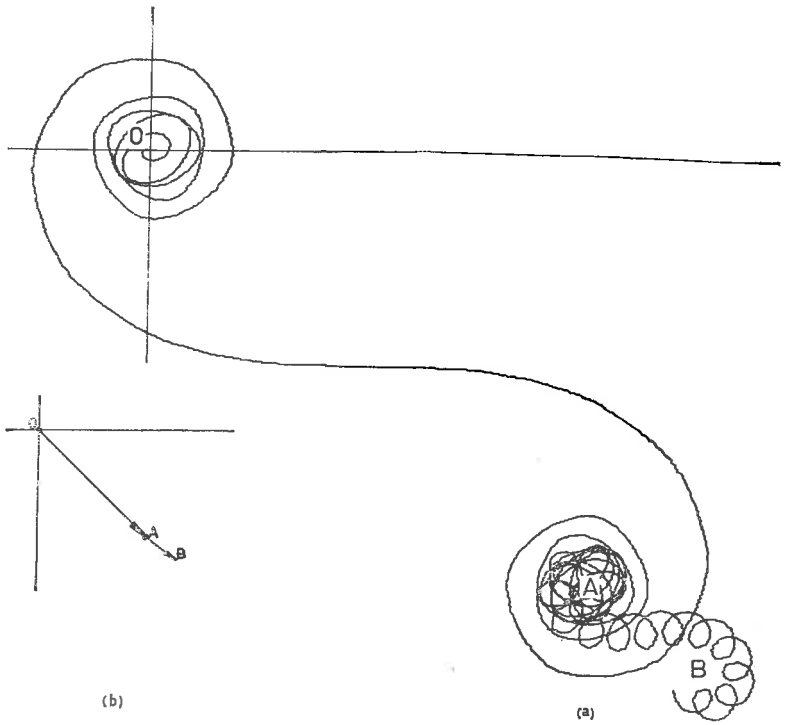

Fig. 3. (a) The vector spiral for the radio signal reflected from the first 9·0 km of a meteor trail with a sinusoidal ionization profile.
The inset (b) shows how this can be considered to consist of a smooth trail signal OA, and a distortion signal AB.

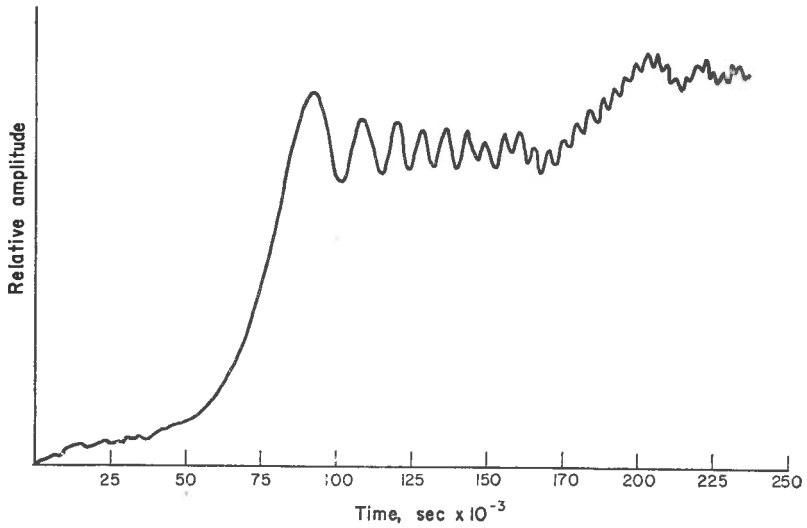

Fig. 3. (c) Diffraction pattern for a meteor whose initial ionization density profile is the sinusoid given in Fig. 1(a). (For a meteoroid with a constant velocity of 40 km/sec.)

close to 0° and there is an enhancement of the amplitude of the echo. In contrast, a phase difference of 180° would have reduced the amplitude of the diffraction pattern.

A typical example of a distorted spiral in the case of a trail with random ionization is shown in Fig. 4(a), and the related diffraction pattern of the radio echo is shown in Fig. 4(b). It is of interest to note that significant oscillations in amplitude can occur during the initial growth of the echo.

For both the random and sinusoidal trails, decay rates were computed for different phases between the principal and distortion signals. This was achieved by moving the trail in 40 m steps parallel to itself, thus shifting the point of specular reflection relative to the irregularities of the trail while maintaining the height of the reflection point at 100 km. The computed decays were all exponential, a result also found for the sinusoidal ionization profile by Rice and Forsyth (1963). Table 1, columns 2 and 3, show an 'apparent height' for the reflection point. This was deduced by making the assumption that the computed signal decay represents the decay of the signal from the principal zone only. By measuring the rate of decay of the echo (T), the coefficient of diffusion (D) for the ionization of the principal zone was determined by using the relation

$$D = \lambda^2/(16\pi^2 T)$$

where λ is the radio wavelength (McKinley 1961). The apparent height (H) of the principal zone was then obtained using the experimental relation

$$\log_{10} D \text{ (m}^2\text{/sec)} = 0{\cdot}067H \text{ (km)} - 5{\cdot}6$$

determined by Greenhow and Neufeld (1955).

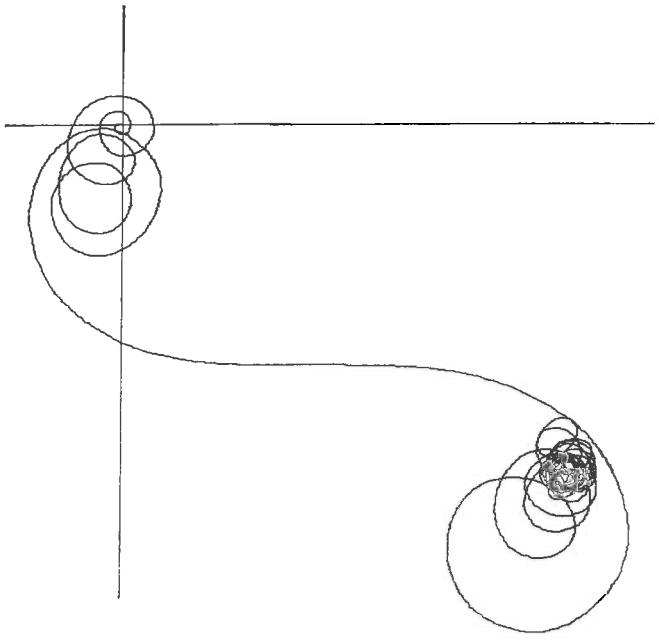

(a)

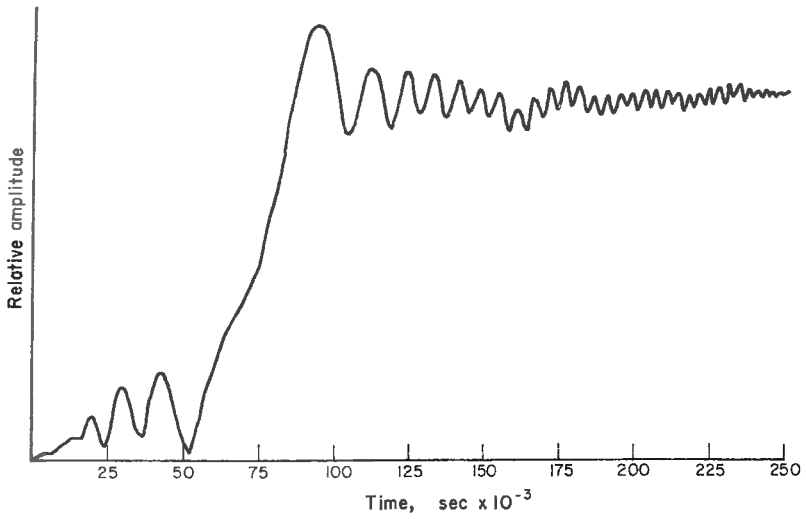

(b)

Fig. 4. (a) The vector spiral for the radio signal reflected from the first 9·0 km of a meteor trail with a random ionization profile.
(b) Diffraction pattern for a meteor whose initial ionization density profile is the random profile given in Fig. 1(b). (For a meteoroid with a constant velocity of 40 km/sec.)

Table 1. Apparent height deduced from the signal decays for meteor trails with sinusoidal and random ionization profiles. Specular reflection occurs initially at a height of 100 km. The first column gives the distance from the upper end of the trail to the initial specular point

Specular position (km)	Apparent height (km) Sinusoidal profile No shear	Random profile No shear	Random profile shear = 20 m/km/sec
2·92	101·0	100·2	100·0
2·96	99·8	100·1	99·0
3·00	99·3	100·1	99·8
3·04	100·0	100·2	99·1
3·08	101·0	100·1	97·3
3·12	99·8	100·0	99·5
3·16	99·3	100·0	101·1
3·20	100·0	100·0	102·2
3·24	101·0	100·0	101·8

(b) *Wind shear*

With a linear wind shear present, the specular point moves along the trail while it is diffusing, owing to the rotation of the trail. For a typical wind shear the change in the height of the specular point only amounts to a few hundred meters, so the decay of the signal reflected from the principal zone is not seriously altered. Ionization irregularities situated in the higher order zones will, however, contribute signals that are continuously changing their phase with respect to the principal zone signal. The resultant signal observed is therefore the sum of a number of vectors all rotating at different rates. The decay should then deviate from the expected exponential decay and show, in some cases, a cyclic variation about an exponential decay.

Figure 5 shows the change in the signal strength with time calculated for a randomly ionized trail, decaying in the presence of a 20 m/sec/km shear. The initial height of the specular point of the trail has been chosen as 100 km. Decays have again been calculated for 40 m shifts of the trail relative to the initial position of the specular point. It can be seen that for this trail profile, the decay of the total signal is almost exponential, but does not occur at the same rate as the decay of the principal signal. The apparent heights assessed from the decay of the total signal in each case are given in Table 1, column 4.

It should be noted that a trail with a similar profile placed lower in the atmosphere so that the specular reflection point is initially at 90 km height, would produce similar effects with a shear of only 5m/sec/km.

6. Discussion

These calculations support the conclusions of Jones (1969), that the effect of random ionization cannot alone explain the large scatter in the observed decay times of meteor echoes at a fixed height. However it has been shown that wind shear can alter the rate of the radio signal decay without significantly changing the exponential appearance. This was so for about half of the cases computed. Thus it would appear that heights deduced from radio echo decays can be significantly in error if the meteor trail is irregularly ionized and subject to wind shear.

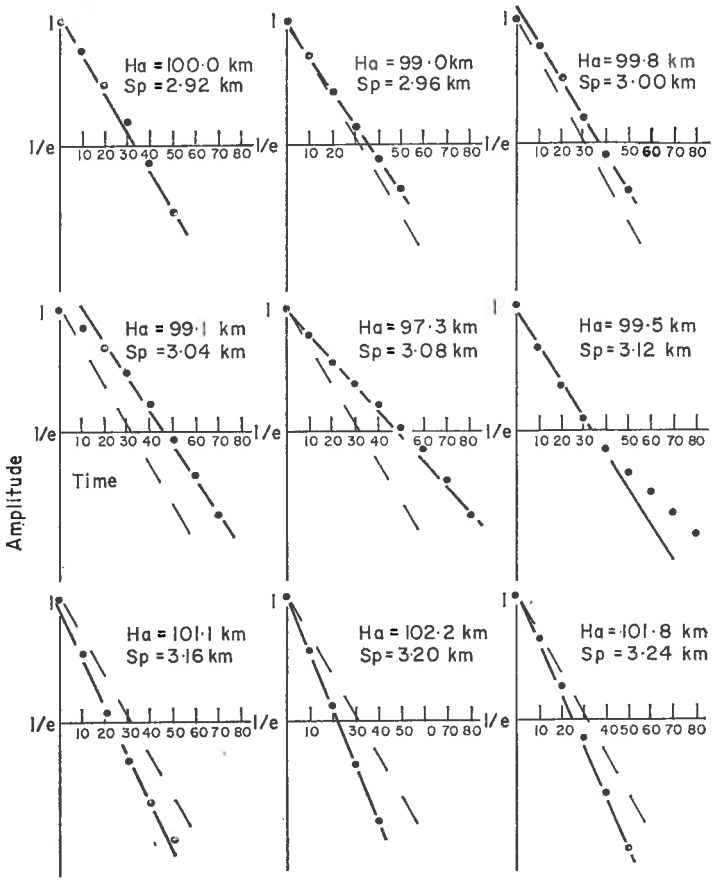

Fig. 5. Plots of log amplitude against time in milliseconds for echoes from a randomly ionized trail subject to a wind shear of 20 m/sec/km. *Ha* is the apparent height and *Sp* the distance of the specular point from the start of the trail. The dashed line represents the decay of the principal signal.

Acknowledgements—This work was supported by a grant from the University of Adelaide.

References

Greenhow J. S. and Hall J. E.	1961	*Planet. Space Sci.* **5,** 109.
Greenhow J. S. and Neufeld E. L.	1955	*J. Atmosph. Terr. Phys.* **6,** 133.
Jones J.	1969	*Planet. Space Sci.* **17,** 1579.
Kaiser T. R.	1953	*Adv. Phys.* **2,** 495.
McKinley D. W. R.	1961	*Meteor Science and Engineering,* p. 203. McGraw-Hill, New York.
Murray E. L.	1959	*Planet. Space Sci.* **1,** 125.
Rice D. W. and Forsyth P. A.	1963	*Can. J. Phys.* **41,** 679.
Rice D. W. and Forsyth P. A.	1964	*Can. J. Phys.* **42,** 2035.